Applying Principles of Developmental Biology to Generate Three-dimensional Lung Organoids from Human Pluripotent Stem Cells

by

Briana Rockich Dye

A dissertation submitted in partial fulfillment
of the requirements for the degree of
Doctor of Philosophy
(Cell and Developmental Biology)
in the University of Michigan
2016

Doctoral Committee

Associate Professor Yukiko M. Yamashita, Chair
Assistant Professor Jason R. Spence
Associate Professor Deneen M. Wellik
Associate Professor Eric S. White

To my husband, parents, and sister for all their encouragement, support, and advice.
Thank you.

TABLE OF CONTENTS

LIST OF FIGURES

LIST OF TABLES

ABSTRACT

The lungs are a complex organ consisting of two main anatomical features, the airways and alveoli. The airways form an arborized network of epithelial tubes surrounded by supporting tissue that conduct air in and out of the body. The airways connect to clusters of alveoli where gas exchange occurs between a thin epithelium and the surrounding vasculature. Any disruption to these tissues leads to the vast number of lung diseases that are known today. The number and severity of diseases affecting human lung development and adult respiratory function has stimulated great interest in deriving new *in vitro* models to study the human lung. Currently, a variety of animal models and cell culturing systems are used to model human lung development and adult homeostasis and disease. As described herein, I have taken two different approaches to understand how the lung develops normally. First, by utilizing mouse models, we have determined that a transcription factor, Sox9, which is expressed during lung development, is necessary to establish the proper arborized network of airways in the adult. Second, I used human pluripotent stem cells, which are grown in a tissue culture dish and are capable to differentiate into any cell type of the human body, in order to investigate human lung development and to derive a model for human lung disease. Using human pluripotent stem cells, we have developed a three-dimensional human lung model system that consists of structures that are similar to the human lung, including complex, multicellular lung epithelium and supporting tissue. This dissertation will describe my efforts to exploit both animal models and human cells grown *in vitro* in

order to better understand how the lung develops into the complex airway and alveolar structures of the adult lung.

CHAPTER 1

INTRODUCTION

Lung Overview

The lungs are the main organ of the respiratory system and function to exchange gas, taking in oxygen and expelling carbon dioxide. The lungs are organized in a branched, tree-like structure that has two major anatomical features, the conducting airways and alveoli. The conducting airways are arranged in a series of tubes that become progressively smaller as they move gas into the alveoli. The conducting airways start as a singular tube, the trachea, which splits into two main bronchi. The main bronchi then further split and branch into smaller airway tubes called the conducting bronchioles. The walls of the conducting airways consist of epithelial cell types surrounded by supporting mesenchyme including fibroblasts, smooth muscle, cartilage, vasculature, and neurons extending the length of the airways (Fig. 1.1). Just before the bronchioles terminate they form a small tube called the alveolar duct, which leads into the thin sac of cells that make up the alveoli. The alveolar epithelium is tightly associated with a capillary network in order for efficient gas exchange to take place.

In order to accommodate diverse functions, the human lung possesses several specialized cell types. The conducting airways are predominated by three epithelial cell types: ciliated, goblet, and basal cells, with ciliated cells being the most dominant cell type in human airways (1). Ciliated cells have multiple cilia that beat in a synchronous

rhythm in order to maintain the flow of mucus across the airway epithelium (2, 3). Goblet cells are secretory cells that secrete mucus on the surface of the airway (4). The basal cells are the adult stem cells of the airways (5-9). In humans, basal cells line the main bronchi and large bronchioles, but begin to decrease in number in the smaller bronchioles toward the alveoli (1, 8, 10, 11). Other, sparse populations of cells in the airway include club cells, which are secretory cells that secrete lubricating glycosaminoglycans and antimicrobial peptides into airways (12), and pulmonary neuroendocrine cells which are innervated on the basal surface and store proteins that are released under a physiological stimulus such as hypoxia (13-16). The alveolar epithelium is comprised of two epithelial cell types, alveolar epithelial type I cells (AECI) and alveolar epithelial type II cells (AECII) (Fig. 1.1). AECIs form a thin, squamous epithelium that covers the majority of the alveolar surface and exchanges gas with neighboring capillaries through diffusion (17-20). AECIIs have a cuboidal shape and secrete surfactant proteins to reduce the surface tension of the alveolar sacs, allowing them to expand and contract without collapsing as breathing takes place (18, 20-22).

The complex architecture of the adult lung is established during early embryonic development. The epithelium of the lung is derived from the embryonic endoderm while much of the structural support of the lung, including fibroblasts, smooth muscle and cartilage, is derived from the embryonic mesoderm. Lung development begins as two buds forming off of a tube of endoderm surrounded by mesoderm called the gut tube. The gut tube gives rise to the entire gastrointestinal tract and associated organs, including lungs, thyroid, liver and pancreas (23-26). The primary lung buds emerge from the gut tube, invade the surrounding mesoderm and continue to elongate in tight

association with the mesoderm throughout development. The lung buds then undergo branching morphogenesis, in which epithelial bud tips continuously bifurcate, forming new branches, until a stereotyped tree-like pattern is formed (27). During branching, a proximal-distal lung axis is established, with proximal lung epithelium giving rise to conducting airways, and the distal tips eventually terminally differentiating into the alveolar sacs (for more detailed reviews see: (28, 29)).

Since lung development is so critical for neonatal life, it has been the focus of intense study. In addition, adult lung diseases are prevalent and can be caused by environmental exposure to pathogens or damaging toxins; however, in many cases, chronic lung diseases are often a result of both genetics and environment. Much of our understanding of aberrant lung development and adult disease has resulted from using animal models and cell culture systems. These approaches have yielded a tremendous amount of insight into the mechanisms that cause disease; however, there are many aspects of human biology and disease that are not reflected in animal models or cell culture systems. In order to address the need for a physiologically relevant human model systems, the past decade has seen several fields turn to human pluripotent stems cells (hPSCs), which include both embryonic stem cells and induced pluripotent stem cells, in an attempt to generate specific cell types and even complex organ-like tissue *in vitro* (30-34). Indeed, the lung field has seen rapid growth in the number of exciting reports generating lung tissue *in vitro* (35-45). In this chapter, I will introduce the developmental biology framework that forms the basis to differentiate lung tissue from hPSCs.

Endoderm and Anterior Foregut Specification

hPSC-derived tissues are often generated using directed differentiation, a process that aims to recapitulate the signals that drive cell or organ specific differentiation in the embryo in an *in vitro* environment (36-46). In the case of the lung, this entails a series of sequential steps to derive endoderm, then anterior foregut endoderm and induction of lung progenitor cells, followed by lung-specific cell type differentiation and maturation. It has long been appreciated that Nodal signaling is necessary to form definitive endoderm during gastrulation in animal models, and is also sufficient to convert non-endodermal lineages (ectoderm) into endoderm in early embryonic tissue (26, 47-51). In cell culture, ActivinA, which is a Tgf□ superfamily member, stimulates the same signaling pathways as Nodal and has been widely used to successfully induce definitive endoderm differentiation from hPSCs (30, 34, 39, 52).

Following gastrulation, the embryo undergoes a series of morphological movements that give rise to the gut tube, which is an endodermal tube surrounded by mesoderm. Embryo and gut tube patterning are guided by a multitude of secreted proteins that both stimulate and inhibit different signaling pathways in order to establish the domains of the gut tube, referred to as the foregut, midgut, and hindgut which form along the anterior-posterior axis of the embryo (for more detailed reviews, see: (26, 53)).

Several secreted inhibitors help to establish the anterior identity of the foregut endoderm, which will give rise to the lungs and thyroid. As the endoderm migrates to form the gut tube during gastrulation, cells at the anterior side of the embryo encounter secreted Nodal inhibitors Lefty1 and Cerberus-like (Cerl) and BMP inhibitors Chordin

and Noggin, which inhibit posterior patterning (54-56). In Xenopus laevis, the Wnt antagonist Sfrp5 is secreted from the endoderm to maintain foregut identity (57). In line with embryonic regulation of anterior endoderm patterning, an activator/inhibitor screen conducted in hPSC-derived endoderm that included inhibitors and activators of Nodal, Hedgehog (HH), WNT, RA, BMP and TGF□ signaling pathways identified that inhibition of the BMP and TGFβ signaling pathways robustly induced anterior foregut genes (58).The observation that inhibition of BMP and TGFβ ("dual smad inhibition") potently stimulates a foregut endoderm fate has been widely adopted by the lung differentiation field (38-41, 45, 58). Interestingly, although secreted Wnt inhibitors help maintain foregut identity *in vivo*, inhibition of Wnt signaling is not necessary to induce foregut endoderm *in vitro* (36, 37, 39-41, 45, 58).

Morphogenesis in a dish

In hPSC-derived endoderm cultures, it has been shown that stimulating WNT and FGF signaling pathways (via WNT3A and FGF4) causes self-aggregation of three-dimensional cell clusters, called spheroids, that delaminate from the tissue culture monolayer (34, 39, 52, 59). While the mechanisms driving three-dimensional spheroid formation in endoderm cultures is not known, it is interesting to speculate that FGF4 and WNT are acting, as they do *in vivo*, to drive cellular reorganization and migration (60-64).

In addition to driving three-dimensional morphogenesis in a dish, WNT3A and FGF4 are potent stimulators of the CDX2+ intestinal lineage *in vitro* (34). However, simultaneous stimulation of WNT/FGF signaling in combination of the *in vitro* anterior foregut

promoting conditions (dual smad inhibition), caused spheroids to take on an anterior foregut fate, including the expression of, NKX2.1, PAX8, and SOX2 (39). Taken together, these studies demonstrated that hPSC-derived definitive endoderm can be directed to become anterior foregut endoderm by mimicking *in vivo* patterning signals.

Lung Induction

During early development, the lung primordium forms along the ventral anterior foregut and expresses transcription factor Nkx2.1, which is required for lung fate (65, 66). Extensive study of lung specification has identified several signaling pathways that are critical for this process, including Fgf, Bmp, Wnt, Hedgehog (Hh) and RA signaling pathways (reviewed in (28, 67)). Bmp signaling to the anterior-ventral foregut endoderm is important to prime the lung domain by inhibiting Sox2, allowing lung specification to take place (67, 68). Additionally, Fgf2 secreted from the cardiac mesoderm, which sits adjacent to the ventral foregut, and Fgf10 secreted from the surrounding lung mesoderm are necessary for Nkx2.1 expression and lung formation (69-72). Similarly, Wnt ligands signaling from the lung mesoderm to the ventral foregut endoderm are also necessary for Nkx2.1 expression and lung induction (28, 73-76). RA promotes Nkx2.1 expression and lung bud formation in part by inhibiting TGFβ and the Wnt antagonist Dkk1, allowing Fgf and Wnt signaling to occur (77, 78). Hh signaling is also critical for lung development, as concurrent deletion of the Hh signaling transcription effectors Gli2 and Gli3 leads to lung agenesis(79).

Since the events required for lung induction are complex and involve multiple signaling pathways that are controlled in very tight temporal and spatial manner *in vivo*,

translating these developmental paradigms in a dish has proven to be challenging. However, many groups have generated hPSC-derived NKX2.1+ lung progenitor populations with varying levels of efficiency (Fig. 1.2A-C) (36-41, 43-46). The majority of methods to derive lung tissue *in vitro* have treated endoderm, or anterior foregut endoderm, in monolayer cultures with FGFs, BMPs, WNTs, and RA to induce NKX2.1+ endoderm. Approaches to induce three-dimensional lung organoids have used a combination of factors to promote spheroid formation by activating FGF4 and WNT signaling, while simultaneously specifying foregut with dual smad inhibition and inducing lung.

To date, the field has primarily focused on differentiating lung epithelial cells from hPSCs, however, the lung mesenchyme also plays a critical role in sending and receiving signals and physically interacting with the lung epithelium during early development (28). Given the important contribution of the mesenchyme to lung development and lung function, modeling this aspect of lung development *in vitro* represents a significant opportunity for furthering the field.

Branching morphogenesis and distal patterning

Lung progenitors

Following the induction of an Nkx2.1+ field of lung progenitor cells, the primordial lung buds undergo branching morphogenesis, giving rise to a patterned epithelium that consists of Sox2+ proximal airways and Sox9+/Id2+/Nmyc+ actively branching epithelium that will eventually differentiate, giving rise to the alveoli (80-83). As bud tips bifuracate forming two new branches, the epithelial and mesenchymal cells are

proliferating and migrating (80, 81, 84-86). In the distal epithelium, epithelial marker Nmyc has been shown to be necessary to maintain the proper level of proliferation and maintain the progenitor identity in the branching tips (81). Although a function has not been defined for Id2 in the distal epithelium, the Id2+ cells have been lineage traced to show that during early development (Embryonic day (E) 10.5-E13.5), the Id2+ cells give rise to all epithelial cell types, but during late development (E15.5-E17.5) the Id2+ cells only give rise to the distal epithelial cells AECI and AECII (83). Previously Sox9 was shown to have no role during lung development when deleted by using SftpCre driver, SftpC is expressed in the distal epithelium then after branching exclusively in AECII cells (82). However, when Sox9 is deleted using a ShhCre driver, which allowed Sox9 epithelial deletion early during lung induction (E9.5), the loss of Sox9 caused severe branching defects (80).

Sox9

Sox9 is part of the sex-determining region Y (SRY)-related high mobility group (HMG)-box (SOX) transcription factors family (87). In humans, mutations in SOX9 can lead to several genetic disorders including campomelic dysplasia (CD), acampomelic campomelic dysplasia (ACD), Cooks syndrome, and Pierre Robin sequence (or syndrome) (88-90). Patients suffering from these diseases have many birth defects including respiratory defects, which can ultimately lead to death (89-94). Sox9 plays many roles during development in a variety of tissues including organs that undergo branching morphogenesis such as the pancreas and kidney. During pancreas development, Sox9 regulates proliferation and differentiation of the pancreatic

progenitors through Wnt , Notch, FGF signaling pathways (95, 96). In the kidney Sox9 is involved in the GDNF/RET pathway and is necessary for branching (97). In the lung Sox9 is necessary for proper branching morphogenesis by primarily regulating ECM deposition, cell cytoskeleton, and epithelial cell migration (80)

Distal patterning

Diffusible growth factors including Bmp4, Fgfs and Wnts are essential for establishing proximal-distal axis and maintaining the distal Sox9+/Id2+/Nmyc+ epithelium. Bmp4 and Wnt2/2b expression in the distal mesenchyme and Wnt7a originating in the distal epithelium signal to the distal epithelium and are essential for maintaining the distal epithelium and promoting branching (98-102). In mice, blocking Wnt signaling by conditional loss of β-Catenin from the epithelium results in disrupted branching and expansion of the proximal epithelium (99, 103). Similarly, Fgf7 and Fgf10 signaling from the distal mesenchyme to the epithelium promotes epithelial growth and branching, and Fgf10 plays a role in maintaining distal progenitor cells during branching morphogenesis (104-108). RA promotes branching by increasing Fgf10 expression in the lung mesenchyme (109). Once the branching program is complete, the distal epithelium differentiates into alveolar cells AECI and AECII. In the mouse lung, both alveolar cell types arise from a distal bipotent progenitor (110), however, the factors that regulate cell fate choice and differentiation of alveolar cell types in the embryo are not well understood.

Efforts to derive distal and alveolar cell types *in vitro* have attempted to recapitulate the signaling factors active around distal buds during branching in the

developing embryo. To date, Huang et al. have provided the most efficient protocol to generate AECI and AECII cells from hPSCs (Fig.1. 2A) (38). hPSC-derived foregut endoderm was cultured with Chir99021 (a GSK3□ antagonist that stabilizes □-catenin), BMP4, FGF10, FGF7 and RA for 15 days at which time the cells were cultured with Chir99021, FGF10 and FGF7 for an additional 25 days, followed by treatment with dexamethasone, cAMP and isobutylmethylxanthine (DCI), which stimulates alveolar cell-specific gene expression *in vitro* (35, 111). Additionally, dexamethasone is administrated to premature infants to accelerate fetal lung maturation, which results in enhanced surfactant secretion from AECIIs (112, 113). These sequential steps resulted in cells expressing AECII protein SFTPB in over 50% of all cells in the culture, with some SFTPB+ cells displaying lamellar bodies and functional release and uptake of surfactant protein. These factors also induced cells to express AECI cell specific markers. While these cells displayed the flat, elongated nuclei typical of AECI cells, they did not exhibit elongated cell bodies or form multi-cellular sac-like alveolar structures (38). Others have found that seeding NKX2.1+ lung progenitors onto human lung extra cellular matrix (ECM) proteins significantly enhanced AECI and AECII cell differentiation, indicating that both the physical and chemical environments are important for alveolar differentiation *in vitro* (42).

More recently, attempts have been made to differentiate three-dimensional lung-like tissues *in vitro* by recreating the embryonic distal lung environment in a dish (Fig.1. 2B) (39). Three-dimensional foregut spheroid cultures grown in an extracellular matrix (Matrigel) with high concentrations of FGF10 led to the formation of lung organoids. Lung organoids possess a distal alveolar cell population that express bipotent

progenitor markers including SFTPC, HOPX, and SOX9 (110) with a few cells expressing mature AECI and AECII mature markers, PDPN and SFTPB, respectively. Alveolar cell types were found in distinct regions of the lung organoid, but true alveolar sac-like structures were not observed (39).

Thus, one of the hurdles that remain in hPSC-derived lung differentiation is to successfully recapitulate alveolar structure *in vitro*. Alveolar-like structures have been derived from primary human AECII cells co-cultured with fetal human lung fibroblast cell lines forming alveolar spheres (alveolospheres). The cultures consist of phenotypic AECI and AECII cells demonstrating proof of concept that achieving such three-dimensional alveolar structure is possible (114). Similar approaches have been attempted with hPSC-derived tissues, where the cell surface marker carboxypeptidase M (CPM) was used to enrich NKX2.1+ progenitors using fluorescent activated cell sorting (FACS). CPM purified lung progenitors were cultured in a three-dimensional extracellular matrix along with FGF7, DCI and a fetal human lung fibroblast cell line. This resulted in three-dimensional spheres comprised of cells expressing AECI and AECII markers, yet proper AECI morphology was not demonstrated (41). Although effective, one of the drawbacks to this approach is that it is unclear if the human fetal feeder cells are providing a physical niche through cell-cell contact, and/or if they secrete important factors (41, 114). While several groups have shown success obtaining distal epithelial cell types *in vitro,* additional work is needed to better understand the mechanisms that control AECI and AECII differentiation to improve upon the efficiency of the differentiation and deriving alveolar structure.

Proximal airway differentiation

In the developing embryo, a variety of factors are important for promoting proximal airway fate in mouse lungs(115). As development progresses the Sox9/Id2/Nmyc bud tips differentiate into proximal tissue and express the marker Sox2. The multipotent Sox2+ airway population will give rise to neuroendocrine, club, ciliated, goblet and basal cells (28). Activation of Notch signaling promotes Sox2+ cells to differentiate into secretory cells, whereas inhibition of Notch signaling promotes ciliated cells and neuroendocrine cell fates (116-118). During late lung development and adult homeostasis, the Fgf signaling ligand Fgf18 is necessary for maintaining basal stem cells in the proximal airways, and Notch signaling acts to control the balance of secretory and ciliated cell types (5, 9, 115, 119, 120).

In order to differentiate proximal airway cell types from hPSC-derived endoderm, approaches to both promote proximal airway differentiation and approaches to reduce distal airway differentiation have been taken (Fig. 1.2C). In order to steer cells away from a distal fate, BMP4 concentrations were reduced and FGF18 was added to promote proximal cell fates, an approach that resulted in over 50% of the cells expressing the basal stem cell marker P63. To further mature proximal cell types, cultures were moved to an air-liquid interface (ALI) resulting in an increase in mature airway cells and polarization of the airway epithelium. The cells on the ALI expressed markers for goblet, club, and ciliated cells along with basal cells (36). Together, these results suggest that foregut endoderm can be directed to a proximal lung fate by a combination of reducing factors that promoted distal fate and adding factors that promoted proximal fate. However, the role of the polarizing ALI environment and the

undefined growth factors present in commercially purchased ALI media in this approach leaves room for further exploration.

In addition to the ALI platform, thee-dimensional airway cultures have been generated from hPSCs, applying similar concepts used to derive “bronchospheres” from human and mouse primary basal cells, an approach first establishing that human basal cells can self-renew and generate ciliated and club cells *in vitro* (5). Successful growth of bronchoshperes from hPSCs has been achieved by using the CPM, similar to the approach used for alveolarspheres (40, 41). Using commercially available ALI media and Notch inhibition, the sorted CPM+ population formed spheres in a three-dimensional matrix from single cells. Spheres consisted of mostly ciliated cells interspersed with neuroendocrine cells with even fewer basal cells and secretory cells. These hPSC-derived bronchospheres represent the first report of beating ciliated cells that are not derived from a primary cell line; however the cells do not organize into a pseudostratified epithelium, as is the case with the lung *in vivo* (40). Foregut spheroids grown in a three-dimensional ECM, Matrigel, overlaid with media containing high concentrations of FGF10 also gave rise to proximal airway-like structures that formed a polarized epithelium organized in a cyst containing a lumen, and surrounded by mesenchyme (Fig. 1.2B). The epithelium consisted of basal cells close to the mesenchymal tissue, with the adjacent epithelial cell types facing toward the lumen and expressing an early marker of ciliated cells, FOXJ1 (39). High FGF10 was required for airway-like epithelium to differentiate in lung organoids, and may act to maintain the basal cell population in lung organoids, however, this has not yet been formally tested. However, recent evidence in mice suggests that high levels of ectopic FGF10

expressed during embryonic development can increase the number of P63+ basal stem cells present in the lung (105). Interestingly, as has been demonstrated in both lung organoids and other hPSC-derived tissues, including hepatocyte-like, □-cell-like, intestinal, stomach and cerebral organoids, even in long term cultures, the organoids retain a transcriptional profile more similar to the fetal tissue than to adult tissue (33, 39, 52, 121-123). Thus, an important unresolved question in the field is to understand how to overcome this developmental barrier *in vitro* in order to obtain more mature adult-like tissue. Achieving this goal could require modulation of the physical or chemical environment to induce further maturation of the tissue.

References

1. Mercer RR, Russell ML, Roggli VL, Crapo JD (1994) Cell number and distribution in human and rat airways. *American Journal of Respiratory Cell and Molecular Biology* 10(6):613–624.

2. Wolff RK (1986) Effects of airborne pollutants on mucociliary clearance. *Environ Health Perspect* 66:223–237.

3. Schum M, Yeh HC (1980) Theoretical evaluation of aerosol deposition in anatomical models of mammalian lung airways. *Bull Math Biol* 42(1):1–15.

4. Rogers DF (1994) Airway goblet cells: responsive and adaptable front-line defenders. *Eur Respir J* 7(9):1690–1706.

5. Rock JR, et al. (2009) Basal cells as stem cells of the mouse trachea and human airway epithelium. *Proceedings of the National Academy of Sciences* 106(31):12771–12775.

6. Hackett T-L, et al. (2008) Characterization of side population cells from human airway epithelium. *STEM CELLS* 26(10):2576–2585.

7. Hong KU, Reynolds SD, Watkins S, Fuchs E, Stripp BR (2004) Basal cells are a multipotent progenitor capable of renewing the bronchial epithelium. *AJPA* 164(2):577–588.

8. Boers JE, Ambergen AW, Thunnissen FB (1998) Number and proliferation of basal and parabasal cells in normal human airway epithelium. *Am J Respir Crit Care Med* 157(6 Pt 1):2000–2006.

9. Pardo-Saganta A, et al. (2015) Injury induces direct lineage segregation of functionally distinct airway basal stem/progenitor cell subpopulations. *Cell Stem Cell* 16(2):184–197.

10. Nakajima M, et al. (1998) Immunohistochemical and ultrastructural studies of basal cells, Clara cells and bronchiolar cuboidal cells in normal human airways. *Pathol Int* 48(12):944–953.

11. Evans MJ, Van Winkle LS, Fanucchi MV, Plopper CG (2001) Cellular and molecular characteristics of basal cells in airway epithelium. *Exp Lung Res* 27(5):401–415.

12. Boers JE, Ambergen AW, Thunnissen FB (1999) Number and proliferation of clara cells in normal human airway epithelium. *Am J Respir Crit Care Med* 159(5 Pt 1):1585–1591.

13. Linnoila RI (2006) Functional facets of the pulmonary neuroendocrine system. *Lab Invest* 86(5):425–444.

14. Domnik NJ, Cutz E (2011) Pulmonary neuroepithelial bodies as airway sensors: putative role in the generation of dyspnea. *Curr Opin Pharmacol* 11(3):211–217.

15. Song H, et al. (2012) Functional characterization of pulmonary neuroendocrine cells in lung development, injury, and tumorigenesis. *Proceedings of the National Academy of Sciences* 109(43):17531–17536.

16. Branchfield K, et al. (2016) Pulmonary neuroendocrine cells function as airway sensors to control lung immune response. *Science*. doi:10.1126/science.aad7969.

17. Williams MC (2003) Alveolar type I cells: molecular phenotype and development. *Annu Rev Physiol* 65:669–695.

18. Féréol S, Fodil R, Pelle G, Louis B, Isabey D (2008) Cell mechanics of alveolar epithelial cells (AECs) and macrophages (AMs). *Respir Physiol Neurobiol* 163(1-3):3–16.

19. Yang J, et al. (2016) The development and plasticity of alveolar type 1 cells. *Development* 143(1):54–65.

20. Branchfield K, et al. (2016) A three-dimensional study of alveologenesis in mouse lung. *Developmental Biology* 409(2):429–441.

21. Castranova V, Rabovsky J, Tucker JH, Miles PR (1988) The alveolar type II epithelial cell: a multifunctional pneumocyte. *Toxicol Appl Pharmacol* 93(3):472–483.

22. Fehrenbach H (2001) Alveolar epithelial type II cell: defender of the alveolus revisited. *Respir Res* 2(1):33–46.

23. Wells JM, Spence JR (2014) How to make an intestine. *Development* 141(4):752–760.

24. Spence JR, Wells JM (2007) Translational embryology: using embryonic principles to generate pancreatic endocrine cells from embryonic stem cells. *Dev Dyn* 236(12):3218–3227.

25. Finkbeiner SR, Spence JR (2013) A gutsy task: generating intestinal tissue from human pluripotent stem cells. *Dig Dis Sci* 58(5):1176–1184.

26. Zorn AM, Wells JM (2009) Vertebrate endoderm development and organ formation. *Annu Rev Cell Dev Biol* 25:221–251.

27. Metzger RJ, Klein OD, Martin GR, Krasnow MA (2008) The branching programme of mouse lung development. *Nature* 453(7196):745–750.

28. Morrisey EE, Hogan BLM (2010) Preparing for the First Breath: Genetic and

Cellular Mechanisms in Lung Development. *Dev Cell* 18(1):8–23.

29. Rawlins EL (2010) The building blocks of mammalian lung development. *Dev Dyn* 240(3):463–476.

30. D'Amour KA, et al. (2005) Efficient differentiation of human embryonic stem cells to definitive endoderm. *Nature Biotechnology* 23(12):1534–1541.

31. Cai J, et al. (2007) Directed differentiation of human embryonic stem cells into functional hepatic cells. *Hepatology* 45(5):1229–1239.

32. Kroon E, et al. (2008) Pancreatic endoderm derived from human embryonic stem cells generates glucose-responsive insulin-secreting cells in vivo. *Nature Biotechnology* 26(4):443–452.

33. Si-Tayeb K, et al. (2010) Highly efficient generation of human hepatocyte-like cells from induced pluripotent stem cells. *Hepatology* 51(1):297–305.

34. Spence JR, et al. (2011) Directed differentiation of human pluripotent stem cells into intestinal tissue in vitro. *Nature* 470(7332):105–109.

35. Longmire TA, et al. (2012) Efficient Derivation of Purified Lung and Thyroid Progenitors from Embryonic Stem Cells. *Stem Cell* 10(4):398–411.

36. Wong AP, et al. (2012) Directed differentiation of human pluripotent stem cells into mature airway epithelia expressing functional CFTR protein. *Nature Biotechnology* 30(9):875–881.

37. Mou H, et al. (2012) Generation of Multipotent Lung and Airway Progenitors from Mouse ESCs and Patient-Specific Cystic Fibrosis iPSCs. *Stem Cell* 10(4):385–397.

38. Huang SXL, et al. (2013) Efficient generation of lung and airway epithelial cells from human pluripotent stem cells. *Nature Biotechnology*. doi:10.1038/nbt.2754.

39. Dye BR, et al. (2015) In vitro generation of human pluripotent stem cell derived lung organoids. *Elife* 4. doi:10.7554/eLife.05098.

40. Konishi S, et al. (2016) Directed Induction of Functional Multi-ciliated Cells in Proximal Airway Epithelial Spheroids from Human Pluripotent Stem Cells. *Stem Cell Reports* 6(1):18–25.

41. Gotoh S, et al. (2014) Generation of alveolar epithelial spheroids via isolated progenitor cells from human pluripotent stem cells. *Stem Cell Reports* 3(3):394–403.

42. Ghaedi M, et al. (2014) Alveolar epithelial differentiation of human induced pluripotent stem cells in a rotating bioreactor. *Biomaterials* 35(2):699–710.

43. Ghaedi M, et al. (2013) Human iPS cell-derived alveolar epithelium repopulates lung extracellular matrix. *J Clin Invest* 123(11):4950–4962.

44. Hannan NRF, Sampaziotis F, Segeritz C-P, Hanley NA, Vallier L (2015) Generation of Distal Airway Epithelium from Multipotent Human Foregut Stem Cells. *Stem Cells Dev* 24(14):1680–1690.

45. Firth AL, et al. (2014) Generation of multiciliated cells in functional airway epithelia from human induced pluripotent stem cells. *Proceedings of the National Academy of Sciences* 111(17):E1723–30.

46. Longmire TA, et al. (2012) Efficient Derivation of Purified Lung and Thyroid Progenitors from Embryonic Stem Cells. *Stem Cell* 10(4):398–411.

47. Schier AF (2003) Nodal signaling in vertebrate development. *Annu Rev Cell Dev Biol* 19:589–621.

48. Schier AF, Shen MM (2000) Nodal signalling in vertebrate development. *Nature* 403(6768):385–389.

49. Aoki TO, et al. (2002) Molecular integration of casanova in the Nodal signalling pathway controlling endoderm formation. *Development* 129(2):275–286.

50. Shen MM (2007) Nodal signaling: developmental roles and regulation. *Development* 134(6):1023–1034.

51. Hagos EG, Dougan ST (2007) Time-dependent patterning of the mesoderm and endoderm by Nodal signals in zebrafish. *BMC Dev Biol* 7:22.

52. McCracken KW, et al. (2014) Modelling human development and disease in pluripotent stem-cell-derived gastric organoids. *Nature* 516(7531):400–404.

53. Rossant J, Tam PPL (2009) Blastocyst lineage formation, early embryonic asymmetries and axis patterning in the mouse. *Development* 136(5):701–713.

54. Yamamoto M, et al. (2004) Nodal antagonists regulate formation of the anteroposterior axis of the mouse embryo. *Nature* 428(6981):387–392.

55. Perea-Gomez A, et al. (2002) Nodal antagonists in the anterior visceral endoderm prevent the formation of multiple primitive streaks. *Dev Cell* 3(5):745–756.

56. Tiso N, Filippi A, Pauls S, Bortolussi M, Argenton F (2002) BMP signalling regulates anteroposterior endoderm patterning in zebrafish. *MECHANISMS OF DEVELOPMENT* 118(1-2):29–37.

57. Li Y, et al. (2008) Sfrp5 coordinates foregut specification and morphogenesis by antagonizing both canonical and noncanonical Wnt11 signaling. *Genes Dev*

22(21):3050–3063.

58. Green MD, et al. (2011) Generation of anterior foregut endoderm from human embryonic and induced pluripotent stem cells. *Nature Biotechnology* 29(3):267–272.

59. McCracken KW, Howell JC, Wells JM, Spence JR (2011) Generating human intestinal tissue from pluripotent stem cells in vitro. *Nat Protoc* 6(12):1920–1928.

60. Schlessinger K, Hall A, Tolwinski N (2009) Wnt signaling pathways meet Rho GTPases. *Genes Dev* 23(3):265–277.

61. Li S, Muneoka K (1999) Cell migration and chick limb development: chemotactic action of FGF-4 and the AER. *Developmental Biology* 211(2):335–347.

62. Sun X, Meyers EN, Lewandoski M, Martin GR (1999) Targeted disruption of Fgf8 causes failure of cell migration in the gastrulating mouse embryo. *Genes Dev* 13(14):1834–1846.

63. Crump JG, Maves L, Lawson ND, Weinstein BM, Kimmel CB (2004) An essential role for Fgfs in endodermal pouch formation influences later craniofacial skeletal patterning. *Development* 131(22):5703–5716.

64. Sherwood RI, Maehr R, Mazzoni EO, Melton DA (2011) Wnt signaling specifies and patterns intestinal endoderm. *MECHANISMS OF DEVELOPMENT*:1–14.

65. Lazzaro D, Price M, de Felice M, Di Lauro R (1991) The transcription factor TTF-1 is expressed at the onset of thyroid and lung morphogenesis and in restricted regions of the foetal brain. *Development* 113(4):1093–1104.

66. Minoo P, Su G, Drum H, Bringas P, Kimura S (1999) Defects in tracheoesophageal and lung morphogenesis in Nkx2.1(-/-) mouse embryos. *Developmental Biology* 209(1):60–71.

67. Rankin SA, Zorn AM (2014) Gene regulatory networks governing lung specification. *J Cell Biochem* 115(8):1343–1350.

68. Domyan ET, et al. (2011) Signaling through BMP receptors promotes respiratory identity in the foregut via repression of Sox2. *Development* 138(5):971–981.

69. Serls AE, Doherty S, Parvatiyar P, Wells JM, Deutsch GH (2005) Different thresholds of fibroblast growth factors pattern the ventral foregut into liver and lung. *Development* 132(1):35–47.

70. Min H, et al. (1998) Fgf-10 is required for both limb and lung development and exhibits striking functional similarity to Drosophila branchless. *Genes Dev* 12(20):3156–3161.

71. Sekine K, et al. (1999) Fgf10 is essential for limb and lung formation. *Nat Genet* 21(1):138–141.

72. Shifley ET, Kenny AP, Rankin SA, Zorn AM (2012) Prolonged FGF signaling is necessary for lung and liver induction in Xenopus. *BMC Dev Biol* 12:27.

73. Goss AM, et al. (2009) Wnt2/2b and β-Catenin Signaling Are Necessary and Sufficient to Specify Lung Progenitors in the Foregut. *Dev Cell* 17(2):290–298.

74. Harris-Johnson KS, Domyan ET, Vezina CM, Sun X β-Catenin promotes respiratory progenitor identity in mouse foregut.

75. Rankin SA, Gallas AL, Neto A, Gomez-Skarmeta JL, Zorn AM (2012) Suppression of Bmp4 signaling by the zinc-finger repressors Osr1 and Osr2 is required for Wnt/ -catenin-mediated lung specification in Xenopus. *Development* 139(16):3010–3020.

76. Miller MF, et al. (2012) Wnt ligands signal in a cooperative manner to promote foregut organogenesis. *Proceedings of the National Academy of Sciences* 109(38):15348–15353.

77. Chen F, et al. (2010) A retinoic acid-dependent network in the foregut controls formation of the mouse lung primordium. *J Clin Invest* 120(6):2040–2048.

78. Chen F, et al. (2007) Inhibition of Tgf beta signaling by endogenous retinoic acid is essential for primary lung bud induction. *Development* 134(16):2969–2979.

79. Motoyama J, et al. (1998) Essential function of Gli2 and Gli3 in the formation of lung, trachea and oesophagus. *Nat Genet* 20(1):54–57.

80. Rockich BE, et al. (2013) Sox9 plays multiple roles in the lung epithelium during branching morphogenesis. *Proceedings of the National Academy of Sciences* 110(47):E4456–64.

81. Okubo T (2005) Nmyc plays an essential role during lung development as a dosage-sensitive regulator of progenitor cell proliferation and differentiation. *Development* 132(6):1363–1374.

82. Perl A-KT, Kist R, Shan Z, Scherer G, Whitsett JA (2005) Normal lung development and function afterSox9 inactivation in the respiratory epithelium. *genesis* 41(1):23–32.

83. Rawlins EL, Clark CP, Xue Y, Hogan BLM (2009) The Id2+ distal tip lung epithelium contains individual multipotent embryonic progenitor cells. *Development* 136(22):3741–3745.

84. Weaver M, Dunn NR, Hogan BL (2000) Bmp4 and Fgf10 play opposing roles during lung bud morphogenesis. *Development* 127(12):2695–2704.

85. Plosa EJ, et al. (2014) Epithelial β1 integrin is required for lung branching morphogenesis and alveolarization. *Development* 141(24):4751–4762.

86. Varner VD, Nelson CM (2014) Cellular and physical mechanisms of branching morphogenesis. *Development* 141(14):2750–2759.

87. Pritchett J, Athwal V, Roberts N, Hanley NA, Hanley KP (2011) Understanding the role of SOX9 in acquired diseases: lessons from development. *Trends Mol Med* 17(3):166–174.

88. Jakobsen LP, et al. (2007) Pierre Robin sequence may be caused by dysregulation of SOX9 and KCNJ2. *J Med Genet* 44(6):381–386.

89. Herman TE, Siegel MJ (2012) Acampomelic campomelic dysplasia in genetic male without sex reversal. *J Perinatol* 32(1):75–77.

90. Mansour S, Hall CM, Pembrey ME, Young ID (1995) A clinical and genetic study of campomelic dysplasia. *J Med Genet* 32(6):415–420.

91. Kwok C, et al. (1995) Mutations in SOX9, the gene responsible for Campomelic dysplasia and autosomal sex reversal. *American Journal of Human Genetics* 57(5):1028–1036.

92. Sock E, et al. (2003) Loss of DNA-dependent dimerization of the transcription factor SOX9 as a cause for campomelic dysplasia. *Human Molecular Genetics* 12(12):1439–1447.

93. Shinwell ES, Hengerer AS, Kendig JW (1988) A third case of bronchoscopic diagnosis of tracheobronchomalacia in campomelic dysplasia. *Pediatr Pulmonol* 4(3):192.

94. Houston CS, et al. (1983) The campomelic syndrome: review, report of 17 cases, and follow-up on the currently 17-year-old boy first reported by Maroteaux et al in 1971. *Am J Med Genet* 15(1):3–28.

95. Belo J, Krishnamurthy M, Oakie A, Wang R (2013) The role of SOX9 transcription factor in pancreatic and duodenal development. *Stem Cells Dev* 22(22):2935–2943.

96. Seymour PA (2014) Sox9: a master regulator of the pancreatic program. *Rev Diabet Stud* 11(1):51–83.

97. Reginensi A, et al. (2011) SOX9 controls epithelial branching by activating RET effector genes during kidney development. *Human Molecular Genetics* 20(6):1143–1153.

98. Weaver M, Yingling JM, Dunn NR, Bellusci S, Hogan BL (1999) Bmp signaling regulates proximal-distal differentiation of endoderm in mouse lung

development. *Development* 126(18):4005–4015.

99. Mucenski ML, et al. (2003) beta-Catenin is required for specification of proximal/distal cell fate during lung morphogenesis. *J Biol Chem* 278(41):40231–40238.

100. De Langhe SP, Reynolds SD (2008) Wnt signaling in lung organogenesis. *organogenesis* 4(2):100–108.

101. Kadzik RS, et al. (2014) Wnt ligand/Frizzled 2 receptor signaling regulates tube shape and branch-point formation in the lung through control of epithelial cell shape. *Proceedings of the National Academy of Sciences* 111(34):12444–12449.

102. Rajagopal J, et al. (2008) Wnt7b stimulates embryonic lung growth by coordinately increasing the replication of epithelium and mesenchyme. *Development* 135(9):1625–1634.

103. Shu W, et al. (2005) Wnt/β-catenin signaling acts upstream of N-myc, BMP4, and FGF signaling to regulate proximal–distal patterning in the lung. *Developmental Biology* 283(1):226–239.

104. Bellusci S, Grindley J, Emoto H, Itoh N, Hogan BL (1997) Fibroblast growth factor 10 (FGF10) and branching morphogenesis in the embryonic mouse lung. *Development* 124(23):4867–4878.

105. Volckaert T, et al. (2013) Localized Fgf10 expression is not required for lung branching morphogenesis but prevents differentiation of epithelial progenitors. *Development* 140(18):3731–3742.

106. Shiratori M, et al. (1996) Keratinocyte growth factor and embryonic rat lung morphogenesis. *American Journal of Respiratory Cell and Molecular Biology* 15(3):328–338.

107. Yano T, et al. (2000) KGF regulates pulmonary epithelial proliferation and surfactant protein gene expression in adult rat lung. *Am J Physiol Lung Cell Mol Physiol* 279(6):L1146–58.

108. Nyeng P, Norgaard GA, Kobberup S, Jensen J (2008) FGF10 maintains distal lung bud epithelium and excessive signaling leads to progenitor state arrest, distalization, and goblet cell metaplasia. *BMC Dev Biol* 8:2.

109. Desai TJ, et al. (2006) Distinct roles for retinoic acid receptors alpha and beta in early lung morphogenesis. *Developmental Biology* 291(1):12–24.

110. Desai TJ, Brownfield DG, Krasnow MA (2014) Alveolar progenitor and stem cells in lung development, renewal and cancer. *Nature*. doi:10.1038/nature12930.

111. Gonzales LW, Guttentag SH, Wade KC, Postle AD, Ballard PL (2002) Differentiation of human pulmonary type II cells in vitro by glucocorticoid plus cAMP. *Am J Physiol Lung Cell Mol Physiol* 283(5):L940–51.

112. Crowley P, Chalmers I, Keirse MJ (1990) The effects of corticosteroid administration before preterm delivery: an overview of the evidence from controlled trials. *Br J Obstet Gynaecol* 97(1):11–25.

113. Wapner R (2004) Antenatal corticosteroids: we continue to learn. *Am J Obstet Gynecol* 190(4):875.

114. Barkauskas CE, et al. (2013) Type 2 alveolar cells are stem cells in adult lung. *J Clin Invest* 123(7):3025–3036.

115. Whitsett JA, et al. (2002) Fibroblast growth factor 18 influences proximal programming during lung morphogenesis. *J Biol Chem* 277(25):22743–22749.

116. Guseh JS, et al. (2009) Notch signaling promotes airway mucous metaplasia and inhibits alveolar development. *Development* 136(10):1751–1759.

117. Morimoto M, et al. (2010) Canonical Notch signaling in the developing lung is required for determination of arterial smooth muscle cells and selection of Clara versus ciliated cell fate. *J Cell Sci* 123(Pt 2):213–224.

118. Zhang S, Loch AJ, Radtke F, Egan SE, Xu K (2013) Jagged1 is the major regulator of Notch-dependent cell fate in proximal airways. *Dev Dyn* 242(6):678–686.

119. Tadokoro T, et al. (2014) IL-6/STAT3 promotes regeneration of airway ciliated cells from basal stem cells. *Proceedings of the National Academy of Sciences* 111(35):E3641–9.

120. Rock JR, et al. (2011) Notch-dependent differentiation of adult airway basal stem cells. *Cell Stem Cell* 8(6):639–648.

121. Hrvatin S, et al. (2014) Differentiated human stem cells resemble fetal, not adult, β cells. *Proceedings of the National Academy of Sciences* 111(8):3038–3043.

122. Finkbeiner SR, et al. (2015) Transcriptome-wide Analysis Reveals Hallmarks of Human Intestine Development and Maturation In Vitro and In Vivo. *Stem Cell Reports*. doi:10.1016/j.stemcr.2015.04.010.

123. Camp JG, et al. (2015) Human cerebral organoids recapitulate gene expression programs of fetal neocortex development. *Proceedings of the National Academy of Sciences* 112(51):15672–15677.

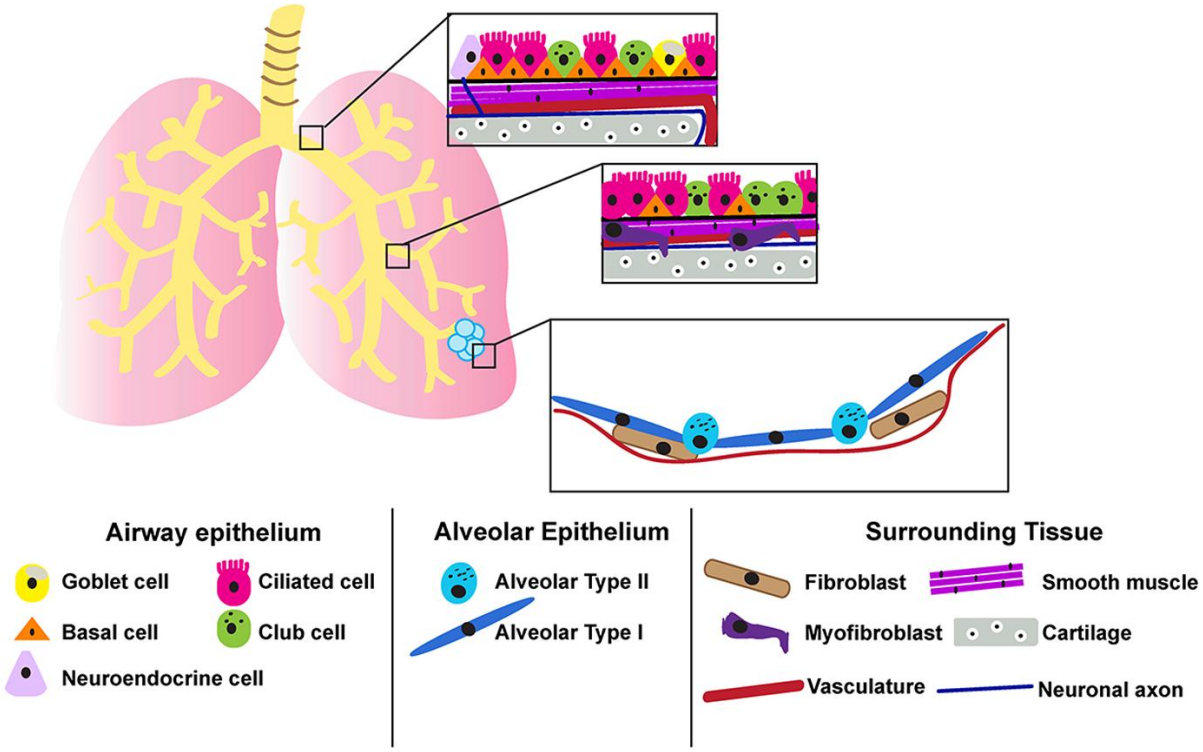

Figure 1.1 A diagram summarizing the lung cell types in and surrounding the airways and alveoli. Upper airways are surrounded by cartilage (brown) and smooth muscle (pink). The upper airway epithelium is lined with basal cells (orange) with ciliated (pink), goblet (yellow), club (green), and neuroendocrine (light purple) cells adjacent to the basal cells facing toward the lumen of the airway. The lower airways possess less basal cells and consist of mostly ciliated and club cells with surrounding tissues consisting of smooth muscle, myofibroblasts (purple), and patches of cartilage. Vessels (red line) and neurons (blue line) line both the upper and lower airways. The alveolar sacs consist of elongated AECI (light blue) and cuboidal AECII cells (dark blue) that are lined with thin vessels in order for gas exchange to occur with few fibroblasts scattered outside the alveolar sac. Note that only the most abundant lung cell types are depicted.

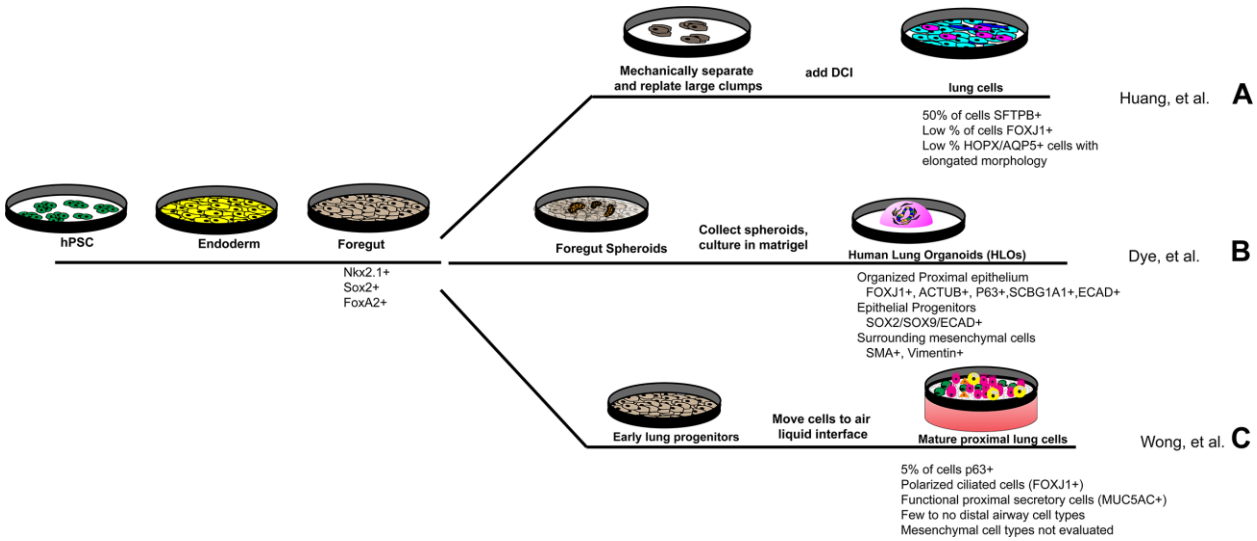

Figure. 1.2 Overview of methods to direct differentiation of hPSCs to lung tissue. The majority of protocols to derive lung cell types from hPSCs have taken a directed differentiation approach. hPSCs are first treated with growth factors, including ActivinA, to derive endoderm, which is further treated to become anterior foregut endoderm. Anterior foregut endoderm cells are marked by Nkx2.1, FoxA2, and Sox2 transcription factors. Different groups have used various methods to derive lung cell types after this stage. (A) Huang et al. grew foregut cultures for 15 days, after which cells were broken up and remaining large clumps were re-plated. On day 25, cells were treated with a DCI cocktail, which has been shown to induce alveolar specific cell-type gene expression *in vitro* [34, 95]. After 48 days in monolayer culture, the majority of cells expressed the AECII marker, SFTPB. A low number of cells also expressed the proximal ciliated cell marker FOXJ1, and some cells expressed markers for mature AECI (HOPX, AQP5) cells and exhibited elongated nuclei. (B) Dye et al. treated foregut cultures with FGF4 and Wnt to induce three-dimensional foregut spheroids, which were cultured in a matrigel droplet. These lung organoids persisted in culture for over 100 days and contained an organized epithelium containing cells positive for proximal airway markers FOXJ1/ACTUB (ciliated cells), p63 (basal stem cells), SCBGA1A1 (club cells), and surrounding mesenchymal tissue positive for smooth muscle (SMA) and vimentin (VIM). Additionally, organoids contained some cells that stained positive for AECI and AECII cell makers, but organized alveolar structures were not observed. (C) Wong et al. used multiple growth factor cocktails over the course of 35 days to induce lung progenitor cells in a monolayer culture. After roughly 5 weeks in culture, cells were moved to an air-liquid interface environment, which resulted in maturation of lung cells. The majority of cells expressed mature proximal cell markers for ciliated cells (FOXJ1) or goblet cells (MUC5AC), and cells exhibited distinct polarization, with the basal side of cells facing the media and the apical side of cells facing the air, similar to the *in vivo* polarization of lung cells with apical surfaces facing the airway lumen.

CHAPTER 2

SOX9 PLAYS MULTIPLE ROLES IN THE LUNG EPITHELIUM DURING BRANCHING MORPHOGENESIS.

Summary

Lung branching morphogenesis is a highly orchestrated process that gives rise to the complex network of gas-exchanging units in the adult lung. Intricate regulation of signaling pathways, transcription factors, and epithelial-mesenchymal cross-talk are critical to ensure that branching morphogenesis occurs properly. Here, we describe a novel role for the transcription factor Sox9 during lung branching morphogenesis. Sox9 is expressed at the distal tips of the branching epithelium in a highly dynamic manner as branching occurs, and is down regulated starting at E16.5, concurrent with the onset of terminal differentiation of Type I and Type II alveolar cells. Using epithelial specific genetic loss- and gain-of-function approaches, our results demonstrate that Sox9 controls multiple aspects of lung branching. Fine regulation of Sox9 levels is required to balance proliferation and differentiation of epithelial tip progenitor cells, and loss of Sox9 leads to direct and indirect cellular defects including extracellular matrix defects, cytoskeletal disorganization and aberrant epithelial movement. Our evidence shows that unlike other endoderm-derived epithelial tissues, such as the intestine, Wnt/β-catenin signaling does not regulate Sox9 expression in the lung. We conclude that Sox9

collectively promotes proper branching morphogenesis by controlling the balance between proliferation and differentiation, and regulating the ECM.

Introduction

Lung epithelial morphogenesis is a highly complex and stereotyped process that gives rise to a tree-like network consisting of proximal conducting airways and distal alveoli where gas exchange occurs in the adult (1-3). In mice, branching morphogenesis begins after the primary lung buds are firmly established and begin to invade into the surrounding mesenchyme at embryonic day (E) 10.5 (E10.5). As the primary lung buds proliferate and continue to invade the surrounding mesenchyme, domain branching initiates (3). The distal tips of the domain branches begin to repetitively bifurcate until terminal saccules form at the canalicular stage (E16.5-E17.5). These saccules will eventually give rise to the mature alveoli in the adult mouse (2-5). Several signaling pathways and transcription factors are known to play roles in branching morphogenesis; however, mechanisms controlling morphogenetic movements in the lungs have only recently started to gain attention (1, 6-11).

During branching morphogenesis, the distal tips of the branching epithelium contain a distinct population of progenitor cells that gives rise to all epithelial cell types early in lung development, but become developmentally restricted after E16.5 (12, 13). Since this distal epithelium is a highly proliferative population of cells, a fine balance between proliferation and differentiation must be maintained during lung development (14). Several transcription factors are expressed specifically in the distal branching

epithelium including Nmyc, Id2, and Sox9 (13-17). Nmyc plays an important role in maintaining the progenitor population in an undifferentiated state and in driving proliferation (14). Lineage tracing experiments have shown that distal tip cells expressing Id2 give rise to both proximal (ciliated, Clara, neuroendocrine cells) and distal cell types (Alveolar type I and II) (13), but a functional role for Id2 in the regulation of lung progenitor cells has not been established. Similarly, Sox9 is expressed in the distal tip epithelium; however, conditional epithelial-specific deletion of Sox9 using SftpC driven ablation (SftpC-rtTa;tetO-cre;Sox9-flox) resulted in normal lung development (15). Using an alternative approach (Shh-cre;Sox9-flox), we now report that early and efficient deletion of Sox9 from the lung epithelium results in dramatic defects in branching morphogenesis.

Sox9 is a member of the SRY-related HMG-box transcription factors family that regulates many developmental processes (18). In humans, mutations in SOX9 can lead to several inherited genetic birth defects, including Campomelic Dysplasia (CD), Acampomelic Campomelic Dysplasia (ACD), Cooks Syndrome and Pierre Robin Sequence (or Syndrome) (19-21). Congenital birth defects associated with these disorders can affect many different organ systems, including the respiratory system. Infants that are born with CD/ACD often die in the neonatal period due to respiratory distress, which can be a result of abnormal upper airway development or hypoplastic lungs (20-25). In other tissues, Sox9 has a diverse array of functions. For example, pancreatic Sox9 is required for proliferation and branching, intestinal Sox9 acts to limit Wnt-stimulated proliferation and Sox9 regulates proliferation and extracellular matrix (ECM) production in chondrocytes (26-32). Using genetic gain- and loss-of-function

models of Sox9, our findings demonstrate that the appropriate level of Sox9 is necessary for controlling the number of proliferating cells and differentiating cells as either loss or gain of Sox9 disrupts this balance. Further, we find dramatic cellular defects when Sox9 is conditionally deleted, which appear to be mediated through both direct and indirect mechanisms. Similar to its role in chondrogenesis, Sox9 transcriptionally regulates ECM genes in the lung epithelium and directly binds to DNA in *Col2a1* regulatory regions. Removing Sox9 leads to a down regulation of *Col2a1* mRNA and reduced protein expression. We also show that Sox9 leads to defects in Laminin deposition, cytoskeletal organization and cellular movement, although these defects may be indirect. Finally, we show that unlike the intestine (29, 33, 34) Wnt/β-Catenin signaling is not required for Sox9 expression during development. Taken together, our results demonstrate that Sox9 plays multiple roles regulating proliferation, differentiation, and the ECM during lung branching morphogenesis.

Results

Epithelial specific loss and gain of Sox9 causes severe branching defects in the lung.

Sox9 is expressed in the distal epithelium during branching morphogenesis (E11.5-E16.5) (Fig. 2.1 B-E and(15)). After E16.5, Sox9 is down regulated, terminal differentiation begins, and only a few cells retain Sox9 expression in late embryonic and postnatal stages. Sox9 is expressed in a manner similar to other distal tip progenitor markers including Nmyc and Id2 (13-15). Previous reports have suggested that epithelial Sox9 is not required for normal lung development (15). We generated lung

epithelial conditional loss-of-function (LOF; Sox9-floxed) (35) and gain-of-function (GOF; Rosa26-tetO-Sox9-mCherry, see methods section) embryos using a well-characterized Sonic hedgehog (Shh) Cre driver (36). Shh-cre shows robust activity in the lung epithelium by E10.5 (Fig. 2.1A and (1-3, 37)). Shh-cre;Sox9-flox/flox lungs (herein referred to as $Sox9^{LOF}$) and Shh-cre;Rosa-LSL-rtTa;Rosa-tetO-Sox9-mCherry lungs (herein referred to as $Sox9^{GOF}$) both develop large cyst-like structures at the distal epithelial branch tips at all developmental time points examined (Fig. 2.2A,C; Fig. 2.3A). Quantitative analysis of branching of *in vitro* cultured lungs showed a significant reduction in branching in $Sox9^{LOF}$ lungs compared to controls at the start of culture E12.5 (0 hours) and after 72 hours in culture (0 hours: 19.9 +/- 1.7 vs. 11.3 +/- 1.5 $p<0.05$, n=3; 72 hours: 57.6 +/- 5.9 vs. 38.0 +/- 1.7, $p<0.05$, n=5) (Fig. 2.2B, Fig 2.3B). We confirmed that Sox9 was deleted or overexpressed in the lung epithelium of the respective models with immunochemistry and qRT-PCR (Fig. 2.2D, Fig. 2.3C-D). Cross sections revealed that these cyst-like structures were the result of larger and rounder branch tips compared to control (Fig. 1E), which led to large open spaces in $Sox9^{LOF}$ lungs (Fig. 2.2F). We observed a reduction in airway spaces in $Sox9^{GOF}$ at E18.5 (Fig. 2.2F), likely due to reduced proliferation in cells expressing ectopic Sox9 (see Figure 2.4 and discussion). By E14.5 $Sox9^{LOF}$ and $Sox9^{GOF}$ lungs were noticeably smaller than control lungs (Fig. 2.2C, Fig. 2.3F). This reduction in size was more apparent by E16.5 (Fig. 2.3E), however, all lungs formed the appropriate number of lobes compared to control (Fig. 2.3F).

Ultimately, loss or gain of Sox9 had severe consequences on health and survival of mice. Of two litters born (to generate $Sox9^{LOF}$), there were 5 wildtype, 5 heterozygous

and 3 $Sox9^{LOF}$ pups. Of the 3 $Sox9^{LOF}$ pups, one died at birth and two others were euthanized at postnatal (P)7 due to poor health and an apparent difficulty breathing. One litter was born to generate $Sox9^{GOF}$ pups (Sftpc-rtTa;tetO-Sox9-mCherry, Dox started at E15.5). Of 6 mice, 3 were controls (Sftpc-rtTa or tetO-Sox9-mCherry) were healthy and thrived at P0, whereas the 3 pups that were $Sox9^{GOF}$ all died at birth. Analysis of the $Sox9^{GOF}$ lungs are discussed below and presented in Fig. 2.9. Taken together, our data suggests that Sox9 has a previously undiscovered role in regulating branching morphogenesis.

Precise regulation of Sox9 is required for appropriate proliferation in lung epithelium.

Recent quantitative and live imaging studies have shown that the process of lung bud bifurcation is dynamic and can be separated into three main stages: bud, flattened, and cleft stages (3, 38). Immunofluorescent staining of Sox9 revealed a dynamic expression pattern during these different stages. Sox9 is expressed highest at the distal-most cells of the budding tip and dissipates toward the parent branch (Fig. 2.4A). During the flat and cleft stage Sox9 is expressed highest where the two new buds will form and lowest where the cleft forms (Fig. 2.4A). Due to the dynamic expression of Sox9 in actively branching buds and previous reports demonstrating increased proliferation in distal lung epithelium (2-5, 14), we wanted to determine if proliferation was affected in $Sox9^{LOF}$ and $Sox9^{GOF}$ lungs compared to controls. To quantitate proximal and distal proliferation, control or $Sox9^{LOF}$ lungs were co-stained with Sox2 (proximal epithelium), E-cadherin (total epithelium), BrdU (proliferation) and Dapi (total

nuclei) (Fig. 2.5). After a 30 minute pulse of BrdU, we determined the percent of proximal (Ecad+, Sox2+) and distal (Ecad+, Sox2-) proliferation in the epithelium of control and $Sox9^{LOF}$ lungs at E14.5. As previously demonstrated (1, 6-11, 14), we confirmed that distal epithelial proliferation was significantly higher than proximal epithelial proliferation in control tissue (40.2% +/- 1.7% vs. 29.6% +/- 1.7%, $p<0.0005$, n=12) (Fig. 2.4B and Fig 2.5). Comparing BrdU incorporation in control and $Sox9^{LOF}$ lungs we found a significant decrease in total epithelial proliferation (37.8% +/- 1.5 vs. 30.2% +/- 2.2%, $p<0.01$, n=12) which was due to reduced proliferation in the distal tip epithelium (40.2% +/- 1.7% vs. 31.3% +/- 2.1%, $p<0.005$, n=12) since there was no change in proliferation of the proximal (Sox2+) epithelium when comparing control and $Sox9^{LOF}$ lungs (29.5% +/- 1.7% vs. 29.4% +/- 3.7%, n=12) (Fig. 2.4B and Fig. 2.5). There was no change in mesenchymal proliferation between groups (Fig. 2.5). $Sox9^{GOF}$ lungs had a more dramatic change in proliferation. In the proximal airways of $Sox9^{GOF}$ lungs, cells ectopically expressing Sox9 had almost no Ki67 staining, whereas Ki67 was present in most cells of the control proximal epithelium (Fig. 2.4C). Similarly, cells highly overexpressing Sox9 in the distal epithelium resulted in weak Ki67 staining (Fig. 2.4C). This data suggests that a fine balance of Sox9 expression is necessary to regulate proper proliferation during branching morphogenesis.

To determine if the perturbations in branching and proliferation in $Sox9^{LOF}$ or $Sox9^{GOF}$ lungs were due to disruption of well characterized signaling pathways that regulate lung development, we examined Wnt, Hh, Fgf, and Bmp signaling (2, 12, 13). Using *in situ* hybridization and/or qRT-PCR in $Sox9^{LOF}$ and $Sox9^{GOF}$ lungs at E12.5 and/or E14.5 we examined key signaling components and target genes and found no

significant changes compared to control lungs (Fig. 2.6A-B). Additionally, our data demonstrates that proximal-distal patterning is not disrupted in Sox9^{LOF} lungs. *In situ* hybridization demonstrates that *Bmp4* expression is localized to distal epithelial tips in control and Sox9^{LOF} lungs (Fig. 2.6B) (14, 39, 40), and proximal Sox2 immunostaining is not changed in Sox9^{LOF} lungs compared to controls (Fig 2.5). Together, our results suggest that loss of Sox9 regulates proliferation without significantly affecting proximal-distal patterning or the major signaling pathways (Wnt, Fgf, Bmp, Hh) known to play a role in lung branching morphogenesis.

Sox9 inhibits differentiation in early lung epithelium

Sox9 is expressed in the distal progenitor population, which gives rise to all cell types of the lung, and Sox9 expression is down regulated concomitant with onset of cytodifferentiation in the distal epithelium (13-17). Additionally, we observed a significant decrease in *Id2* mRNA expression in Sox9^{LOF} lungs at E14.5 by qRT-PCR (Fig. 2.6C). These results, combined with the observed decrease in proliferation in Sox9^{LOF} lungs, led us to hypothesize that Sox9 prevents differentiation of distal progenitors. Differentiation occurs in a proximal-to-distal direction starting at E14.5 with the differentiation of proximal airway cell types and ending with alveolar type I and II cell differentiation at E17.5 in the distal airways (2, 15). We examined markers for both proximal and distal epithelial cell types with qRT-PCR and immunostaining. Appropriate temporal differentiation of proximal cell types (Clara and Ciliated cells) and distal type I cells occurred in Sox9^{LOF} lungs (Fig. 2.7 and Fig. 2.8). Surfactant protein C (Sftpc) is

typically associated with type II alveolar cells. However, Sftpc in the early lung marks all distal tip progenitor cells, and recent studies have demonstrated that Sftpc positive cells in the adult are alveolar stem cells (41). Given that Sftpc can mark progenitor cells, alveolar stem cells and type II differentiated cells, we used Surfactant protein B (Sftpb) as type II alveolar cell marker, since it is normally expressed starting at E17.5 (18, 42, 43). In controls we observed that Sftpb protein was close to background at E14.5 by immunostaining whereas Sftpb staining in $Sox9^{LOF}$ lungs was readily detectable at this time (Fig. 2.4D). These results were supported by qRT-PCR, which showed a significant increase in *Sftpb* mRNA levels in E14.5 $Sox9^{LOF}$ lungs (Fig. 2.4E), providing evidence that the loss of Sox9 causes precocious differentiation of Type II cells. In contrast, $Sox9^{GOF}$ lungs demonstrated evidence that terminal differentiation was inhibited. When Sox9 is overexpressed throughout the lung epithelium (Shh-cre, Doxycycline administered starting at E9.5, Fig. 2.4 H-I and Figs. 2.7,2.8) or ectopically expressed in the distal lung epithelium (Sftpc-rtTa, Doxycycline administered starting at E15.5, Fig. 2.9) and lungs were analyzed at E18.5 or P0, respectively, there was decreased expression of proximal and distal differentiation markers (Fig. 2.4H-I, Figs. 2.7-2.9). It is important to point out that differentiated cells observed in $Sox9^{GOF}$ lungs were always Sox9-negative, indicating that they escaped transgene expression, whereas Sox9 positive cells did not express differentiation markers. During terminal differentiation starting around E17.5, the distal epithelium undergoes a columnar to squamous epithelial transition giving rise to alveolar sacs comprised of Type I and Type II alveolar cells. Accordingly, air spaces in control lungs at E18.5 were lined by a squamous epithelium; however, the distal epithelium of $Sox9^{GOF}$ lungs remains columnar (Fig.

2.4J). Collectively, our results suggest that Sox9 activity maintains the undifferentiated status of distal lung progenitors. Removing Sox9 leads to early differentiation and increasing Sox9 prevents differentiation and inhibits the epithelial transition from columnar to squamous epithelium that allows the adult alveoli to form.

Loss of Sox9 leads to multiple cellular defects in the distal progenitor cells

Since perturbations of epithelial Sox9 led to branching defects and cystic terminal branches, we wanted to detail the cellular events associated with the cystic structures observed in mutant mice. To examine possible cellular defects, we performed transmission electron microscopy in control and $Sox9^{LOF}$ lungs, and observed striking disruptions in the $Sox9^{LOF}$ lungs. Whereas the distal epithelial tips of control lungs showed a relatively uniform apical surface with microvilli, apical tight junctions and a flat, uniform basal surface (Fig. 2.10A), $Sox9^{LOF}$ lungs had a range of defects with varying levels of severity (Fig. 2.10B). $Sox9^{LOF}$ lungs showed defects on the apical surface of the cell. While tight junctions were observed, apical membranous blebs protruded into the lumen. In some cases, microvilli were absent, and the apical surface appeared rounded and smooth (Fig. 2.10B, lower panel). Cell-cell adhesion also appeared to be disrupted in $Sox9^{LOF}$ lungs. While control epithelial cells were in close apposition with occasional gaps, cell-cell adhesion appeared uniformly disrupted in $Sox9^{LOF}$ lungs, with large gaps filled with pseudopodia between the lateral membranes of neighboring cells (Fig. 2.10B). These pseudopodia are similarly observed in lungs with disrupted Cdc42, which have defective epithelial organization (7). Lastly, the control epithelium has a

relatively flat and uniform basal surface that contacts the lung mesenchyme (Fig. 2.10A). In contrast, the basal epithelial surface in Sox9^{LOF} lungs was not uniform, with many cells having a rounded appearance and with membranous blebs projecting into the subcellular space (Fig. 2.10B). Surprisingly, the apparent cell adhesion defects we observed by TEM were not obvious when examining E-cadherin immunofluorescence, although we did note that the epithelium in Sox9^{LOF} lungs was taller than in controls (17.2 μm +/- .24 μm vs. 15.2 μm +/- .21 μm, $p<0.0001$, n=192) (Fig. 2.11). Given that Sox9 controls multiple cellular processes in different contexts (see introduction, discussion), we examined apical-basal polarity and ECM proteins in Sox9^{LOF} and control lungs and found that polarity was unaffected (Fig. 2.12). However, upon examining several proteins that make up and interact with the ECM of the distal lung epithelium (Fig. 2.12), we found that two proteins (Col2a1 and Laminin) were disrupted (Figs. 2.13 and 2.14).

Type II collagen (Col2a1), which is directly regulated by Sox9 in other contexts, and is highly expressed in the distal lung epithelium at E12.5 (44), was significantly reduced in Sox9^{LOF} lungs compared to control (Fig. 2.13). Immunofluorescence of Col2a1 protein at E12.5 (Fig. 2.13A) and e14.5 (Fig. 2.15) showed a reduction of staining specifically in distal epithelial buds. This was supported by qRT-PCR on whole lungs at E12.5 and E14.5, which demonstrated significant *Col2a1* down regulation at both times in whole Sox9^{LOF} lungs (Fig. 2.13B). To determine if Sox9 is directly binding *Col2a1* regulatory elements in the distal lung epithelium, we performed Sox9 chromatin immunoprecipitation using FACS purified distal lung epithelium from transgenic Sox9-eGFP mice (Fig. 2.15B, C) (45). Using qRT-PCR, we observed that Sox9 was able to

bind to a previously characterized consensus binding site located in intron 1 of the *Col2a1* gene with a ~5-fold higher affinity than an IgG control antibody (Fig 2.10C). In contrast the same Sox9 antibody did not have increased binding to a non-specific region of DNA located near the *Col2a1* intron 1 (negative control in Fig. 2.13C), whereas an antibody to Histone H3 was used as a positive control and bound to both regions of DNA. Collectively, these results are consistent with Sox9 direct regulating of *Col2a1* transcription resulting in proper protein expression

We also observed defects in Laminin deposition in both $Sox9^{LOF}$ and $Sox9^{GOF}$ lungs (Fig. 2.14, Fig. 2.16), however, these effects may be indirect, since we did not detect a transcriptional change in several *Laminin* mRNAs by qRT-PCR (Fig. 2.16). By examining Stage 1 bud tips (Fig. 2.4A) we observed that Laminin is deposited by the epithelium as a fine border along the basal side of the epithelial buds in controls (Fig. 2.4A and Fig. 2.14A,B). In contrast, $Sox9^{LOF}$ lungs have a fragmented border around the distal epithelium with Laminin staining being found within the epithelial cell rather than in the basement membrane (Fig. 2.14, Fig. 2.16, Fig. 2.17). This staining includes large, Laminin positive intercellular punctae observed on the apical and basal surfaces of the cell (Fig. 2.14, Fig. 2.16, Fig. 2.17). In $Sox9^{LOF}$ lungs we found that intercellular Laminin punctae associate with the Golgi marker gm130 and with the Endoplasmic Reticulum (ER) marker KDELR (Fig. 2.16 C,D).

Given the severe cellular disruptions observed by TEM (Fig. 2.10), we also examined the lung epithelial cytoskeleton, which is important during branching morphogenesis (29, 33, 34, 46, 47). We analyzed the cytoskeleton by staining acetylated tubulin (AcTub) and F-actin (Phalloidin) staining (Fig. 2.18, Fig. 2.19).

Phalloidin staining is strongest on the apical surface of the cells, but is also observed along the basal-lateral surfaces and was not different between control and $Sox9^{LOF}$ lungs (Fig. 2.19A). In contrast, we observed a stark reduction in AcTub staining along the basal surface of the epithelial cells in $Sox9^{LOF}$ lungs (Fig. 2.18A). This indicates that stabilized tubulin is disrupted at the basal surfaces of the epithelial cells in $Sox9^{LOF}$. In $Sox9^{GOF}$ lungs the cytoskeletal organization was not perturbed compared to control lungs (Fig. 2.19A-B).

Loss of Sox9 disrupts epithelial movement

Since the ECM and microtubule dynamics are strongly associated with cell movement/migration (13-15, 48, 49), and we observed disrupted ECM and stabilized (acetylated) microtubules in $Sox9^{LOF}$ epithelium along the basal surface of the cells, we wanted to determine if this had an effect on cell movements/migration. As the lung branches, the lung bud grows by coordinating epithelial movement and proliferation (15, 40). Epithelial movement was quantified using an *in vitro* cell migration scratch assay that has previously been used to assay movement in kidney epithelial buds during branching morphogenesis (35, 50); isolated E12.5 $Sox9^{LOF}$ and control epithelial buds were plated *in vitro,* and exhibited delayed scratch closure compared to controls (Fig. 2.18B-C, Fig. 2.19). The control epithelial cells migrated 50.1% (+/- 5.3%, n=8 epithelial buds) of the scratch in 3 hours and 79.2% (+/- 5.8%, n=8) in 6 hours compared to $Sox9^{LOF}$ cells, which only travelled 33.9% (+/- 2.3%, n=16 epithelial buds) in 3 hours and 65.5% (+/-3.7%, n=16) in 6 hours ($p<0.005$, $p<0.01$ respectively) (Fig. 2.18C, Fig.

2.19C). Epithelial buds were stained for ActTub, and similar to lung buds *in vivo,* we observed that stabilized microtubules were disrupted in isolated Sox9^{LOF} buds *in vitro,* whereas control cells showed uniform organization of the microtubules along the wound edge (Fig. 2.18D).

Sox9 expression is not regulated by Wnt/β-Catenin in the lung epithelium.

Since Sox9 is a well-established direct target of β-catenin-dependent Wnt signaling in the intestine (29, 33, 34, 36), and our data shows that the Wnt target gene *Axin2* is higher in distal epithelium than proximal epithelium in control lungs by *in situ* hybridization (Fig. 2.6B), we investigated whether Sox9 is also regulated by Wnt/β-catenin in the developing lung. We generated two Wnt loss-of-fucnction models (β-Catenin^{LOF}: Sox9CreER^{T2};β-Catenin-flox/flox lungs and Lrp5/6^{LOF}: Sox9CreER^{T2};Lrp5/6-flox/flox) (Fig. 2.20) (51, 52). In both β-Catenin^{LOF} and Lrp5/6^{LOF} lungs, Sox9 expression is not lost, but expands into the proximal airway, creating a Sox9+/Sox2+ intermediate population of cells that is not seen in control lungs throughout development (Fig S14). From these results, we conclude that canonical Wnt signaling is not necessary for Sox9 expression in the lung epithelium.

Discussion

In a previous report, deletion of Sox9 in lung epithelium (Sftpc-rtTa;tetO-cre;Sox9-flox/flox) at E12.5 produced no deleterious developmental consequences in

the lung (15). Here, using an earlier and more complete Sox9 deletion (Shh-cre;Sox9-flox/flox) (E9.5), we document an important role for Sox9 in branching morphogenesis. We observe an obvious branching defect as early as E12.5 along with the complete loss of protein by this time, indicating that Sox9 function is important at the beginning of branching. Importantly, Perl et al. also reported that Sox4 and Sox11 are present and unchanged in Sox9 mutant lung epithelium at E12.5 and E13.5, suggesting that loss of Sox9 on or after E12.5 may be compensated for by other Sox genes. The strategy that we take here and the phenotypes that develop may be highly relevant to the congenital birth defects in CD/ACD, making this an applicable mouse model for the further investigation of those devastating human conditions.

Many signaling pathways and transcription factors are essential for branching morphogenesis. In many cases, when these factors and pathways are perturbed, the consequence is a cystic phenotype, similar to the phenotype seen in both $Sox9^{LOF}$and $Sox9^{GOF}$ lung (7, 10, 14, 53-59). The fact that both gain and loss of Sox9 resulted in a similar phenotype is likely reflected in the small number of possible outcomes when branching morphogenesis is perturbed; that is, if an epithelial bud cannot properly bifurcate, it give rise to a larger, cystic sac. We also observed that the E14.5 $Sox9^{GOF}$ cystic phenotype was not present at E18.5 in $Sox9^{GOF}$ lungs (Fig. 2.2E-F). This change in phenotype at E18.5 could be explained by the smaller numbers of cells expressing ectopic Sox9 at this time, likely due to the fact that cells expressing high levels of ectopic Sox9 had reduced proliferation and a selective disadvantage over developmental time (Fig. 2.4 H-J, Fig. 2.7, Fig. 2.8). It is highly possible that cells

expressing ectopic Sox9 were outcompeted by normal cells leading to a partial resolution of the phenotype.

Sox9 influences ECM and cell movement

In addition to proliferation and differentiation, we investigated if the cystic phenotype resulting from Sox9 perturbations may be due to abnormal cellular consequences. Many studies have shown that Sox9 plays critical roles in both ECM deposition and cell migration in various tissues and diseases (18). In the heart, Sox9 is required for proper organization the valvular ECM proteins (60), while in the gonads, Sox9 regulates many ECM proteins as well as modifiers of the ECM such as matrix metaloproteinases (61, 62). Sox9 also plays a role in many fibrotic and sclerotic disorders in various tissues, in which Sox9 causes excessive and inappropriate ECM deposition by activating various ECM proteins (63-68). Furthermore, Sox9 plays a critical role during chondrogenesis (30), and ChiP analysis in chondrocytes has shown that Sox9 directly binds to loci of 18 different ECM genes, including *Col2a1* (69). Our results support Sox9 as a regulator of ECM in the lung as well, demonstrating that it can transcriptionally regulate *Col2a1* and lead abnormal protein deposition in the basal lamina. We also observed defects in Laminin deposition with loss or gain of Sox9 in the branching lung, however this seems to be an indirect effect of Sox9 perturbations since we did not observe transcriptional changes in Laminin genes. These results also highlight that some of the cellular defects observed in the $Sox9^{LOF}$ or $Sox9^{GOF}$ phenotype may be indirect. Elucidating additional detail as to how perturbations in Sox9

directly and indirectly affect lung epithelial cell morphology and behavior will be an active area of future investigation.

In many contexts the ECM has a dynamic role associating with and influencing reorganizing the cytoskeleton (70, 71). For example, Laminin-integrin based cell adhesion functions to anchor stabilized microtubule “plus-ends” and maintain the proper microtubule density on the basal surface of epithelial cells (72). Therefore, our results demonstrating disruption of the stabilized microtubule network on the basal side of the lung epithelium in $Sox9^{LOF}$ lungs, and the disorganized microtubule network observed in $Sox9^{LOF}$ distal epithelial cells in the *in vitro* migration assay may be explained by perturbations in the ECM. Although the link between Sox9 and cell migration/microtubule organization may be indirect, in other systems Sox9 is critical for cell migration including neural crest cells during development (73) and tumor metastasis in breast, colon, prostate, and melanoma cancers (74-77). In future studies, it will be pertinent to determine how Sox9 is mechanistically regulating acetylated tubulin and epithelial cell movement during lung branching morphogenesis.

β-catenin dependent Wnt signaling and Sox9

Sox9 contributes to diverse range of functions in several endodermally derived organs, including the pancreas, lung and intestine (26, 27, 78, 79). Wnt signaling is critical for the development of these organ systems, and it has been shown in the developing intestine that Sox9 is a direct target of Wnt signaling (29, 33, 34). Here, we find that in contrast to the lung, Sox9 transcription is not regulated by Wnt/β-catenin

signaling. It will be interesting to determine how these context dependent differences for Sox9 within endodermal lineages are established.

Taken together, our results have established a novel role for Sox9 during lung branching morphogenesis. We have demonstrated that Sox9 is a multi-faceted transcription factor that directly and indirectly regulates proliferation, differentiation, the ECM, cytoskeletal organization, cell shape and cellular movement.

Materials and Methods

Mouse strains

All mice used in these studies were housed at the University of Michigan mouse facility, and were maintained according to institutional protocols. *Shh-Cre, Sox9CreER, Sox9^{Flox}, β-Catenin^{Flox}, Rosa-rtTa, SftpC-rtTa, Lrp5/6^{Flox}, Sox9-eGFP* mice have all been previously described (35, 36, 45, 80-82). Description of the Rosa26-tetO-Sox9 mice is currently under review elsewhere (Philip A. Seymour, Hung Ping Shih, Richard Behringer, Mark Magnuson, and Maike Sander). Briefly, the pTight tetracycline responsive (tetO) promoter driving bi-directional expression of Sox9 and mCherry was targeted to the Rosa26 locus. An active tetracycline transactivator protein (tTa or rtTa) causes transcription of both alleles to be driven independently from the same promoter.

Doxycycline and Tamoxifen administration.

Doxycycline was administered in the drinking water at (2mg/mL) supplemented with 2.5 mg/mL of sucrose started at E9.5 until the time of harvest. Tamoxifen (50 ug/g) was dissolved in corn oil and given via oral gavage once a day for two consecutive days, E11.5 and E12.5.

Lung Explant Cultures

Lung explant cultures were performed *in vitro* as previously described (83). E12.5 lungs were cultured on Nucleopore polycarbonate track-etch membranes for up to 72 hours at 37°C in a 5% CO_2 incubator. Images of explants were taken on a Leica M125 stereomicroscope. Branches were counted manually.

Migration Scratch Assay

Isolation of epithelial buds from the surrounding mesenchyme of E12.5 lungs was previously described (50). Briefly, lung epithelial buds were placed on BD Matrigel hESC-qualified matrix (BD Biosciences) coated plates with DMEM/F-12 supplemented with 50 units/mL of penicillin-streptomycin and 0.1% Fetal bovine serum (Gibco). Epithelial buds grew into colonies by 48 hours at 37°C in a 5% CO_2 incubator. Lung bud cultures were scratched with a micropipette tip and images were taken on an Olympus SZX16 microscope at 0, 3, and 6 hours post scratch. Scratch width was measured with ImageJ software.

Immunohistochemistry and in situ hybridization

Immunostaining was carried out as previously described (84, 85). Antibody information and dilutions can be found in Table 2.1. All immunofluorescence images were taken on a Nikon A1 confocal microscope. All DAB images were taken on an Olympus IX71 microscope. For section *in situ* hybridization, embryos were collected in PBS and fixed overnight in 4% paraformaldehyde in PBS (PFA) at 4°C. Embryos were then rinsed in PBS and immersed in 30% sucrose at 4°C overnight prior to embedding into OCT media. 12 to 16 µm frozen sections were cut and slides were stored at −80°C. *In situ* hybridization (ISH) was performed as previously described(86, 87). *Axin2, Bmp4*and *Shh in situ* probes were previously described (88-90).

qRT-PCR

RNA was extracted from E12.5 or E14.5 lungs using Purelink RNA Mini Kit (Life Technologies). RNA quantity and quality were determined spectrophotometrically using a Nano Drop 2000 (Thermoscientific). Reverse transcription was conducted using the SuperScript VILO kit (Invitrogen) according to manufacturer's protocol. Finally, qRT-PCR was carried out using Quantitect Sybr Green MasterMix (Qiagen) on a Step One Plus Real-Time PCR system (Life Technologies). For a list of primer sequences see Table 2.2.

Proliferation Quantification

Quantification of BrdU positive cells that co-localized with E-Cadherin, Sox2, Dapi was counted with Metamorph cell counting software.

Transmission electron microscopy

E14.5 lungs were processed as previously described (91). 70 nm sections were imaged using a Philips CM-100 electron microscope.

Fluorescence-activated cell sorting (FACS)

E14.5 Sox9-eGFP and control lungs were minced and resuspended in 2mg/mL Collagenase D (Roche) and 40 units TURBO DNase (Life Technologies) for 2 mins. This was then repeated with 2x TrypLE SELECT (Life Technologies) and DNase for 5 mins at 37°C. The cells were gravity filtered through a 70 micron filter. Both Sox9-eGFP and control cells were sorted (Fig. 2.13)

Chromatin immunoprecipitation assay

Sox9-eGFP positive FACS sorted distal lung progenitor cells were fixed with 1% formaldehyde for 10 mins. The reaction was quenched with glycine and washed in 1x PBS. The Cell Signaling SimpleChIP® Enzymatic ChIP Kit was used as described by the manufacturer, with the following modification: MNase was not used, rather, nuclei

were sonicated (Branson Sonifier 250) 10x for 30 sec bursts at 25% duty, output 3.5 with 1 min on ice in between bursts.

Cell Length Quantification

Height of cells was measured from the apical to basal surface of the cell indicated by E-Cad stain. Cell height was measured using ImageJ software.

Statistical Analysis

All data are shown as the mean of at least 3 independent biological replicates and error bars represent SEM. Statistical differences between experimental and control groups were assessed with Prism software using multiple t-tests. Results were considered statistically significant at $p<0.05$.

Acknowledgements

Dr. Bart O. Williams for kindly providing the Lrp5 and Lrp6 floxed mice. This work was supported in part by the following: Bradley M. Patten Student Fellowship to BER; MICHR PTSP fellowship and an NIH training fellowship (T32 HL 7749-20) to SMH; University of Michigan Department of Internal Medicine, Biological Sciences Scholars Program (BSSP), Center for Organogenesis and March of Dimes Basil O'Connor Research Award to JRS and by the NHLBI (R01-HL119215) to JRS and DMW.

References

1. Domyan ET, Sun X (2010) Patterning and plasticity in development of the respiratory lineage. *Dev Dyn* 240:477–485.

2. Morrisey EE, Hogan BLM (2010) Preparing for the First Breath: Genetic and Cellular Mechanisms in Lung Development. *Dev Cell* 18:8–23.

3. Metzger RJ, Klein OD, Martin GR, Krasnow MA (2008) The branching programme of mouse lung development. *Nature* 453:745–750.

4. Rawlins EL (2010) The building blocks of mammalian lung development. *Dev Dyn* 240:463–476.

5. Warburton D et al. (2005) Molecular mechanisms of early lung specification and branching morphogenesis. *Pediatr Res* 57:26R–37R.

6. Yates LL et al. (2013) Scribble is required for normal epithelial cell-cell contacts and lumen morphogenesis in the mammalian lung. *Developmental Biology* 373:267–280.

7. Wan H et al. (2013) CDC42 is required for structural patterning of the lung during development. *Developmental Biology* 374:46–57.

8. Nechiporuk T, Klezovitch O, Nguyen L, Vasioukhin V (2013) Dlg5 maintains apical aPKC and regulates progenitor differentiation during lung morphogenesis. *Developmental Biology* 377:375–384.

9. Yates LL, Dean CH (2011) Planar polarity: a new player in both lung development and disease. *organogenesis* 7:209–216.

10. Yates LL et al. (2010) The PCP genes Celsr1 and Vangl2 are required for normal lung branching morphogenesis. *Human Molecular Genetics* 19:2251–2267.

11. Tian Y et al. (2011) Regulation of lung endoderm progenitor cell behavior by miR302/367. *Development* 138:1235–1245.

12. Perl A-KT, Wert SE, Nagy A, Lobe CG, Whitsett JA (2002) Early restriction of peripheral and proximal cell lineages during formation of the lung. *Proc Natl Acad Sci USA* 99:10482–10487.

13. Rawlins EL, Clark CP, Xue Y, Hogan BLM (2009) The Id2+ distal tip lung

epithelium contains individual multipotent embryonic progenitor cells. *Development* 136:3741–3745.

14. Okubo T (2005) Nmyc plays an essential role during lung development as a dosage-sensitive regulator of progenitor cell proliferation and differentiation. *Development* 132:1363–1374.

15. Perl A-KT, Kist R, Shan Z, Scherer G, Whitsett JA (2005) Normal lung development and function afterSox9 inactivation in the respiratory epithelium. *genesis* 41:23–32.

16. Herriges JC et al. (2012) Genome-scale study of transcription factor expression in the branching mouse lung. *Dev Dyn* 241:1432–1453.

17. Rawlins EL, Ostrowski LE, Randell SH, Hogan BLM (2007) Lung development and repair: contribution of the ciliated lineage. *Proc Natl Acad Sci USA* 104:410–417.

18. Pritchett J, Athwal V, Roberts N, Hanley NA, Hanley KP (2011) Understanding the role of SOX9 in acquired diseases: lessons from development. *Trends Mol Med* 17:166–174.

19. Jakobsen LP et al. (2007) Pierre Robin sequence may be caused by dysregulation of SOX9 and KCNJ2. *J Med Genet* 44:381–386.

20. Herman TE, Siegel MJ (2012) Acampomelic campomelic dysplasia in genetic male without sex reversal. *J Perinatol* 32:75–77.

21. Mansour S, Hall CM, Pembrey ME, Young ID (1995) A clinical and genetic study of campomelic dysplasia. *J Med Genet* 32:415–420.

22. Kwok C et al. (1995) Mutations in SOX9, the gene responsible for Campomelic dysplasia and autosomal sex reversal. *American Journal of Human Genetics* 57:1028–1036.

23. Sock E et al. (2003) Loss of DNA-dependent dimerization of the transcription factor SOX9 as a cause for campomelic dysplasia. *Human Molecular Genetics* 12:1439–1447.

24. Shinwell ES, Hengerer AS, Kendig JW (1988) A third case of bronchoscopic diagnosis of tracheobronchomalacia in campomelic dysplasia. *Pediatr Pulmonol* 4:192.

25. Houston CS et al. (1983) The campomelic syndrome: review, report of 17 cases, and follow-up on the currently 17-year-old boy first reported by Maroteaux et al in 1971. *Am J Med Genet* 15:3–28.

26. Seymour PA et al. (2008) A dosage-dependent requirement for Sox9 in pancreatic endocrine cell formation. *Developmental Biology* 323:19–30.

27. Seymour PA et al. (2007) From the Cover: SOX9 is required for maintenance of the pancreatic progenitor cell pool. *Proceedings of the National Academy of Sciences* 104:1865–1870.

28. Lynn FC et al. (2007) Sox9 coordinates a transcriptional network in pancreatic progenitor cells. *Proc Natl Acad Sci USA* 104:10500–10505.

29. Mori Akiyama Y et al. (2007) SOX9 is required for the differentiation of paneth cells in the intestinal epithelium. *YGAST* 133:539–546.

30. Akiyama H (2008) Control of chondrogenesis by the transcription factor Sox9. *Mod Rheumatol* 18:213–219.

31. Lefebvre V, Dumitriu B, Penzo-Méndez A, Han Y, Pallavi B (2007) Control of cell fate and differentiation by Sry-related high-mobility-group box (Sox) transcription factors. *Int J Biochem Cell Biol* 39:2195–2214.

32. Liu C-J et al. (2007) Transcriptional activation of cartilage oligomeric matrix protein by Sox9, Sox5, and Sox6 transcription factors and CBP/p300 coactivators. *Front Biosci* 12:3899–3910.

33. Bastide P et al. (2007) Sox9 regulates cell proliferation and is required for Paneth cell differentiation in the intestinal epithelium. *J Cell Biol* 178:635–648.

34. Blache P et al. (2004) SOX9 is an intestine crypt transcription factor, is regulated by the Wnt pathway, and represses the CDX2 and MUC2 genes. *J Cell Biol* 166:37–47.

35. Kist R, Schrewe H, Balling R, Scherer G (2002) Conditional inactivation of Sox9: a mouse model for campomelic dysplasia. *genesis* 32:121–123.

36. Harfe BD et al. (2004) Evidence for an expansion-based temporal Shh gradient in specifying vertebrate digit identities. *Cell* 118:517–528.

37. Harris KS, Zhang Z, McManus MT, Harfe BD, Sun X (2006) Dicer function is essential for lung epithelium morphogenesis. *Proc Natl Acad Sci USA* 103:2208–

2213.

38. Schnatwinkel C, Niswander L (2013) Multiparametric image analysis of lung-branching morphogenesis. *Dev Dyn* 242:622–637.

39. Weaver M, Batts L, Hogan BLM (2003) Tissue interactions pattern the mesenchyme of the embryonic mouse lung. *Developmental Biology* 258:169–184.

40. Weaver M, Dunn NR, Hogan BL (2000) Bmp4 and Fgf10 play opposing roles during lung bud morphogenesis. *Development* 127:2695–2704.

41. Barkauskas CE et al. (2013) Type 2 alveolar cells are stem cells in adult lung. *J Clin Invest* 123:3025–3036.

42. Weaver TE, Whitsett JA (1989) Processing of hydrophobic pulmonary surfactant protein B in rat type II cells. *Am J Physiol* 257:L100–8.

43. Glasser SW et al. (1987) cDNA and deduced amino acid sequence of human pulmonary surfactant-associated proteolipid SPL(Phe). *Proc Natl Acad Sci USA* 84:4007–4011.

44. Elluru RG, Whitsett JA (2004) Potential role of Sox9 in patterning tracheal cartilage ring formation in an embryonic mouse model. *Arch Otolaryngol Head Neck Surg* 130:732–736.

45. Gong S et al. (2003) A gene expression atlas of the central nervous system based on bacterial artificial chromosomes. *Nature* 425:917–925.

46. Moore KA et al. (2005) Control of basement membrane remodeling and epithelial branching morphogenesis in embryonic lung by Rho and cytoskeletal tension. *Dev Dyn* 232:268–281.

47. Moore KA, Huang S, Kong Y, Sunday ME, Ingber DE (2002) Control of embryonic lung branching morphogenesis by the Rho activator, cytotoxic necrotizing factor 1. *Journal of Surgical Research* 104:95–100.

48. Ganguly A, Yang H, Sharma R, Patel KD, Cabral F (2012) The role of microtubules and their dynamics in cell migration. *J Biol Chem* 287:43359–43369.

49. Ridley AJ et al. (2003) Cell migration: integrating signals from front to back. *Science* 302:1704–1709.

50. Kuure S et al. (2010) Actin depolymerizing factors cofilin1 and destrin are required for ureteric bud branching morphogenesis. *PLoS Genet* 6:e1001176.

51. Zhong Z, Baker JJ, Zylstra-Diegel CR, Williams BO (2012) Lrp5 and Lrp6 play compensatory roles in mouse intestinal development. *J Cell Biochem* 113:31–38.

52. Joeng KS, Schumacher CA, Zylstra-Diegel CR, Long F, Williams BO (2011) Lrp5 and Lrp6 redundantly control skeletal development in the mouse embryo. *Developmental Biology* 359:222–229.

53. Metzger DE, Stahlman MT, Shannon JM (2008) Misexpression of ELF5 disrupts lung branching and inhibits epithelial differentiation. *Developmental Biology* 320:149–160.

54. Yin Y, Wang F, Ornitz DM (2011) Mesothelial- and epithelial-derived FGF9 have distinct functions in the regulation of lung development. *Development* 138:3169–3177.

55. Rajagopal J et al. (2008) Wnt7b stimulates embryonic lung growth by coordinately increasing the replication of epithelium and mesenchyme. *Development* 135:1625–1634.

56. Goss AM et al. (2009) Wnt2/2b and β-Catenin Signaling Are Necessary and Sufficient to Specify Lung Progenitors in the Foregut. *Dev Cell* 17:290–298.

57. Schnatwinkel C, Niswander L (2012) Nubp1 Is Required for Lung Branching Morphogenesis and Distal Progenitor Cell Survival in Mice. *PLoS ONE* 7:e44871.

58. Abler LL, Mansour SL, Sun X (2009) Conditional gene inactivation reveals roles for Fgf10and Fgfr2in establishing a normal pattern of epithelial branching in the mouse lung. *Dev Dyn* 238:1999–2013.

59. El-Hashash AHK et al. (2011) Six1 transcription factor is critical for coordination of epithelial, mesenchymal and vascular morphogenesis in the mammalian lung. *Developmental Biology* 353:242–258.

60. Lincoln J, Kist R, Scherer G, Yutzey KE (2007) Sox9 is required for precursor cell expansion and extracellular matrix organization during mouse heart valve development. *Developmental Biology* 305:120–132.

61. Georg I, Barrionuevo F, Wiech T, Scherer G (2012) Sox9 and Sox8 are required for basal lamina integrity of testis cords and for suppression of FOXL2 during embryonic testis development in mice. *Biol Reprod* 87:99.

62. Nakamura S et al. (2012) Analysis of medaka sox9 orthologue reveals a conserved role in germ cell maintenance. *PLoS ONE* 7:e29982.

63. Naitoh M et al. (2005) Gene expression in human keloids is altered from dermal to chondrocytic and osteogenic lineage. *Genes Cells* 10:1081–1091.

64. Hanley KP et al. (2008) Ectopic SOX9 mediates extracellular matrix deposition characteristic of organ fibrosis. *J Biol Chem* 283:14063–14071.

65. Bennett MR et al. (2007) Laser capture microdissection-microarray analysis of focal segmental glomerulosclerosis glomeruli. *Nephron Exp Nephrol* 107:e30–40.

66. Sumi E et al. (2007) SRY-related HMG box 9 regulates the expression of Col4a2 through transactivating its enhancer element in mesangial cells. *AJPA* 170:1854–1864.

67. Airik R et al. (2010) Hydroureternephrosis due to loss of Sox9-regulated smooth muscle cell differentiation of the ureteric mesenchyme. *Human Molecular Genetics* 19:4918–4929.

68. Schulick AH et al. Overexpression of transforming growth factor β1 in arterial endothelium causes hyperplasia, apoptosis, and cartilaginous metaplasia.

69. Oh C-D et al. (2010) Identification of SOX9 Interaction Sites in the Genome of Chondrocytes. *PLoS ONE* 5:e10113.

70. Hay ED (1982) Interaction of embryonic surface and cytoskeleton with extracellular matrix. *Am J Anat* 165:1–12.

71. Nishizaka T, Shi Q, Sheetz MP (2000) Position-dependent linkages of fibronectin-integrin-cytoskeleton. *Proc Natl Acad Sci USA* 97:692–697.

72. Hotta A et al. (2010) Laminin-based cell adhesion anchors microtubule plus ends to the epithelial cell basal cortex through LL5alpha/beta. *J Cell Biol* 189:901–917.

73. Betters E, Liu Y, Kjaeldgaard A, Sundström E, García-Castro MI (2010) Analysis of early human neural crest development. *Developmental Biology* 344:578–592.

74. Chakravarty G et al. (2011) Prognostic significance of cytoplasmic SOX9 in invasive ductal carcinoma and metastatic breast cancer. *Exp Biol Med (Maywood)* 236:145–155.

75. Bowen KA et al. (2009) PTEN loss induces epithelial--mesenchymal transition in human colon cancer cells. *Anticancer Res* 29:4439–4449.

76. Wang H et al. (2008) SOX9 is expressed in human fetal prostate epithelium and enhances prostate cancer invasion. *Cancer Research* 68:1625–1630.

77. Rao P, Fuller GN, Prieto VG (2010) Expression of Sox-9 in metastatic melanoma--a potential diagnostic pitfall. *Am J Dermatopathol* 32:262–266.

78. Seymour PA et al. (2012) A Sox9/Fgf feed-forward loop maintains pancreatic organ identity. *Development* 139:3363–3372.

79. Furuyama K et al. (2011) Continuous cell supply from a Sox9-expressing progenitor zone in adult liver, exocrine pancreas and intestine. *Nat Genet* 43:34–41.

80. Kopp JL et al. (2011) Sox9+ ductal cells are multipotent progenitors throughout development but do not produce new endocrine cells in the normal or injured adult pancreas. *Development* 138:653–665.

81. Brault V et al. (2001) Inactivation of the beta-catenin gene by Wnt1-Cre-mediated deletion results in dramatic brain malformation and failure of craniofacial development. *Development* 128:1253–1264.

82. Belteki G et al. (2005) Conditional and inducible transgene expression in mice through the combinatorial use of Cre-mediated recombination and tetracycline induction. *Nucleic Acids Research* 33:e51.

83. Del Moral P-M, Warburton D (2010) Explant culture of mouse embryonic whole lung, isolated epithelium, or mesenchyme under chemically defined conditions as a system to evaluate the molecular mechanism of branching morphogenesis and cellular differentiation. *Methods Mol Biol* 633:71–79.

84. Spence JR et al. (2011) Directed differentiation of human pluripotent stem cells into intestinal tissue in vitro. *Nature* 470:105–109.

85. Spence JR et al. (2009) Sox17 regulates organ lineage segregation of ventral foregut progenitor cells. *Dev Cell* 17:62–74.

86. Di Giacomo G et al. (2006) Spatio-temporal expression of Pbx3 during mouse organogenesis. *Gene Expr Patterns* 6:747–757.

87. Mendelsohn C, Batourina E, Fung S, Gilbert T, Dodd J (1999) Stromal cells mediate retinoid-dependent functions essential for renal development. *Development* 126:1139–1148.

88. Jones CM, Lyons KM, Hogan BL (1991) Involvement of Bone Morphogenetic Protein-4 (BMP-4) and Vgr-1 in morphogenesis and neurogenesis in the mouse. *Development* 111:531–542.

89. Li X et al. (2009) Dynamic patterning at the pylorus: formation of an epithelial intestine-stomach boundary in late fetal life. *Dev Dyn* 238:3205–3217.

90. Echelard Y et al. (1993) Sonic hedgehog, a member of a family of putative signaling molecules, is implicated in the regulation of CNS polarity. *Cell* 75:1417–1430.

91. Prasov L, Nagy M, Rudolph DD, Glaser T (2012) Math5 (Atoh7) gene dosage limits retinal ganglion cell genesis. *Neuroreport* 23:631–634.

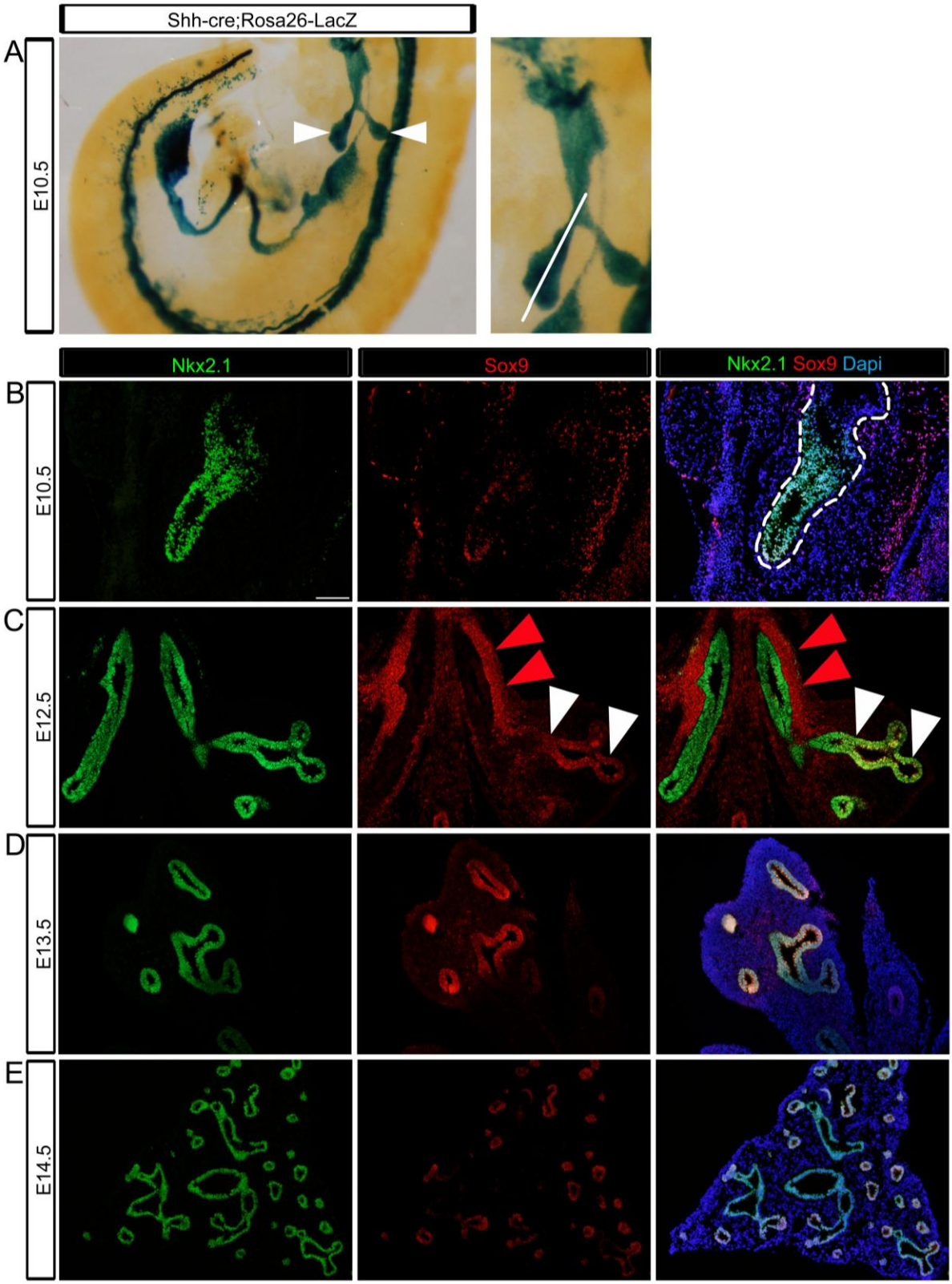
Shh-cre;Rosa26-LacZ
A
E10.5
Nkx2.1
Sox9
Nkx2.1 Sox9 Dapi
B
E10.5
C
E12.5
D
E13.5
E
E14.5

Figure 2.1. Sox9 expression through lung development. (A) Shh-cre expression at E10.5 using a LacZ reporter. White arrowheads indicate the lung buds. White line through the lung bud represents the cross section of the lung bud in (B). (B-D) At all time points Nkx2.1 (green) marks total lung epithelium, Sox9 (red) is expressed in the distal epithelium (white arrowheads in C) and proximal mesenchyme (red arrowheads in C). Dapi (blue) marks total nuclei. Scale bars in B-D represent 100 μm.

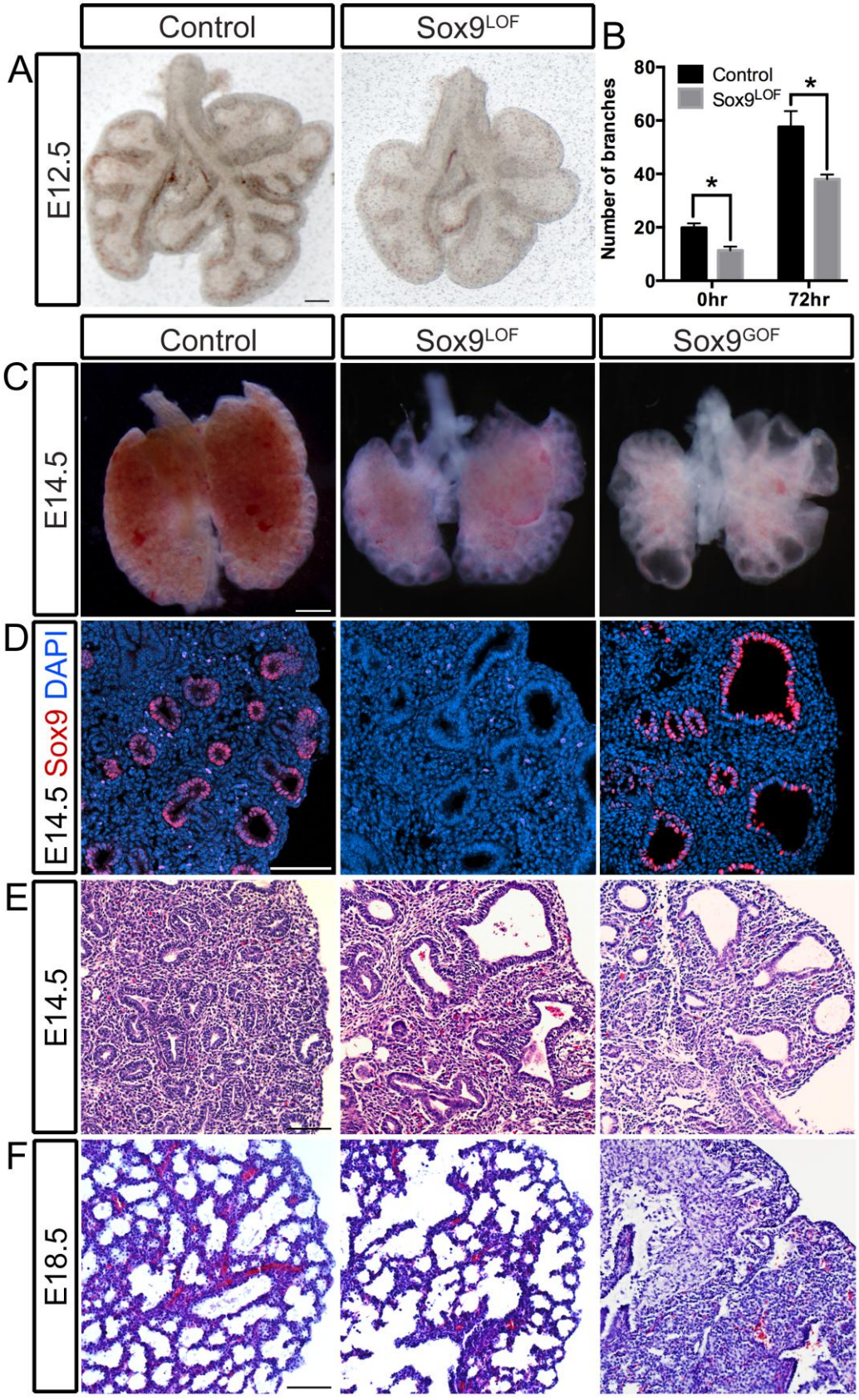
Control
Sox9LOF
A
E12.5
B
Number of branches
Control
Sox9LOF
80
60
40
20
0
*
*
0hr
72hr
Control
Sox9LOF
Sox9GOF
C
E14.5
D
E14.5 Sox9 DAPI
E
E14.5
F
E18.5

Figure 2.2. Sox9 is critical for proper branching morphogenesis. (A) Whole mount images of control and $Sox9^{LOF}$ lungs demonstrate that loss of Sox9 results in fewer domain branches with terminal cystic structures. (B) The number of branches were quantified on E12.5 explant lung cultures immediately after dissection (0 hours (hr)) and after 72hr in culture. $Sox9^{LOF}$ lungs had significantly fewer branches at both time points. (C) Whole mount lungs from E14.5 $Sox9^{LOF}$ and $Sox9^{GOF}$ embryos had cystic structures at the distal epithelial tips rather than smaller bifurcations seen in the control lungs. (D) Sox9 expression (red) in control, $Sox9^{LOF}$ and $Sox9^{GOF}$ lungs at E14.5. Control lungs had Sox9 expression in the distal epithelial tips. Epithelial Sox9 protein was undetectable in $Sox9^{LOF}$ lungs. $Sox9^{GOF}$ lungs demonstrated robust Sox9 expression in the distal epithelium and ectopic Sox9 expression in the proximal airways. (E) H&E staining on sections of E14.5 control, $Sox9^{LOF}$ and $Sox9^{GOF}$ lungs. Staining showed fewer large cystic buds rather than numerous small buds seen in control lungs. (F) H&E staining at E18.5 demonstrate that epithelial cysts led to larger airspaces in $Sox9^{LOF}$ lungs compared to controls. Cystic buds in $Sox9^{GOF}$ lungs appear to have collapsed by E18.5. Scale bars in A and C represent 200 μm, D-F represent 100 μm.* indicates $p<0.05$ and error bars represent SEM.

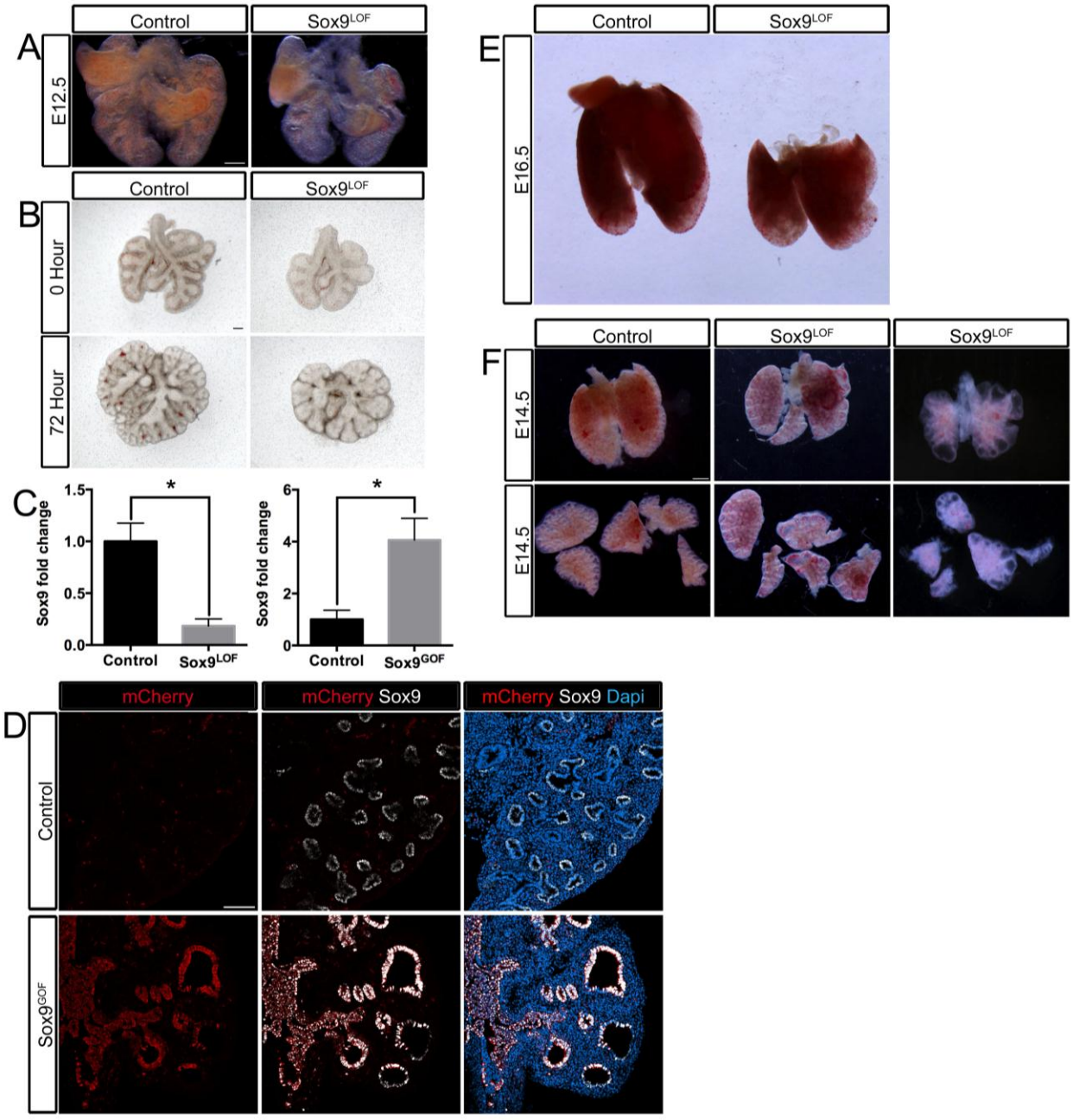

Figure 2.3. Sox9 is critical for branching morphogenesis. (A) Whole mount images of control and Sox9^{LOF} lungs demonstrate that loss of Sox9 results in fewer domain branches with terminal cystic structures at E12.5. (B) E12.5 lung explant cultures were grown *in vitro* for up to 72 hr. Sox9^{LOF} lungs at 0hr and 72hr had fewer branches with terminal cystic structures compared to control explants.(C) Sox9 transcript levels, measured by qRT-PCR in whole E14.5 lungs. Sox9 was significantly down regulated in Sox9^{LOF} lungs and significantly up regulated in Sox9^{GOF} lungs compared to control lung Sox9 transcript. (D) In E14.5 control lungs, Sox9 (white) protein expression is only observed in the distal lung epithelium. E14.5 Sox9^{GOF} lungs (Shh-cre;Rosa26-rtTa;tetO-

Sox9-mCherry +Doxycycline (Sox9 ON) at E9.5) had transgenic Sox9 expression, marked by mCherry (red) throughout the proximal and distal epithelium. mCherry expression correlated with Sox9 (white) protein expression. Control lungs had no mCherry expression. (E) Whole mount image of control and $Sox9^{LOF}$ lung demonstrated a size difference at E16.5.(F) Whole mount lungs from E14.5 $Sox9^{LOF}$ and $Sox9^{GOF}$ embryos had terminal cystic structures, but had same number of lobes compared to control lungs. Scale bars in A-B,F represent 200 µm and in D represent 100 µm.* indicates $p<0.05$ and error bars represent SEM.

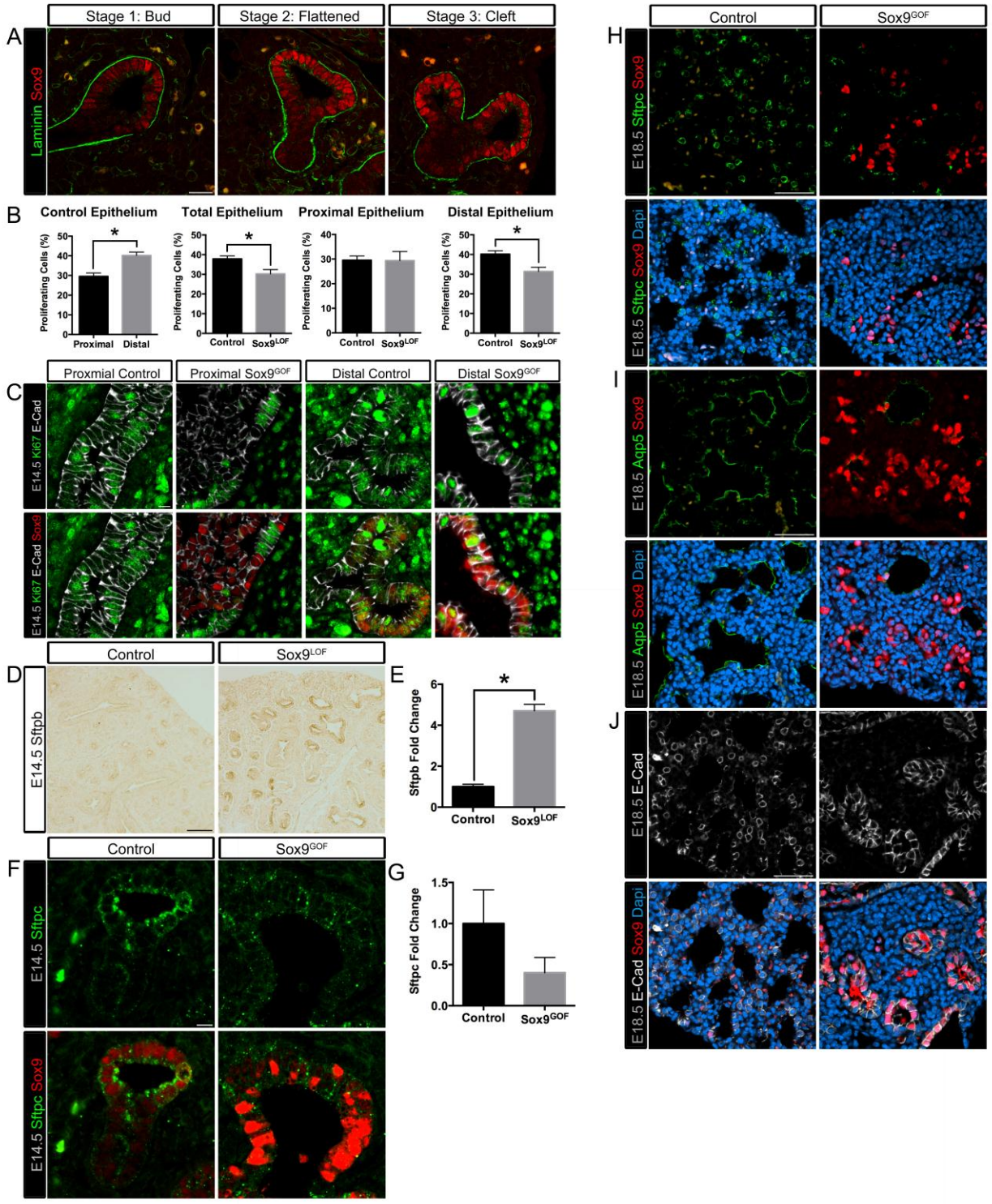

Figure 2.4. Sox9 is required for proper proliferation and differentiation of the lung epithelium during branching morphogenesis. (A) Sox9 is dynamically expressed during branch bifurcation. Sox9 (red) is expressed highest at the budding tip in Stage 1 and the newly formed budding tips in Stage 2 and 3. Sox9 expression dissipates toward

the parent branch in all three stages and the cleft in Stage 3. Laminin staining (green) is less robust at the budding tip and most stable at the parent branch and cleft. (B) Proliferation in control and $Sox9^{LOF}$ lung epithelium at E14.5 was assessed by BrdU incorporation. In control epithelium, proliferation is significantly higher in distal compared to proximal epithelium ("Control Epithelium"). There is significantly less proliferation in total $Sox9^{LOF}$ epithelium compared to controls ("Total Epithelium"). Comparing proliferation in proximal or distal epithelium of controls versus $Sox9^{LOF}$ lung epithelium demonstrated that proximal proliferation did not change ("Proximal Epithelium") whereas a significant reduction in distal epithelial proliferation was seen in $Sox9^{LOF}$ lungs ("Distal Epithelium"). (C) Proliferation in control and $Sox9^{GOF}$ lung epithelium at E14.5 was assessed by Ki67 staining. Compared to controls, a dramatic decrease in Ki67 staining (green) was seen in both proximal and distal epithelium (E-cad, white) of $Sox9^{GOF}$ lungs, specifically in cells overexpressing Sox9. (D-E) Sox9 inhibits differentiation. Sftpb protein is below detection using immunostaining in control epithelium at E14.5, but was readily detected in $Sox9^{LOF}$ lungs E14.5. qRT-PCR confirmed a greater than 4-fold increase in Sftpb mRNA in $Sox9^{LOF}$ lungs compared to controls at E14.5. (F-G) In E18.5 $Sox9^{GOF}$ lungs, ectopic Sox9 (red) leads to a reduction in Sftpc staining (H, green) and Aqp5 (I, green) staining. (H) E-Cad staining (white) revealed that distal $Sox9^{GOF}$ epithelium (red) fails to undergo the columnar-to-squamous epithelial transition seen in lower airways of control lungs. Scale bars in A represent 20 µm, C and F represent 10 µm, D represent 100 µm, H-J represent 50 µm. * indicates $p<0.01$ and error bars represent SEM. Scale bars in A-B represent 200 µm, D,F represent 100 µm.

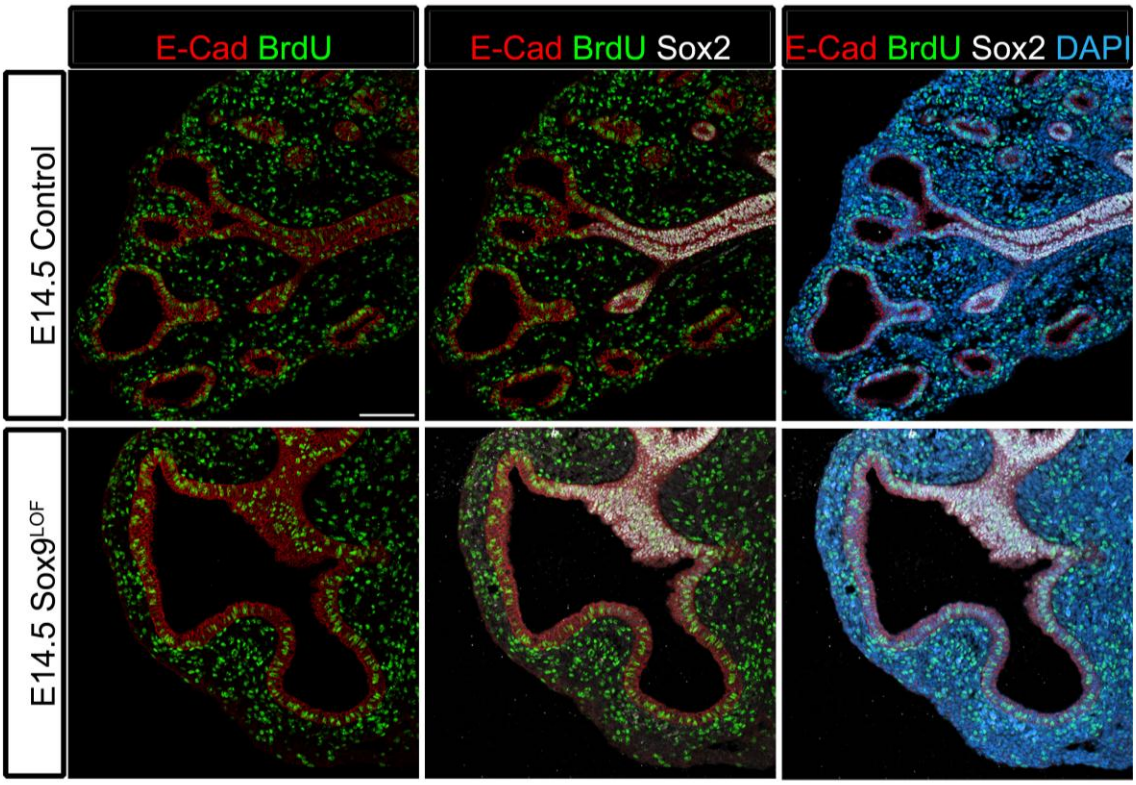

Figure 2.5. Effect of loss and gain of Sox9 on proliferation. BrdU (green) was injected into timed pregnant females 30 minutes prior to embryo harvest. BrdU staining (green) marks proliferating cells, Sox2 (white) labels the proximal epithelium and E-Cad (red) labels the total epithelium. For quantitation, Ecad+/Sox2+ cells were considered proximal epithelium and Ecad+/Sox2- cells were considered distal epithelium. At E14.5 $Sox9^{LOF}$ lungs had less distal epithelial proliferation than control lungs (See quantitation in Fig 2B). Control and $Sox9^{LOF}$ lungs had the same levels of proliferation in the proximal epithelium and mesenchyme.Scale bar represents 100 µm.

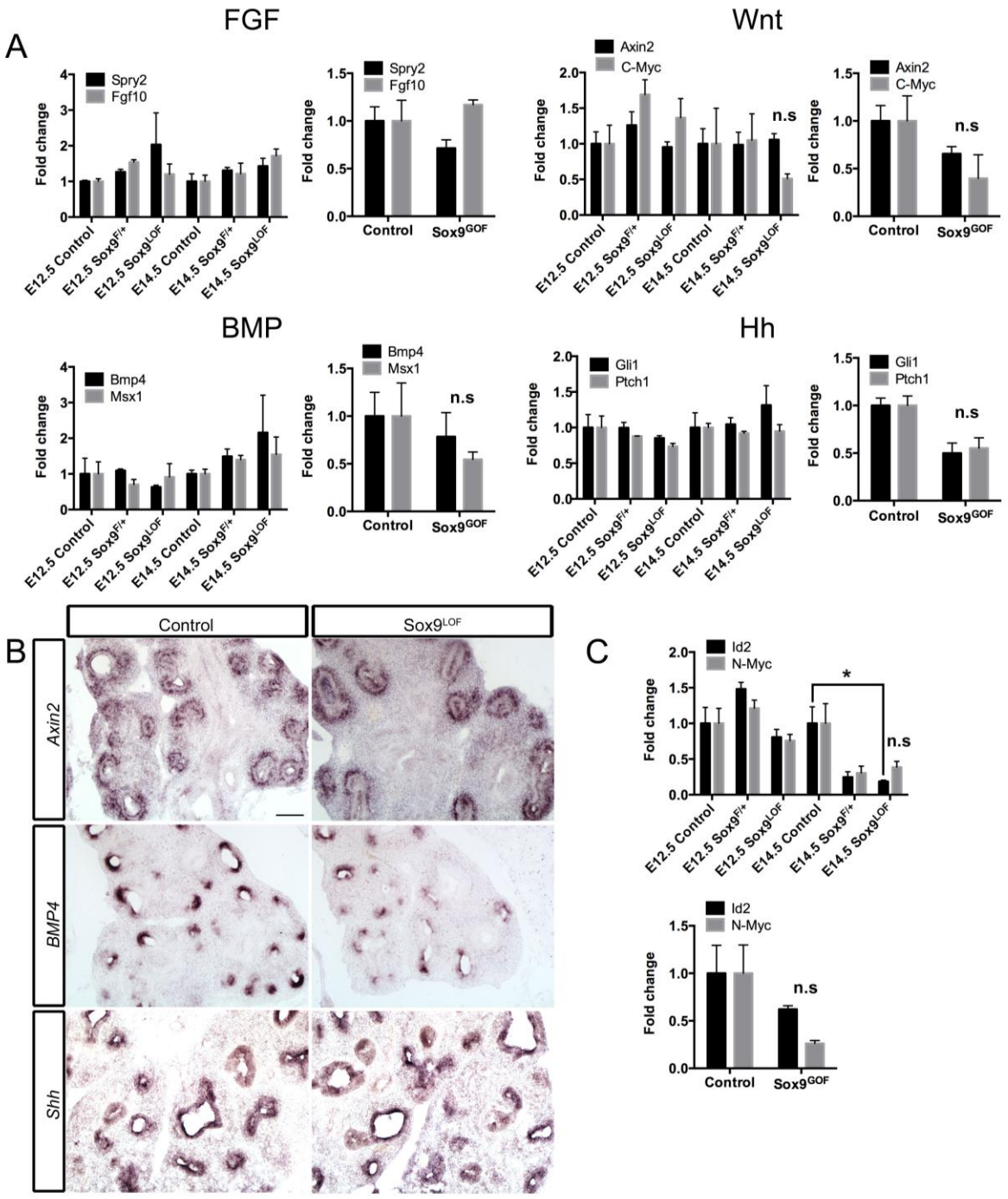

Figure 2.6. The effect of Sox9 loss and gain on the major signaling pathways of lung development. (A) Transcripts for key members or targets of the FGF, Wnt, BMP, and Hh signaling pathways were quantified by qRT-PCR at E12.5 and E14.5 for control and Sox9^{LOF}, and at E14.5 for control and Sox9^{GOF}. There were no significant differences among E12.5 and E14.5 control, Sox9 heterozygous (Sox9$^{F/+}$), Sox9^{LOF}, and E14.5 Sox9^{GOF} lungs. (B) *In situ* hybridizations were done on Axin2 (Wnt target), BMP4 and Shh. There were no differences in localization or expression levels between E14.5

control and $Sox9^{LOF}$ lungs. (C) Transcript levels of distal lung progenitor markers Id2 and Nmyc were examined by qRT-PCR in E12.5 and E14.5 control, Sox9 heterozygous (Shh-cre;$Sox9^{F/+}$), $Sox9^{LOF}$, and E14.5 $Sox9^{GOF}$ lungs. While some trends of down regulation were apparent, only Id2 expression at E14.5 in $Sox9^{LOF}$ lungs showed a statistically significant down regulation. * indicates $p<0.05$ and error bars represent SEMScale bars in B represent 100 µm.**Note**: For all qRT-PCR experiments, 3 independent biological samples were analyzed (n=3 independent lungs).

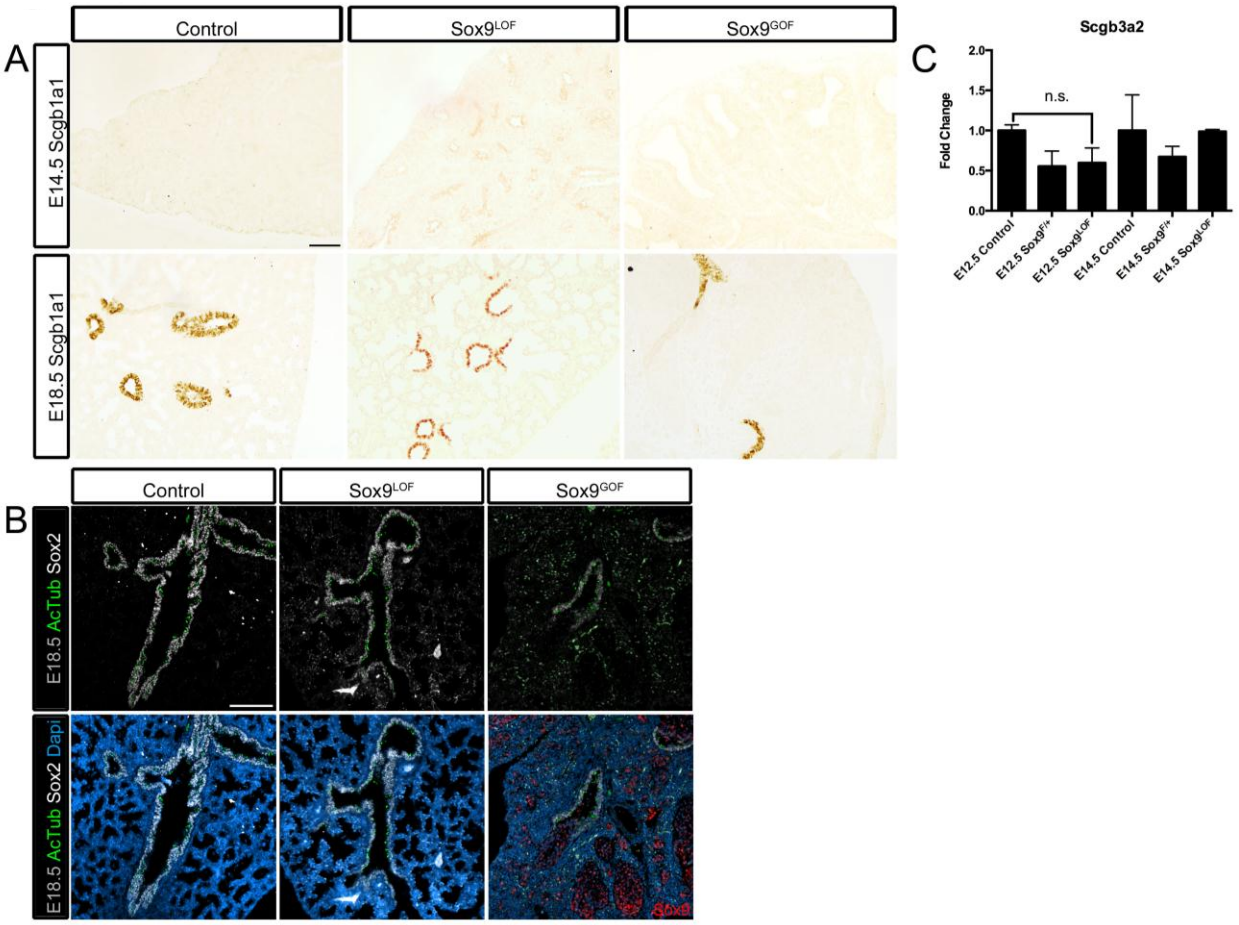

Figure 2.7. The effect of Sox9 loss and gain on differentiation of proximal cell types. (A-C) Immunostaining for Scgb1a1 (Clara cells) and AcTub (Ciliated cells) and qRT-PCR of Scgb3a2 (Clara cells). At E14.5 and/or E18.5 there was no difference in Scgb1a1 or ActTub staining (A-B) or significant difference in Scgb3a2 mRNA levels (C) between E12.5 and E14.5 Sox9^{LOF} lungs and control lungs. In Sox9^{GOF} lungs (Shh-cre;Rosa26-rtTa;tetO-Sox9-mCherry +Doxycycline (Sox9 ON) at E9.5), cells ectopically expressing Sox9 did not co-stain for Ciliated cell markers (AcTub) at E18.5 (B). Since Sox9 has scattered ectopic expression in E18.5 Sox9^{GOF} lungs, the epithelial cells expressing proximal markers do not express the Sox9 transgene. Scale bars in A-B represent 100 µm. Error bars in C represent SEM.

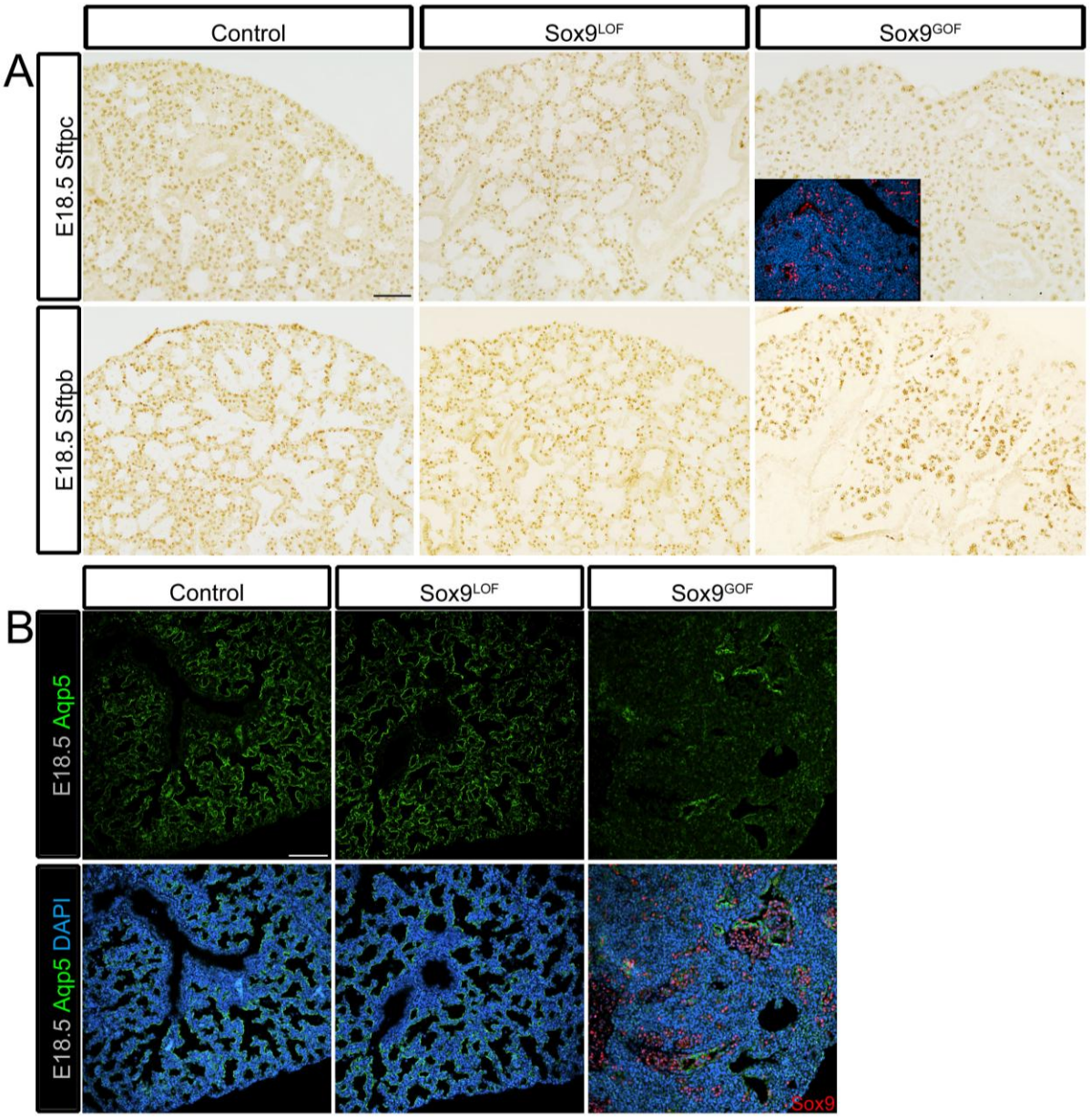

Figure 2.8. The effect of Sox9 loss and gain on differentiation of distal cell types. (A-B) Immunostaining for Sftpc and Sftpb (Alveolar type II cells) and Aqp5 (Alveolar type I cells) at E18.5. (A) At E18.5 there was no apparent difference in Sftpc and Sftpb expression between control and $Sox9^{LOF}$ or $Sox9^{GOF}$ lungs (Shh-cre;Rosa26-rtTa;tetO-Sox9-mCherry +Doxycycline (Sox9 ON) at E9.5). However, upon closer inspection, cells in the $Sox9^{GOF}$ model that express the Sox9 transgene do not co-express differentiation markers (inset in A, B).(B) Aqp5 staining did not appear to be different between control and $Sox9^{LOF}$ lungs, whereas the $Sox9^{GOF}$ lungs had reduced Apq5 staining at E18.5.Scale bars in A-B represent 100 µm.

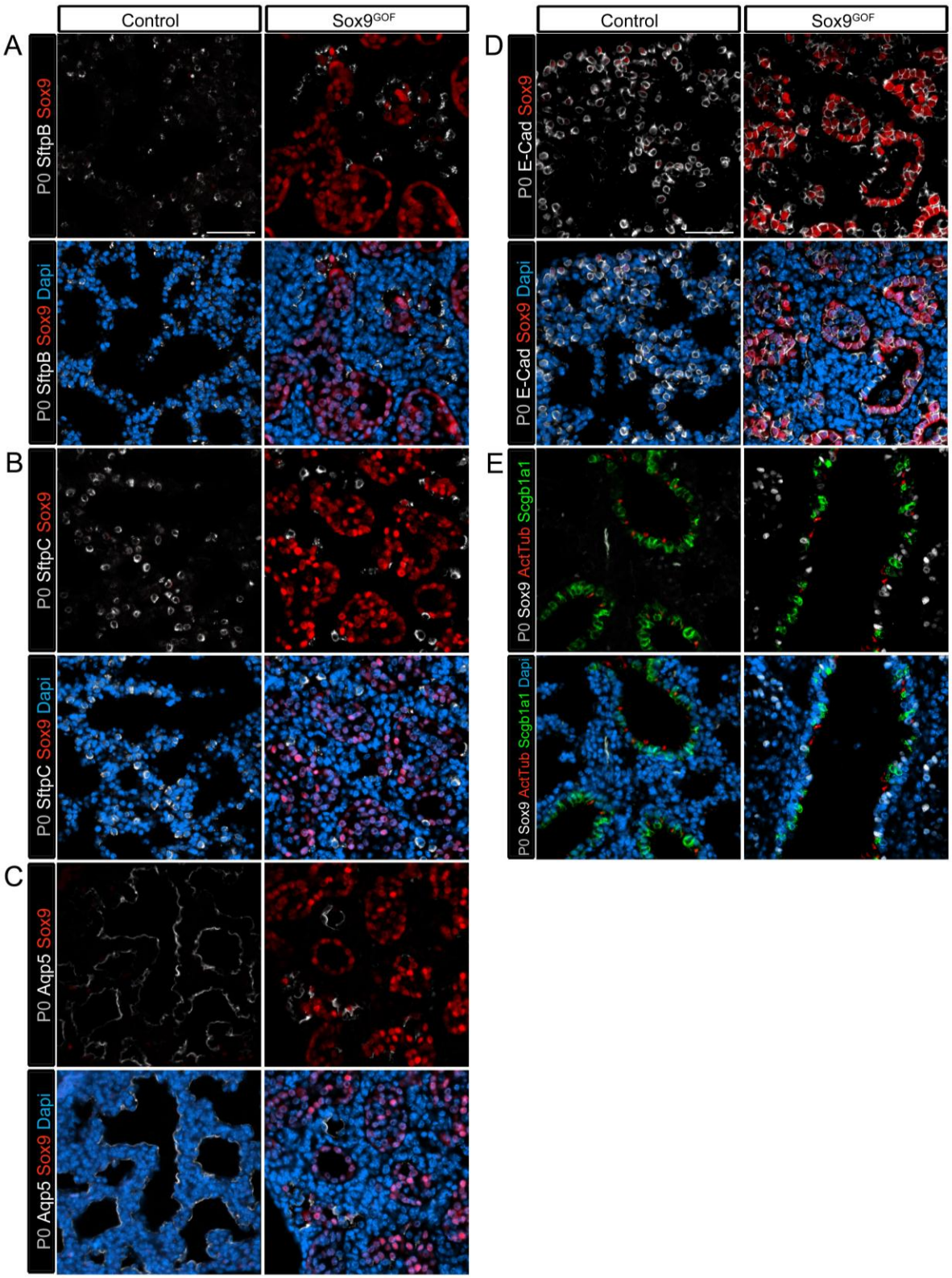

Figure 2.9. Ectopic Sox9 inhibits differentiation. For Figure 2.9, mice used were Sftpc-rtTa;tetO-Sox9-mCherry. Doxycycline was administered at E15.5 and lungs were

harvested at P0, which resulted in ectopic Sox9 expression when the epithelium is transitioning from the branching columnar epithelium to a terminally differentiated squamous epithelium. (A-C) In P0 $Sox9^{GOF}$ lungs, ectopic Sox9 (red) leads to a reduction in Type II alveolar cell markers SftpB and SftpC staining (A-B, white) and Type I cell marker Aqp5 (C, green) staining. (D) E-Cad staining (white) revealed that distal $Sox9^{GOF}$ epithelium (red) fails to undergo the columnar-to-squamous epithelial transition seen in lower airways (alveoli) of control lungs. (E) Proximal cell types, Clara (Scgb1a1) and Ciliated cells (ActTub) were reduced in $Sox9^{GOF}$ lungs where Sox9 was ectopically expressed compared to control lungs.All scale bars represent 50 µm.

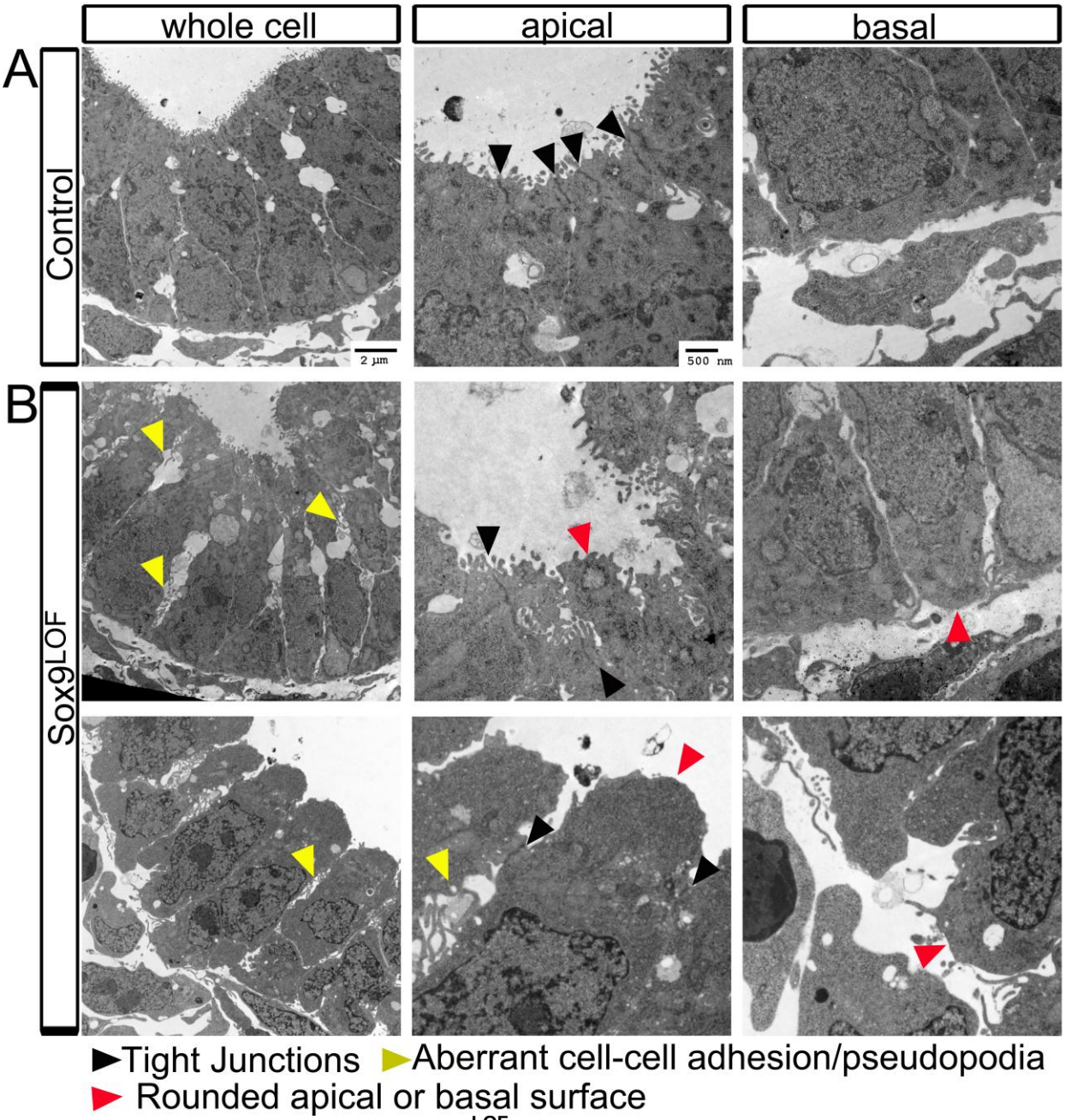

Figure 2.10. Cellular defects in Sox9^{LOF} lung epithelium. (A-B) TEM images of E14.5 control and Sox9^{LOF} lungs revealed intact tight junctions (black arrows). (B) Sox9^{LOF} lungs exhibited moderate (B, middle row) and severe (B, bottom row) degrees of cellular disruption. This included rounded apical surfaces, loss of microvilli, apical blebbing and irregular basal surfaces (red arrows). In addition Sox9^{LOF} lungs had large spaces between adjacent cell membranes that contained pseudopidia (yellow arrows).

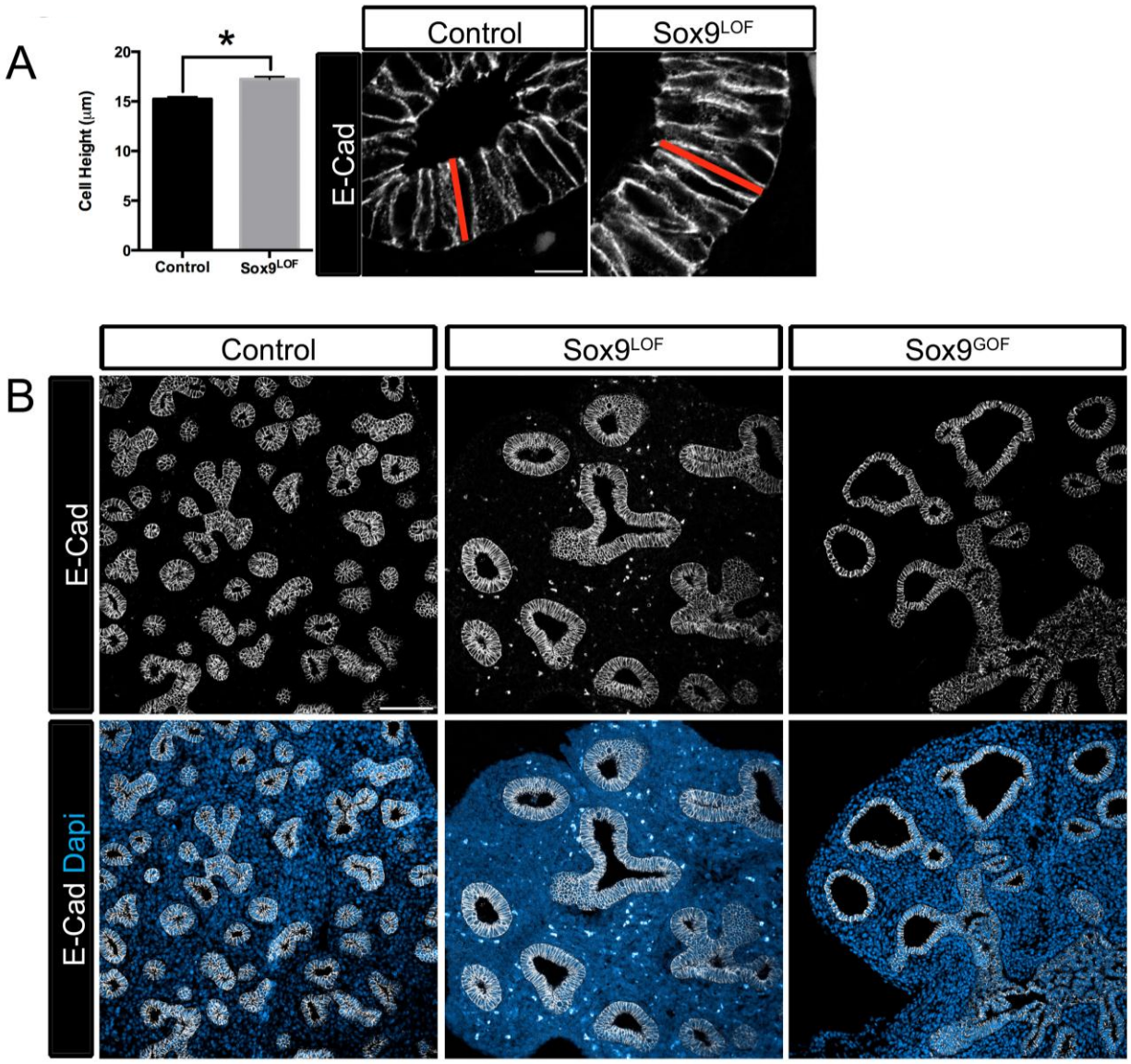

Figure 2.11. Sox9^{LOF} have perturbed cell shape.(A) Epithelial cell shape is perturbed at E14.5 in Sox9^{LOF} lungs. Cells were labeled with E-cadherin (white) and cell height was quantified by measuring from the apical to basal surfaces of the cell indicated by the red line. Sox9^{LOF} had significantly taller epithelial cells at the bud tips than the control epithelium. (B) At E14.5 lower magnification images of E-Cad (white) staining shows differences in the epithelium between control, Sox9^{LOF} and Sox9^{GOF} lungs. Scale bars in A represent 50 µm and B represent 100 µm

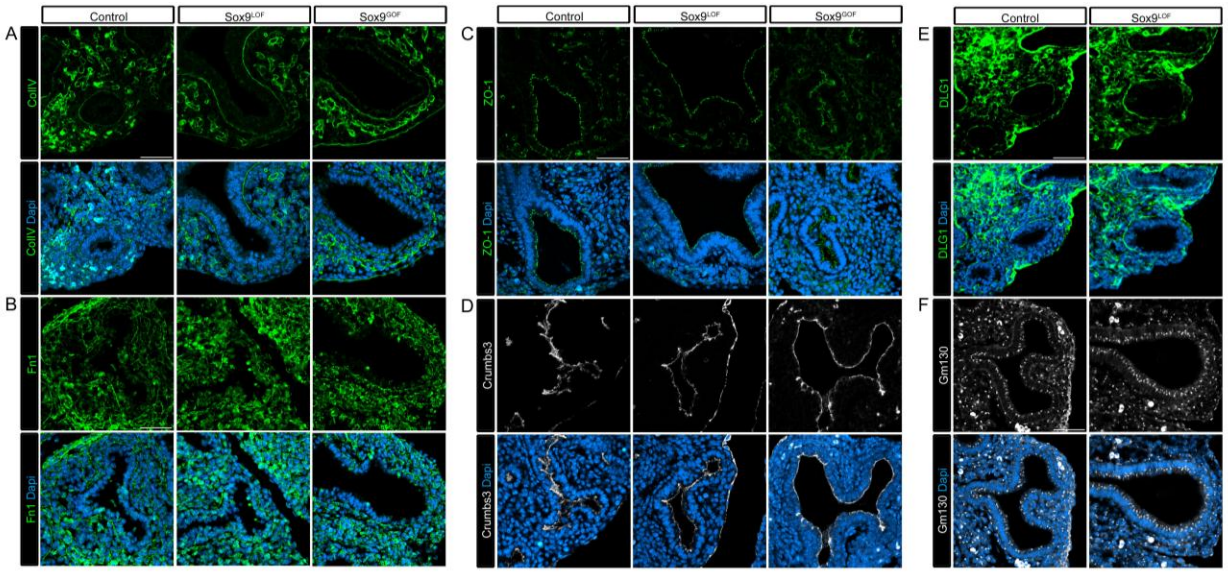

Figure 2.12. Loss or gain of Sox9 does not affect some ECM proteins or apical-basal polarity in the lung. (A-B,E) ColIV (A), Fibronectin (Fn1) (B), and DLG1 (E) mark the basal lamina. There was no difference in ColIV or Fn1 expression or localization between control and $Sox9^{LOF}$ or $Sox9^{GOF}$ lungs at E14.5. There were also no changes in DLG1 between control and $Sox9^{LOF}$ at E14.5.(C-D, F) ZO-1 (C), Crumbs3 (D) marks the apical surface and Gm130 marks the golgi on the nucleus and apical surface of the cell. There was no difference in ZO-1 or Crumbs3 expression or localization between control and $Sox9^{LOF}$ or $Sox9^{GOF}$ lungs at E14.5. There were also no changes in Gm130 between control and $Sox9^{LOF}$ at E14.5.All scale bars represent 50 µm.

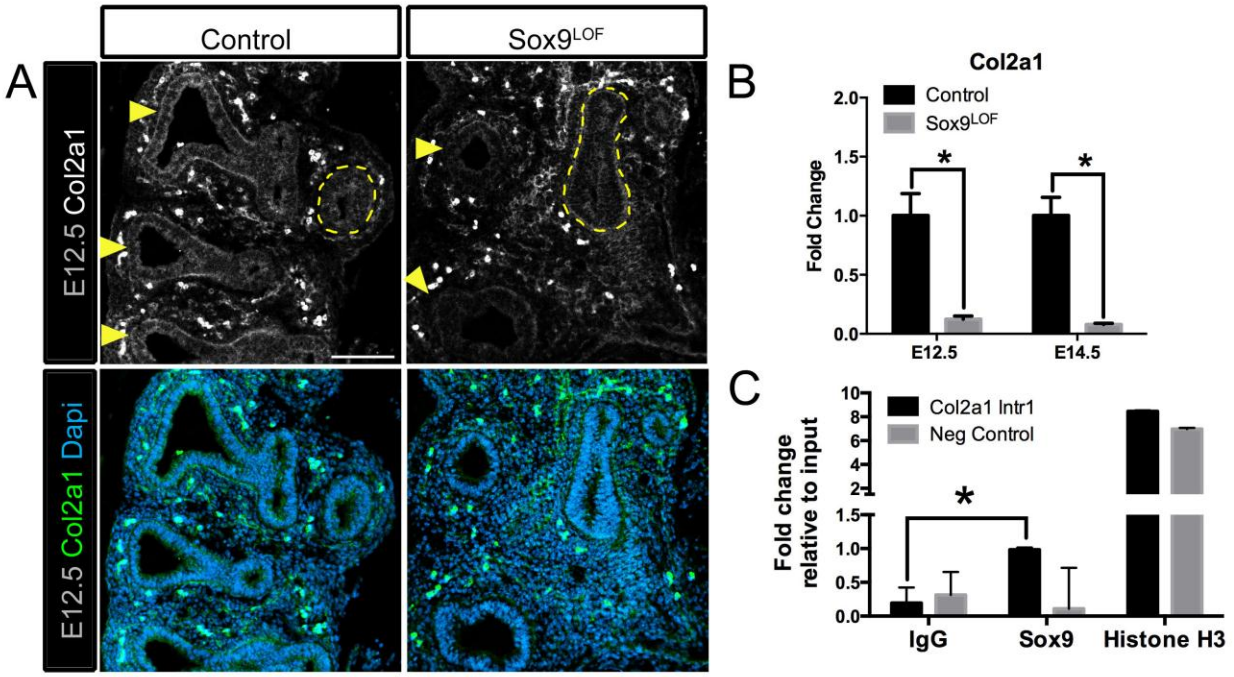

Figure 2.13. Sox9 regulates ECM protein Col2a1.(A) Col2a1 staining (white, top; green, bottom) was reduced in E12.5 distal buds (yellow arrows) compared to control lungs. Proximal airways are outlined with a yellow dotted line. (B) Col2a1 mRNA levels are reduced by an 8 fold decrease in E12.5 and a 12 fold decrease E14.5 lungs compared to control lungs. (C) ChIP assay was performed on FACS purified Sox9-eGFP distal lung epithelial cells. Compared to a non-specific rabbit anti-IgG, anti-Sox9 preferentially (5 fold enrichment) pulled down a previously characterized Sox9 binding site in Col2a1 intron1 (Col2a1 Intr1, black bars), whereas anti-Sox9 did not preferentially pull down non-specific DNA near the Col2a1 gene compared with anti-IgG negative control (Neg Control, grey bars). Both Col2a1 Intr1 and Neg Control sites were pulled down with the positive control, anti-Histone H3. All fold changes were normalized to 2% input. Scale bars in A represent 100 μm. * indicates $p<0.005$ in A and $P<.05$ in C. All error bars represent SEM

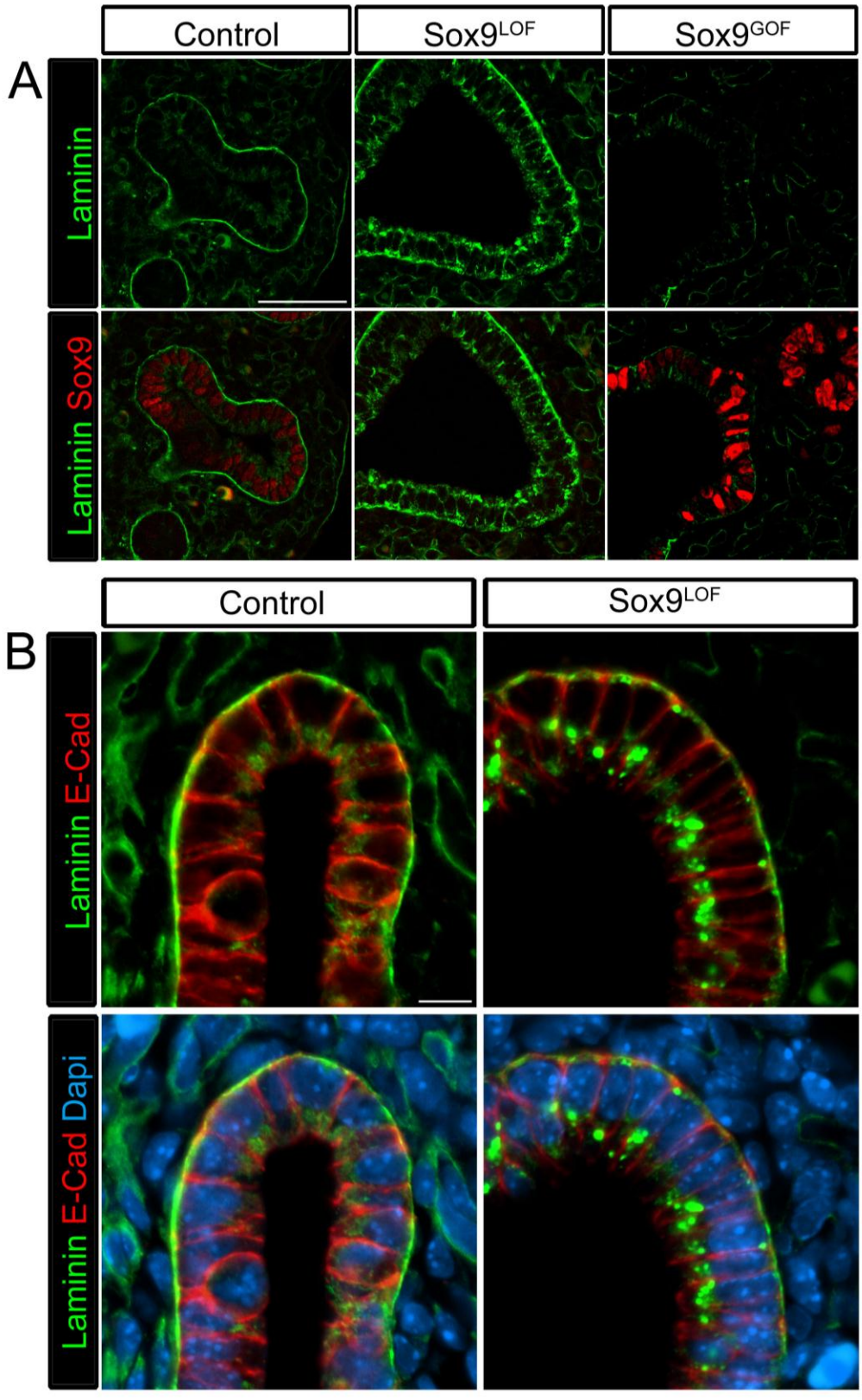
A
Control
Sox9LOF
Sox9GOF
Laminin
Laminin Sox9
B
Control
Sox9LOF
Laminin E-Cad
Laminin E-Cad Dapi

Figure 2.14. Gain or loss of Sox9 disrupts basement membrane laminin deposition. (A) Laminin staining (green) in control lungs at E14.5 shows robust staining in the basement membrane of Sox9+ (red) branching epithelial tips. In contrast, $Sox9^{LOF}$ lungs showed mislocalized staining, and $Sox9^{GOF}$ had a reduction in Laminin staining. (B) In $Sox9^{LOF}$ lungs, intracellular Laminin staining (green) is observed as punctae on both the apical and basal surfaces of the epithelial (E-cad, red) cells compared to controls, where Laminin is part of the ECM of the basement membrane. Scale bars in A represent 50 μm and in B represent 10 μm.

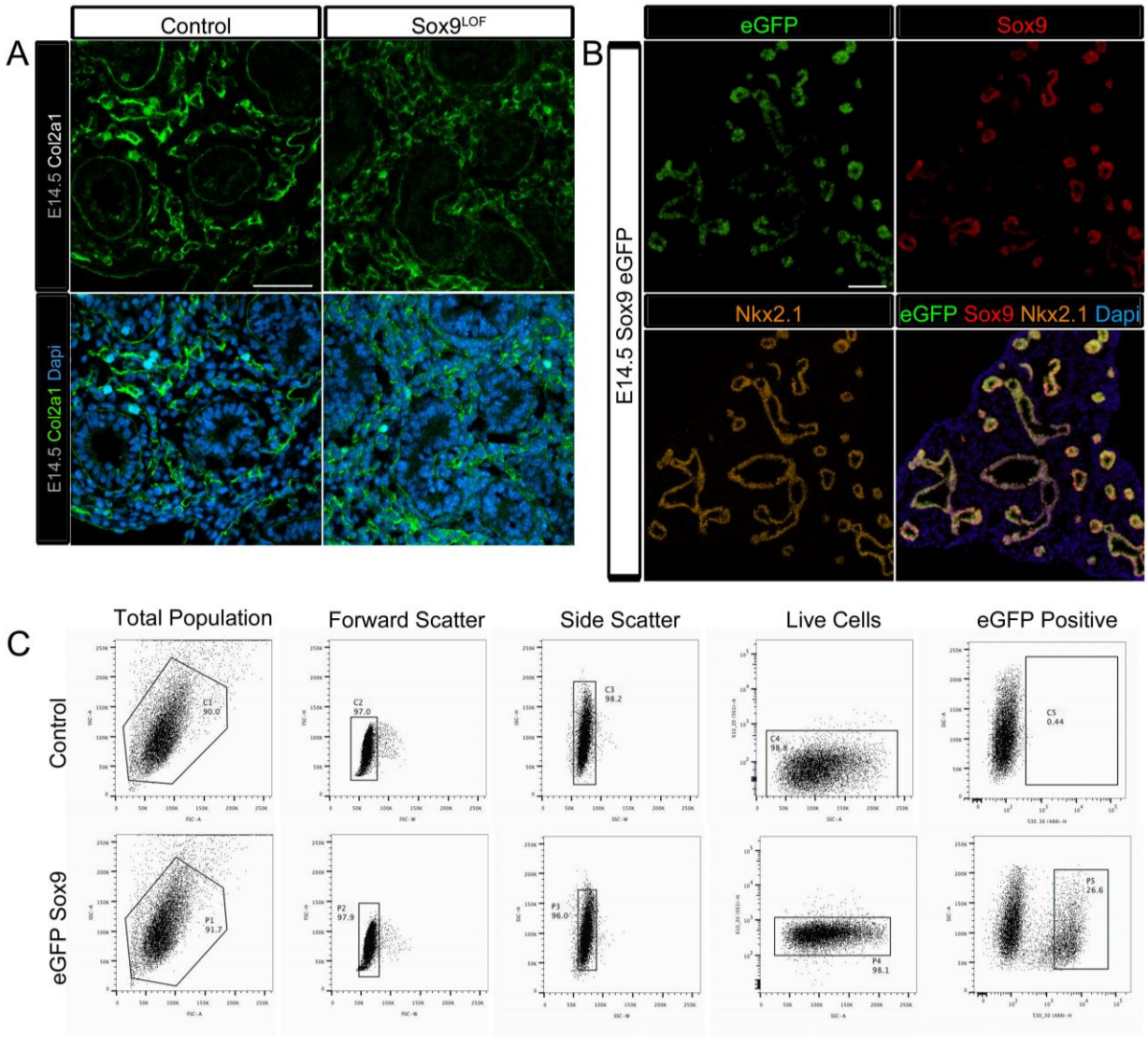

Figure 2.15. Col2a1 expression is reduced in Sox9^{LOF} lungs.(A) Col2a1 immuno staining was reduced in the distal epithelial buds of E14.5 Sox9^{LOF} lungs compared to controls. In controls, a thin ring of staining was seen around distal buds, whereas Sox9^{LOF} distal epithelial buds had weak and diffuse staining around distal buds. Mesenchymal Col2a1 expression did not appear to be different. (B) Sox9-eGFP transgeneic mouse had GFP staining in the distal lung epithelium, which correlated with the Sox9 (red) immunostaining. (C) Sox9-eGFP positive cells were sorted by FACS for the ChIP assay. Panel C shows the different gates used to isolate these cells. Live/dead dells were determined by Propidium Iodide exclusion from live cells. An eGFP^{High} population of cells were collected and used for ChIP analysis.Scale bars in A represent 50 µm and B represent 100 µm.

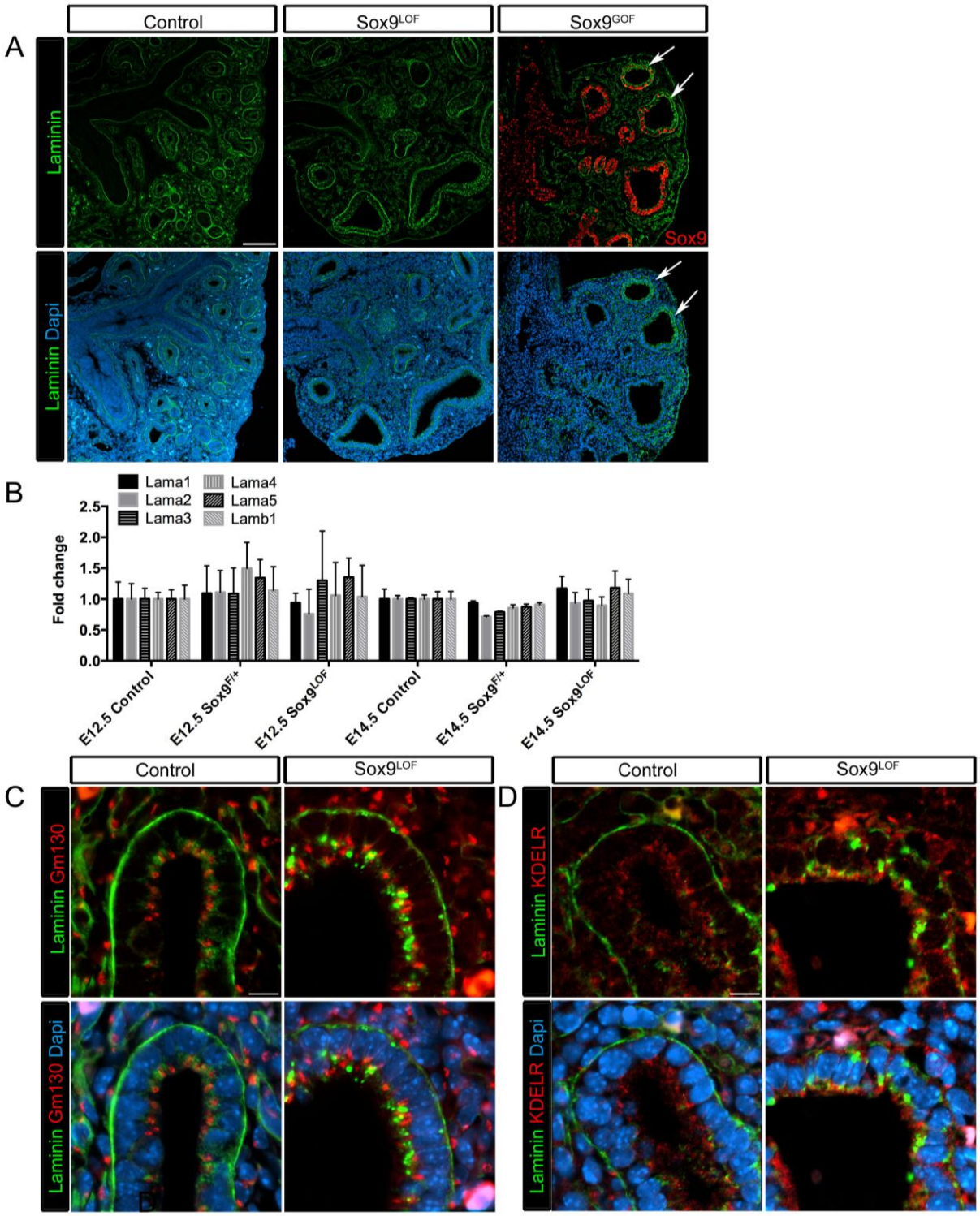

Figure 2.16. Loss of Sox9 causes Laminin deposition defects in the lung epithelium.(A) Laminin (green) stains the basal lamina throughout the proximal and distal lung epithelium in control lungs at E14.5. In contrast, Sox9^{LOF} lungs showed mislocalized Laminin staining in the distal epithelium, and Sox9^{GOF} had a reduction in

Laminin staining both in the proximal and distal epithelium, (B) Various *Laminin* isoform transcripts were quantified by qRT-PCR. There were no significant differences in expression levels among control, Sox9 heterozygous ($Sox9^{F/+}$), $Sox9^{LOF}$ lungs at E12.5 and E14.5. (n=3 independent lungs) (C-D) Some of the punctate Laminin staining (green) associates (co-localizes) with the golgi marker Gm130 (C, red – co-localization is yellow) and ER marker KDELR (D, red – co-localization is yellow). In control epithelium, co-localization was not apparent. Scale bars in A represent 100 μm and C-D represent 10 μm.Error bars in B represent SEM.

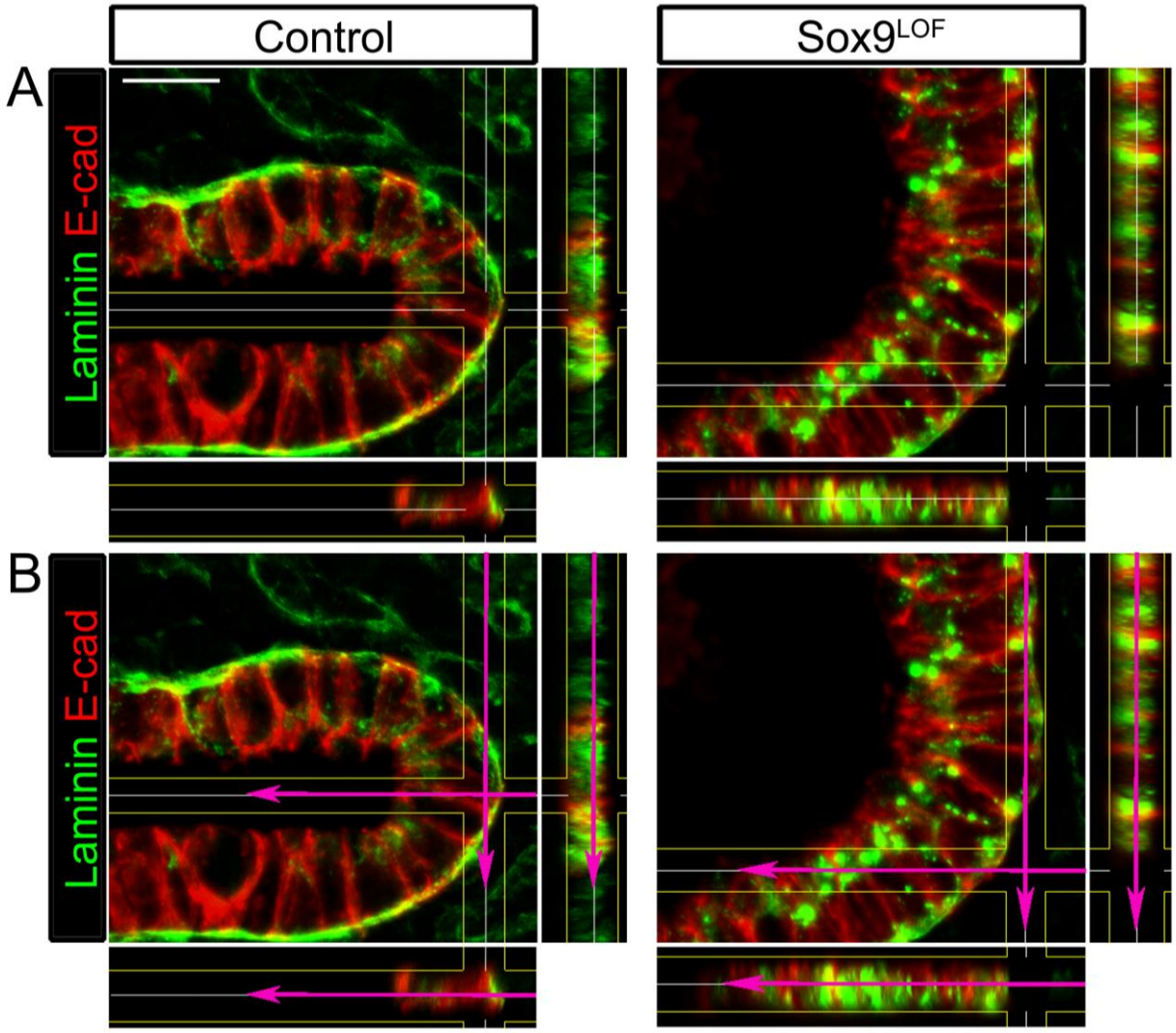

Figure 2.17. Loss of Sox9 causes mislocalization of Laminin within the distal epithelial cells. (A-B) High magnification confocal microscopy Z-stacks to examine Laminin expression in control and Sox9^{LOF} lungs. In control lungs, Laminin (green) stains the basal lamina and a view through the cell from basal-to-apical demonstrates that Laminin is on the basal side of the E-cad staining (bottom panel in A, pink arrow at bottom). In Sox9^{LOF} lungs, strong, punctate Laminin staining is observed inside the epithelial cells marked by E-cad.. Pink arrows indicate the orientation of the Z-stack. Scale bars in A-B represent 10 μm.

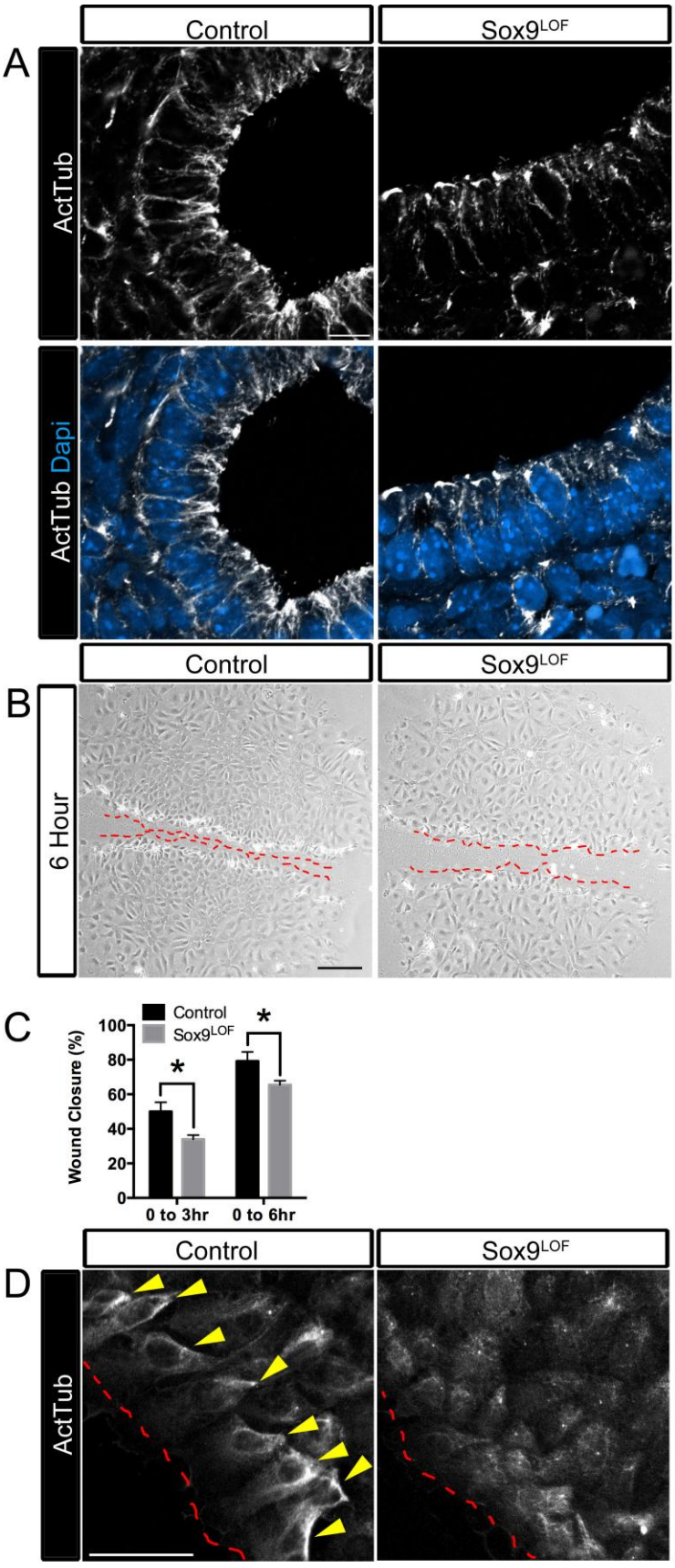
A
Control
Sox9LOF
ActTub
ActTub Dapi
B
Control
Sox9LOF
6 Hour
C
Control
Sox9LOF
Wound Closure (%)
100
80
60
40
20
0
*
*
0 to 3hr
0 to 6hr
D
Control
Sox9LOF
ActTub

Figure 2.18. Sox9 is required for proper cytoskeleton organization and *in vitro* cellular migration. (A) $Sox9^{LOF}$ lungs have a disrupted microtubule cytoskeleton. Stabilized acetylated tubulin (AcTub, white) is observed on the apical, lateral and basal surfaces of control epithelium at E14.5. In contrast $Sox9^{LOF}$ epithelium has reduced AcTub staining on the lateral surfaces and no staining along the basal surface of the epithelium. (B-C) A scratch assay was performed on isolated control and $Sox9^{LOF}$ epithelial buds cultured *in vitro* to examine epithelial movement characteristics. The red-dotted line indicates the scratch. Compared to controls, migration of $Sox9^{LOF}$ epithelial cells were significantly delayed at both 3 hour (hr) and 6hr time points, indicating that $Sox9^{LOF}$epithelial cells have impaired cellular migration/movement. Closure of the scratch was quantitated over time (D). ActTub staining revealed that in control lungs the cells lining the scratch had accumulated stabilized tubulin on the side furthest from the scratch (arrows) compared to the $Sox9^{LOF}$ cells, which had no aggregation of ActTub. Scale bars in A represent 50 µm, B represent 200 µm, and C represent 100 µm.* indicates $p<0.01$ and error bars represent SEM

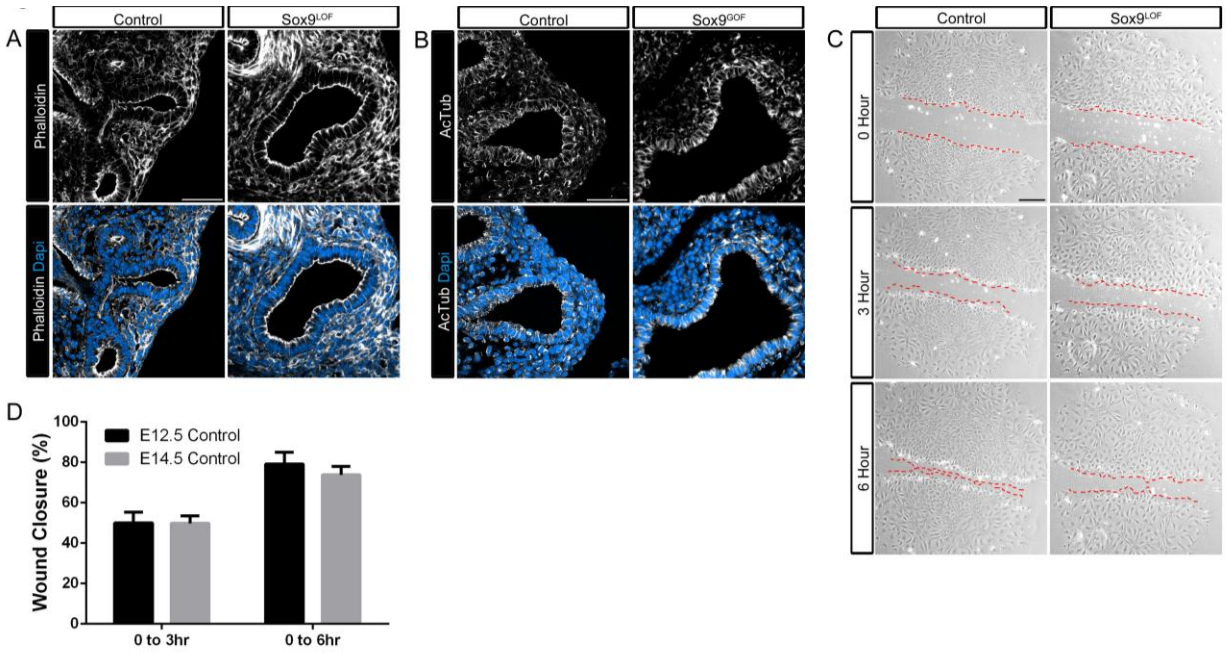

Figure 2.19. The effects of Sox9 loss and gain on cytoskeleton organization and cell shape. (A) Phalloidin (white) labels the F-actin filaments of the cytoskeleton. There was no difference in F-actin localization or expression between control and $Sox9^{LOF}$ lungs. (B) Acetylated tubulin (AcTub) (white) stains the stabilized microtubules. There was no difference in acetylated tubulin localization or expression between control and $Sox9^{GOF}$ lungs.(C-D) A scratch assay was performed on isolated control and $Sox9^{LOF}$ epithelial buds cultured *in vitro* to examine epithelial movement characteristics. The red-dotted line indicates the scratch. Compared to controls, migration of $Sox9^{LOF}$ epithelial cells were significantly delayed at both 3 hour (hr) and 6hr time points, indicating that $Sox9^{LOF}$epithelial cells have impaired cellular migration/movement (C). In E12.5 and E14.5 control lungs there was no difference in wound closure, indicating the rate of migration is the same at both time points (D). Scale bars in A-B represent 50 µm and C represent 200 µm. Error bars in D represent SEM.

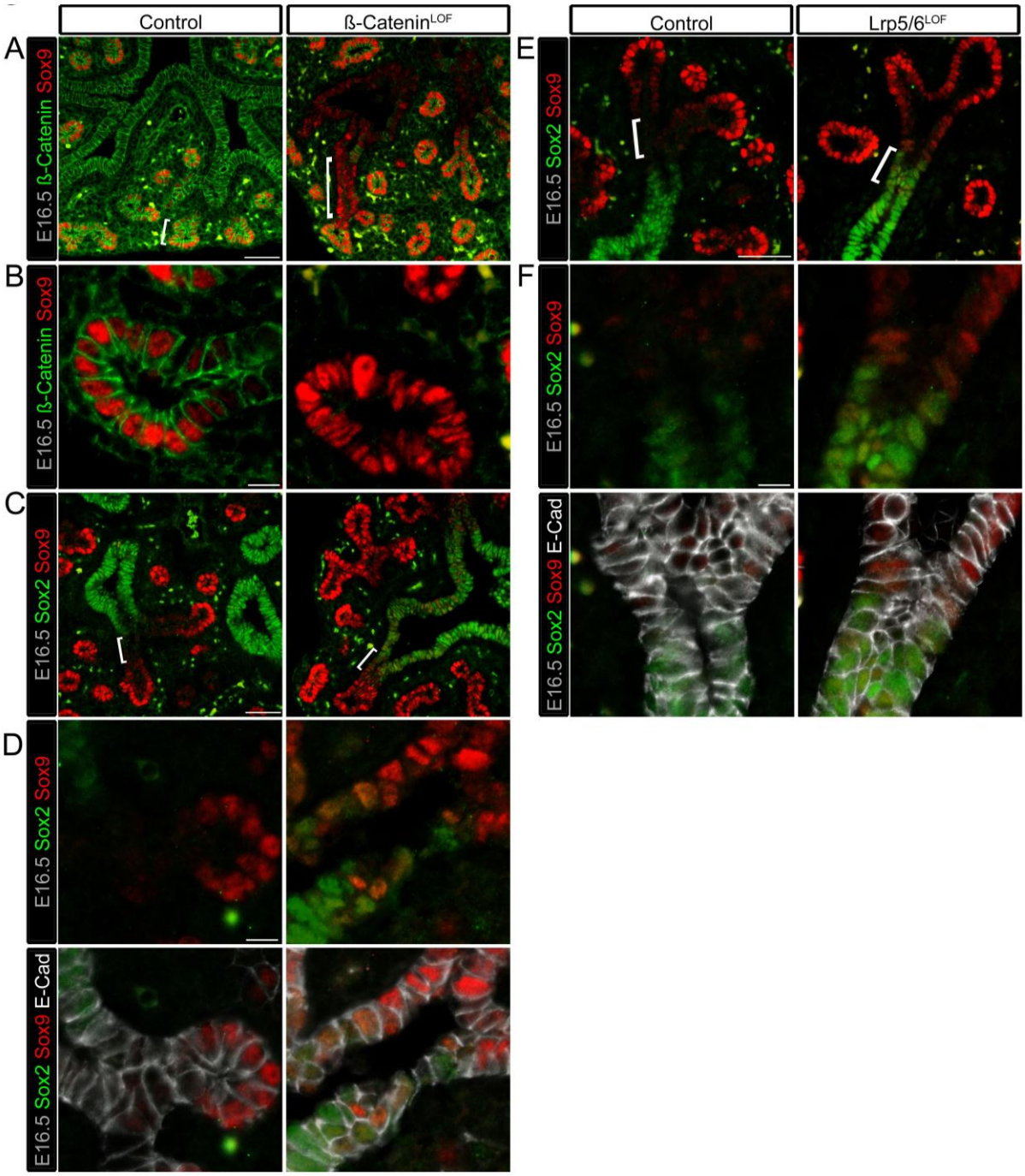

Figure 2.20. ß-Catenin/Wnt Signaling is sufficient, but not necessary for Sox9 expression during branching morphogenesis. (A-B) Control and ß-Catenin^{LOF} lungs (Sox9-creER;β-catenin$^{Flox/Flox}$) at E16.5 (Tamoxifen injections given at E11.5 and E12.5). In controls Sox9 (red) marks the distal lung epithelium (A: highlighted by white bar) while β -Catenin (green) marks both mesenchyme and epithelium. Mosaic loss of β -Catenin protein specifically in the epithelium is seen in β -Catenin^{LOF} lungs. In regions where β -Catenin has been deleted both in the proximal airways (A) and distal buds (B), Sox9 expression expands into the proximal airways (A: highlighted by white bar) and

normal Sox9 expression in the distal buds (B).(C-D) Sox9 (red) and Sox2 (green) staining in control and β -Catenin^{LOF} lungs at E16.5. In controls, these markers stain the distal and proximal airways, respectively and do not overlap. A Sox2/Sox9 negative zone is observed between the two domains (highlighted by white bar in control (C)). Conditional deletion of β -Catenin causes a proximal expansion of Sox9 causing a Sox2+/Sox9+ intermediate population (highlighted by white bar in β -Catenin^{LOF} (C)). E-Cad (white) staining in β-Catenin^{LOF} resembled control lungs (D).(E-F) Wnt loss of function (Lrp5/6^{LOF}) (Sox9-creER;Lrp5$^{Flox/Flox}$;Lrp6$^{Flox/Flox}$, Tamoxifen injections given at E11.5 and E12.5) model was generated in order determine if the phenotype in A-D was due to adhesive functions of β –Catenin. Similar to β -Catenin^{LOF} lungs, a Sox2+/Sox9+ intermediate population was observed in Lrp5/6^{LOF} lungs (highlighted by the white bar (E)) compared to the Sox2/Sox9 negative zone in the control lungs. E-Cad (white) staining in Lrp5/6^{LOF} resembled control lungs. Scale bars in A,C,E represent 50 μm and B,D,F represent 10 μm.

Table 2.1 List of primary and secondary antibodies

Primary Antibody	**Source**	**Catalog #**	**Dilution**
Alexa Fluor 546 – Phalloiden**	Invitrogen	A22283	1:50Frozen
Goat anti-E-Cadherin (E-cad)	R & D Systems	AF748	1:100
Goat anti-Sox9 (for IF)	R & D Systems	AF3075	1:500
Rabbit anti-Sox9 (for IF, ChIP)	Millipore	AB5535	1:500
Mouse anti-Acetylated Tubulin (AcTub)	Sigma-Aldrich	T7451	1:1000
Mouse anti-DLG1*	Santa Cruz Biotechnology	sc-9961	1:100Frozen
Mouse anti-E-Cadherin (E-cad)	BD Transduction Laboratories	610181	1:500
Mouse anti-Fibronectin (Fn1)*	DSHB	B3/D6	1:100
Mouse anti-Gm130	BD Transduction Laboratories	610822	1:200
Mouse anti-KDEL Receptor (KDELR)	Stressgen Bioreagents	VAA-PT048	1:100
Rabbit anti-Aquaporin 5 (Aqp5)	Abcam	ab78486	1:1000
Rabbit anti-CCSP	Seven Hills Bioreagents	WRAB-3950	1:1000
Rabbit anti-Collagen, Type IV (Col IV)	Millipore	AB756P	1:500
Rabbit anti-Collagen2 (Col2a1)	Novus	NB100-91715	1:100
Rabbit anti-Crumbs3	Makarova et al. 2003		1:1000
Rabbit anti-Histone H3 (ChIP)	Cell Signaling Technology	4620	1:50
Rabbit anti IgG (ChIP)	Cell Signaling Technology	2729	1:500
Rabbit anti-Ki67	Thermo Scientific	RM-9106-S1	1:500
Rabbit anti-Laminin	Abcam	ab14055	1:200
Rabbit anti-N-Terminal Pro SP-C (Sftpc)	Seven Hills Bioreagents	WRAB-9337	1:100
Rabbit anti-Sox2	Seven Hills Bioreagents	WRAB-SOX2	1:500
Rabbit anti-Sufactant Protein B (Sftpb)	Santa Cruz Biotechnology	sc-13978	1:500
Rabbit anti-TTF1 (Nkx2.1)	Epitomics	2044-1	1:500
Rabbit anti-ZO-1	Invitrogen	33-9100	1:500
Rabbit anti-β-catenin	Santa Cruz Biotechnology	sc-1496	1:500
Rat anti-BrdU	Abcam	ab6326	1:1000
Secondary Antibody	**Source**	**Catalog #**	**Dilution**
Biotin anti-mouse	Jackson Immuno	715-065-150	1:500
Biotin anti-rabbit	Jackson Immuno	711-065-152	1:500
Biotin anti-rat	Jackson Immuno	712-065-150	1:500
Donkey anti-goat 488	Jackson Immuno	705-545-147	1:500
Donkey anti-goat 647	Jackson Immuno	705-605-147	1:500
Donkey anti-goat Cy3	Jackson Immuno	705-165-147	1:500
Donkey anti-mouse 488	Jackson Immuno	715-545-150	1:500
Donkey anti-mouse 647	Jackson Immuno	415-605-350	1:500
Donkey anti-mouse Cy3	Jackson Immuno	715-165-150	1:500

Donkey anti-rabbit 488	Jackson Immuno	711-545-152	1:500
Donkey anti-rabbit 647	Jackson Immuno	711-605-152	1:500
Donkey anti-rabbit Cy3	Jackson Immuno	711-165-102	1:500
Streptavidin 488	Jackson Immuno	160-540-084	1:500

*Amplfication kit required
**Primary conjugated to secondary antibody

Table 2.2 List of primers for qRT-PCR and genotyping

Primer Name	Forward Sequence	Reverse Sequence
Axin2	TGCATCTCTCTCTGGAGCTG	ACTGACCGACGATTCCATGT
BMP4	TGGACTGTTATTATGCCTTGTTT	CTCCTAGCAGGACTTGGCAT
Col2a1	CTACGGTGTCAGGGCCAG	GCAAGATGAGGGCTTCCATA
C-Myc	AGAGCTCCTCGAGCTGTTTG	TGAAGTTCACGTTGAGGGG
Fgf10	GCAACAACTCCGATTTCCAC	GATTGAGAAGAACGGCAAGG
Gli1	GGATGAAGAAGCAGTTGGGA	ATTGGATTGAACATGGCGTC
Id2	GTCCTTGCAGGCATCTGAAT	AGAAAAGAAAAAGTCCCCAAATG
Lama1	CTGTCACCCTGGACTTACGG	GCTCCAAAATCCAGTTTCCA
Lama2	CTCGAAGGCTCCCAGACTC	TGCATTCGAAGCAAGATTCA
Lama3	ACACCTGGGACGTGGATTG	CTTGCAGGGTGAATGCTTCAT
Lama4	GAGACTAGCGACTCAGGCGT	AGGGTGCACATTCTCCTGAC
Lama5	CTGGCGGAGATCCCAATCAG	GTGTGACGTTGACCTCATTGT
Lamb1	GCATTCCTTTGGGCCATC	CAGGGTCTCCCCAGAAGAG
Msx1	GAAACTAGATCGGACCCCGT	GTTGGTCTTGTGCTTGCGTA
Nmyc	AGCACCTCCGGAGAGGATA	TCTCTACGGTGACCACATCG
Ptch1	CTCCTCATATTTGGGGCCTT	AATTCTCGACTCACTCGTCCA
Scgb3a2	TCACAGGCACCAGCTATGAA	GTCAACAACAGGGAGACGGT
Sftpb	TTCTCTGAGCAACAGCTCCC	ACAGCCAGCACACCCTTG
Sftpc	AGCAAAGAGGTCCTGATGGA	ATGAGAAGGCGTTTGAGGTG
Sox9	AGGAAGCTGGCAGACCAGTA	TCCACGAAGGGTCTCTTCTC
Spry2	AGAGGATTCAAGGGAGAGGG	CATCAGGTCTTGGCAGTGTG

Note: All above primer sequences were obtained from http://mouseprimerdepot.nci.nih.gov/

Primer Name	Forward Sequence	Reverse Sequence
Col2a1 Intron 1*	TGAAACCCTGCCCGTATTTATT	GCTTTTCTCAAGCGCATACAGA
Col2a1 Neg Control	GGGGCGCTTTGTATGAAAGG	GTGAGCCAGTCTGGGTTTGA

Note: All annealing temperatures 60°C.

* Primer Sequences obtained from: Oh C-D et al. (2010) Identification of SOX9 Interaction Sites in the Genome of Chondrocytes. *PLoS ONE* 5:e10113.

CHAPTER 3

IN VITRO GENERATION OF HUMAN PLURIPOTENT STEM CELLS DERIVED LUNG ORGANOIDS

Summary

Recent breakthroughs in 3-dimensional (3D) organoid cultures for many organ systems have led to new physiologically complex *in vitro* models to study human development and disease. Here, we report the step-wise differentiation of human pluripotent stem cells (hPSCs) (embryonic and induced) into lung organoids. By manipulating developmental signaling pathways hPSCs generate ventral-anterior foregut spheroids, which are then expanded into human lung organoids (HLOs). HLOs consist of epithelial and mesenchymal compartments of the lung, organized with structural features similar to the native lung. HLOs possess upper airway-like epithelium with basal cells and immature ciliated cells surrounded by smooth muscle and myofibroblasts as well as an alveolar-like domain with appropriate cell types. Using RNA-sequencing, we show that HLOs are remarkably similar to human fetal lung based on global transcriptional profiles, suggesting that HLOs are an excellent model to study human lung development, maturation and disease.

Introduction

Several reports have demonstrated that directed differentiation of human pluripotent stem cells (hPSCs), which include embryonic (hESCs) and induced (iPSCs),

is one of the most efficient approaches to achieving differentiation of a cell or tissue of interest (1-5). Using this approach, differentiation of hPSCs into lung lineages has been achieved using diverse methodology with varying degrees of success(5-11).

Thus far, the majority of efforts to differentiate lung lineages from hPSCs have focused on using 2-dimensional (2D) monolayer cultures. Several recent advances in generating 3-dimensional (3D) organ-like tissues, called “organoids”, have been reported (1,2,12-16) Such 3D models offer several advantages; they often possess structural organization similar to the native organ, cell types from multiple germ layers (for example, mesoderm and endoderm (1,16,17), and multiple cellular lineages making them a physiologically complex model to study developmental processes, tissue homeostasis and pathological conditions *in vitro*.

Previous work has demonstrated that activation of FGF and WNT signaling synergistically drives CDX2+ intestinal lineage commitment in hPSC-derived endoderm and also drives “morphogenesis in a dish”, where the 2D tissue self-organizes into 3D spheroids comprised of mesenchymal and polarized epithelial layers that detach from the adherent cell layer (1). It has also been demonstrated that inhibition of BMP and TGFβ signaling is able to drive tissue into a SOX2+ foregut lineage (16,18). Building on these previous studies, we show that simultaneous stimulation of WNT and FGF signaling while inhibiting BMP/TGFβ signaling pathways in hPSC-derived endoderm cultures prevents intestinal lineage commitment, and instead, favors a SOX2+ anterior foregut fate while also robustly generating SOX2+ anterior foregut 3D spheroid structures.

In order to further restrict foregut spheroids to the lung lineage, the current study focused on manipulating FGF and HH signaling. In the mouse, high levels of Fgf signaling have been shown to induce Shh expression in the lung endoderm (19-21) which is accompanied by induction of the Nkx2.1+ lung progenitor field (20,22). Shh then signals from the endoderm to the mesoderm, and mutations in *Shh, Gli2* or *Gli3* lead to perturbed lung development, with *Gli2/Gli3* double knockout mice showing lung agenesis(23-25). Our results demonstrate that FGF2 induces NKX2.1, PAX8, and SHH in human foregut endoderm cultures. By using pharmacological inhibitors of FGF and HH signaling we demonstrate that SHH is required for NKX2.1 expression downstream of FGF2, and that FGF2 also induces PAX8 independently of HH signaling. These observations suggest a paradigm where FGF^{Lo}/HH^{Hi} conditions preferentially induce $PAX8^{Lo}/NKX2.1^{Hi}$ lung progenitors and FGF^{Hi}/HH^{Lo} conditions favor a $PAX8^{Hi}/NKX2.1^{Lo}$ fate. Given that Pax8 is required for thyroid development, we focused on defining the most robust conditions to induce NKX2.1 while minimizing PAX8 expression (24,26-32). By applying HH^{Hi} conditions during generation of foregut spheroids we were able to enhance NKX2.1 expression in foregut spheroids and subsequently expand spheroids in media containing FGF10, allowing them to grow into organoids. Organoids persisted in culture for over 100 days and developed well-organized proximal-like airway epithelial structures that had many cell types found in the proximal lung epithelium, including basal and ciliated cells along with rare club cells. Moreover, proximal airway structures were often surrounded by smooth muscle actin (SMA) positive mesenchymal tissue. Organoids also possessed distal-like epithelial cells that co-expressed progenitor markers, SFTPC/SOX9 and HOPX/SOX9, consistent with early bipotent alveolar

progenitor cells seen in mice (33,34). To support the idea that organoids may be more similar to a developing lung with abundant progenitor cells, we used RNA-sequencing to compare the global transcriptional profile of organoids to the human fetal and adult lung, undifferentiated hESCs and definitive endoderm. Principal component analysis, hierarchical clustering and Spearman's correlation all show that organoids have striking similarity to the human fetal lung.

Taken together, our data demonstrates an efficient and robust *in vitro* system to generate complex, 3D human lung organoids that are immature /fetal in nature. We anticipate that this model will serve as an unparalleled novel model for the study of human lung development, maturation and disease.

Results

Differentiation of hPSCs into anterior foregut spheroids

We and others have reported efficient induction of human endoderm using ActivinA (1,2,35), and a further lineage restriction into SOX2+ anterior foregut endoderm using inhibition of BMP and TGFβ signaling (18,36). We have recently demonstrated that inhibition of BMP signaling during intestinal lineage induction with WNT and FGF ligands is sufficient to inhibit intestinal CDX2 and induce SOX2+ posterior foregut spheroids capable of giving rise to human gastric (antral) organoids(16). Given that the lung is derived from the anterior foregut, we sought to define conditions to generate ventral anterior foregut spheroids. To do this, we tested if dual inhibition of BMP and TGFβ was able to anteriorize cultures, as previously described (18). We treated hESCs with ActivinA (100ng/mL) for four days to induce endoderm, followed by four days of

Noggin (NOG, 200ng/mL) and the small molecule TGFβ inhibitor, SB431542 (SB, 10μM). We confirmed that these conditions were able to induce robust mRNA and protein expression of SOX2, which co-expressed with endodermal marker FOXA2, while repressing the intestinal lineage marker CDX2 (Fig. 3.1A-C,Fig. 3.2A). QRT-PCR analysis also showed that compared to controls (in which endoderm was induced but was not exposed to NOG/SB), exposure to NOG/SB robustly induced ventral anterior foregut genes *NKX2.1* and *PAX8*, while the posterior foregut transcript, *PDX1* was reduced. *HHEX,* which is expressed in the developing liver, biliary system and thyroid, but is absent from the lung primordium, remained unchanged (Fig.3.1B). Given that NKX2.1 is expressed in the lung and thyroid primordium, and PAX8 is expressed in the thyroid primordium, these results suggest that 4 day ActivinA treatment followed by a 4 day NOG/SB treatment biases the cultures towards ventral-anterior foregut lineages.

Addition of FGF4 plus WNT3A (or Chir99021, a GSK3β inhibitor that enhances β-catenin dependent WNT signaling) promotes CDX2 intestinal lineage commitment and 3D spheroid formation in endoderm cultures (1,18,37,38). Based on our results in Fig. 3.1B-C, we hypothesized that combining FGF, Chir99021, NOG and SB would result in the generation of SOX2+ ventral-anterior foregut spheroids. To test this, we generated endoderm (4 days ACTA) and added no growth factors (Endoderm controls) or NOG, SB, FGF4, and Chir99021 (NOG/SB/F/Ch) (Fig. 3.1D). Addition of all four factors resulted in the generation of 3-dimensional SOX2+, CDX2- spheroids (Fig. 3.1E, F). SOX2+ spheroids also expressed the endodermal protein FOXA2, and were epithelial, co-expressing E-Cadherin (ECAD) (Fig. 3.1F, Fig. 3.3). In addition to SOX2, spheroids exhibited higher mRNA expression of anterior foregut lineage markers *NKX2.1* and

PAX8 compared to endoderm controls, suggesting that they are ventral-anterior foregut spheroids (Fig. 3.1E), however, immunofluorescence revealed that levels of NKX2.1 protein were just above the detection threshold (Fig. 3.3). Spheroids also possess a minor population of cells that are mesodermal in origin staining positive for Vimentin protein (VIM) (Fig. 3.4). Given that neural tissues also express NKX2.1, PAX8, SOX2, and FOXA2, and that neural induction protocols use dual BMP and TGFβ inhibition, we wanted to exclude the possibility that spheroids were neural in nature. To do this, we generated endoderm control cultures, foregut spheroids (ActivinA followed by NOG/SB/F/Ch), and induced neural tissue by adding NOG/SB to hESC cultures that were not treated with ActivinA (39). By examining induction of the neural markers *NESTIN, SOX1,* and *PAX6*, we confirmed that these transcripts were highly induced in dual NOG/SB neural cultures, but were low in ventral foregut spheroid cultures. In contrast, *FOXA2*, which is expressed in the foregut (40,41) and in some neural tissues (1,3,4,42-45), had high expression in ventral foregut spheroids, but was significantly reduced in dual NOG/SB neural conditions (Fig. 3.5). Taken together, these results strongly suggest spheroids are indeed foregut, and not of neural origin.

Induction of anterior foregut endoderm into a lung lineage through modulation of FGF and HH signaling

Many signaling pathways are important for lung induction and development (reviewed in (5-9,11,19,21,46,47)). High levels of Fgf signaling have been shown to induce Shh and Nkx2.1 expression in the foregut endoderm in mice (1,2,12-15,20,22); furthermore, Gli2/3 null mouse embryos fail to form lungs (1,17,23) and Hh signaling is

important for lung mesenchyme proliferation *in vivo*(25). These data confirm that Fgf and Hh signaling are critical for lung specification and ligands from both signaling pathways have been applied to hPSC derived lung lineages in 2D cultures (1,5,6). In our cultures we have reported that approximately 85-95% of cells are endoderm, but a portion of the remaining cells are mesodermal and this small mesodermal population is maintained in the spheroids and organoids (1,16,18) (Fig. 3.4). Therefore, based on mouse and hPSC studies, we hypothesized that FGF and/or HH signaling would induce an NKX2.1+ lung lineage in anterior foregut endoderm. To test our hypothesis we initially focused on adherent endoderm monolayer cultures to optimize induction conditions. Cultures were treated for 4 days with ActivinA followed by an additional 4 days with NOG/SB (Referred to as Foregut). Controls consisted of ActivinA treatment only followed by no additional growth factors (Endoderm controls), or ActivinA followed by NOG/SB, followed by no additional factors (Foregut controls). All experimental groups were compared to both endoderm and foregut controls (Fig. 3.6). We first tested the ability of FGF2 to induce *SHH*, *NKX2.1* and *PAX8* by exposing foregut cultures to low and high concentrations of FGF2 (50, 500ng/mL) (Fig. 3.6A). We observed a robust concentration dependent increase in *SHH* and *PAX8* mRNA expression compared to foregut or endoderm controls, and a modest increase of *NKX2.1* expression at the highest dose of FGF2 (500ng/mL) (Fig. 3.6A). We also observed that dual NOG/SB inhibition in endoderm cultures induced robust *NKX2.1* and *PAX8* expression without adding FGF2 (Fig. 3.1B, Fig. 3.6A). Thus, we wanted to determine if *NKX2.1* expression in foregut cultures was due to endogenous FGF and/or HH signaling. To test this, we inhibited the FGF or HH pathway with small molecules SU5402 (SU, 10µm) and Sant-2

(10µm) respectively (Fig. 3.6B-C). Treating foregut cultures with the FGF inhibitor SU caused a significant, robust reduction in *PAX8* and a modest reduction in *SHH*, while *NKX2.1* expression was unchanged compared to foregut control (Fig. 3.6B). Conversely, inhibition of HH signaling caused a significant reduction in *NKX2.1* expression, but not *PAX8* compared to untreated foregut. When FGF2 was added to the cultures, we observed a modest increase in *NKX2.1* expression, and when FGF was added along with Sant-2, *NKX2.1* expression was significantly reduced (Fig. 3.6C). Together our results suggest a hierarchy where FGF is upstream of SHH and PAX8, and where SHH is upstream of NKX2.1. To test if HH signaling was able to induce NKX2.1 in foregut cultures, we added the Smoothened agonist, SAG (1µM) to foregut cultures. The addition of SAG induced a 6.5 fold increase of *NKX2.1* expression above foregut controls (Fig. 3.6D). However, SAG alone did not reduce *PAX8* expression.

Based on these results, we further hypothesized that enhancing HH signaling would result in increased *NKX2.1* expression downstream of FGF, and that simultaneous inhibition of FGF signaling would reduce PAX8 expression; therefore, we inhibited endogenous FGF signaling with SU while activating HH with SAG (Fig. 3.6D). This combination caused an additional increase in *NKX2.1* expression (21 fold vs. 6.5 fold with SAG only, when compared to foregut) and a concomitant decrease in *PAX8* mRNA (Fig. 3.6D). Importantly, immunofluorescence correlated with QRT-PCR data showing an increased number of NKX2.1+ cells with the addition of SAG only. SAG+SU treated cultures showed a further increase in the number of NKX2.1 expressing cells, with ~77% of all cells expressing NKX2.1 compared to ~20% in foregut controls, and nearly undetectable levels of PAX8 expressing cells (Fig. 3.7). SAG and SAG+SU

treated cells also co-expressed FOXA2 and SOX2 confirming their endodermal origin (Fig. 3.2).

HH-induced foregut spheroids give rise to human lung organoids (HLOs)

Based on the observations that stimulating HH and inhibiting FGF signaling strongly enhances NKX2.1 expression while reducing PAX8 expression (Fig. 3.6), we tested multiple conditions of HH activation and FGF inhibition to induce $NKX2.1^{HI}/PAX8^{LO}$ foregut spheroids (NOG/SB/F/Ch) (Summarized in Fig. 3.8). Consistent with the important roles of FGF signaling in lung growth and branching morphogenesis (19-21,46-48), we found that conditions where FGF inhibition was used led to a reduction of epithelial tissue relative to mesenchymal tissue, which could be due to a loss of epithelium or an overgrowth of mesenchyme; this suggests that endogenous FGF signaling is necessary to maintain the epithelial tissue in 3D cultures (Fig. 3.9). Therefore, we also tested several conditions that stimulated HH signaling using SAG only, without FGF inhibition. We found that the most efficient method to enhance NKX2.1 expression was by adding SAG during the foregut spheroid phase (Fig. 3.10A). Comparing foregut spheroids (NOG/SB/F/Ch) with those treated with SAG (NOG/SB/F/Ch/SAG), we observed a substantial decrease in *SOX2* expression compared to NOG/SB/F/Ch spheroids and a significant increase in *NKX2.1* mRNA. Additionally, nuclear NKX2.1 protein expression was found in ECAD+ epithelium which co-expressed endoderm epithelial markers FOXA2 and SOX2 (Fig. 3.10B-C, Fig.3.11). Interestingly, during lung specification in mice, the gut tube initially expresses Sox2 throughout the endoderm, but Sox2 is down-regulated in the lung field during lung

specification and Nkx2.1 induction (20,22,49). Thus, concomitant down-regulation of *SOX2* and increased *NKX2.1* observed in SAG treated foregut spheroids is consistent with early transcriptional changes that occur during lung specification in mice.

We also observed a slight, but non-significant increase in *PAX8* transcript level in NOG/SB/F/Ch/SAG treated foregut spheroids (Fig. 3.10). Importantly, PAX8 protein expression was undetectable in NOG/SB/F/Ch/SAG treated foregut spheroids and expression remained low/undetectable throughout time in culture (Fig. 3.12). Similar to NOG/SB/F/Ch treated spheroids, the NOG/SB/F/Ch/SAG treated spheroids had a minor population of cells within the spheroids of mesodermal in origin, expressing Vimentin (VIM) (Fig. 3.13)

NOG/SB/F/Ch/SAG treated foregut spheroids were embedded in Matrigel to provide a 3D growth environment. Spheroids maintained in basal media (see methods) supplemented with 1% FBS lost ECAD+ epithelial structures and were mainly comprised of mesenchyme within 20 days of 3D culture (Fig. 3.9D,E). FGF10 is essential for branching morphogenesis and maintenance of lung progenitor cells during development as well as tissue homeostasis in the adult lung (23-25,46,47,50,51). We observed that the addition of FGF10 (500ng/mL) allowed spheroids to expand and be passaged for over 100 days. FGF10 promoted the maintenance of ECAD+ epithelial structures with less mesenchymal contributions compared to both basal and FGF inhibitor conditions (Fig. 3.10D). NOG/SB/F/Ch/SAG cultured for 15 days in FGF10 possessed abundant ECAD+ epithelium that expressed the proximal lung marker SOX2 and distal lung marker SOX9. SOX2+ domains and SOX9+ domains were distributed throughout the entire HLO as determined by whole mount immunofluorescence and

confocal Z-sections. (Fig. 3.14). FGF10 treated foregut spheroids maintained *NKX2.1* expression over time; however, consistent with mouse development, distal progenitor markers, *NMYC* and *ID2* mRNA expression decreased over time while distal Alveolar Type I and II cell markers, *HOPX* and *SFTPC* increased over time (24,26-32,52,53) (Fig. 3.10). These data suggest that HLOs pass through a stage resembling early fetal lung development in mice.

HLOs possess proximal airway-like structures

HLOs cultured longer than 2 months had striking epithelial structures resembling proximal airways, expressing proximal cell type-specific markers, including basal cells (P63), ciliated cells (FOXJ1, ACTTUB) and club cells (SCGB1A1) (Fig.3.15). Proximal-like airway tissues were often surrounded by a smooth muscle actin positive (SMA+) mesenchyme compartment. Although *P63* mRNA expression is maintained throughout culture (Fig. 3.15A), it is only in prolonged cultures (> 2 months) where the P63+ cells are spatially arranged along the basal side of the epithelial tube-like structures, adjacent to SMA+ mesenchyme, similar to human bronchi and bronchioles (Fig. 3.15B)(1,2,35,54-57). By 65 days *in vitro* (D65) proximal-like epithelial structures form a cyst-like structure that expresses P63, as determined by whole mount immunofluorescence staining and confocal z-stacks. Moreover, SMA expression is strongest at the periphery of the HLO (Fig. 3.16). P63+ proximal airway-like cells also co-express SOX2 and NKX2.1 as determined on serial sections (Fig. 3.17). Located on the luminal surface of HLO proximal airway-like structures are cells expressing the multi-ciliated cell transcription factor FOXJ1 (Fig. 3.15B). Very few cells expressed the

club cell marker SCGB1A1, and this protein was observed in a pixilated expression pattern (Fig. 3.15D). Multi-ciliated and club cell specific mRNAs, *FOXJ1* and *SCGB1A1* respectively, were significantly increased in prolonged HLO culture (Fig. 3.15A). Although the goblet cell marker *MUC5AC* mRNA expression was detected, protein expression was not detected by immunofluorescence (Fig. 3.15A and data not shown).

Although the multi-ciliated cell transcription factor FOXJ1 was abundant in proximal airway-like structures, we observed that ACTTUB was localized to the apical side of these cells, but did not appear to be localized to cilia on the apical cell surface (Fig. 3.15C), suggesting that this may represent a cell that has not fully differentiated. Others have demonstrated that robust differentiation of multi-ciliated cells from hPSCs require modified culture conditions to promote differentiation of functional cell types (7,18,36). Thus, it is possible that the HLO environment, such as Matrigel or media rich in FGF10, does not promote terminal differentiation of all cell types. In order to alter the HLO environment, we seeded NOG/SB/F/Ch/SAG foregut spheroids onto an acellular human lung matrix (18,58). Spheroids seeded on slices of acellular lung matrix predominantly gave rise to proximal airway-like structures in which stereotypical tufts of ACTTUB positive ciliated structures on the apical surface of cells were observed facing into a lumen. In serial sections, these airways had abundant FOXJ1+ cells (Fig. 3.15E). Thus, HLOs have the capacity to generate more mature ciliated cells given the correct stimulus or environment.

As noted, proximal airways are often closely associated with the SMA+ mesenchyme (Fig. 3.15B) whereas in the adult murine lung, proximal airways are also associated with Pdgfrα+ and Vim+ mesenchymal cells (59-61). Thus, we investigated

the mesenchymal population within the HLOs in more detail. Immunofluorescence revealed that D65 HLOs have both PDGFRα+/VIM+ double positive and PDGFRα-/VIM+ cell populations, which indicative of myofibroblasts and fibroblasts respectively (Fig. 3.17A). Adult murine myofibroblasts also co-express Sma and Pdgfrα whereas differentiated smooth muscle is Sma+/Pdgfra- (59-63),and we observe PDGFRα+/SMA+ and PDGFRα-/SMA+ populations of cells indicating that HLOs possess myofibroblasts and smooth muscle cells (Fig. 3.17B). The HLOs did not stain positive for SafraninO indicating there is no cartilage tissue, whereas iPSC derived teratomas had abundant cartilage (Fig. 3.17C). Taken together, the HLO mesenchymal population is diverse with myofibroblasts, fibroblasts, and smooth muscle cells.

HLOs possess immature alveolar airway-like structures

The distal lung epithelium in mouse and human make up the gas-exchanging alveoli, consisting of type I and type II alveolar epithelial cells (AECI, AECII). During development, the distal lung epithelium expresses progenitor markers including SOX9, ID2, and NMYC (1,18,37,38,52,53,64,65). All distal markers are present in the HLOs; however, *ID2* and *NMYC* are expressed at high levels in early cultures, but are down regulated in prolonged culture (Fig. 3.10F) while *SOX9* expression remains consistent across time in culture (Fig. 3.19A).

Recently, there have been major advances in mice toward defining a bipotent alveolar progenitor population during the late fetal/early neonatal period (33,34,39), and this work has highlighted the fact that many markers previously considered terminal differentiation markers are co-expressed in the bipotent progenitors. Specifically, the

AECII marker SftpC and AECI marker Hopx can be co-expressed in a bipotent progenitor before becoming committed to one lineage or the other. Moreover, we have shown that Sox9 marks an early progenitor population in the developing mouse lung and Sox9 also marks the bipotent progenitor in late fetal life (34,40,41,64). In HLOs grown in prolonged culture (> 2 months), we observed that AECII (SFTPC, SFTPB) and AECI (PDPN, HOPX) cell-type markers were present (Fig. 3.19A-B). However, we also observed that *SFTPC* levels were very low (Fig. 3.10F), and that SFTPB+ cells were rare (Fig. 3.19B). This suggested that the distal airway cells present in HLOs might be a progenitor-like population. To test this possibility, we co-stained SFTPC (AECII) or HOPX (AECI) with SOX9 and found abundant SFTPC/SOX9 and HOPX/SOX9 double positive cells (Fig. 3.19B). Co-staining in serial sections suggests that SFTPC/SOX9 double positive cells are also NKX2.1+ (Fig. 3.20). In contrast these co-expressing cells were not found in the adult human lung (Fig. 3.19C). Although rare, the few SFTPB+ observed in HLOs resemble AECII cells seen in the adult human lung, and PDPN+ cells resembled the elongated AECI cells in the human lung (Fig. 3.19B-C). In order to improve confidence that cells expressing AECII markers are AECII cells, we used transmission electron microscopy (TEM) to determine if HLOs possessed cells containing lamellar bodies, which are necessary for surfactant protein trafficking and secretion (66-68). Using TEM, we observed lamellar bodies both in cells within HLOs, and in open spaces between cells, indicating that lamellar bodies are being secreted (Fig. 3.19D). Taken together, our data suggests that HLOs predominantly possess an undifferentiated alveolar progenitor cells with rare differentiated AECI and AECII cells interspersed throughout the distal-like tissue.

Quantitative assessment of HLO composition

We have shown that HLOs have both proximal-like and distal-like epithelium in addition to surrounding mesenchymal tissue. In order to better gauge the composition of HLOs, we performed a detailed quantitative analysis of cell types and structures. We sectioned 48 individual HLOs, and examined them for P63+ proximal airway-like structures (as shown in Fig. 3.15B-D), and distal-airway like structures (as shown in Fig. 3.20). We found that 39/48 (81%) of the HLOs have proximal airway epithelial structures while 48/48 (100%) of HLOs have distal airway-like structures (Fig. 3.21). We then calculated the average cross-sectional area of comprised of P63+ proximal airway-like and P63- distal airway-like tissue and found that proximal structures comprised 14.5% (+/- 0.6%) of the entire area of the HLO, whereas 85.5% (+/- 0.6%) were distal in nature (including epithelium and mesenchyme) (Fig. 3.21B). To determine the percentage of certain cell types within an HLO, we sectioned and stained 15 individual HLOs (n=15) and counted cells positive for specific markers, and the total number of Dapi+ nuclei within a section (Fig. 3.21C-G). On average, 57% of all cells in the HLOs were NKX2.1+ (Fig. 3.21C), 39% of all cells were P63+, 3% were FOXJ1+, 5% were SFTPC+ 4% of all cells were HOPX+ (Fig. 3.21D-G).

HLOs are globally similar to human fetal lung

Accumulating evidence suggests that HLOs are immature. For example, distal progenitor markers are initially robustly expressed whereas SFTPC expression is very low across time in HLOs (Fig. 3.10E), FOXJ1+ cells do not appear to form mature multi-

ciliated structures until placed onto a decelluarized lung matrix (Fig. 3.15B, E) and rare SCGB1A1+ cells do not resemble mature club cells (Fig. 3.15D). Moreover, the majority of the distal-like epithelium expresses bipotent progenitor markers (Fig. 3.18). In order to directly address the maturity of HLOs, we conducted RNA-sequencing (RNAseq) on HLOs (n=6; 3 D65 HLOs, 3 D110 HLOs), on undifferentiated hESCs and on definitive endoderm. We also took advantage of publicly available RNAseq datasets for human fetal lung representing a range of gestational stages, and for adult human lung (Table 3.1). In order to determine global similarity among these tissues relative to HLOs, we conducted principal component (PC) analysis (Fig. 3.22 A,B)(69), hierarchical clustering (Fig. 3.22C)(70) and Spearmans rank-order correlation matrix analysis (Fig. 3.22D) of the complete tabulated FPKM matrix generated from RNA sequences datasets and representing the total gene expression complement in each sample (71). Consistent across all three types of informatics analysis, transcriptional activity in the HLOs shares the greatest degree of similarity to human fetal lung. These data strongly suggest that global transcription of HLOs is highly similar to human fetal lung, and support the idea that HLOs are in a less differentiated, fetal state when grown in the conditions described here.

Discussion

To date, a number of groups have defined methods to generate lung specific cell types utilizing 2D culture systems (5,6,8-11,18). Although lung lineage cells have been generated with varying efficiency (~30-80% NKX2.1+ cells (5-7)) and can generate both both proximal (~5-36% of cells (5-7))and distal cell types (up to ~50% of cells (6)) with

varying efficiency, proper spatial organization of the cell types and specific tissue morphology have not been reported in 2D systems. Here, we show that HLOs possess both mesenchymal and lung epithelial (~60% NKX2.1+) cells with proximal airway-like structures that possess P63+ (~40%) and FOXJ1+ cells (~3%) along with distal airway-like structures that possess SFTPC+ (~5%) and HOPX+ (~4%) cells.

It is currently unclear if 2D culture systems described have the capability to give rise to mesodermal lineages. Thus, HLOs allow one to address questions regarding spatial tissue organization and epithelial-mesenchymal interactions. Since HLOs form organized structures that resemble bronchi and bronchioles with adjacent mesenchyme, these complex, organized tissues may allow exploration, for example, of airway remodeling after injury. Moreover, the spatial arrangement of specific cell types will be critical to study proximal airway dynamics during homeostasis and injury. For example, the location of P63+ cells adjacent to FOXJ1+ cells in the HLOs will be necessary to study basal cell differentiation into different proximal airway cell types during homeostasis or after injury. In addition to tissue morphology and structure during prolonged culture, the HLOs consist of both epithelium and mesenchyme in early cultures that are maintained over time. Since lung development requires extensive cross talk between the epithelium and mesenchyme in order to regulate developmental processes, proliferation and differentiation, HLOs may be an ideal *in vitro* system to study these complex tissue-tissue interactions.

Recently, there has been a push to define progenitor populations during lung development and adult homeostasis in order to better understand differentiation and the transition between branching and alveolarization. Two groups have defined a bipotent

progenitor population in the embryonic/neonatal lung that gives rise to both AECI and AECII cells (33,34). These bipotent cells express the distal progenitor marker Sox9 along with differentiation markers of AECI and AECII cells, including SftpC, HopX, and Pdpn. We demonstrate that HLOs expressed both AECI and II markers; however, the majority of these cells also expressed SOX9 suggesting that the majority of the distal epithelium is comprised of bipotent progenitors. Thus, HLOs will allow us to gain insight into this bipotent population, explore how bipotent progenitors are regulated, and define the mechanisms of how fate-decisions are made as terminal differentiation occurs. For example, it will allow us to examine signaling pathways or transcription factors that instruct the bipotent progenitor to differentiate into a mature AECII cell, instead of an AECI cell.

The evidence supporting that HLOs are fetal in nature could reflect the fact that a block to full maturation exists *in vitro,* as is the case with other endoderm lineage organoids (intestinal and gastric), which appear to be immature. That is, while they possess committed lineage-specific cell types, the cells may not exhibit fully matured adult-like function (16,72). This is also the case for pancreatic β-like cells and hepatocyte-like cells generated *in vitro* (4,73). Alternatively, the progenitor state may reflect the high levels of FGF10 in the culture media, since FGF10 is known to maintain progenitor cells in the lung (74,75). Given that HLOs are similar to human fetal lung, this tissue is an ideal model to study lung maturation of both the proximal and distal epithelium along with epithelial-mesenchymal interactions in a developmental context.

While the multi-lineage, multi-cellular composition of HLOs is a major advantage, one of the caveats to this system is that HLOs do not appear to undergo *bona fide*

branching morphogenesis or possess transitional zones found in the adult lung, such as the bronchioalveolar ductal junction (BADJ). The HLOs possess proximal SOX2+ domain and distal SOX9+ domains observed during branching morphogenesis, but this regionalization occurs without setting up the stereotyped branching pattern. This may be due to the fact that the organoids are surrounded by media supplemented with FGF10 compared to the *in vivo* situation where FGF10 is expressed in a dynamic, spatially restricted manner in the distal mesenchyme(48,74,76). However, it has recently been demonstrated that localized expression FGF10 is not required for branching (51), so this may not be the reason HLOs don't branch. Alternatively, similar to other endoderm-derived organoid models, HLOs lack several components of the native organ, including immune cells, vasculature, and innervation. Thus, it is possible that cellular inputs important for branching morphogenesis are missing from HLOs. Indeed, recent reports have shown that innervation is required for proper branching(77), and while vasculature may not be important for lung branching(78), others have shown the vascular endothelium is required to induce a branching-like program of isolated airway epithelium in 3D cultures (79). Lastly, the microenvironment is essential for branching morphogenesis to occur including dynamic changes in the extracellular matrix around branching lung bud tips where the ECM is constantly changing and interacting with the cytoskeleton of the branching epithelium in order to facilitate cell movement and branching bifurcations (80-82). It is possible that in the future, co-culture with additional cellular inputs may prove to enhance HLO branching.

Taken together, we describe here a novel system to generate human lung organoids from human pluripotent stem cells. HLOs possess both mesenchymal and

epithelial lineages, as well as organized proximal airway structures with multiple cell types and surrounded by mesenchyme. HLOs also possess distal epithelial cells that are reminiscent of a bipotent alveolar progenitor cell recently described in mice which is likely a reflection of the similarities of HLOs to the human fetal lung. We believe that HLOs will be an excellent new human system to model lung differentiation, homeostasis and disease *in vitro*.

Materials and Methods

Maintenance of hESCs

Human ES cell lines H1 (NIH registry #0043) and H9 (NIH registry #0062) were obtained from WiCell Research Institute. Human ES line UM77-2 (NIH registry #0278) was obtained from the University of Michigan. iPSC lines 3-5 and 20-1 were generated at Cincinnati Children's Hospital and have been previously described (1). Stem cells were maintained on Matrigel (BD Biosciences) in mTesR1 medium (STEM CELL Technologies). HESCs were passaged as previously described (1).

Differentiation of PSCs into definitive endoderm

Differentiation into definitive endoderm was carried out as previously described (1,42). Briefly, a 4-day Activin A (R&D systems) differentiation protocol was used. Cells were treated with Activin A (100 ng ml^{-1}) for three consecutive days in RPMI 1640 media (Life Technologies) with increasing concentrations of 0%, 0.2% and 2% HyClone defined fetal bovine serum (dFBS, Thermo Scientific).

Differentiation of definitive endoderm into anterior foregut

After differentiation into definitive endoderm, foregut endoderm was differentiated, essentially as described (18). Briefly, cells were incubated in foregut media: Advanced DMEM/F12 plus N-2 and B27 supplement, 10mM Hepes, 1x L-Glutamine (200mM), 1x Penicillin-streptomycin (5,000 U/mL, all from Life Technologies) with 200ng/mL Noggin (NOG, R&D Systems) and 10µM SB431542 (SB, Stemgent) for 4 days. For long term maintenance, cultures were maintain in “basal” foregut media without NOG and SB, or in the presence of growth factors including 50, 500 ng/mL FGF2 (R&D systems), 10µM Sant-2 (Stemgent), 10µM SU5402 (SU, Stemgent), 100 ng/mL SHH (R&D systems), and SAG (Enzo Life Sciences) for 8 days.

Directed differentiation into anterior foregut spheroids and lung organoids

After differentiation into definitive endoderm, cells were incubated in foregut media with NOG, SB, 500ng/mL FGF4 (R&D Systems), and 2 µM CHIR99021 (Chiron, Stemgent) for 4-6 days. After 4 days with treatment of growth factors, three-dimensional floating spheroids were present in the culture. Three-dimensional spheroids were transferred into Matrigel to support 3D growth as previously described (83). Briefly, spheroids were embedded in a droplet of Matrigel (BD Bioscience #356237) in one well of a 24 well plate, and incubated at room temperature for 10 minutes. After the Matrigel solidified, foregut media with 1% Fetal bovine serum (FBS, CAT#: 16000-044, Life Technologies) or other growth factors and small molecules were overlaid and replaced every 4 days. Organoids were transferred into new Matrigel droplets every 10 to 15 days.

Immunohistochemistry

Immunostaining was carried out as previously described (64,84). Antibody information and dilutions can be found in Table 3.2. All images were taken on a Nikon A1 confocal microscope or an Olympus IX71 epifluorescent microscope.

RNA extraction and qRT-PCR

RNA was extracted from monolayers, spheroids, and organoids using a MagMAX-96 Total RNA Isolation Kit (Life Technologies) and MAG Max Express (Applied Biosystems). RNA quantity and quality were determined spectrophotometrically, using a Nano Drop 2000 (Thermoscientific). Reverse transcription was conducted using the SuperScript VILO kit (Invitrogen), according to manufacturer's protocol. Finally, qRT-PCR was carried out using Quantitect Sybr Green MasterMix (Qiagen) on a Step One Plus Real-Time PCR system (Life Technologies). For a list of primer sequences see Table 3.3.

Seeding lung spheroids on decellularized human lung matrices

Human lungs deemed to be unsuitable for lung transplantation were obtained from beating-heart (or warm autopsy) donors through Gift of Life Michigan and lungs were decellularized as previously described (58). Slices were prepared using a sterile tissue punch (Fisher) and sterilized with 0.18% peracetic acid and 4.8% EtOH. Matrix slices were placed in a 96 well plate and approximately 50 NOG+SB+F+Ch+SAG spheres were pipetted directly onto the matrices. Samples were centrifuged for 2min at

2000rpm and then incubated at 37C for 30min without media. Foregut media supplemented with 1%FBS and 500ng/mL FGF10 was then added to the matrices. Media was changed daily.

Transmission Electron Microscopy

D50 HLOs were processed as previously described (64,85). 70nm sections were sections were imaged using a Philips CM-100 electron microscope.

Area and Cell Quantification

HLOs with P63+ cells were counted as having proximal airway-like epithelium and HLOs with SFTPC+ cells were counted as having distal airway-like epithelium. The area of proximal epithelium was determined by P63+ECAD+ staining. Area was measured using ImageJ software. Cell quantification of NKX2.1, P63, and DAPI was counted by Metamorph cell counting software. FOXJ1, SFTPC, and HOPX were counted in ImageJ using the cell counter plugin.

Statistical Analysis and Experimental Replicates

All immunofluorescence and qRT-PCR experiments were carried out at least two times with three (n=3) independent biological samples per experiment. The only exceptions to this were experiments that included human adult lung samples in the analysis. For these experiments, n=1 biological human lung sample was used in statistical replicates (triplicates) whereas all other samples used biological replicates (n=3). For quantification in Fig. 3.21, a total of 48 different HLOs (n=48) were counted

for HLO composition. For the proximal epithelial area, 29 different HLOs were counted (n=29). For cell quantification, 15 different HLOs were counted (n=15). Statistical differences between groups were assessed with Prism software, using multiple t tests. All error bars represent SEM. Results were considered statistically significant at $P < 0.05$.

RNA Sequencing and Analysis

Sequencing of HLOs (n=3 D65, n=3 D110) was performed by the University of Michigan DNA Sequencing Core, using the Illumina Hi-Seq platform. Sequencing of H9 Stem Cells (SC) and Definitive Endoderm (DE) was performed by the University of California, San Francisco DNA Sequencing Core using the Illumina Hi-Seq platform. All sequences were deposited in the EMBL-EBI ArrayExpress database using Annotare 2.0 and are catalogued under the accession number E-MTAB-3339 for the HLOs and E-MTAB-3158 for SC and DE. The University of Michigan Bioinformatics Core obtained the reads files and concatenated those into a single .fastq file for each sample. The Bioinformatics Core also downloaded reads files from EBI-AE database (Adult lung Samples) and NCBI-GEO (SRA) database (Fetal lung samples) (Supplemental Table 3.1). The quality of the raw reads data for each sample was evaluated using FastQC (version 0.10.1) to identify features of the data that may indicate quality problems (e.g. low quality scores, over-represented sequences, inappropriate GC content, etc.). Initial QC report indicated over-representation of Illumina adapter sequences in samples from EBI-AE data set and NCBI-GEO data set. Adapter sequences were trimmed from the reads using Cutadapt (version 0.9.5)(86). Briefly, we aligned reads to the reference

transcriptome (UCSC hg19) using TopHat (version 2.0.9) and Bowtie (version 2.1.0.0)(87). We used Cufflinks/CuffNorm (version 2.2.1) for expression quantitation and differential expression analysis(88), using UCSC hg19.fa as the reference genome sequence and UCSC hg19.gtf as the reference transcriptome annotation. For this analysis, we used parameter settings: “–multi-read-correct” to adjust expression calculations for reads that map in more than one locus, as well as “–compatible-hits-norm” and “–upper-quartile –norm” for normalization of expression values. Normalized FPKM tables were generated using the CuffNorm function found in Cufflinks. Transcriptional quantitation analysis in Cufflinks was conducted using the 64-bit Debian Linux stable version 7.8 ("Wheezy") platform. The complete FPKM matrix, containing frequency counts for all 24,010 genes contained in the reference genome for all 23 RNAseq samples, was evaluated using unscaled principle component analysis (PCA) to visualize and quantify multi-dimensional variation between samples(69). Of the 24,010 genes annotated in the reference genome, 2,815 (11.7%) were not detected in the RNAseq analysis of any of the 23 samples. Principle components were calculated using the function ’prcomp’ found in the R (version 3.1.2) statistical programming language (http://www.R-project.org/) and plotted using the R package ’ggplot2’ (89). Hierarchical cluster analysis based on the Canberra distance(70) between FPKM vectors was used to classify discrete RNAseq samples according to the degree of total transcriptional dissimilarity indicated by the normalized FPKM values. Bootstrap analysis was used to assess the uncertainty in the assigned hierarchical clustering relationships. 10,000 bootstraping iterations were generated by repeatedly randomly sampling the FPKM dataset. The bootstrap probability (BP) of a cluster is defined as the frequency of a

given relationship among the bootstrap replicates. Multiscale bootstrap resampling was used to calculate an approximately unbiased (AU) p-value for a given relationship, with AU > 95 indicating a high degree of statistical significance. Analyses were conducted using R package 'pvclust'(90). Spearman correlation was applied as an additional assessment of the cumulative degree of correlation among RNAseq datasets. In addition, we computed Spearman rank correlation coefficients (ρ) in a pairwise manner among all 23 RNAseq samples using the complete normalized FPKM data. The Spearman coefficients were plotted as a heatmap using the function 'heatmap.2' in the R package 'gplots' (http://CRAN.R-project.org/package=gplots). Complete data analysis scripts are available at https://github.com/hilldr/HLO_eLife2015.

Acknowledgements

JRS is supported by the NHLBI (R21HL115372, R01HL119215), and by career development grants from the NIDDK (K01DK091415) and the March of Dimes (Basil O'Connor starter scholar award).

References

1. Spence JR, Mayhew CN, Rankin SA, Kuhar MF, Vallance JE, Tolle K, Hoskins EE, Kalinichenko VV, Wells SI, Zorn AM, Shroyer NF, Wells JM. Directed differentiation of human pluripotent stem cells into intestinal tissue in vitro. Nature. 2011 Feb 3;470(7332):105–9. PMCID: PMC3033971

2. D'Amour KA, Agulnick AD, Eliazer S, Kelly OG, Kroon E, Baetge EE. Efficient differentiation of human embryonic stem cells to definitive endoderm. Nat Biotechnol. 2005 Oct 28;23(12):1534–41.

3. Kroon E, Martinson LA, Kadoya K, Bang AG, Kelly OG, Eliazer S, Young H, Richardson M, Smart NG, Cunningham J, Agulnick AD, D'Amour KA, Carpenter MK, Baetge EE. Pancreatic endoderm derived from human embryonic stem cells generates glucose-responsive insulin-secreting cells in vivo. Nat Biotechnol. 2008 Feb 20;26(4):443–52.

4. Si-Tayeb K, Noto FK, Nagaoka M, Li J, Battle MA, Duris C, North PE, Dalton S, Duncan SA. Highly efficient generation of human hepatocyte-like cells from induced pluripotent stem cells. Hepatology. 2009 Oct 1;51(1):297–305. PMCID: PMC2946078

5. Wong AP, Bear CE, Chin S, Pasceri P, Thompson TO, Huan L-J, Ratjen F, Ellis J, Rossant J. Directed differentiation of human pluripotent stem cells into mature airway epithelia expressing functional CFTR protein. Nat Biotechnol. 2012 Aug 26.

6. Huang SXL, Islam MN, O'Neill J, Hu Z, Yang Y-G, Chen Y-W, Mumau M, Green MD, Vunjak-Novakovic G, Bhattacharya J, Snoeck H-W. efficient generation of lung and airway epithelial cells from human pluripotent stem cells. Nat Biotechnol. Nature Publishing Group; 2013 Dec 1;:1–11. PMCID: PMC4101921

7. Firth AL, Dargitz CT, Qualls SJ, Menon T, Wright R, Singer O, Gage FH, Khanna A, Verma IM. Generation of multiciliated cells in functional airway epithelia from human induced pluripotent stem cells. Proceedings of the National Academy of Sciences. 2014 Apr 29;111(17):E1723–30. PMCID: PMC4035971

8. Mou H, Zhao R, Sherwood R, Ahfeldt T, Lapey A, Wain J, Sicilian L, Izvolsky K, Musunuru K, Cowan C, Rajagopal J. Generation of Multipotent Lung and Airway Progenitors from Mouse ESCs and Patient-Specific Cystic Fibrosis iPSCs. Cell Stem Cell. 2012 Apr 6;10(4):385–97. PMCID: PMC3474327

9. Ghaedi M, Calle EA, Mendez JJ, Gard AL, Balestrini J, Booth A, Bove PF, Gui L, White ES, Niklason LE. Human iPS cell-derived alveolar epithelium repopulates lung extracellular matrix. J. Clin. Invest. 2013 Nov 1;123(11):4950–62. PMCID: PMC3809786

10. Kadzik RS, Morrisey EE. Directing lung endoderm differentiation in pluripotent

stem cells. Cell Stem Cell. 2012 Apr 6;10(4):355–61. PMCID: PMC3366272

11. Longmire TA, Ikonomou L, Hawkins F, Christodoulou C, Cao Y, Jean JC, Kwok LW, Mou H, Rajagopal J, Shen SS, Dowton AA, Serra M, Weiss DJ, Green MD, Snoeck H-W, Ramirez MI, Kotton DN. Efficient derivation of purified lung and thyroid progenitors from embryonic stem cells. Cell Stem Cell. 2012 Apr 6;10(4):398–411. PMCID: PMC3322392

12. Lancaster MA, Renner M, Martin C-A, Wenzel D, Bicknell LS, Hurles ME, Homfray T, Penninger JM, Jackson AP, Knoblich JA. Cerebral organoids model human brain development and microcephaly. Nature. 2013 Sep 19;501(7467):373–9. PMCID: PMC3817409

13. Takebe T, Sekine K, Enomura M, Koike H, Kimura M, Ogaeri T, Zhang RR, Ueno Y, Zheng YW, Koike N, Aoyama S, Adachi Y, Taniguchi H. Vascularized and functional human liver from an iPSC-derived organ bud transplant. Nature. 2013 Jul 25;499(7459):481–4.

14. Nakano T, Ando S, Takata N, Kawada M, Muguruma K, Sekiguchi K, Saito K, Yonemura S, Eiraku M, Sasai Y. Self-formation of optic cups and storable stratified neural retina from human ESCs. Cell Stem Cell. 2012 Jun 14;10(6):771–85.

15. Meyer JS, Howden SE, Wallace KA, Verhoeven AD, Wright LS, Capowski EE, Pinilla I, Martin JM, Tian S, Stewart R, Pattnaik B, Thomson JA, Gamm DM. Optic vesicle-like structures derived from human pluripotent stem cells facilitate a customized approach to retinal disease treatment. Stem Cells. 2011 Aug;29(8):1206–18. PMCID: PMC3412675

16. McCracken KW, Catá EM, Crawford CM, Sinagoga KL, Schumacher M, Rockich BE, Tsai Y-H, Mayhew CN, Spence JR, Zavros Y, Wells JM. Modelling human development and disease in pluripotent stem-cell-derived gastric organoids. Nature. Nature Publishing Group; 2014 Oct 29;:1–19.

17. Wells JM, Spence JR. How to make an intestine. Development. 2014 Feb;141(4):752–60. PMCID: PMC3912826

18. Green MD, Chen A, Nostro M-C, d'Souza SL, Schaniel C, Lemischka IR, Gouon-Evans V, Keller G, Snoeck H-W. Generation of anterior foregut endoderm from human embryonic and induced pluripotent stem cells. Nat Biotechnol. Nature Publishing Group; 2011 Feb 27;:1–7.

19. Rankin SA, Zorn AM. Gene Regulatory Networks Governing Lung Specification. J Cell Biochem. 2014 Mar 19.

20. Hebrok M, Kim SK, Melton DA. Notochord repression of endodermal Sonic hedgehog permits pancreas development. Genes & Development. 1998.

21. Morrisey EE, Hogan BLM. Preparing for the First Breath: Genetic and Cellular Mechanisms in Lung Development. Developmental Cell. Elsevier Inc; 2010 Jan 19;18(1):8–23. PMCID: PMC3736813

22. Serls AE. Different thresholds of fibroblast growth factors pattern the ventral foregut into liver and lung. Development. 2004 Dec 2;132(1):35–47.

23. Motoyama J, Liu J, Mo R, Ding Q, Post M, Hui CC. Essential function of Gli2 and Gli3 in the formation of lung, trachea and oesophagus. Nat Genet. 1998 Sep;20(1):54–7.

24. Li Y, Zhang H, Choi SC, Litingtung Y, Chiang C. Sonic hedgehog signaling regulates Gli3 processing, mesenchymal proliferation, and differentiation during mouse lung organogenesis. Developmental Biology. 2004 Jun 1;270(1):214–31.

25. Bellusci S, Furuta Y, Rush MG, Henderson R, Winnier G, Hogan BL. Involvement of Sonic hedgehog (Shh) in mouse embryonic lung growth and morphogenesis. Development. 1997 Jan;124(1):53–63.

26. Kimura S, Hara Y, Pineau T, Fernandez-Salguero P, Fox CH, Ward JM, Gonzalez FJ. The T/ebp null mouse: thyroid-specific enhancer-binding protein is essential for the organogenesis of the thyroid, lung, ventral forebrain, and pituitary. Genes & …. 1996.

27. Yuan B, Li C, Kimura S, Engelhardt RT, Smith BR, Minoo P. Inhibition of distal lung morphogenesis inNkx2.1(?/?) embryos. Dev. Dyn. 2000 Feb;217(2):180–90.

28. Narumi S, Araki S, Hori N, Muroya K, Yamamoto Y, Asakura Y, Adachi M, Hasegawa T. Functional characterization of four novel PAX8 mutations causing congenital hypothyroidism: new evidence for haploinsufficiency as a disease mechanism. Eur. J. Endocrinol. 2012 Nov;167(5):625–32.

29. Vilain C, Rydlewski C, Duprez L, Heinrichs C, Abramowicz M, Malvaux P, Renneboog B, Parma J, Costagliola S, Vassart G. Autosomal dominant transmission of congenital thyroid hypoplasia due to loss-of-function mutation of PAX8. J. Clin. Endocrinol. Metab. 2001 Jan;86(1):234–8.

30. Mansouri A, Chowdhury K, Gruss P. Follicular cells of the thyroid gland require Pax8 gene function. Nat Genet. 1998 May;19(1):87–90.

31. Kusakabe T, Kawaguchi A, Hoshi N, Kawaguchi R, Hoshi S, Kimura S. Thyroid-specific enhancer-binding protein/NKX2.1 is required for the maintenance of ordered architecture and function of the differentiated thyroid. Mol. Endocrinol. 2006 Aug;20(8):1796–809. PMCID: PMC2588428

32. Carré A, Szinnai G, Castanet M, Sura-Trueba S, Tron E, Broutin-L'Hermite I, Barat P, Goizet C, Lacombe D, Moutard M-L, Raybaud C, Raynaud-Ravni C, Romana S, Ythier H, Léger J, Polak M. Five new TTF1/NKX2.1 mutations in

brain–lung–thyroid syndrome: rescue by PAX8 synergism in one case. Human molecular …. 2009.

33. Desai TJ, Brownfield DG, Krasnow MA. Alveolar progenitor and stem cells in lung development, renewal and cancer. Nature. 2014 Feb 5.

34. Treutlein B, Brownfield DG, Wu AR, Neff NF, Mantalas GL, Espinoza FH, Desai TJ, Krasnow MA, Quake SR. Reconstructing lineage hierarchies of the distal lung epithelium using single-cell RNA-seq. Nature. 2014 May 15;509(7500):371–5. PMCID: PMC4145853

35. Zhang M, Wang H, Teng H, Shi J, Zhang Y. Expression of SHH signaling pathway components in the developing human lung. Histochem. Cell Biol. 2010 Oct;134(4):327–35.

36. Loh KM, Ang LT, Zhang J, Kumar V, Ang J, Auyeong JQ, Lee KL, Choo SH, Lim CYY, Nichane M, Tan J, Noghabi MS, Azzola L, Ng ES, Durruthy-Durruthy J, Sebastiano V, Poellinger L, Elefanty AG, Stanley EG, Chen Q, Prabhakar S, Weissman IL, Lim B. Efficient endoderm induction from human pluripotent stem cells by logically directing signals controlling lineage bifurcations. Cell Stem Cell. 2014 Feb 6;14(2):237–52. PMCID: PMC4045507

37. Xue X, Ramakrishnan S, Anderson E, Taylor M, Zimmermann EM, Spence JR, Huang S, Greenson JK, Shah YM. Endothelial PAS Domain Protein 1 Activates the Inflammatory Response in the Intestinal Epithelium to Promote Colitis in Mice. Gastroenterology. 2013 Jul 13. PMCID: PMC3799890

38. Chen Y-J, Finkbeiner SR, Weinblatt D, Emmett MJ, Tameire F, Yousefi M, Yang C, Maehr R, Zhou Q, Shemer R, Dor Y, Li C, Spence JR, Ben Z Stanger. De Novo Formationof Insulin-Producing "'Neo-b Cell Islets'" from Intestinal Crypts. Cell Rep. The Authors; 2014 Mar 4;:1–13. PMCID: PMC4245054

39. Chambers SM, Fasano CA, Papapetrou EP, Tomishima M, Sadelain M, Studer L. Highly efficient neural conversion of human ES and iPS cells by dual inhibition of SMAD signaling. Nat Biotechnol. 2009 Mar 1;27(3):275–80. PMCID: PMC2756723

40. Monaghan AP, Kaestner KH, Grau E, Schütz G. Postimplantation expression patterns indicate a role for the mouse forkhead/HNF-3 alpha, beta and gamma genes in determination of the definitive endoderm, chordamesoderm and neuroectoderm. Development. 1993 Nov;119(3):567–78.

41. Ang SL, Rossant J. HNF-3 beta is essential for node and notochord formation in mouse development. Cell. 1994 Aug 26;78(4):561–74.

42. D'Amour KA, Agulnick AD, Eliazer S, Kelly OG, Kroon E, Baetge EE. Efficient differentiation of human embryonic stem cells to definitive endoderm. Nat Biotechnol [Internet]. 2005 Oct 28;23(12):1534–41. Retrieved from:

http://www.nature.com/nbt/journal/v23/n12/abs/nbt1163.html

43. Stott SRW, Metzakopian E, Lin W, Kaestner KH, Hen R, Ang SL. Foxa1 and Foxa2 Are Required for the Maintenance of Dopaminergic Properties in Ventral Midbrain Neurons at Late Embryonic Stages. Journal of Neuroscience. 2013 May 1;33(18):8022–34.

44. D'Amour KA, Bang AG, Eliazer S, Kelly OG, Agulnick AD, Smart NG, Moorman MA, Kroon E, Carpenter MK, Baetge EE. Production of pancreatic hormone-expressing endocrine cells from human embryonic stem cells. Nat Biotechnol. 2006 Nov;24(11):1392–401.

45. DeLaForest A, Nagaoka M, Si-Tayeb K, Noto FK, Konopka G, Battle MA, Duncan SA. HNF4A is essential for specification of hepatic progenitors from human pluripotent stem cells. Development. 2011 Oct;138(19):4143–53.

46. Min H, Danilenko DM, Scully SA, Bolon B, Ring BD, Tarpley JE, DeRose M, Simonet WS. Fgf-10 is required for both limb and lung development and exhibits striking functional similarity to Drosophila branchless. Genes & Development. 1998 Oct 15;12(20):3156–61. PMCID: PMC317210

47. Weaver M, Dunn NR, Hogan BL. Bmp4 and Fgf10 play opposing roles during lung bud morphogenesis. Development. 2000 Jun;127(12):2695–704.

48. Abler LL, Mansour SL, Sun X. Conditional gene inactivation reveals roles for Fgf10 and Fgfr2 in establishing a normal pattern of epithelial branching in the mouse lung. Dev. Dyn. 2009 Aug;238(8):1999–2013.

49. Domyan ET, Ferretti E, Throckmorton K, Mishina Y, Nicolis SK, Sun X. Signaling through BMP receptors promotes respiratory identity in the foregut via repression of Sox2. Development. 2011 Feb 8;138(5):971–81. PMCID: PMC4074297

50. Agha El E, Herold S, Alam Al D, Quantius J, MacKenzie B, Carraro G, Moiseenko A, Chao CM, Minoo P, Seeger W, Bellusci S. Fgf10-positive cells represent a progenitor cell population during lung development and postnatally. Development. 2013 Dec 18. PMCID: PMC3879811

51. Volckaert T, Campbell A, Dill E, Li C, Minoo P, De Langhe S. Localized Fgf10 expression is not required for lung branching morphogenesis but prevents differentiation of epithelial progenitors. …. 2013.

52. Okubo T. Nmyc plays an essential role during lung development as a dosage-sensitive regulator of progenitor cell proliferation and differentiation. Development. 2005 Feb 9;132(6):1363–74.

53. Rawlins EL, Clark CP, Xue Y, Hogan BLM. The Id2+ distal tip lung epithelium contains individual multipotent embryonic progenitor cells. Development. 2009 Nov;136(22):3741–5. PMCID: PMC2766341

54. Evans MJ, Van Winkle LS, Fanucchi MV, Plopper CG. Cellular and molecular characteristics of basal cells in airway epithelium. Exp. Lung Res. 2001 Jul;27(5):401–15.

55. Rock JR, Onaitis MW, Rawlins EL, Lu Y, Clark CP, Xue Y, Randell SH, Hogan BLM. Basal cells as stem cells of the mouse trachea and human airway epithelium. Proceedings of the National Academy of Sciences. 2009 Aug 4;106(31):12771–5. PMCID: PMC2714281

56. Nakajima M, Kawanami O, Jin E, Ghazizadeh M, Honda M, Asano G, Horiba K, Ferrans VJ. Immunohistochemical and ultrastructural studies of basal cells, Clara cells and bronchiolar cuboidal cells in normal human airways. Pathol. Int. 1998 Dec;48(12):944–53.

57. Boers JE, Ambergen AW, Thunnissen FB. Number and proliferation of basal and parabasal cells in normal human airway epithelium. American Journal of Respiratory and Critical Care Medicine. 1998 Jun;157(6 Pt 1):2000–6.

58. Booth AJ, Hadley R, Cornett AM, Dreffs AA, Matthes SA, Tsui JL, Weiss K, Horowitz JC, Fiore VF, Barker TH, Moore BB, Martinez FJ, Niklason LE, White ES. Acellular normal and fibrotic human lung matrices as a culture system for in vitro investigation. American Journal of Respiratory and Critical Care Medicine. 2012 Nov 1;186(9):866–76. PMCID: PMC3530219

59. Chen L, Acciani T, Le Cras T, Lutzko C, Perl A-KT. Dynamic regulation of platelet-derived growth factor receptor α expression in alveolar fibroblasts during realveolarization. American Journal of Respiratory Cell and Molecular Biology. 2012 Oct;47(4):517–27. PMCID: PMC3488620

60. Hinz B, Phan SH, Thannickal VJ, Galli A, Bochaton-Piallat M-L, Gabbiani G. The myofibroblast: one function, multiple origins. The American Journal of Pathology. 2007 Jun;170(6):1807–16. PMCID: PMC1899462

61. Boucherat O, Benachi A, Barlier-Mur A-M, Franco-Montoya M-L, Martinovic J, Thébaud B, Chailley-Heu B, Bourbon JR. Decreased lung fibroblast growth factor 18 and elastin in human congenital diaphragmatic hernia and animal models. American Journal of Respiratory and Critical Care Medicine. 2007 May 15;175(10):1066–77.

62. Leslie KO, Mitchell JJ, Woodcock-Mitchell JL, Low RB. Alpha smooth muscle actin expression in developing and adult human lung. Differentiation. 1990 Aug;44(2):143–9.

63. Low RB, White SL. Lung smooth muscle differentiation. Int. J. Biochem. Cell Biol. 1998 Aug;30(8):869–83.

64. Rockich BE, Hrycaj SM, Shih H-P, Nagy MS, Ferguson MAH, Kopp JL, Sander M, Wellik DM, Spence JR. Sox9 plays multiple roles in the lung epithelium during

branching morphogenesis. Proceedings of the National Academy of Sciences. 2013 Nov 4. PMCID: PMC3839746

65. Chang DR, Martinez Alanis D, Miller RK, Ji H, Akiyama H, McCrea PD, Chen J. Lung epithelial branching program antagonizes alveolar differentiation. Proceedings of the National Academy of Sciences. 2013 Sep 20.

66. Weaver TE, Na C-L, Stahlman M. Biogenesis of lamellar bodies, lysosome-related organelles involved in storage and secretion of pulmonary surfactant. Seminars in Cell & Developmental Biology. 2002 Aug;13(4):263–70.

67. Schmitz G, Müller G. Structure and function of lamellar bodies, lipid-protein complexes involved in storage and secretion of cellular lipids. J. Lipid Res. 1991 Oct;32(10):1539–70.

68. Stahlman MT, Gray MP, Falconieri MW, Whitsett JA, Weaver TE. Lamellar body formation in normal and surfactant protein B-deficient fetal mice. Lab. Invest. 2000 Mar;80(3):395–403.

69. Ringnér M. What is principal component analysis? Nat Biotechnol. 2008 Mar;26(3):303–4.

70. Eisen MB, Spellman PT, Brown PO, Botstein D. Cluster analysis and display of genome-wide expression patterns. Proceedings of the …. 1998.

71. Daxin Jiang, Chun Tang, Aidong Zhang. Cluster analysis for gene expression data: a survey. IEEE Trans. Knowl. Data Eng. 2004 Nov;16(11):1370–86.

72. Watson CL, Mahe MM, Múnera J, Howell JC, Sundaram N, Poling HM, Schweitzer JI, Vallance JE, Mayhew CN, Sun Y, Grabowski G, Finkbeiner SR, Spence JR, Shroyer NF, Wells JM, Helmrath MA. An in vivo model of human small intestine using pluripotent stem cells. Nat Med. 2014 Oct 19.

73. Hrvatin S, O'Donnell CW, Deng F, Millman JR, Pagliuca FW, DiIorio P, Rezania A, Gifford DK, Melton DA. Differentiated human stem cells resemble fetal, not adult, β cells. Proceedings of the National Academy of Sciences. 2014 Feb 25;111(8):3038–43. PMCID: PMC3939927

74. Nyeng P, Norgaard GA, Kobberup S, Jensen J. FGF10 maintains distal lung bud epithelium and excessive signaling leads to progenitor state arrest, distalization, and goblet cell metaplasia. BMC Dev Biol. 2008;8(1):2.

75. Ramasamy SK, Mailleux AA, Gupte VV, Mata F, Sala FG, Veltmaat JM, Del Moral PM, De Langhe S, Parsa S, Kelly LK. Fgf10 dosage is critical for the amplification of epithelial cell progenitors and for the formation of multiple mesenchymal lineages during lung development. Developmental Biology. 2007 Jul 15;307(2):237–47. PMCID: PMC3714306

76. Bellusci S, Grindley J, Emoto H, Itoh N, Hogan BL. Fibroblast growth factor 10 (FGF10) and branching morphogenesis in the embryonic mouse lung. Development. 1997 Dec;124(23):4867–78.

77. Bower DV, Lee H-K, Lansford R, Zinn K, Warburton D, Fraser SE, Jesudason EC. Airway branching has conserved needs for local parasympathetic innervation but not neurotransmission. BMC Biol. 2014 Nov 11;12(1):92. PMCID: PMC4255442

78. Havrilak JA, Shannon JM. Branching of lung epithelium in vitro occurs in the absence of endothelial cells. Dev. Dyn. 2015 Jan 7.

79. Franzdóttir SR, Axelsson IT, Arason AJ, Baldursson O, Gudjonsson T, Magnusson MK. Airway branching morphogenesis in three dimensional culture. Respir Res. 2010;11:162. PMCID: PMC3002372

80. Moore KA, Polte T, Huang S, Shi B, Alsberg E, Sunday ME, Ingber DE. Control of basement membrane remodeling and epithelial branching morphogenesis in embryonic lung by Rho and cytoskeletal tension. Dev. Dyn. 2005 Feb;232(2):268–81.

81. Kim HY, Nelson CM. Extracellular matrix and cytoskeletal dynamics during branching morphogenesis. Organogenesis. 2012 Apr;8(2):56–64. PMCID: PMC3429513

82. Wan H, Liu C, Wert SE, Xu W, Liao Y, Zheng Y, Whitsett JA. CDC42 is required for structural patterning of the lung during development. Developmental Biology. 2013 Feb 1;374(1):46–57. PMCID: PMC3549046

83. McCracken KW, Howell JC, Spence JR, Wells JM. Generating human intestinal tissue from pluripotent stem cells in vitro. Nature Protocols. Nature Publishing Group; 2011 Nov 10;6(12):1920–8. PMCID: PMC3896236

84. Spence JR, Lange AW, Lin S-CJ, Kaestner KH, Lowy AM, Kim I, Whitsett JA, Wells JM. Sox17 Regulates Organ Lineage Segregation of Ventral Foregut Progenitor Cells. Developmental Cell. Elsevier Ltd; 2009 Jul 21;17(1):62–74. PMCID: PMC2734336

85. Prasov L, Nagy M, Rudolph DD, Glaser T. Math5 (Atoh7) gene dosage limits retinal ganglion cell genesis. Neuroreport. 2012 Jul 11;23(10):631–4. PMCID: PMC3733793

86. Chen C, Khaleel SS, Huang H, Wu CH. Software for pre-processing Illumina next-generation sequencing short read sequences. Source Code Biol Med. 2014;9:8. PMCID: PMC4064128

87. Langmead B, Trapnell C, Pop M, Salzberg SL. Ultrafast and memory-efficient alignment of short DNA sequences to the human genome. Genome Biol. 2009;10(3):R25. PMCID: PMC2690996

88. Trapnell C, Roberts A, Goff L, Pertea G, Kim D, Kelley DR, Pimentel H, Salzberg SL, Rinn JL, Pachter L. Differential gene and transcript expression analysis of RNA-seq experiments with TopHat and Cufflinks. Nature Protocols. 2012 Mar;7(3):562–78. PMCID: PMC3334321

89. Wickham H. ggplot2: Elegant Graphics for Data Analysis - Hadley Wickham - Google Books. 2009.

90. Suzuki R, Shimodaira H. Pvclust: an R package for assessing the uncertainty in hierarchical clustering. Bioinformatics. 2006 Jun 15;22(12):1540–2.

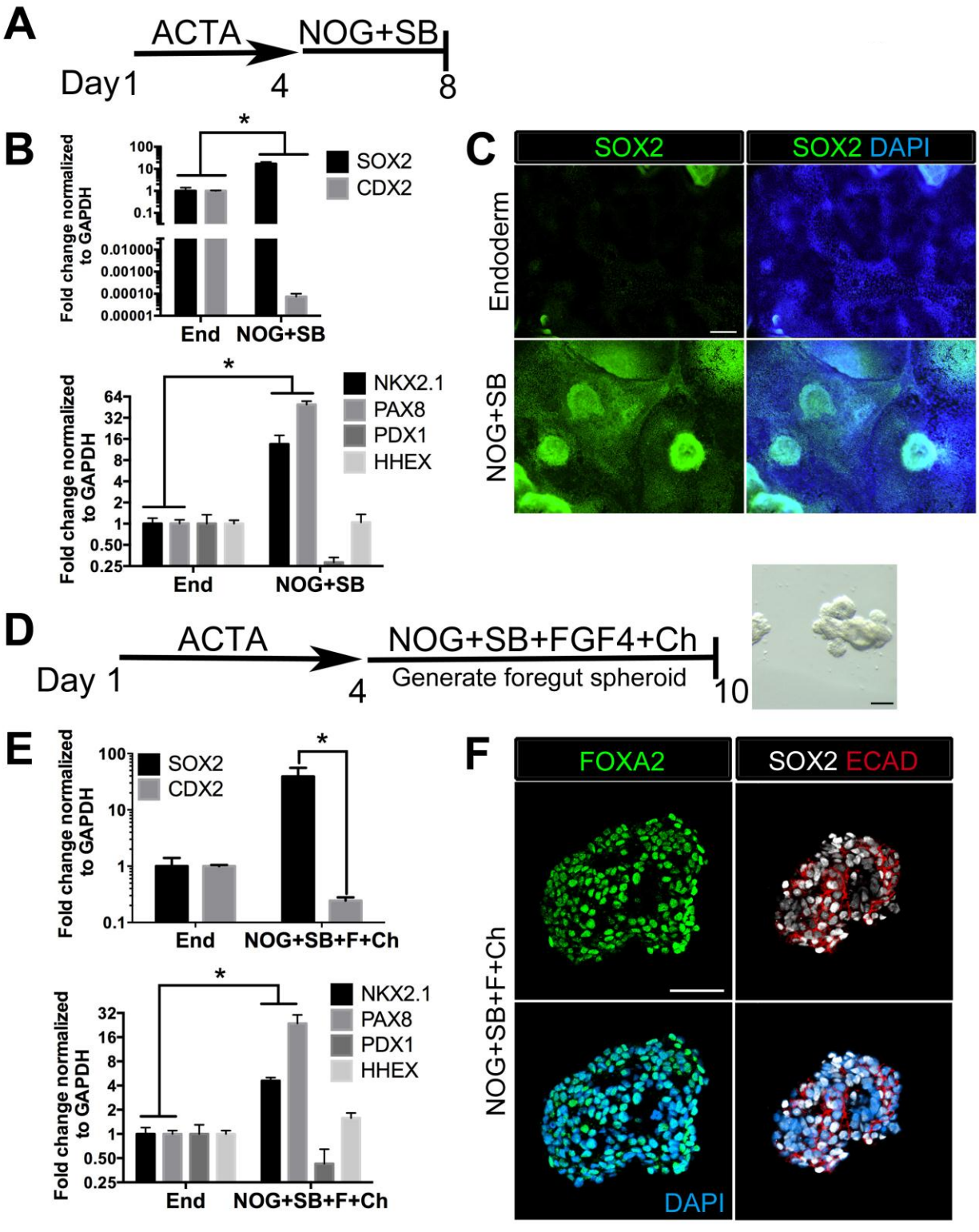

Figure 3.1. Generation of three-dimensional ventral anterior foregut spheroids from endoderm monolayers. (A) hESCs were differentiated into foregut endoderm by

treating cells with 4 days of Activin A (ACTA) followed by 4 days of NOG+SB. (B) Foregut endoderm (NOG+SB) had high expression of the foregut marker *SOX2* while the hindgut marker *CDX2* was significantly reduced compared to untreated endoderm controls (End). NOG+SB monolayer had high expression of ventral anterior foregut genes *NKX2.1* and *PAX8* while the posterior foregut marker *PDX1* was reduced. The foregut marker *HHEX* is expressed in the developing liver, biliary system, and thyroid and remained unchanged. (C) The majority of cells in NOG+SB treated cultures were SOX2 positive (green) compared to the control, in which only scattered clusters of cells were SOX2 positive. Scale bar represents 200 µm. (D) hESCs were differentiated into foregut spheroids by treating cells with 4 days of ACTA and then additional 4 to 6 days of NOG+SB+FGF4+Ch. Representative images of a spheroid in a matrigel droplet shown as whole mount image. Scale bar represents 100 µm. (E) Foregut spheroids (NOG+SB+FGF4+Ch) had high expression of the foregut marker *SOX2* while the hindgut marker *CDX2* was significantly reduced compared to untreated endoderm control (End) (top panel). Spheroids had high expression of anterior foregut genes *NKX2.1* and *PAX8* while the posterior foregut marker *PDX1* was reduced and HHEX was unchanged (bottom panel). *$p<0.05$, error bars represent SEM. (F) The majority of cells in foregut spheroids are FOXA2+ (green, left panel) and SOX2+ (white, right panel) and ECAD+ (red, right panel). Scale bar represent 50µm.

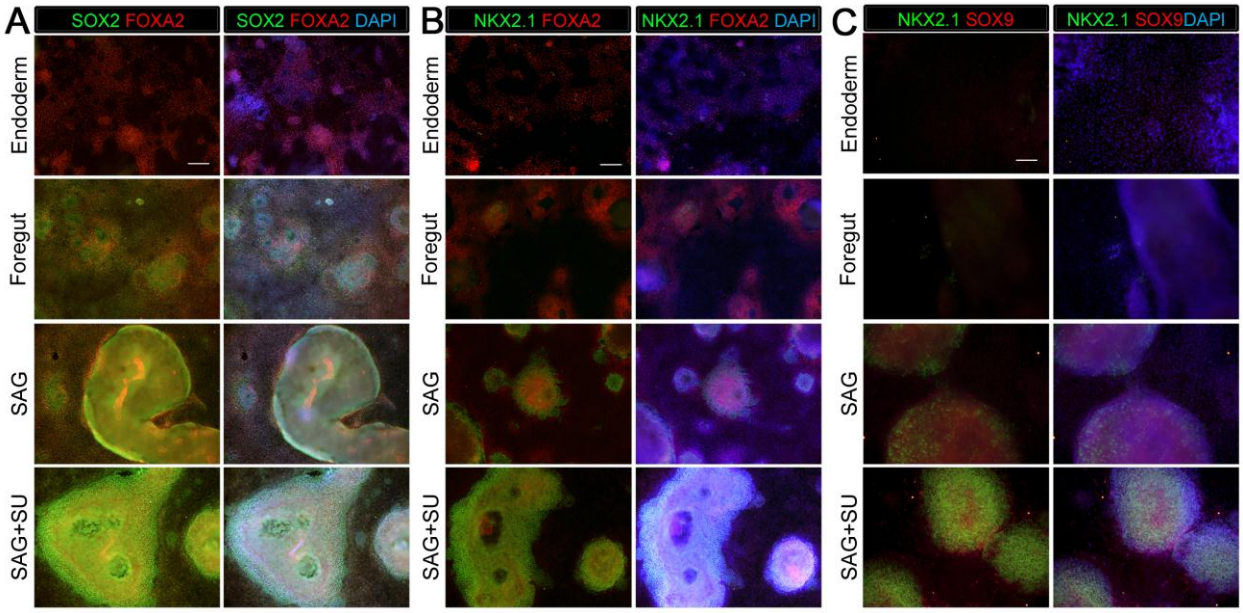

Figure 3.2. Monolayer cultures express lung specific markers.
Immunohistochemistry for markers expressed in endoderm, ventral foregut or lung epithelium were assessed (SOX2, FOXA2, NKX2.1, SOX9) in endoderm controls, foregut controls or foregut cultures treated with SAG or SAG+SU. (A) All conditions express endoderm marker FOXA2 (red), but the foregut (NOG+SB) control, SAG and SAG+SU treated cultures have co-expression of FOXA2 (red) and SOX2 (green) in the majority of cells. (B) All conditions expressed endoderm marker FOXA2 (red), but only foregut endoderm treated with SAG and SAG+SU have robust NKX2.1+ cells (green) that also express FOXA2 (red). (A-B) Scale bars represent 200 µm and apply to all images. (C) Only foregut endoderm treated with SAG and SAG+SU have robust NKX2.1+ cells (green) with the majority of cell co-expressing with lung epithelial marker SOX9 (red). Scale bar represents 100µm.

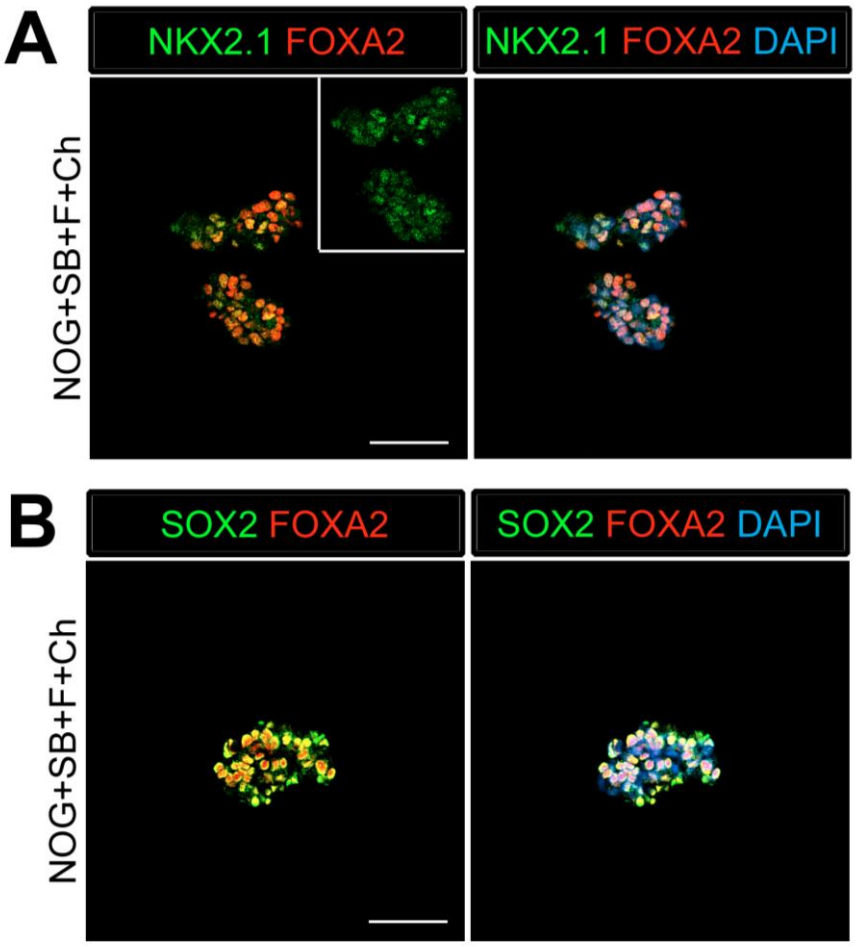

Figure 3.3. Foregut spheroids co-express endoderm and lung specific markers. (A) NOG/SB/FGF4/Ch spheroids have weak NKX2.1 (green) expression which co-expresses with endoderm marker FOXA2 (red). (B) The majority of cells in the spheroid express SOX2 (green) and co-stain with FOXA2 (red). Scale bars represent 50μM.

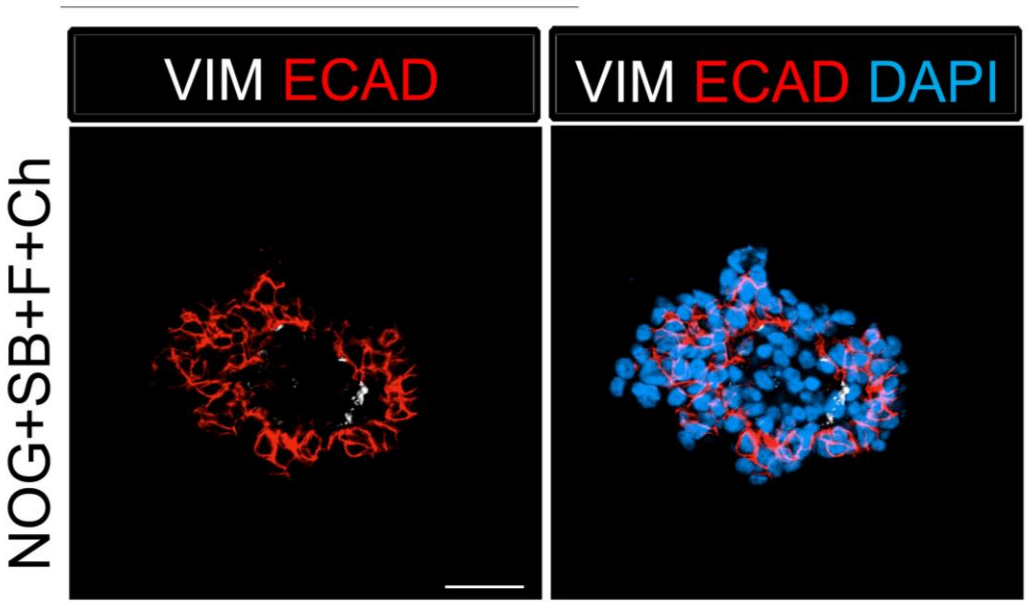

Figure 3.4. Foregut spheroids consist of both epithelial and mesenchymal cells. NOG/SB/FGF4/Ch spheroids have a minor population of Vimentin (VIM, white) positive mesenchymal cells, while the majority of cells are epithelial and express ECAD (red). Scale bar represents 50μM.

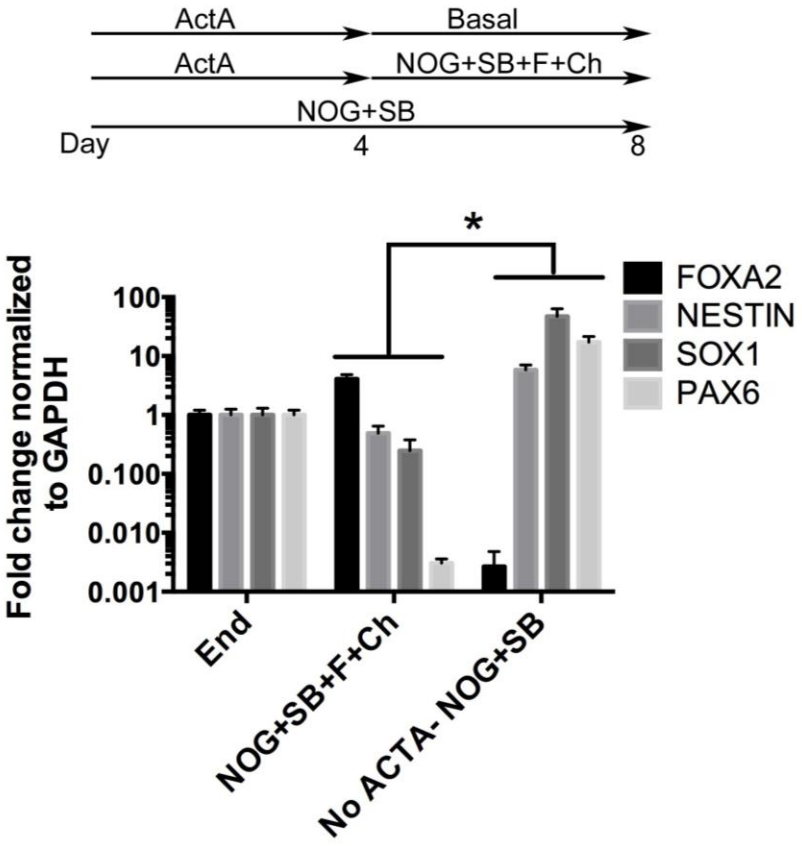

Figure 3.5. NOG+SB+FGF4+Ch spheroids do not express neural markers. hESCs were differentiated into endoderm by treating with 4 days of ActivinA (ACTA) and spheroids were generated with an additional 4 days of NOG+SB+FGF4+Ch. Neural cultures were not treated with ACTA, but were treated with NOG+SB for 8 days. Compared to foregut spheroids (NOG+SB+FGF4+Ch), NOG+SB neural cultures had a significant increase in neural markers *NESTIN*, *SOX1*, and *PAX6* and significant decrease in *FOXA2,* which is highly expressed in endoderm. *p<0.05, error bars represent SEM.

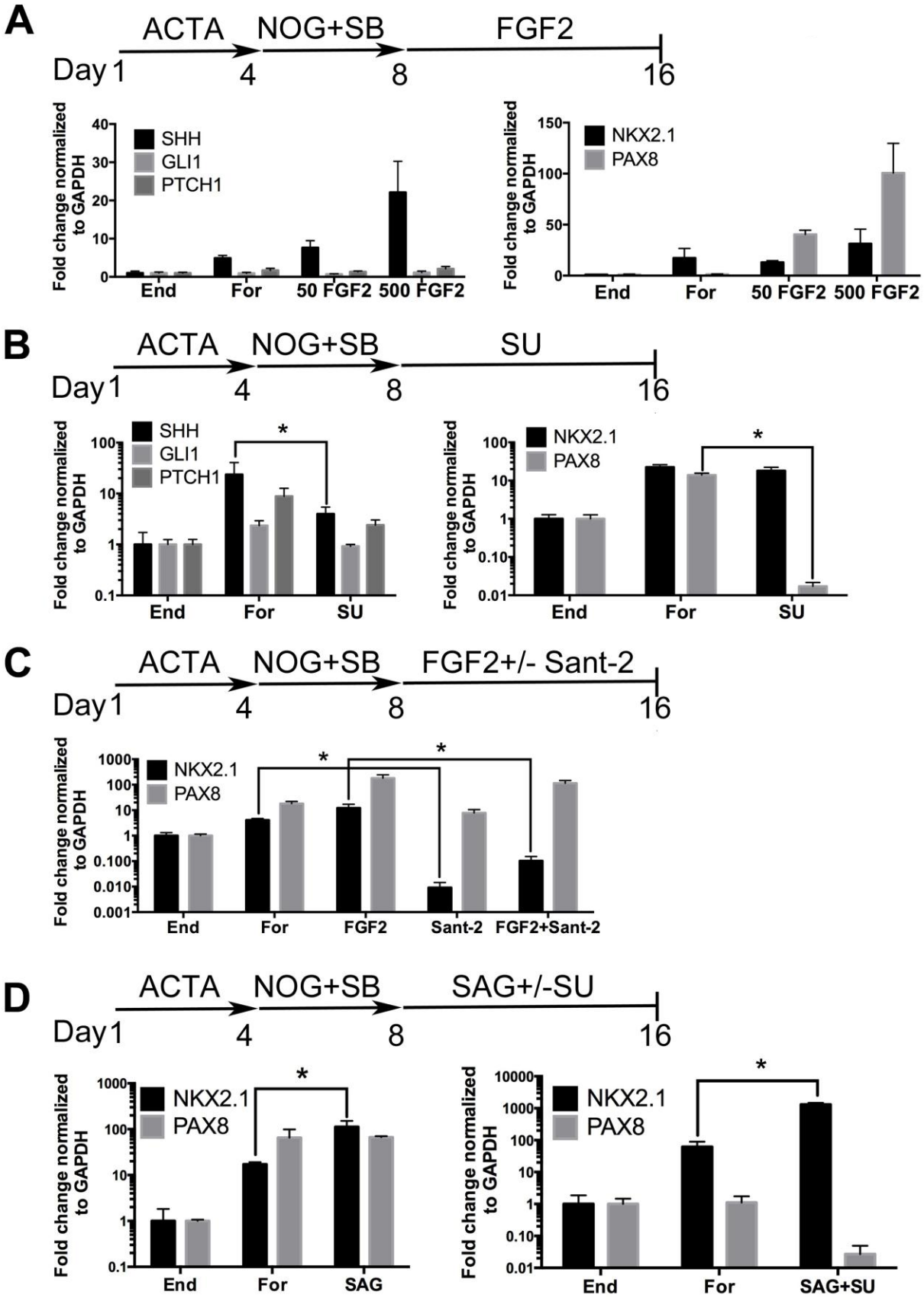
A
ACTA
NOG+SB
FGF2
Day 1
4
8
16
Fold change normalized to GAPDH
SHH
GLI1
PTCH1
End
For
50 FGF2
500 FGF2
NKX2.1
PAX8
B
SU
*
SU
C
FGF2+/- Sant-2
FGF2
Sant-2
FGF2+Sant-2
D
SAG+/-SU
SAG
SAG+SU

Figure 3.6. Induction of NKX2.1 in anterior foregut endoderm by modulating FGF and HH signaling. (A) hESCs were differentiated into endoderm (End) or anterior foregut with NOG+SB (For). Anterior foregut was treated with low (50ng/mL) and high (500ng/mL) concentrations of FGF2. FGF2 caused a dose dependent increase in *SHH* and *PAX8* expression with a modest increase in *NKX2.1* expression compared to untreated endoderm controls. Note that *NKX2.1* expression is increased by NOG+SB exposure alone (no FGF2). (B) Addition of the FGF inhibitor SU5402 (SU) to NOG+SB foregut cultures (For) caused a significant reduction of *SHH* and *PAX8* expression, but *NKX2.1, GLI1*, and *PTCH1* were not significantly different compared to the foregut controls, in which no growth factors were added after SB+NOG. (C) Addition of the HH inhibitor Sant-2 caused a significant reduction in *NKX2.1* compared to foregut control. Similarly when FGF2 (500 ng/mL) and Sant-2 were added simultaneously, the modest *NKX2.1* induction caused by FGF2 was significantly reduced whereas *PAX8* expression remained unchanged. (D) Foregut endoderm treated with SAG or SAG+SU for 8 days had a 6.5 fold and 21 fold increase of *NKX2.1* expression, respectively, compared to untreated foregut controls. *PAX8* expression was unchanged in the SAG treated cultures whereas SAG+SU treated cultures demonstrated a 41 fold decrease in *PAX8* expression. End=endoderm; For=foregut in all panels. *$p<0.05$, error bars represent SEM.

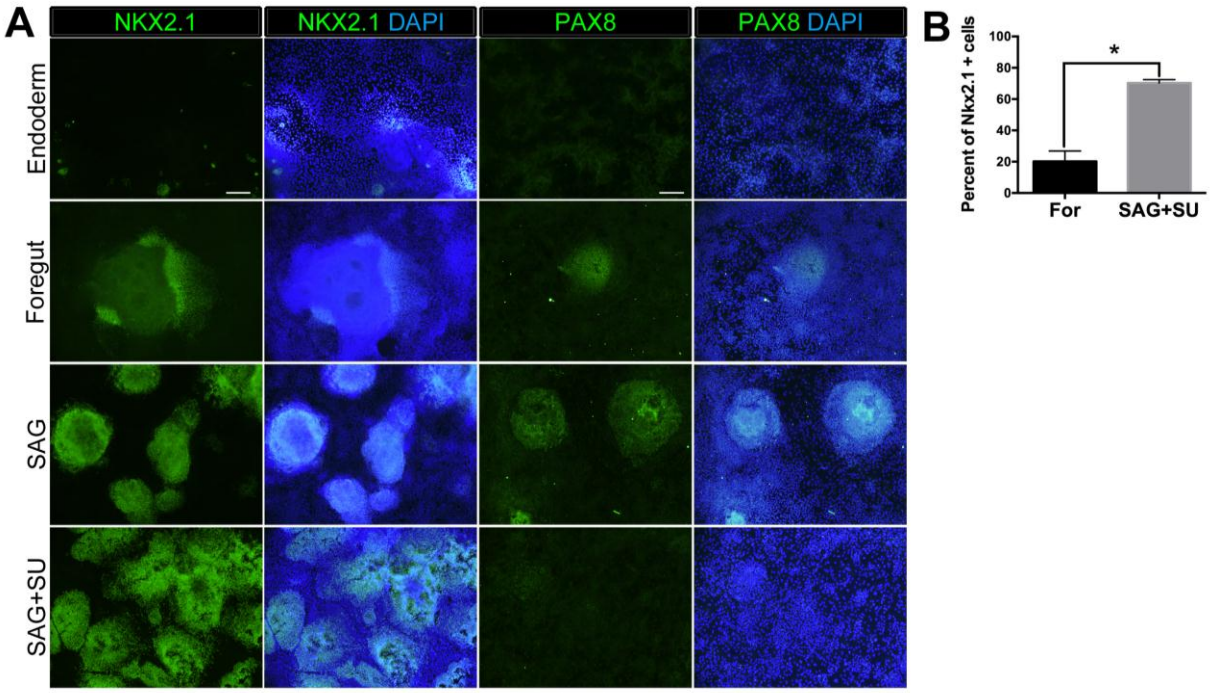

Figure 3.7. Robust induction of NKX2.1 in foregut endoderm with HH stimulation and FGF inhibition. (A) Immunohistochemistry of NKX2.1 and PAX8 in endoderm controls, foregut controls or foregut cultures treated with SAG or SAG+SU. Treatment of foregut cultures with SAG or SAG+SU resulted in more NKX2.1+ cells compared to endoderm and foregut controls. Scale bars represent 200 μm and apply to all images. (B) Quantification showed that 20% +/-4% of cells in foregut controls were NKX2.1+, whereas 72% +/- 3% cells were positive in SAG+SU treated cultures (*$p<0.05$). All error bars represent SEM.

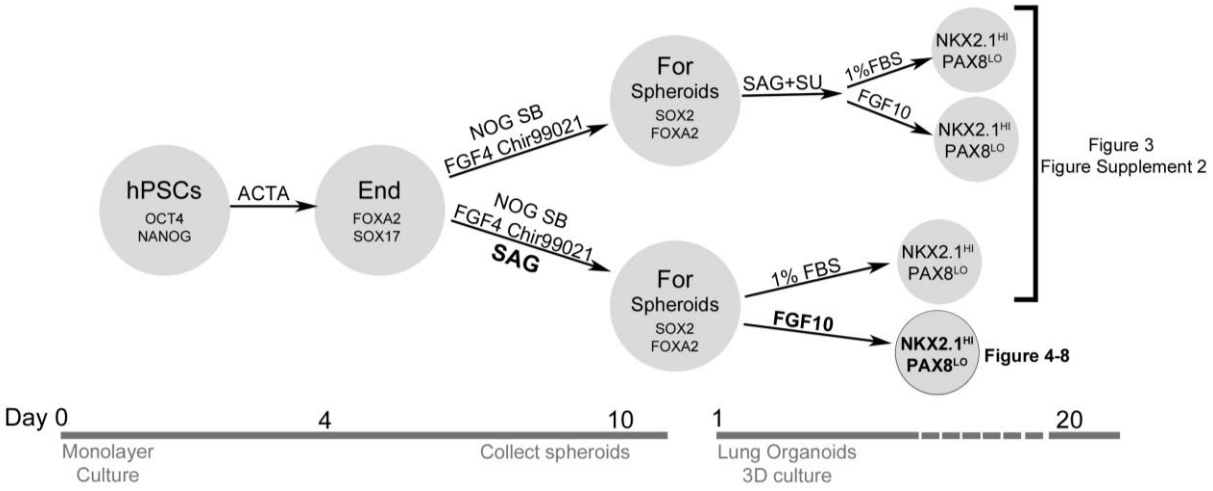

Figure 3.8. Overview of conditions tested to generate human lung organoids. hPSCs are OCT4 and NANOG positive. After 4 days of 100 ng/mL Activin A, definitive endoderm (FOXA2 and SOX17 positive) was generated and then treated with two different conditions. In the top branch, NOG+SB+FGF4+Ch spheroids were generated, and different conditions were tested to promote lung organoid differentiation. In the bottom branch, NOG+SB+FGF4+Ch+SAG spheroids were generated, and different conditions were tested to promote lung organoid differentiation. Ultimately, we determined that spheroids generated with NOG+SB+FGF4+Ch+SAG and that were subsequently embedded in Matrigel and expanded in FGF10 gave rise to “Human Lung Organoids” (HLOs).

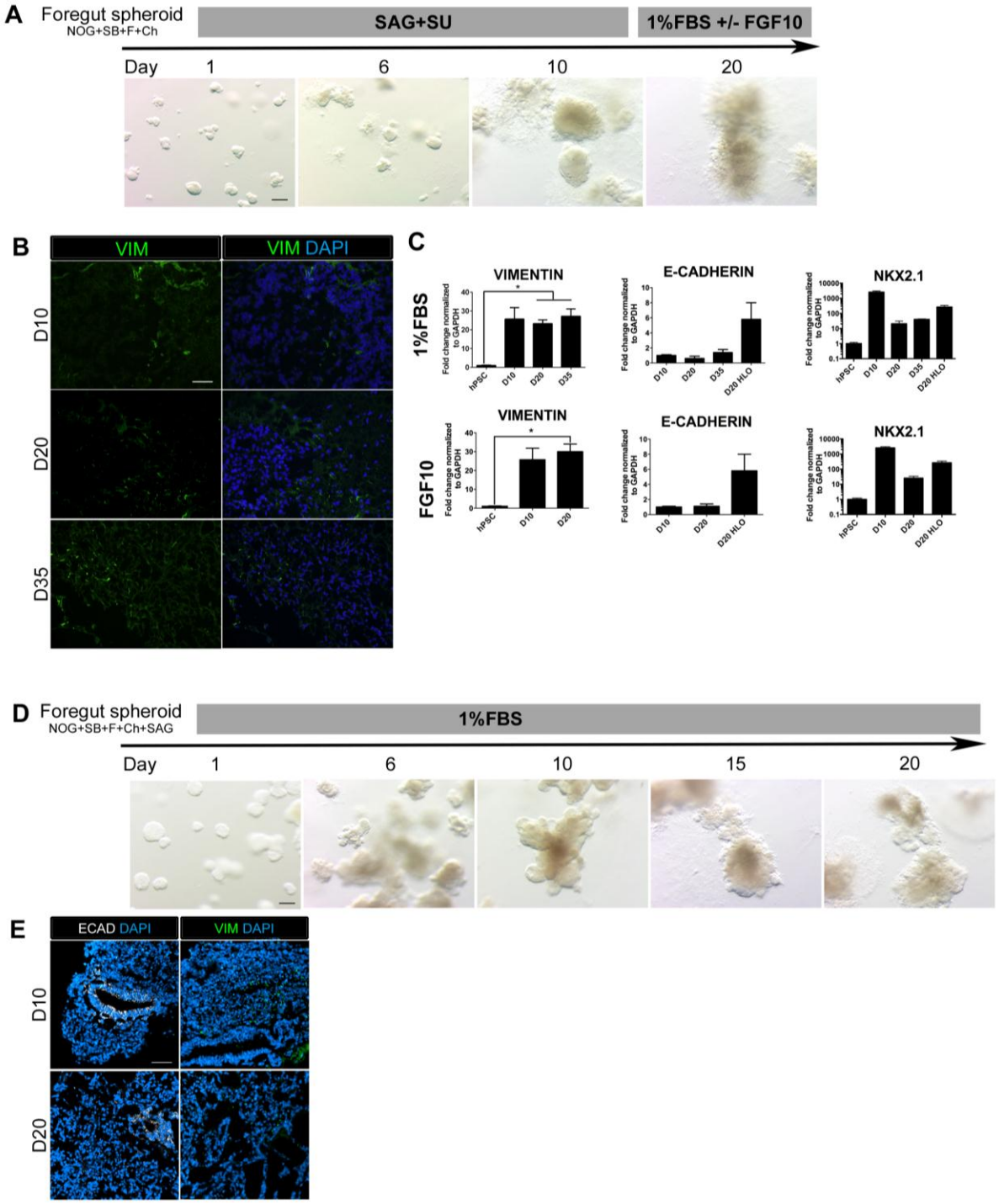

Figure 3.9. FGF-low culture conditions cause a loss of organoid epithelium over time. (A) NOG+SB+F+Ch foregut spheroids were generated and then cultured in SAG+SU for 10 days followed by 1%FBS +/- FGF10. Timeline images show organoids cultured in 1%FBS. By day 20, 3D structures appeared “fuzzy”, which indicates an outgrowth of mesenchymal tissue. Scale bar represents 200μm. (B) NOG+SB+F+Ch foregut spheroids treated with SAG+SU and maintained in 1%FBS showed an increase

in Vimentin (VIM, green) immunofluorescence over time. Scale bar represents 50μM. (C) NOG+SB+F+Ch foregut spheroids treated with SAG+SU and maintained in 1%FBS (upper panel) or 1%FBS+FGF10 (lower panel) had a significant increase of *VIM* expression starting at day 20 (D20) compared to hPSCs and showed very weak *E-CADHERIN* (*CDH1)* expression compared to D20 HLOS (optimized conditions, as described in Figure 3). Lastly, both conditions appeared to lose *NKX2.1* expression over time. (D) NOG+SB+F+Ch+SAG spheroids maintained in 1%FBS (basal media) also appear to lose epithelial structures over time. Scale bar represents 200μm. (E) By day 20 (D20) the tissue had very few epithelial structures expressing ECAD (white, left panel) and there was robust VIM expression (green, right panel) at both time points. Scale bar represents 50μm. HLO. *$p<0.05$. All error bars represent SEM.

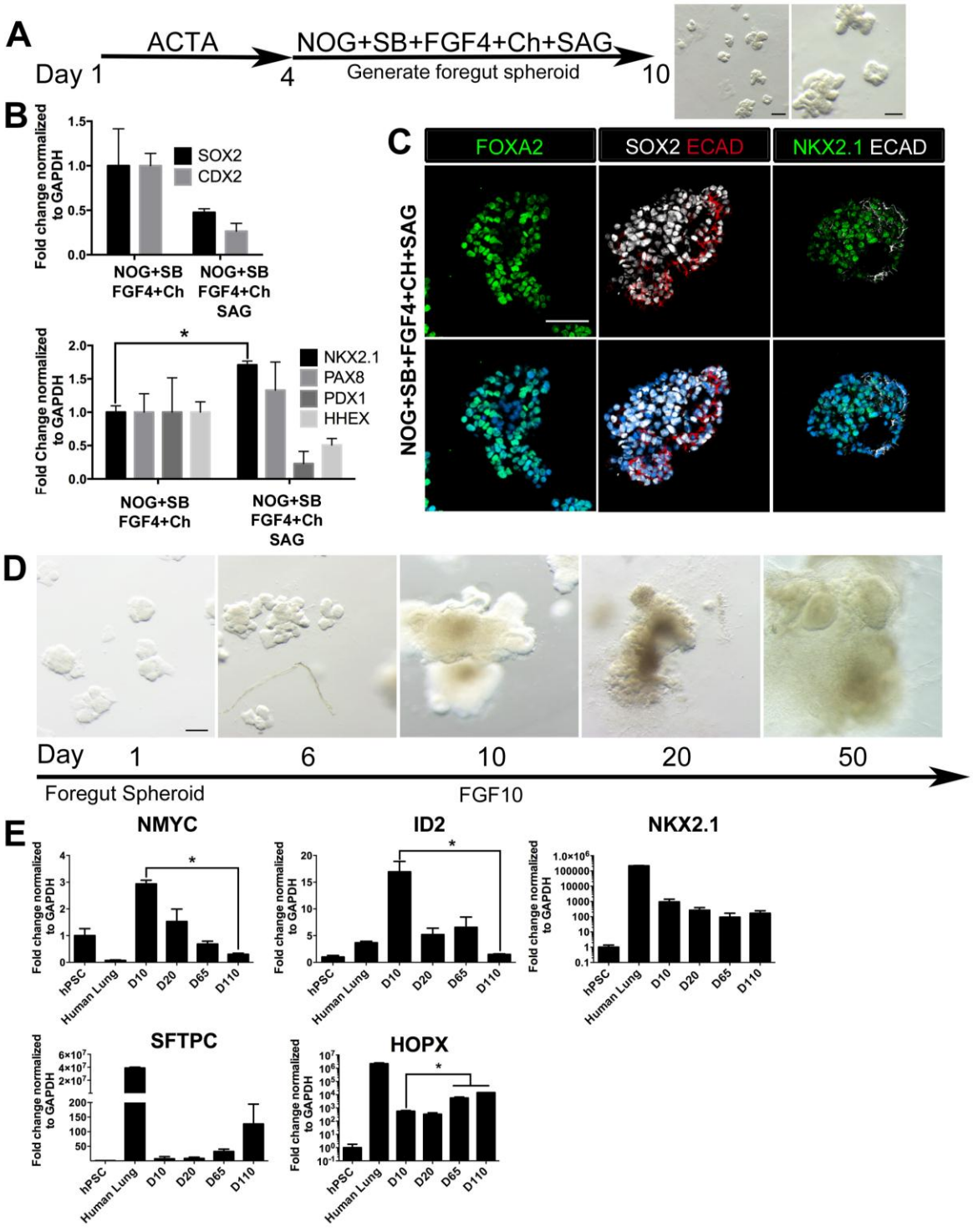

Figure 3.10. HH-induced ventral foregut spheroids give rise to lung organoids. (A) hESCs were differentiated into foregut spheroids by treating cells with 4 days of ACTA and then additional 4 to 6 days of NOG+SB+FGF4+Ch with the addition of the HH agonist SAG. Representative whole mount images of spheroids in a matrigel droplet are shown at low (left, scale bar 200 µm) and high magnification (right, scale bar 100 µm).

(B) The addition of SAG to the NOG+SB+FGF4+Ch spheres caused a reduction in *SOX2* and *CDX2* transcripts (top panel) and a significant increase of *NKX2.1* transcript (bottom panel) compared to NOG+SB+FGF4+Ch spheres (without SAG). Other foregut lineages (*PAX8, PDX1, HHEX*) were not significantly different when SAG was added. (C) The majority of the cells in NOG+SB+FGF4+Ch+SAG spheres expressed FOXA2, SOX2 and NKX2.1 protein. Scale bars represent 50µm. (D) Timeline showing NOG+SB+FGF4+Ch+SAG induced foregut spheroids grown and maintained in FGF10. Note that Day 1 is the day spheroids were plated in Matrigel. Scale bar represents 100µm. (E) Organoids express lung markers in a manner consistent with mouse lung development. All expression is shown relative to undifferentiated pluripotent stem cells (hPSC), and adult human lung is shown as a reference. Lung progenitor markers *NMYC* and *ID2* were very low in adult lung, and were expressed at high levels in early organoid cultures, but were reduced over time (D=Days in culture), whereas *NKX2.1* expression remained relatively constant. In contrast, *SFTPC* is known to be expressed at low levels in distal lung progenitors, but increases and is highly expressed in AECII cells. Consistently, *SFTPC* is highly expressed in adult human lungs and increases over time in organoid cultures and the AECI marker *HOPX* is also highly expressed in adult human lung and increases over time in organoids. *$p<0.05$. All error bars represent SEM.

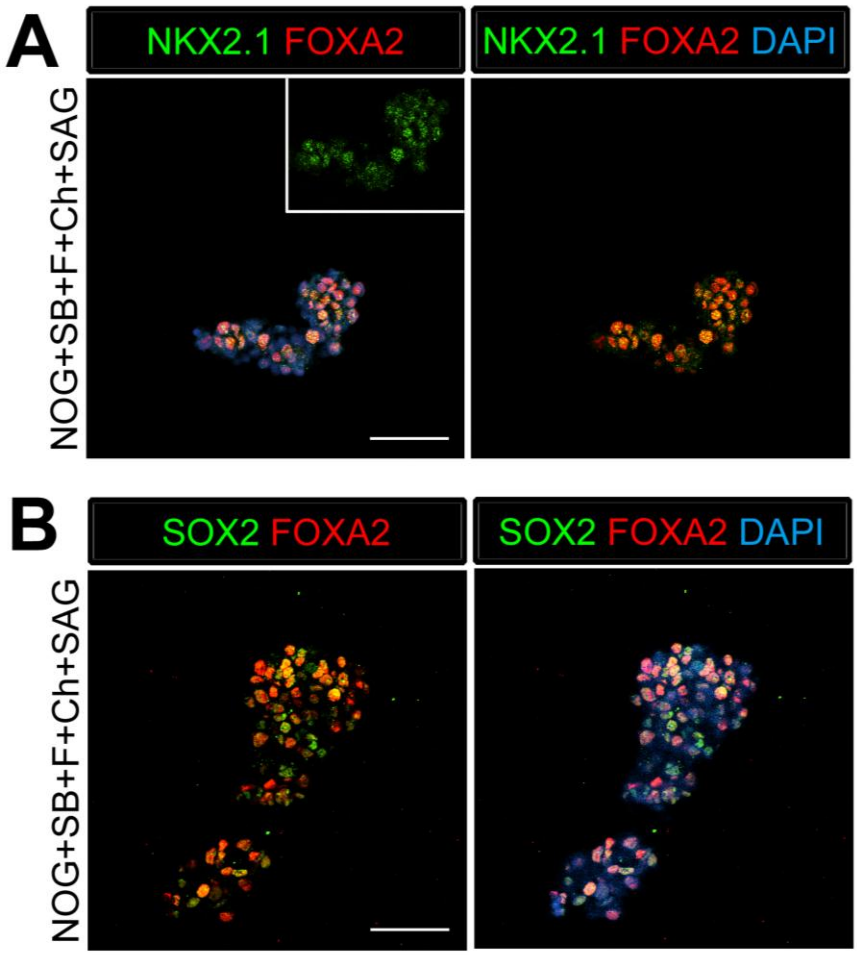

Figure 3.11. Foregut spheroids express lung and foregut specific markers. (A) NOG/SB/FGF4/Ch/SAG spheroids coexpress NKX2.1 (green) and the endoderm marker FOXA2 (red). (B) The majority of the cells in the spheroid co-expresses SOX2 (green) and FOXA2 (red). Scale bars represent 50μM.

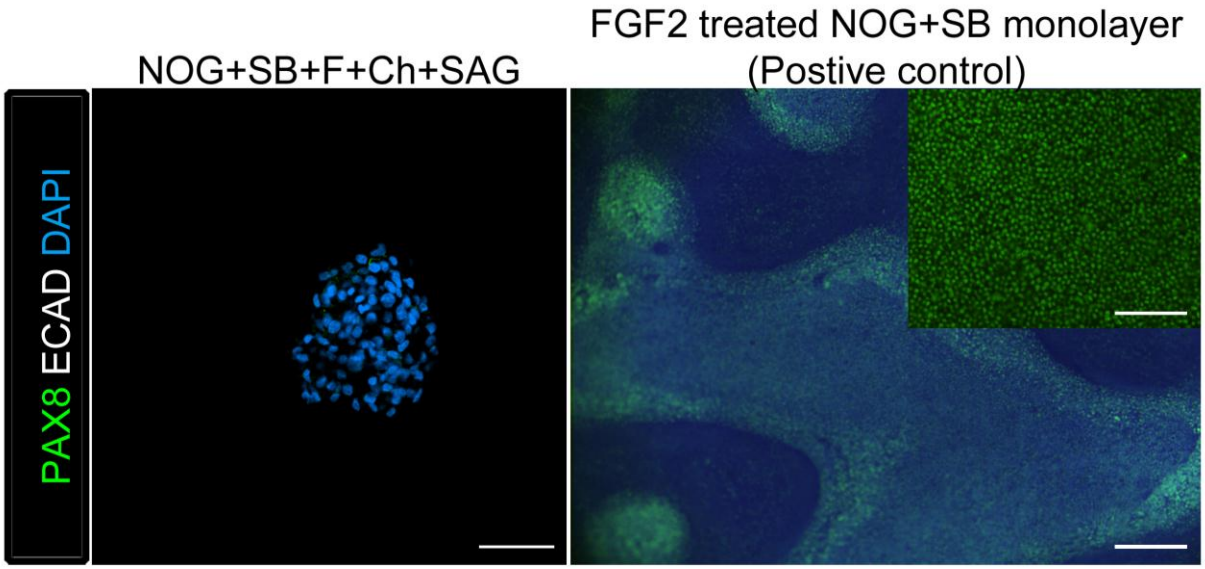

Figure 3.12. Ventral foregut spheroids do not express appreciable levels of PAX8 protein. Although NOG+SB+FGF4+Ch+SAG ventral foregut spheroids expressed *PAX8* mRNA (Figure 3B), we did not detect PAX8 protein in spheroids using immunofluorescence, whereas PAX8 protein in FGF2 8 day treated foregut monolayers (ACTA followed by NOG/SB) was readily detectable. Left panel: scale bar represents 50µm. Right panel: scale bar represents 200µm, inset scale bar represents 100µm.

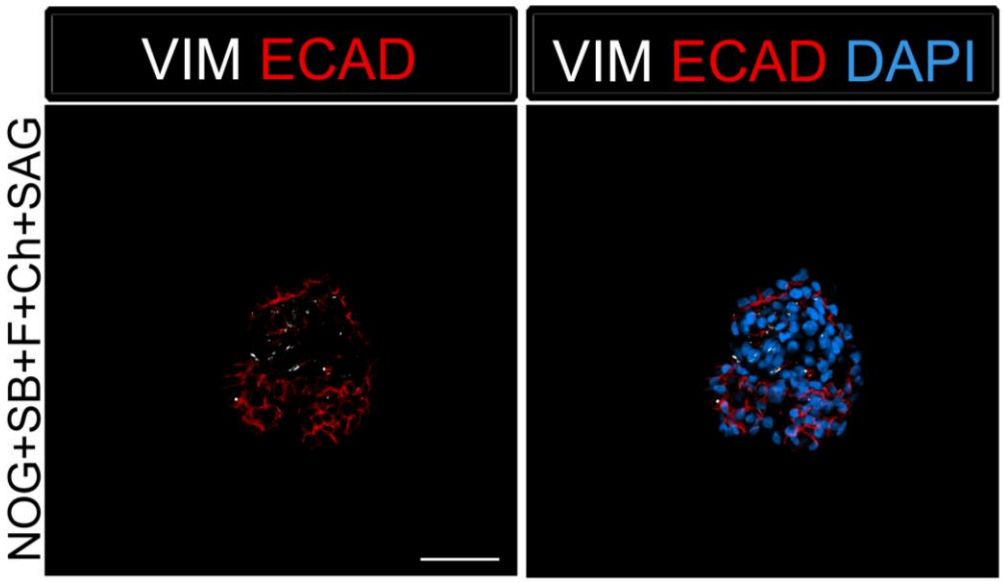

Figure 3.13. Foregut spheroids consist of both epithelial and mesenchymal cells. NOG/SB/FGF4/Ch/SAG spheroids have a minor population of Vimentin (VIM, white) positive mesenchymal cells, while the majority of cells are epithelial and express ECAD (red). Scale bar represents 50μM.

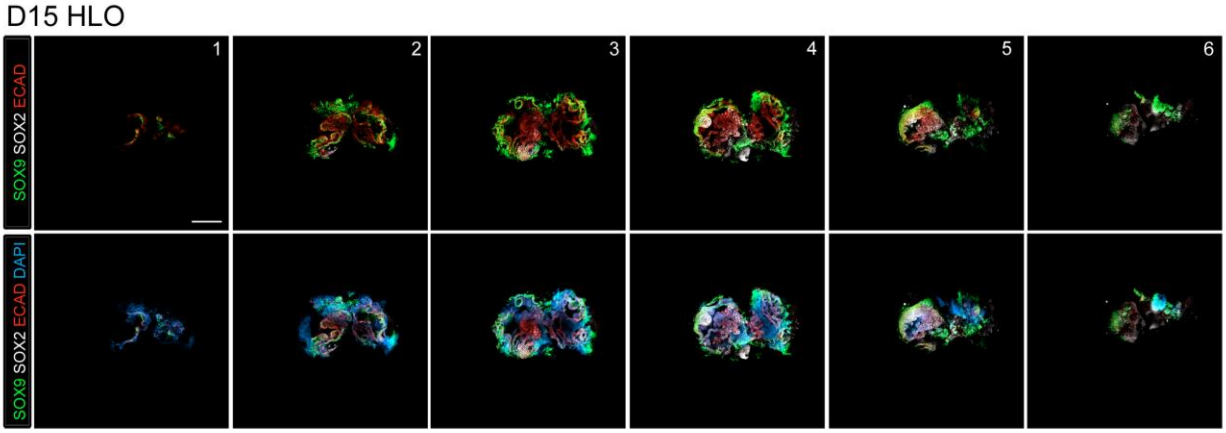

Figure 3.14. Lung organoids contain both proximal and distal domains. NOG/SB/FGF4/Ch/SAG spheroids cultured for 15 days with FGF10 express the distal lung epithelium marker SOX9 (green) and proximal marker SOX2 (white) as separate domains in the epithelium labeled by ECAD (red). Z-stack images are shown every 40µm sections through the HLO. Scale bar represents 200µm.

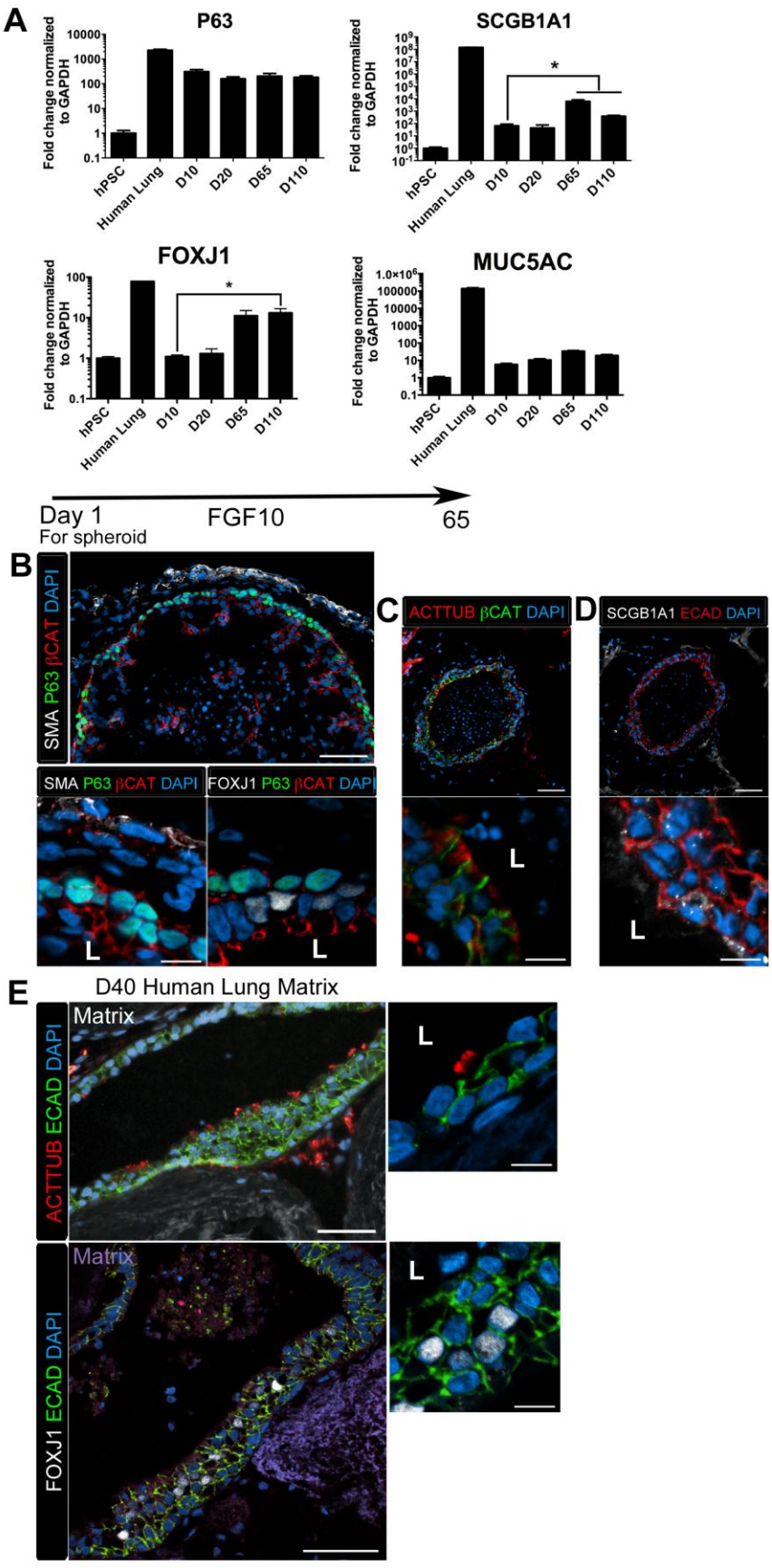
A
P63
SCGB1A1
FOXJ1
MUC5AC
Fold change normalized to GAPDH
hPSC
Human Lung
D10
D20
D65
D110
*
Day 1
For spheroid
FGF10
65
B
SMA P63 βCAT DAPI
FOXJ1 P63 βCAT DAPI
C
ACTTUB βCAT DAPI
D
SCGB1A1 ECAD DAPI
L
E
D40 Human Lung Matrix
Matrix
ACTTUB ECAD DAPI
FOXJ1 ECAD DAPI

Figure 3.15. Lung organoids form proximal airway-like structures. (A) Genes expressed in the proximal airway were examined in organoids across time. The proximal airway cell marker *SOX2* decreased over time in HLOs cultures compared to D10 HLOs. Compared to undifferentiated hPSCs, organoids expressed high levels of the basal cell marker *P63* at all time points, while the club cell marker *SCGB1A1* and ciliated cell marker *FOXJ1* had a significant increase of expression in prolonged cultures (compared to D10 HLOs). There was an increasing but non-significant trend in goblet cell *MUC5AC* expression over time in culture. (B) D65 HLOs had structures resembling the proximal airway, in which the epithelium (β-catenin, red) possesses P63+ basal cells (green), and is surrounded by SMA+ (white, upper and lower left panel) mesenchymal tissue. Adjacent to the P63 positive basal cell layer (green, lower, right panel) were FOXJ1 positive cells (white). Scale bars represent 50μM (top) and 10μM (bottom). (C) Proximal airway-like epithelium (β-catenin, green) co-stained for ACTTUB on the apical side of the cell (red). Scale bars represent 50μM (top) and 10μM (bottom). (D). Proximal airway-like epithelium (E-cadherin, red) also co-stained with Club cell marker CC10 (white, right panel). Scale bars represent 50μM (top) and 10μM (bottom). (E) Acellular human lung matrix was seeded with spheroids and cultured for 40 days (D40). Matrices had abundant proximal airway-like structures that had multi-ciliated cells on the apical surfaced labeled by ACTTUB (red, top panel) in low (scale bar 50μM) and high magnification (scale bar 10μM). Serial sections showed that cells were also FOXJ1 positive (white, lower panel) with the epithelium outlined in ECAD (green) in low (scale bar 50μM) and high magnification (scale bar 10μM). (B-D) 'L' in high magnification images indicates the lumen. *$p<0.05$. All error bars represent SEM.

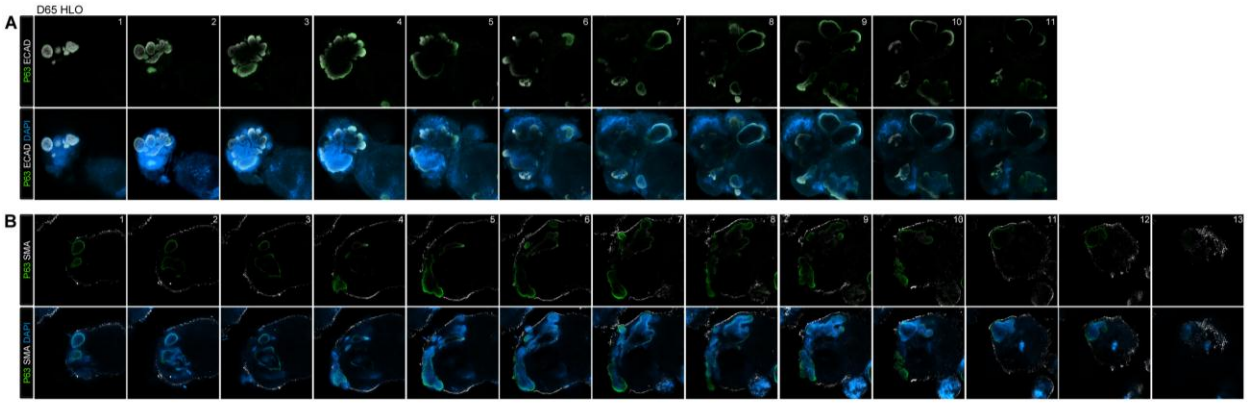

Figure 3.16. Lung organoids have P63+ epithelium throughout the organoid. (A) Confocal Z-slices taken at every 40µm show P63+ (green) and ECAD+ (white) structures through the D65 HLO. (B) Z-slices taken at every 40µm show SMA (white) surrounding the periphery the HLO with P63 (green) staining within the HLO. Scale bars represent 200µm.

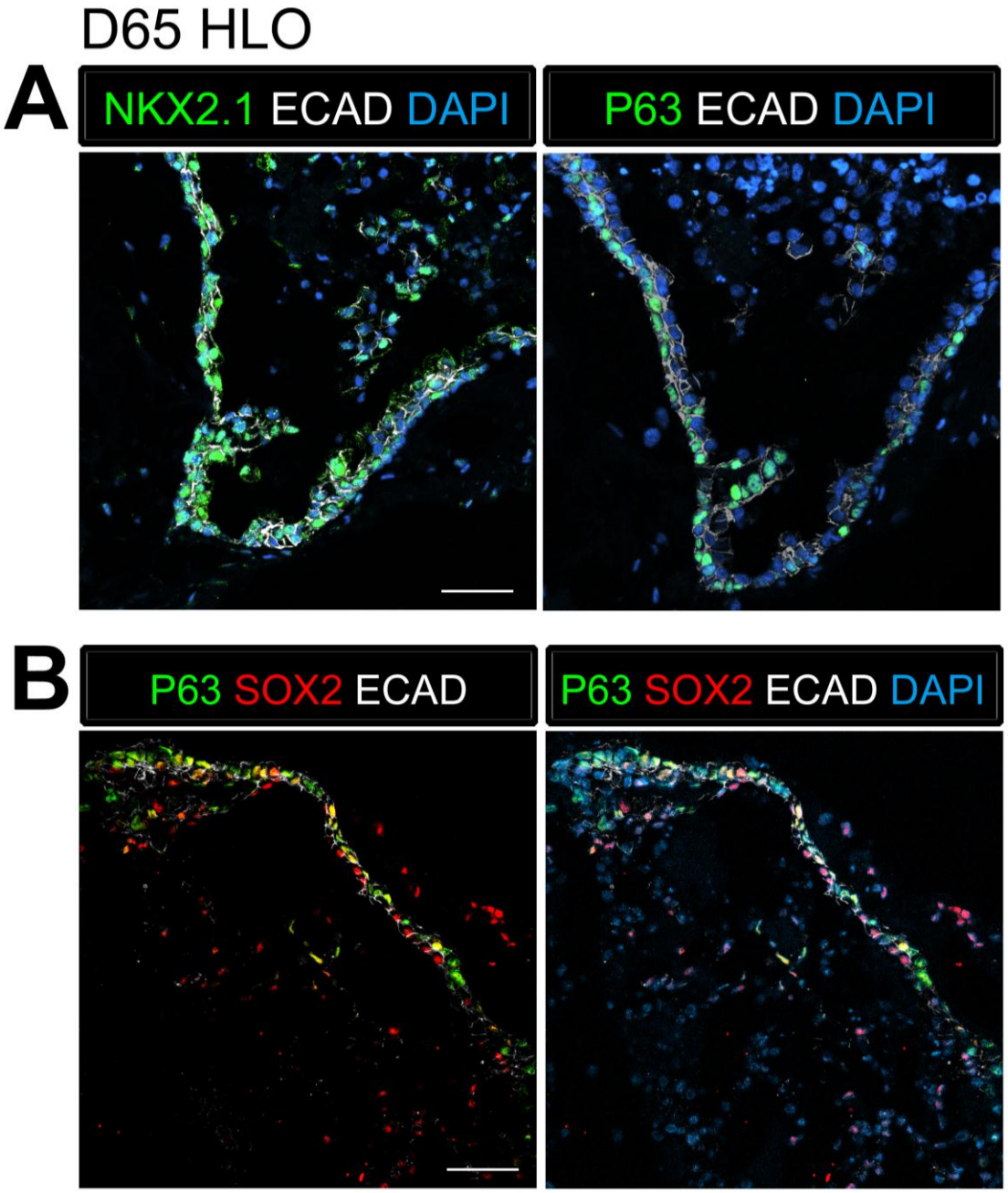

Figure 3.17. P63+ cells have an NKX2.1+ lung identity. (A) Serial sections were stained with NKX2.1 and P63 respectively. The adjacent sections expressed ECAD (white) and NKX2.1 (green) in the first section and P63 (green) in the second section. (B) P63+ cells (green) co-expressed the proximal lung marker SOX2 (red) in the epithelium labeled by ECAD (white). Scale bars represent 50μm.

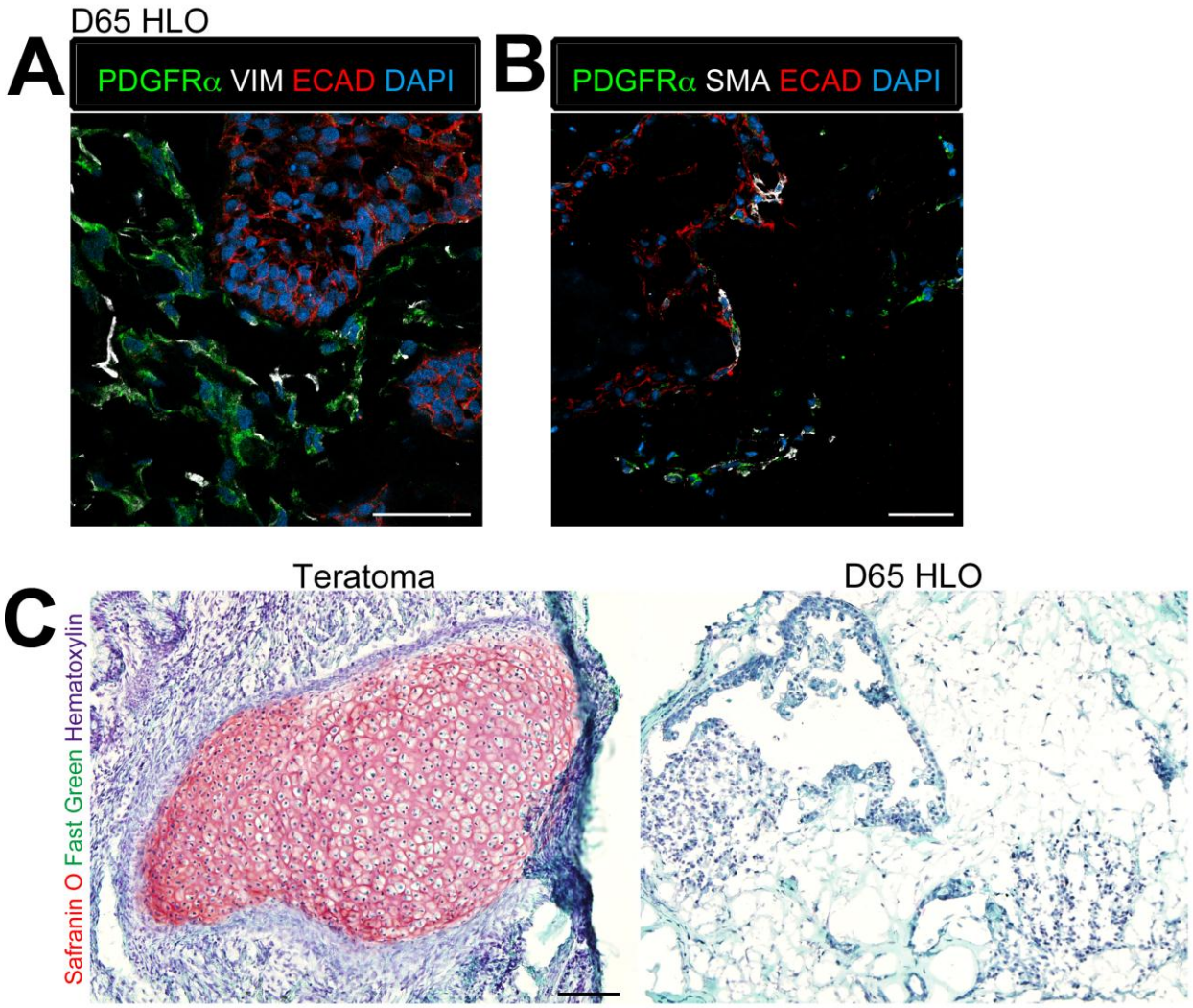

Figure 3.18. Lung organoids possess multiple types of mesenchymal cells. (A) D65 HLOs have PDGFRα+ (green) VIM+ (white) double-positive myofibroblasts and PDGFRα-/VIM+ fibroblasts. Scale bar represents 50μm. (B) D65 HLOs also possesses PDGFRα+ (green) SMA+ (white) double-positive myofibroblasts and PDGFRα-/SMA+ smooth muscle and myofibrblasts. Scale bar represents 50μm. (C) D65 HLO do not contain any cartilage whereas positive control iPSC derived teratoma had clear SafraninO staining specific to cartilage. Fast green marks the cytoplasm and hematoxylin the nuclei of both tissues. Scale bar represents 100μm.

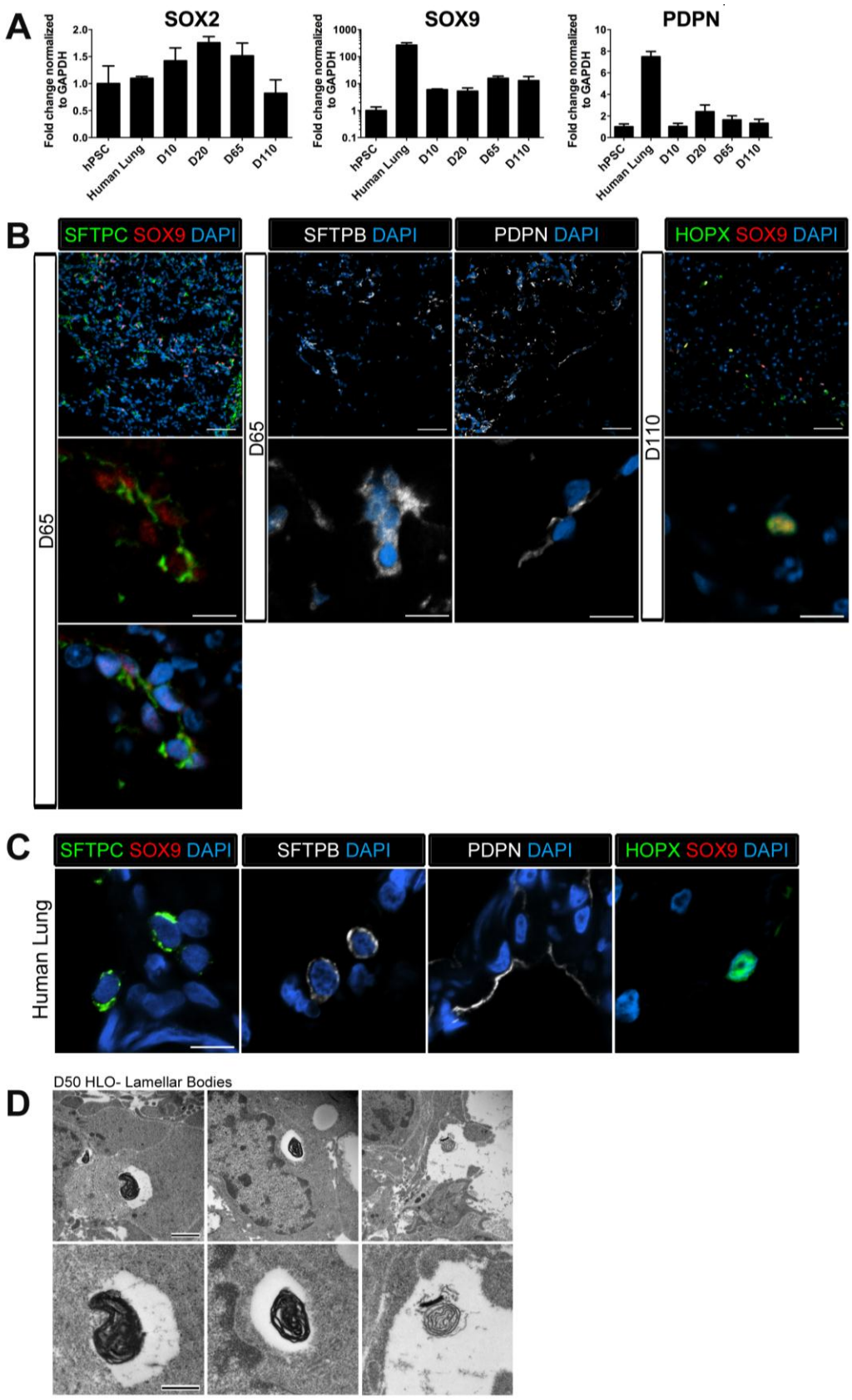
A
SOX2
SOX9
PDPN
Fold change normalized to GAPDH
hPSC
Human Lung
D10
D20
D65
D110
B
SFTPC SOX9 DAPI
SFTPB DAPI
PDPN DAPI
HOPX SOX9 DAPI
D65
D65
D110
C
SFTPC SOX9 DAPI
SFTPB DAPI
PDPN DAPI
HOPX SOX9 DAPI
Human Lung
D
D50 HLO- Lamellar Bodies

Figure 3.19. Lung organoids possess abundant distal bipotent progenitor cells. (A) The expression of the distal progenitor marker *SOX9* remained unchanged over time and the AECI marker *PDPN* had low expression in HLO cultures. (B) The majority of SFTPC+ cells (green, left panel) co-expressed SOX9 (red). Similarly, many cells expressing the AECI early marker HOPX+ (green, right panel) co-expressed SOX9 (red). Few, scattered cells expressed the late AECII marker SFTPB (white, second panel) or the AECI marker, PDPN (third panel, white). Few PDPN+ cells also showed elongated, squamous morphology seen in the adult lung. (C) Human lung AECII cells labeled with SFTPC (green, left panel) did not co-express SOX9. SFTPB+ cells (white, second panel) in the adult human lung have similar morphology to SFTPB+ cells in HLOs. Human lung AECI cells expressed PDPN (white, third panel), and show characteristic AECI cell shape. Human AECI cells express HOPX (green, right panel), but did not co-express SOX9. (B-C) Scale bar in lower magnification images in B (upper panel) represent 50μM and higher magnification in B,C (lower panel) represent 10μM. (D) D50 HLOs contain lamellar bodies which are organelles specific to AECII cells. Scale bars represent 500nm.

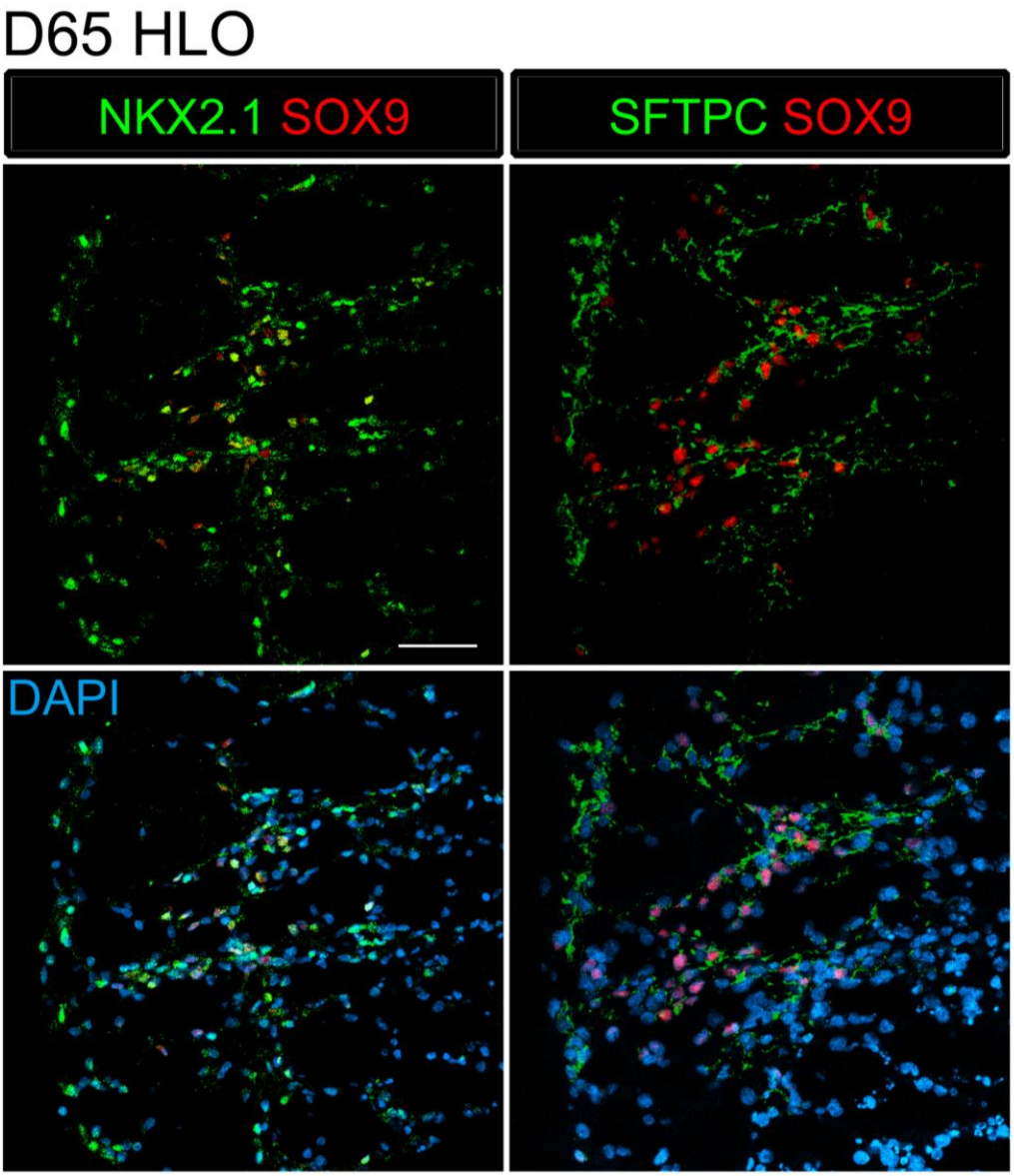

Figure 3.20. SFTPC+ cells express lung specific markers. D65 HLOs express lung epithelial markers NKX2.1 (green) and SOX9 (red) and the adjacent section expresses SFTPC (green) and SOX9 (red). Scale bar represents 50μm.

A

Structural composition of HLOs		
	N	%
Proximal airway-like epithelium	39/48	81%
Distal airway-like epithelium	48/48	100%

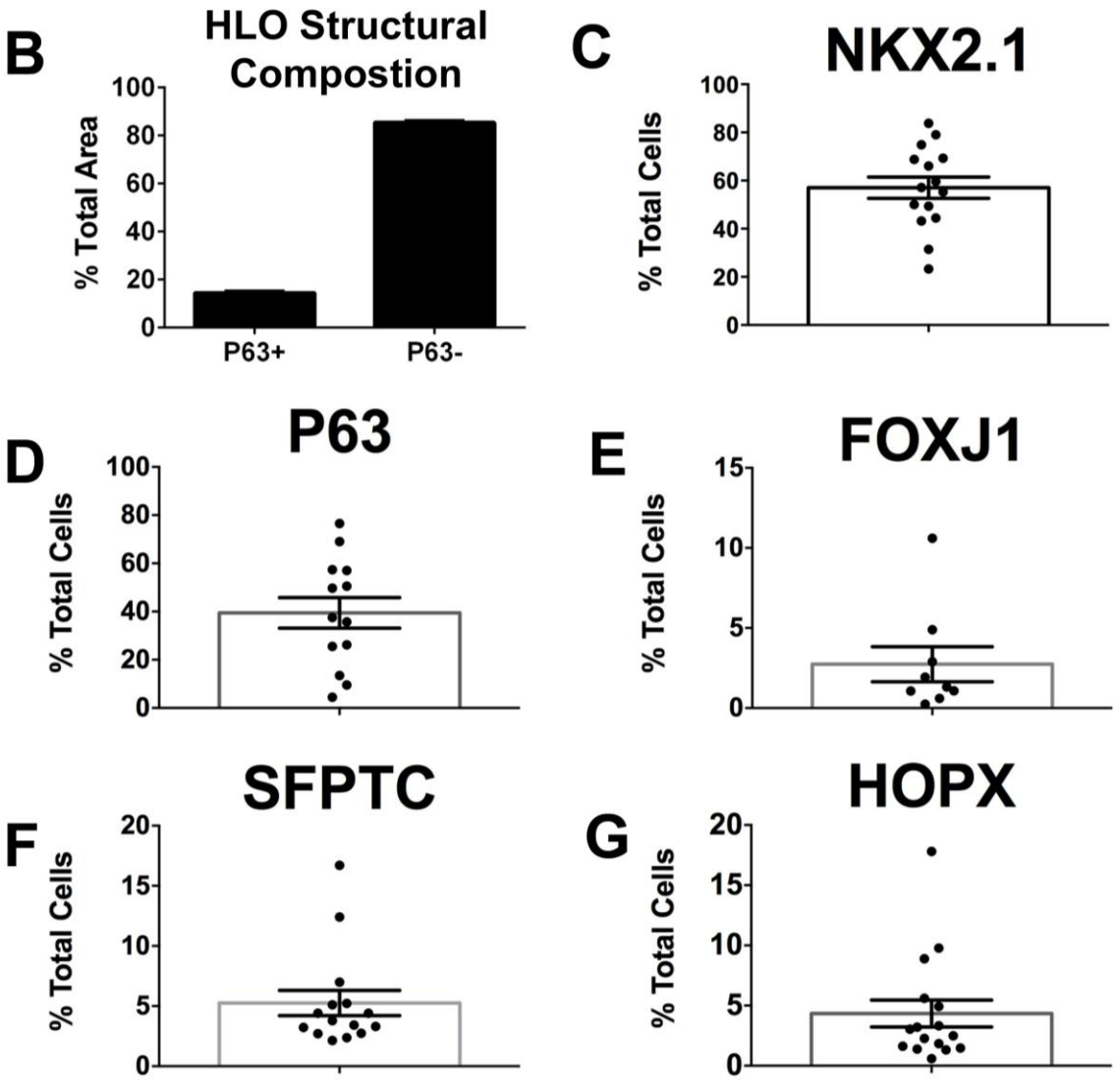

Figure 3.21. Quantitative assessment of the composition of lung organoids. (A) HLOs were assessed for proximal airway-like structures (P63+) and distal airway-like structures (P63-/SFTPC+). 81% of HLOs have proximal airway-like epithelium while

100% have distal airway-like epithelium (n=48 individual HLOs). (B) The average cross-sectional area within an HLO that is comprised of P63+ proximal airway-like and P63- distal airway-like epithelium was calculated. Proximal structures comprised 14.5% (+/- 0.6%) of the entire area of the HLO (P63+), whereas 85.5% (+/- 0.6%) of HLO was distal-like epithelium and mesenchyme (P63-). (C-G) The percent of specific cell markers present in an organoid was determined by dividing by the total number of Dapi+ nuclei within the same section (n=15 individual HLOs). Each point represents the data from an individual HLO while the open bar represents the average percent of cells. (C) On average, 57% of all cells in the HLOs were NKX2.1+, (D) 39% of all cells were P63+, (E) 3% were FOXJ1+, (F) 5% were SFTPC+, (G) 4% of all cells were HOPX+. (B-G) Error bars represent SEM.

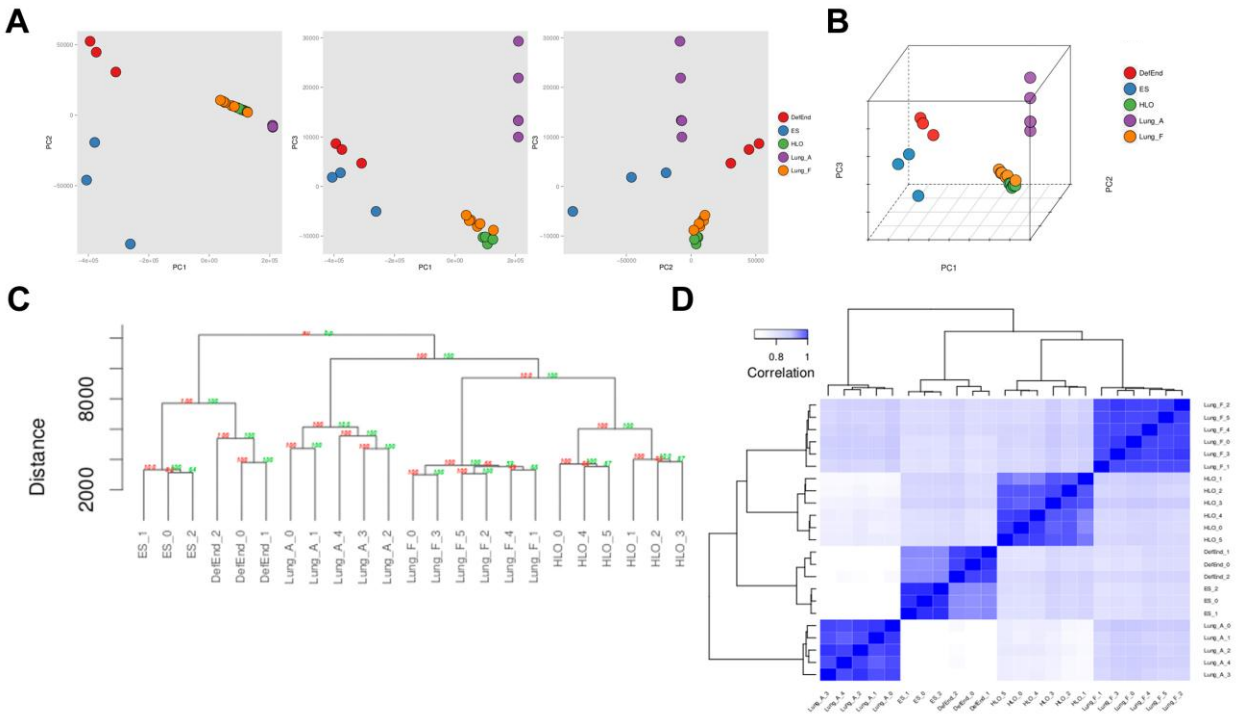

Figure 3.22. **RNA sequencing analysis associates HLOs with fetal lung tissue.** 6 HLOs (n=3 D65 HLOs and n=3 D110 HLOs) were compared to the undifferentiated H9 stem cells (SC) and definitive endoderm (Def End) and publicly available datasets of adult and fetal human lungs (see Supplemental Table 3.1). (A-B) Principle component (PC) analysis, (C) hierarchical clustering, and (D) Spearman's correlation all demonstrate that HLOs are most closely related to the fetal lung.

Table 3.1 Human tissue information

Sample Label	Description	Source	Donor ID	Accession #
Lung_A_1	Adult Lung 3e	EMBL-EBI ArrayExpress	V80	E-MTAB-1733
Lung_A_2	Adult Lung 3f	EMBL-EBI ArrayExpress	V81	E-MTAB-1733
Lung_A_3	Adult Lung 4a	EMBL-EBI ArrayExpress	V130	E-MTAB-1733
Lung_A_4	Adult Lung 4b	EMBL-EBI ArrayExpress	V131	E-MTAB-1733
Lung_A_5	Adult Lung 4d	EMBL-EBI ArrayExpress	V133	E-MTAB-1733
Lung_A_6	Fetal day 105, lung	GEO Datasets	H-24005	GSM1101693
Lung_F_2	Fetal day 105, lung	GEO Datasets	H-24111	GSM1101708
Lung_F_3	Fetal day 108, lung	GEO Datasets	H-23887	GSM1101684
Lung_F_4	Fetal day 91, lung	GEO Datasets	H-23914	GSM1101685
Lung_F_5	Fetal day 96, lung	GEO Datasets	H-24089	GSM1101699
Lung_F_6	Fetal day 98, lung	GEO Datasets	H-23964	GSM1101687

Table 3.2 List of primary and secondary Antibodies

Primary Antibody	Source	Catalog #	Dilution	Clone
Chicken anti-GFP	Abcam	Ab13970	1:500	polyclonal
Goat anti-β-Catenin (βCAT)	Santa Cruz Biotechnology	sc-1496	1:200	C-18
Goat anti-CC10	Santa Cruz Biotechnology	sc-9770	1:200	C-20
Goat anti-E-Cadherin (ECAD)	R&D Systems	AF748	1:100	N-19
Goat anti-FOXA2	Santa Cruz Biotechnology	sc-6554	1:100	M-20
Goat anti-SOX2	Santa Cruz Biotechnology	sc-17320	1:100	Y-17
Goat anti-SOX9	R&D Systems	AF3075	1:500	polyclonal
Goat anti-SOX17	R&D Systems	AF1924	1:500	polyclonal
Goat anti-VIMENTIN (VIM)	Santa Cruz Biotechnology	sc-7558	1:100	S-20
Mouse anti-Acetylated Tubulin (ACTTUB)	Sigma-Aldrich	T7451	1:1000	6-11B-1
Mouse anti-E-Cadherin (ECAD)	BD Transduction Laboratories	610181	1:500	36/E-Cadherin
Mouse anti-FOXJ1	eBioscience	14-9965-82	1:500	2A5
Rabbit anti-FOXA2	Seven Hills Bioreagents	WRAB-FOXA2	1:1000	aa7-86
Rabbit anti-NKX2.1	Abcam	ab76013	1:200	EP1584Y
Rabbit anti-P63	Santa Cruz Biotechnology	sc-8344	1:200	H-129
Rabbit anti-PAX8	Proteintech Group	10336-1-AP	1:500	Ag0306
Rabbit anti-PDPN	Santa Cruz Biotechnology	sc-134482	1:200	FL-162
Rabbit anti-N-Terminal Pro SP-C (SFTPC)	Seven Hills Bioreagents	WRAB-9337	1:200	aa1-35
Rabbit anti-SOX2	Seven Hills Bioreagents	WRAB-SOX2	1:500	polyclonal
Cy3- Mouse anti Actin-alpha smooth muscle (SMA)*	Sigma	C6198	1:400	MonoClonal
Rabbit anti-Sufactant Protein B (SFTPB)	Santa Cruz Biotechnology	sc-13978	1:200	H-300
Secondary Antibody	**Source**	**Catalog #**	**Dilution**	
Donkey anti-goat 488	Jackson Immuno	705-545-147	1:500	
Donkey anti-goat 647	Jackson Immuno	705-605-147	1:500	
Donkey anti-goat Cy3	Jackson Immuno	705-165-147	1:500	
Donkey anti-mouse 488	Jackson Immuno	715-545-150	1:500	
Donkey anti-mouse 647	Jackson Immuno	415-605-350	1:500	
Donkey anti-mouse Cy3	Jackson Immuno	715-165-150	1:500	
Donkey anti-rabbit 488	Jackson Immuno	711-545-152	1:500	
Donkey anti-rabbit 647	Jackson Immuno	711-605-152	1:500	
Donkey anti-rabbit Cy3	Jackson Immuno	711-165-102	1:500	
Donkey anti-goat 488	Jackson Immuno	705-545-147	1:500	
Donkey anti-goat 647	Jackson Immuno	705-605-147	1:500	

Donkey anti-goat Cy3	Jackson Immuno	705-165-147	1:500	
Donkey anti-mouse 488	Jackson Immuno	715-545-150	1:500	
Donkey anti-mouse 647	Jackson Immuno	415-605-350	1:500	
Donkey anti-mouse Cy3	Jackson Immuno	715-165-150	1:500	
Donkey anti-rabbit 488	Jackson Immuno	711-545-152	1:500	
Donkey anti-rabbit 647	Jackson Immuno	711-605-152	1:500	
Donkey anti-rabbit Cy3	Jackson Immuno	711-165-102	1:500	

***Secondary antibody conjugated to the primary antibody**

Table 3.3 List of primers for qRT-PCR

Primer Name	Forward Sequence	Reverse Sequence
CDX2	GGGCTCTCTGAGAGGCAGGT	GGTGACGGTGGGGTTTAGCA
ECADHERIN	TTGACGCCGAGAGCTACAC	GACCGGTGCAATCTTCAAA
FOXA2	CGACTGGAGCAGCTACTATGC	TACGTGTTCATGCCGTTCAT
FOXJ1	CAACTTCTGCTACTTCCGCC	CGAGGCACTTTGATGAAGC
HHEX	CCTCTGTACCCCTTCCCG	GGGGCTCCAGAGTAGAGGTT
HOPX	GCCTTTCCGAGGAGGAGAC	TCTGTGACGGATCTGCACTC
ID2	GACAGCAAAGCACTGTGTGG	TCAGCACTTAAAAGATTCCGTG
*MUC5AC**	GCACCAACGACAGGAAGGATGAG	CACGTTCCAGAGCCGGACAT
NKX2.1	CTCATGTTCATGCCGCTC	GACACCATGAGGAACAGCG
NMYC	CACAGTGACCACGTCGATTT	CACAAGGCCCTCAGTACCTC
P63	CCACAGTACACGAACCTGGG	CCGTTCTGAATCTGCTGGTCC
PAX8	TGCCTCACAACTCCATCAGA	CAGGTCTACGATGCGCTG
PDPN	ACATCCTTTGTTTTTGCCCA	AGTGTCATCTTCTGGCTGGC
PDX1	CGTCCGCTTGTTCTCCTC	CCTTTCCCATGGATGAAGTC
SCGB1A1	ATGAAACTCGCTGTCACCCT	GTTTCGATGACACGCTGAAA
SFTPC	AGCAAAGAGGTCCTGATGGA	CGATAAGAAGGCGTTTCAGG
SOX2	GCTTAGCCTCGTCGATGAAC	AACCCCAAGATGCACAACTC
SOX9	GTACCCGCACTTGCACAAC	GTGGtCCTTCTTGTGCTGC
VIMENTIN	CTTCAGAGAGAGGAAGCCGA	ATTCCACTTTGCGTTCAAGG

Note: All above primer sequences were obtained from http://primerdepot.nci.nih.gov/ and all annealing temperatures 55°C unless stated otherwise.

**MUC5AC* Huang, SX *et al.* Efficient generation of lung and airway epithelial cells from human pluripotent stem cells. *Nature Biotechnol*. 1–11 (2013). doi:10.1038/nbt.2754

Annealing temperature 60°C

CHAPTER 4

HUMAN PLURIPOTENT STEM CELL DERIVED LUNG ORGANOIDS GENERATED MATURE AIRWAY-LIKE STRUCTURES WHEN GROWN IN AN *IN VIVO* ENVIRONMENT

Summary

Previously we have reported a three-dimensional human lung model derived from human pluripotent stem cells (hPSCs) that resemble fetal lung tissue called human lung organoids (HLO). Recent reports using other organoid models have demonstrated that an *in vivo* environment can further mature hPSC derived organoids. Applying this approach, HLOs were seeded onto a microporous scaffold and transplanted into the highly vascular mouse epididymis fat pad. The transplanted HLOs (tHLOs) possessed mature airway-like structures consisting of an organized tube of pseudostratified epithelium expressing basal, ciliated, goblet, and club cell markers that were surrounded by mesenchymal cells expressing myofibroblast, smooth muscle and cartilage markers. The tHLO airway structures can be isolated and cultured *in vitro*. The mature airway-like structures provide an ideal model to study human adult airway disease and regeneration.

Introduction

In order to recapitulate the complex structures and cellular organization of the adult human lung, three-dimensional tissue models have been generated (1-10). More recently, three-dimensional lung models such as human lung orgnaoids (HLOs) have been derived by directing the differentiation of human pluripotent stem cells (hPSCs) including embryonic stem cells (hESCs) and induced pluripotent stem cells (iPSCs) (3, 4, 10).

HLOs were generated by directing the differentiation of hPSCs in a stepwise process, which mimics lung developmental events. HLOs possessed lung airway-like structures, which consisted of proximal epithelial cells that expressed markers of ciliated and basal cells. The airway-like structures were surrounded by mesenchyme, including cells positive for smooth muscle and myofibroblast markers (10). However, the airway structures did not possess mature airway cell types including secretory cells. In support with these results, the global transcriptome of the lung organoids closely associated to the fetal lung transcriptome. Taken together, the lung organoids were similar to the fetal lung (10) and can be applied to study lung development and maturation of developmental progenitors. However, the notable lack of mature airway cell types prevents the use of the current HLO model to study adult lung homeostasis and regeneration.

Similar to the HLOs, human intestinal organoids (HIOs), which are an *in vitro* three-dimensional model of the human intestine derived from hPSCs, closely resembled the fetal intestine (11). Strikingly, when HIOs were placed in an *in vivo* environment, under the mouse kidney capsule, the HIOs expressed mature intestinal markers and gained relevant adult structures including villi and crypts (11, 12). In order to develop a

model of human adult lung tissue, we exploited a similar approach using the HLOs. Distinct from HIOs, lung organoids placed under the mouse kidney capsule did not generate mature lung structures or cell types, and upon further examination the transplanted tissue did not express the lung marker NKX2.1.

The microenvironment of the mouse kidney capsule did not provide the necessary cues to maintain or mature the HLO tissue. Other transplantation sites and techniques such as biosynthetic scaffolds and transplant sites have been employed to maintain and mature *in vitro* grown tissue and may provide a different physical and chemical context that is necessary to mature the HLO tissue. Microporous poly (lactide-co-glycolide) (PLG) scaffolds have been used to mature hPSC derived and primary pancreatic beta cells by seeding the cells onto the honeycomb pattern of pores that are molded into a flattened cylinder. The pores resemble the shape of pancreatic islets for the beta cells to adhere to and allow for the host vascular to infiltrate the scaffold (13-17). In the native lung, the physical forces generated by the extracellular matrix (ECM) and from the surrounding tissues are critical for proper lung development and adult homeostasis (18-20). The PLG scaffold provides a rigid environment for HLOs to adhere to while the porous structure permits tissue growth and vasculature infiltration. The earliest stage of HLOs, foregut spheroids, were seeded onto microporous PLG scaffolds and were cultured for 5 to 7 days *in vitro* before being transplanted into the mouse epididymis fat pad, a highly vascularized environment that could accommodate the scaffold. After 8 weeks, the retrieved transplanted HLOs (tHLOs) possessed impressive mature airway-like structures with a proper organized pseudostratified epithelium that expressed mature cell markers of basal, ciliated, and secretory cells.

The tHLO airway structures were surrounded by mesenchymal cells that expressed both smooth muscle and myofibroblast markers, along with pockets of cartilage. The derived airways were then isolated from the transplants and cultured *in vitro*. This is the first three-dimensional mature airway model derived from hPSCs that consists of a pseudostratified tube of epithelium expressing mature airway cell markers surrounded by lung mesenchyme. The tHLO is an ideal human airway model to study airway diseases and regeneration.

Results

HLOs do not mature when placed in an in vivo environment

Previously, it has been shown that hPSC derived intestinal organoids gain physiological relevant structures of the adult intestine along with mature cell types by growing the HIOs in an *in vivo* environment, the mouse kidney capsule (11,12). In order to mature the HLO model, the same approach was applied, in which day 35 HLOs were placed under the kidney capsule of NOD-scid IL2Rgnull (NSG) mice and were harvested after 4 weeks (Fig. 4.1A-B). The retrieved organoids expressed the human mitochondria marker (huMITO), but lost expression of the lung epithelial marker NKX2.1 (Fig. 4.1C). We then hypothesized that an earlier stage of HLO cultures that expressed early lung developmental markers would be more susceptible to the micro-environmental cues of the kidney capsule than the later stage HLO cultures (10). The earliest stage of HLO three-dimensional cultures called foregut spheroids, which consist of lung progenitors with few mesenchymal cells, were injected underneath the kidney

capsule (Fig. 4.1D). After 6 weeks, the spheroids expanded surpassing the size of the kidney (Fig. 4.1E); however, further analysis demonstrated expression of huMITO, but no NKX2.1 was detected (Fig. 4.1F). Thus, neither spheroids nor day 35 HLOs transplanted under the kidney capsule gave rise to mature lung tissue.

Next, we assessed the effect of the transplant site on HLO maturation. The native lung epithelium is closely associated to the vasculature, thus a highly vascular transplant site may allow the HLO to mature. Day 35 HLOs were sewn into the omentum, the fatty fold of peritoneum attached to the stomach that is highly vascularized, and were harvested after 12 weeks (Fig. 4.1 G-H). The majority of the tissue retrieved from the omentum did not express NKX2.1, but expressed huMITO (Fig. 4.1I). Only 2 of the 13 transplants demonstrated airway-like structures similar to *in vitro* HLOs as indicated by expression of the basal cell marker P63 and ciliated cell marker FOXJ1 along with NKX2.1 and huMITO expression (Fig. 4.2) (10). Overall, the transplantation site, *in vitro* culture time of HLOs prior to transplantation, and the time the tissue was harvested did not improve the maturity of the HLO tissue.

Transplanted HLOs using a scaffold derived mature airway-like structures

The physical environment of the lung including the extracellular matrix (ECM) and the forces generated by the surrounding tissues play a critical role during development and adult homeostasis (18-20). We hypothesized that the HLOs required a rigid structural platform to grow and mature in an *in vivo* environment. Microporous PLG scaffolds provided a rigid platform while the porous structure would permit growth

of airway structures and infiltration of vasculature. Previously PLG scaffolds were transplanted into the mouse fat pad with primary and hPSC derived pancreatic beta cells and the mouse vasculature was able infiltrate the scaffold (13-17, 21). For HLO transplants, the PLG scaffold was coated with Matrigel diluted with DMEM/F12, then seeded with foregut spheroids suspended in 100% Matrigel. The PLG scaffolds were cultured for 5 to 7 days *in vitro* submersed in 500ng/mL FGF10 supplemented media (Fig. 4.3A-B), the same media used to grow HLOs *in vitro* (10). The scaffolds were then either dipped in Matrigel supplemented with FGF10 or no Matrigel then transplanted into the mouse epididymal fat pad (Matrigel n=8, No Matrigel n=3 Fig. 4.3A). Both conditions resulted in mature airway-like structures (airway structures characterized in Fig. 4.5). The fat pad is highly vascularized similar to the omentum, but provides greater surface area than the omentum, which then can accommodate the scaffold. When scaffolds were harvested at 4 weeks, the transplanted foregut spheroids resembled *in vitro* HLOs (10). The retrieved tissue expressed the lung marker NKX2.1 and huMITO while possessing airway-like structures that consisted of cells expressing the basal cell marker P63 and ciliated marker FOXJ1, but club cell marker CC10 was not detected (Fig. 4.4A-B). The 4 week scaffold transplants caused the foregut spheroids to mature, but the transplants still resulted in tissue similar to fully grown *in vitro* HLOs.

Since the lung epithelium was maintained and some maturation occurred after 4 weeks, we predicted that extending the transplant time to 8 weeks would increase the maturation of the transplanted foregut spheroids. The tHLOs harvested after 8 weeks ranged in size from 0.5cm to 1.5cm and extended beyond the dimensions of the scaffold (Fig. 4.5A-B). The histology of the transplanted tissue showed airway-like

structures tightly surrounded by mesenchymal shaped cells. In addition, there were pockets of cartilage throughout the transplants (Fig. 4.5C). The airway-like epithelium expressed the lung marker NKX2.1 and huMiTO (Fig. 4.5D).

In the adult native lung, airways are organized into a pseudostratified epithelium with basal and ciliated cells being the most prevalent cell types in the airway. Secretory cells, goblet and club cells, are scattered throughout mature airways (22). The tHLOs recapitulate a mature airway by possessing a tightly organized pseudostratified epithelium (outlined in red in Fig. 4.5 E-F) that consisted of cells lining the basal lamina that expressed basal cell markers P63 and CK5 (Fig. 4.5E, Fig. 4.6). The cells facing in towards the lumen of the tHLOs were multi-ciliated cells that expressed ACTTUB and the ciliated cell marker FOXJ1 (Fig. 4.5E, Fig. 4.7). The majority of the cells in the transplant expressed markers of basal cells and ciliated cells that were organized into a tube structure where the FOXJ1+ cells lined the lumen while the P63+cells lined the outside of the tube along the basal lamina similar to mature airways. The tHLOs possessed cells scattered throughout the airway structures that expressed club cell marker CC10 and goblet cell marker MUC5AC (Fig. 4.5F-G). Thus, the cellular ratios of basal, ciliated, goblet, and club cells in the tHLO reflected the cellular ratios in adult native lung airways. Foregut spheroids grown on the scaffold *in vitro* for 4 to 8 weeks had significantly less growth and although expressed lung marker NKX2.1 did not possess any airway structures (Fig. 4.8). This suggests that the scaffold alone does not induce maturation, but the combination of the scaffold and the *in vivo* environment allowed for rapid growth and maturation.

Along with the epithelium, native adult airways are surrounded by smooth muscle, myofibroblasts, and cartilage. The tHLO airway structures were surrounded by cells expressing smooth muscle actin and PDGFRα positive (SMA+/PDGFRα+) and SMA+PDGFRα- (Fig. 4.9A), which are markers for myofibroblasts and smooth muscle respectively in mice (23-25). HLOs grown *in vitro* expressed the same combination of mesenchymal markers except the HLOs did not possess cartilage nor did the control 8wk *in vitro* grown scaffolds (10). The tHLOs possess pockets of cartilage indicated by the cell morphology and the cells were positive for SafraninO, a stain specific for cartilage (Fig. 4.5C bottom panel, Fig. 4.9B). In adult airways vasculature and neurons line the airways surrounded by mesenchyme. Similarly, neuron marker TUJ1 positive cells and vasculature marker PECAM positive cells surrounded some of tHLO airway-like structures (Fig. 4.10).

Transplanted lung organoids can be cultured after transplantation

The airway-like structures were mechanically isolated from the transplant and cultured in a Matrigel droplet overlaid with media supplemented with FGF10 and Rho-associated protein kinase (ROCK) inhibitor, Y27632. Previously, ROCK inhibition has been shown to increase epithelial proliferation in mouse and human cell lines and more specifically enhanced lung basal cell proliferation *in vitro* (26-28). These cultures had a mix of morphology including cyst-like structures, budding structures, and dense clumps (Fig. 4.11A). The cultures were analyzed after 5 days in culture by immunofluorescence. The majority of the cells expressed the lung marker NKX2.1 and basal cell marker P63

(Fig. 4.11B). These data suggest that high FGF10 and Y27632 cause the tHLO airway cultures to maintain basal cells, airway stem cell population (2, 29-33). This is in line with previous data that ROCK inhibition increases basal cell proliferation *in vitro* (26) and FGF10 maintains the basal cell population in the mouse trachea (34). Moving forward, changes to the culture media will need to be implemented in order to still maintain the basal cell population, but in addition maintain other airway cells including ciliated and secretory cells.

Discussion

To date, groups have derived three-dimensional lung models derived from both primary cell lines and hPSCs that consist of adult epithelial airway cells. However, these models do not generate a pseudostratified epithelium that reflects the cellular ratio of basal, ciliated, and secretory cells found in the native adult airways. In addition, previous three-dimensional models only consist of epithelial cells. The tHLO airway-like structures are surrounded by lung mesenchyme, vasculature and neurons, in which all these tissues surround the native adult lung airways.

In order to utilize the derived mature airway-like structures, the tHLO airway cultures need to maintain the basal, ciliated, and secretory cell expression. Notch signaling has been shown to be necessary to maintain the balance of mature airway cells and basal cells (2, 33, 35-38). In derived human lung cultures, Notch inhibition by DAPT caused a significant increase in ciliated and neuroendocrine cells (4). In addition, FGF18 has been shown to be sufficient to generate proximal airways while inhibiting

distal epithelial identity in mice (39). By inhibiting Notch and/or the addition of FGF18 may cause the tHLO airway structures to maintain the expression of mature airway cells. Similarly, air-liquid interface media (ALI), a manufactured media to culture primary bronchial epithelial cells *ex vivo,* has been applied to hPSC derived lung progenitors and caused the progenitors to express mature airway cell markers including ciliated and secretory cells (4, 40, 41).

After determining the ideal combination of growth factors and media to maintain the tHLO adult airway structures, the next step will be to apply these models to study airway diseases and acute injuries. Since the tHLOs form a lumen in culture, these lumens can be microinjected with pathogens or toxins that have been shown to disrupt airway homeostasis, including human respiratory syncytial virus, SO2, naphthalene, and allergens (2, 42-46). This technique has been demonstrated by injecting pathogens into the intestinal organoid lumen (47). In addition to environmental factors, there are genetic disorders including cystic fibrosis that affect lung airway funtion. Since the tHLOs are derived from hPSCs, iPSC lines derived from patients with airway genetic disorders can be generated, and then the tHLOs containing the genetic mutations can be challenged with different toxins. Along the lines of diseases, inflammatory cytokines such as IL-13 and IL-17A have been introduced into human airway models and have been shown to disrupt the cellular composition of the airways (48). Taken together, disease models, acute injuries, and cytokines can be introduced into tHLO cultures in order to study human airway maintenance and regeneration including the balance between ciliated and secretory cell populations, mucus secretion, and mesenchymal population changes.

The *in vivo* environment of the mouse fat pad consists of several cell types and tissues that can affect the transplant chemically and physically. However, by breaking down the environment by tissue or cell type may lead us to the key cell/tissues that are necessary for airway maturation *in vitro.* For instance, the transplant was infiltrated with mouse vasculature suggesting that the vasculature plays a key part in the maturation process of the tHLO. Vasculature cells, endothelial cells, can be derived from hPSCs (49-51). Thus by deriving endothelial cells and foregut spheroids separately then combining the two derived tissues may cause airway maturation *in vitro.*

The tHLO is the first adult airway model to possess a pseudostratified tube of epithelial airway cells surrounded by lung mesenchyme. In addition, tHLO airways recapitulate the cellular ratio of the adult airway by the majority of the cells expressing basal cell markers, P63 and CK5, and ciliated cell markers, FOXJ1 and ACTTUB, with fewer cells expressing secretory cell markers, goblet cell marker MUC5AC and club cell marker CC10. These cells are surrounded by mesenchyme expressing myofibroblast and smooth muscle markers along with pockets of cartilage. The mature airway-like structures can be removed from the transplant and cultured *in vitro.* Overall, tHLOs provide a novel human airway model to study airway diseases and regeneration.

Materials and Methods

Maintenance of hESCs and generation of foregut spheroids and HLOs

Human ES line UM63-1 (NIH registry #0278) was obtained from the University of Michigan. Stem cells were maintained on Matrigel (BD Biosciences) in mTesR1 medium

(STEM CELL Technologies). HESCs were passaged as previously described (52). HLOs were generated as previously described (10).

Kidney Capsule and Omentum Transplants

D35 HLOs were placed under the kidney capsule of male NOD-scid IL2Rgnull (NSG) by forceps. The mice were sacrificed and transplant retrieved after 4 weeks. Foregut spheroids mixed with 100% Matrigel were pipetted underneath the mouse kidney capsule and transplants were retrieved after 6 weeks. D30 HLOs were sewn into the mouse omentum and transplants were retrieved after 12 weeks.

Scaffolds Transplants

PLG scaffolds were washed in ddH2O for two 1 hour washes. The scaffold were then washed in 70% EtOH for 2 minutes and dried for 5 minutes. PLG scaffolds were filled with 15µL of cold Matrigel diluted in DMEM/F12 (dilution factor is lot dependent) and incubated at 37°C for 15 minutes. This step was repeated twice. Lung spheroids were mixed with 100% Matrigel and pipetted into the scaffold. The seeded scaffolds were incubated for 15 minutes at 37°C and then overlaid with HLO media (500ng/mL FGF10 and 1% FBS in basal foregut media described in (10)). Scaffolds were cultured for 5 to 7 days *in vitro* with media being changed every other day. Scaffolds cultured with spheroids were removed from culture and were then immersed in Matrigel supplemented with 500ng/mL FGF10, allowed to solidify for 5 minutes or no Matrigel.

The epididymal fat pads of male NOD-scid IL2Rgnull (NSG) were exposed using a lower midline incision. Matrigel coated scaffolds were then placed along the epididymal blood vessels and covered with epididymal fat. The incision was closed in 2-layers using absorbable suture. Mice were sacrificed 4 and 8 weeks post-transplant.

Immunohistochemistry

Immunostaining was carried out as previously described (19). Antibody information and dilutions can be found in Table 1. All images were taken on a Nikon A1 confocal microscope or an Olympus IX71 epifluorescent microscope.

Experimental Replicates

All immunofluorescence (IF) were done on at least three (n=3) independent biological samples per experiment except for foregut spheroids injected into the kidney capsule. Only 1 out 3 transplanted foregut spheroids under the kidney capsule worked; therefore only 1 sample was used for the IF analysis.

References

1. Barkauskas CE, et al. (2013) Type 2 alveolar cells are stem cells in adult lung. *J Clin Invest* 123(7):3025–3036.

2. Rock JR, et al. (2009) Basal cells as stem cells of the mouse trachea and human airway epithelium. *Proceedings of the National Academy of Sciences* 106(31):12771–12775.

3. Gotoh S, et al. (2014) Generation of alveolar epithelial spheroids via isolated progenitor cells from human pluripotent stem cells. *Stem Cell Reports* 3(3):394–403.

4. Konishi S, et al. (2016) Directed Induction of Functional Multi-ciliated Cells in Proximal Airway Epithelial Spheroids from Human Pluripotent Stem Cells. *Stem Cell Reports* 6(1):18–25.

5. Vaughan MB, Ramirez RD, Wright WE, Minna JD, Shay JW (2006) A three-dimensional model of differentiation of immortalized human bronchial epithelial cells. *Differentiation* 74(4):141–148.

6. Pageau SC, Sazonova OV, Wong JY, Soto AM, Sonnenschein C (2011) The effect of stromal components on the modulation of the phenotype of human bronchial epithelial cells in 3D culture. *Biomaterials* 32(29):7169–7180.

7. Fessart D, Begueret H, Delom F (2013) Three-dimensional culture model to distinguish normal from malignant human bronchial epithelial cells. *Eur Respir J* 42(5):1345–1356.

8. Franzdóttir SR, et al. (2010) Airway branching morphogenesis in three dimensional culture. *Respir Res* 11:162.

9. Kaisani A, et al. (2014) Branching morphogenesis of immortalized human bronchial epithelial cells in three-dimensional culture. *Differentiation*. doi:10.1016/j.diff.2014.02.003.

10. Dye BR, et al. (2015) In vitro generation of human pluripotent stem cell derived lung organoids. *Elife* 4. doi:10.7554/eLife.05098.

11. Finkbeiner SR, et al. (2015) Transcriptome-wide Analysis Reveals Hallmarks of Human Intestine Development and Maturation In Vitro and In Vivo. *Stem Cell Reports*. doi:10.1016/j.stemcr.2015.04.010.

12. Watson CL, et al. (2014) An in vivo model of human small intestine using pluripotent stem cells. *Nature Medicine* 20(11):1310–1314.

13. Gibly RF, Zhang X, Lowe WL, Shea LD (2013) Porous scaffolds support extrahepatic human islet transplantation, engraftment, and function in mice. *Cell Transplant* 22(5):811–819.

14. Blomeier H, et al. (2006) Polymer scaffolds as synthetic microenvironments for extrahepatic islet transplantation. *Transplantation* 82(4):452–459.

15. Hlavaty KA, et al. (2014) Enhancing human islet transplantation by localized release of trophic factors from PLG scaffolds. *Am J Transplant* 14(7):1523–1532.

16. Graham JG, et al. (2013) PLG scaffold delivered antigen-specific regulatory T cells induce systemic tolerance in autoimmune diabetes. *Tissue Eng Part A* 19(11-12):1465–1475.

17. Kheradmand T, et al. (2011) Permanent protection of PLG scaffold transplanted allogeneic islet grafts in diabetic mice treated with ECDI-fixed donor splenocyte infusions. *Biomaterials* 32(20):4517–4524.

18. Kim HY, Nelson CM (2012) Extracellular matrix and cytoskeletal dynamics during branching morphogenesis. *organogenesis* 8(2):56–64.

19. Rockich BE, et al. (2013) Sox9 plays multiple roles in the lung epithelium during branching morphogenesis. *Proceedings of the National Academy of Sciences* 110(47):E4456–64.

20. Harunaga JS, Doyle AD, Yamada KM (2014) Local and global dynamics of the basement membrane during branching morphogenesis require protease activity and actomyosin contractility. *Developmental Biology* 394(2):197–205.

21. Gibly RF, et al. (2011) Extrahepatic islet transplantation with microporous polymer scaffolds in syngeneic mouse and allogeneic porcine models. *Biomaterials* 32(36):9677–9684.

22. Mercer RR, Russell ML, Roggli VL, Crapo JD (1994) Cell number and distribution in human and rat airways. *American Journal of Respiratory Cell and Molecular Biology* 10(6):613–624.

23. Boucherat O, et al. (2007) Gene expression profiling in lung fibroblasts reveals new players in alveolarization. *Physiol Genomics* 32(1):128–141.

24. Hinz B, et al. (2007) The myofibroblast: one function, multiple origins. *AJPA* 170(6):1807–1816.

25. Chen L, Acciani T, Le Cras T, Lutzko C, Perl A-KT (2012) Dynamic regulation of platelet-derived growth factor receptor α expression in alveolar fibroblasts during realveolarization. *American Journal of Respiratory Cell and Molecular Biology* 47(4):517–527.

26. Horani A, Nath A, Wasserman MG, Huang T, Brody SL (2013) Rho-associated protein kinase inhibition enhances airway epithelial Basal-cell proliferation and lentivirus transduction. *American Journal of Respiratory Cell and Molecular Biology* 49(3):341–347.

27. Liu X, et al. (2012) ROCK inhibitor and feeder cells induce the conditional reprogramming of epithelial cells. *Am J Pathol* 180(2):599–607.

28. Hegab AE, et al. (2015) Mimicking the niche of lung epithelial stem cells and characterization of several effectors of their in vitro behavior. *Stem Cell Res* 15(1):109–121.

29. Hackett T-L, et al. (2008) Characterization of side population cells from human airway epithelium. *STEM CELLS* 26(10):2576–2585.

30. Hong KU, Reynolds SD, Watkins S, Fuchs E, Stripp BR (2004) Basal cells are a multipotent progenitor capable of renewing the bronchial epithelium. *AJPA* 164(2):577–588.

31. Boers JE, Ambergen AW, Thunnissen FB (1998) Number and proliferation of basal and parabasal cells in normal human airway epithelium. *Am J Respir Crit Care Med* 157(6 Pt 1):2000–2006.

32. Pardo-Saganta A, et al. (2015) Injury induces direct lineage segregation of functionally distinct airway basal stem/progenitor cell subpopulations. *Cell Stem Cell* 16(2):184–197.

33. Nakajima M, et al. (1998) Immunohistochemical and ultrastructural studies of basal cells, Clara cells and bronchiolar cuboidal cells in normal human airways. *Pathol Int* 48(12):944–953.

34. Volckaert T, et al. (2013) Localized Fgf10 expression is not required for lung branching morphogenesis but prevents differentiation of epithelial progenitors. *Development* 140(18):3731–3742.

35. Tadokoro T, et al. (2014) IL-6/STAT3 promotes regeneration of airway ciliated cells from basal stem cells. *Proceedings of the National Academy of Sciences* 111(35):E3641–9.

36. Rock JR, et al. (2011) Notch-dependent differentiation of adult airway basal stem cells. *Cell Stem Cell* 8(6):639–648.

37. Morimoto M, et al. (2010) Canonical Notch signaling in the developing lung is required for determination of arterial smooth muscle cells and selection of Clara versus ciliated cell fate. *J Cell Sci* 123(Pt 2):213–224.

38. Zhang S, Loch AJ, Radtke F, Egan SE, Xu K (2013) Jagged1 is the major regulator of Notch-dependent cell fate in proximal airways. *Dev Dyn* 242(6):678–686.

39. Whitsett JA, et al. (2002) Fibroblast growth factor 18 influences proximal programming during lung morphogenesis. *J Biol Chem* 277(25):22743–22749.

40. Wong AP, et al. (2012) Directed differentiation of human pluripotent stem cells into mature airway epithelia expressing functional CFTR protein. *Nature Biotechnology* 30(9):875–881.

41. Wong AP, et al. (2015) Efficient generation of functional CFTR-expressing airway epithelial cells from human pluripotent stem cells. *Nat Protoc* 10(3):363–381.

42. Borthwick DW, Shahbazian M, Krantz QT, Dorin JR, Randell SH (2001) Evidence for stem-cell niches in the tracheal epithelium. *American Journal of Respiratory Cell and Molecular Biology* 24(6):662–670.

43. Rawlins EL, Hogan BLM (2008) Ciliated epithelial cell lifespan in the mouse trachea and lung. *Am J Physiol Lung Cell Mol Physiol* 295(1):L231–4.

44. Stripp BR, Maxson K, Mera R, Singh G (1995) Plasticity of airway cell proliferation and gene expression after acute naphthalene injury. *Am J Physiol* 269(6 Pt 1):L791–9.

45. Rock JR, Randell SH, Hogan BLM (2010) Airway basal stem cells: a perspective on their roles in epithelial homeostasis and remodeling. *Dis Model Mech* 3(9-10):545–556.

46. Collins PL, Graham BS (2008) Viral and host factors in human respiratory syncytial virus pathogenesis. *J Virol* 82(5):2040–2055.

47. Leslie JL, et al. (2015) Persistence and toxin production by Clostridium difficile within human intestinal organoids result in disruption of epithelial paracellular barrier function. *Infect Immun* 83(1):138–145.

48. Danahay H, et al. (2015) Notch2 is required for inflammatory cytokine-driven goblet cell metaplasia in the lung. *Cell Rep* 10(2):239–252.

49. Levenberg S, Golub JS, Amit M, Itskovitz-Eldor J, Langer R (2002) Endothelial cells derived from human embryonic stem cells. *Proc Natl Acad Sci USA* 99(7):4391–4396.

50. Kane NM, et al. (2010) Derivation of endothelial cells from human embryonic stem cells by directed differentiation: analysis of microRNA and angiogenesis in vitro and in vivo. *Arterioscler Thromb Vasc Biol* 30(7):1389–1397.

51. Costa M, et al. (2013) Derivation of endothelial cells from human embryonic stem cells in fully defined medium enables identification of lysophosphatidic acid and platelet activating factor as regulators of eNOS localization. *Stem Cell Res* 10(1):103–117.

52. Spence JR, et al. (2011) Directed differentiation of human pluripotent stem cells into intestinal tissue in vitro. *Nature* 470(7332):105–109.

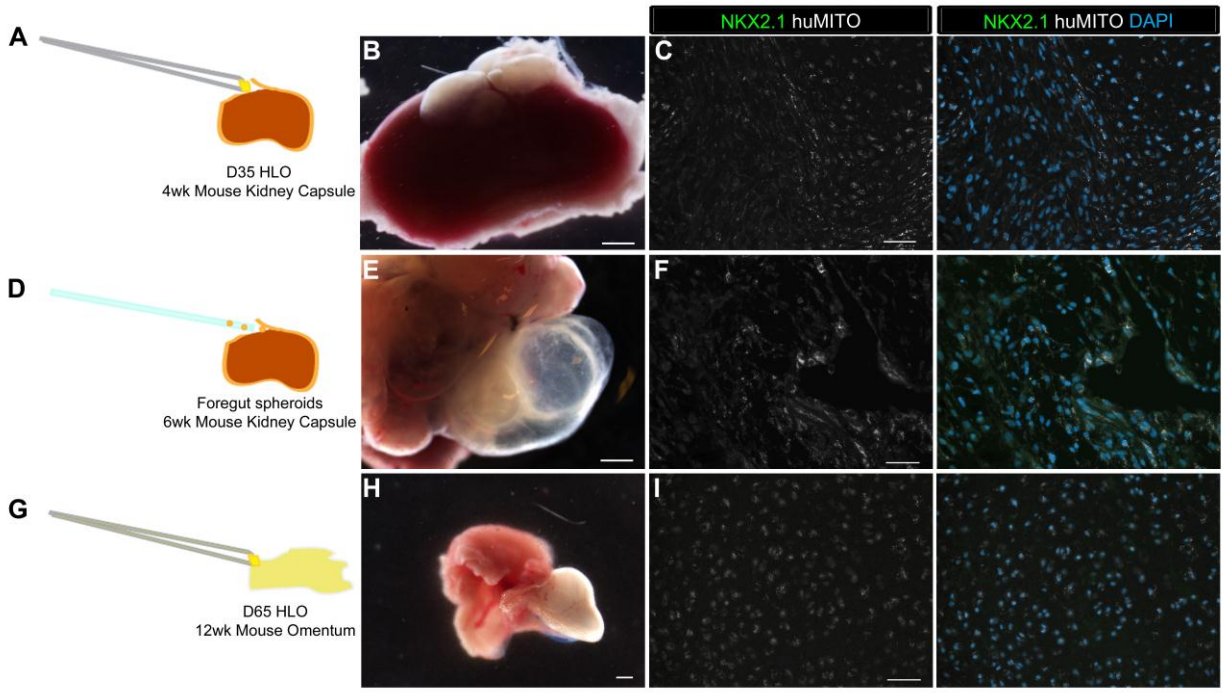

Figure 4.1 Various *in vivo* environments did not maintain lung identify. (A) D35 HLOs were placed under a mouse kidney capsule and retrieved after 4 weeks. (B) Wholemount of the retrieved tissue within the kidney capsule. The white bumps on top of the kidney was the transplanted tissue. (C) Tissue retrieved from the kidney capsule did not express lung marker NKX2.1 (green), but expressed human mitochondria marker (huMITO, white) n=6. (D) Foregut spheroids were placed under the kidney capsule and retrieved after 6 weeks. (E) The foregut spheroids grew out from the kidney capsule and consisted of transparent and dense white tissue. (F) Tissue retrieved from the kidney capsule did not express NKX2.1 (green), but expressed huMITO (white) n=1. (G) D65 HLOs were sewn into the omentum, fat tissue surrounding the stomach and proximal intestine. The tissue was retrieved after 12 weeks. (H) The white outgrowth is the transplant after 12 weeks. (I) The majority of the tissue did not express NKX2.1 (green), but all the retrieved tissue expressed huMITO n=13 Scale bars in B,E,H represent 250µm and scale bars in C,F,I represent 50µm.

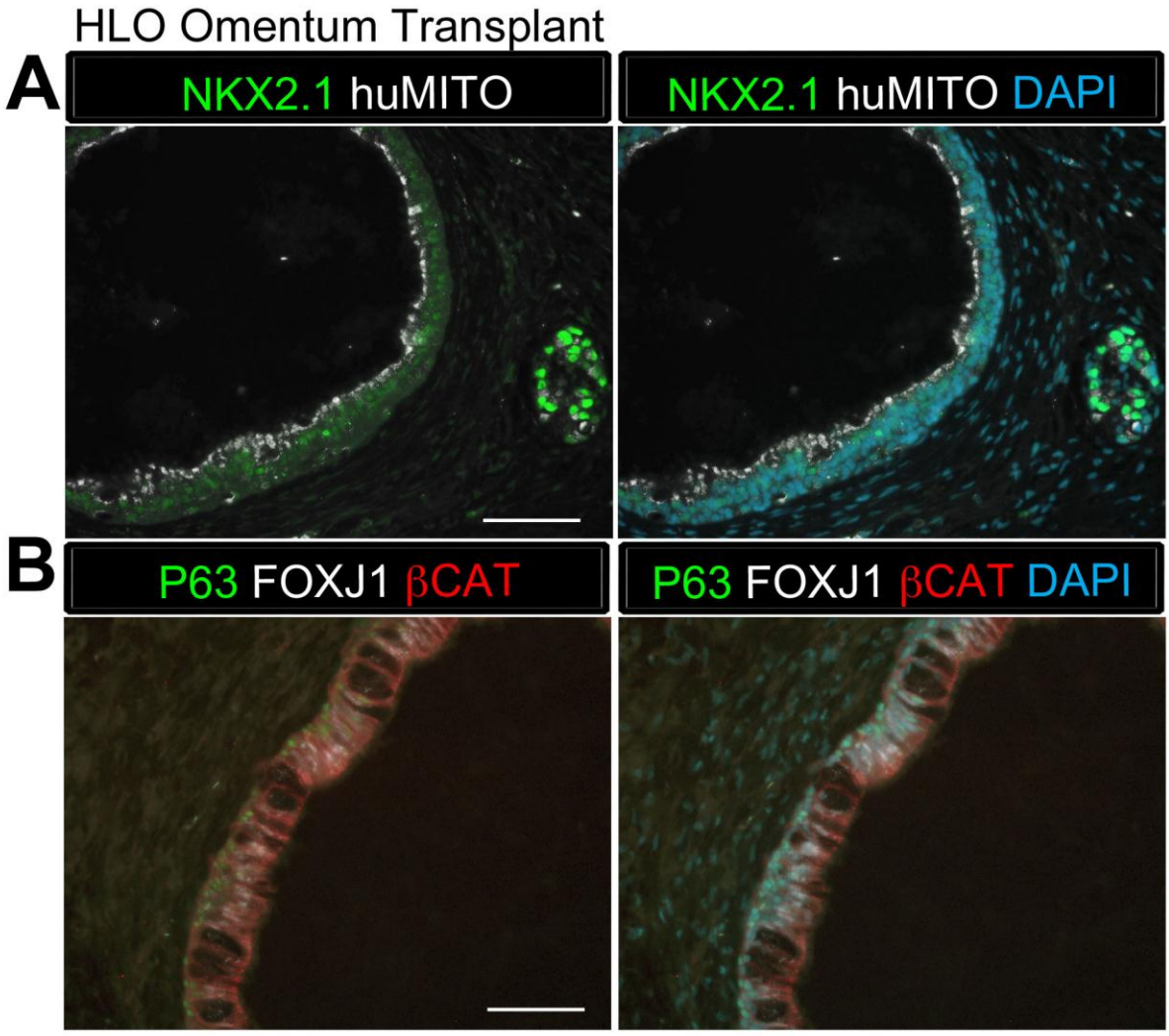

Figure 4.2 Only 2 out of 13 HLO omentum transplants maintained lung identity. (A) 2 out of 13 HLO omentum transplants expressed lung marker NKX2.1 (green) and all the transplant tissue expressed human mitochondria marker (huMITO, white). (B) 2 out 13 transplants possessed airway-like structures that expressed basal cell marker P63 (green) and ciliated cell marker FOXJ1 (white), which were similar to HLOs grown *in vitro* for 50 days (Chapter 3). Scale bars represent in A-B 50µm.

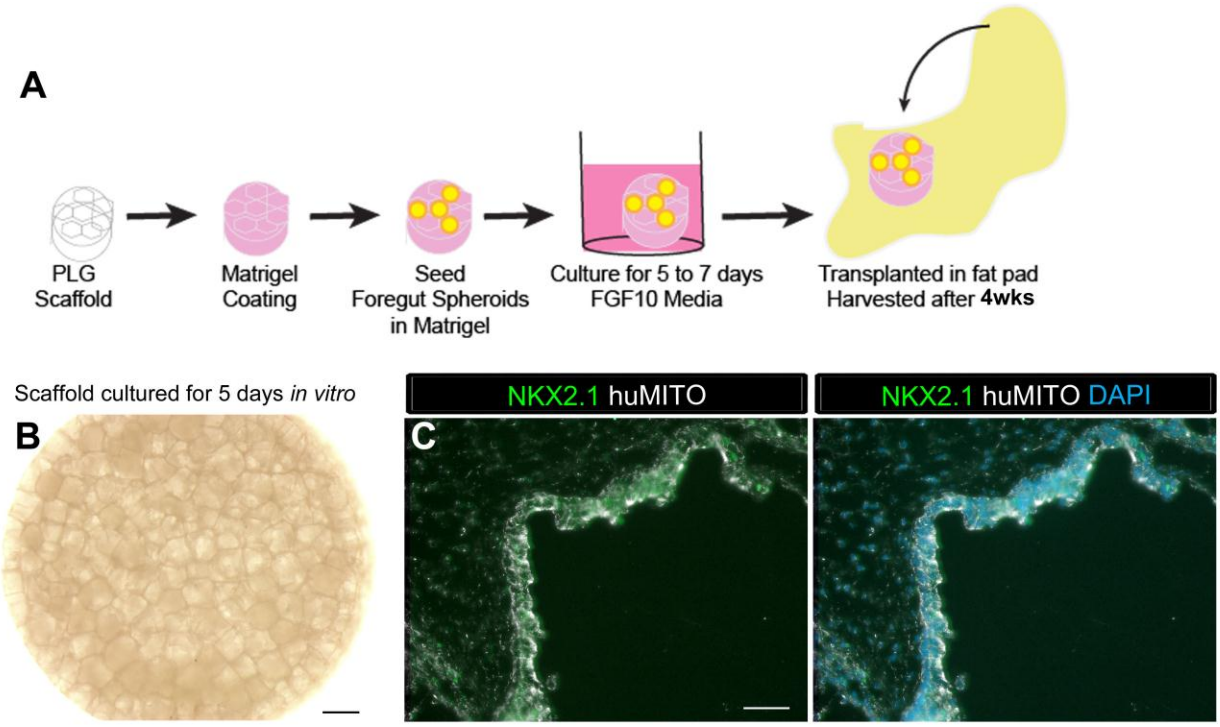

Figure 4.3 Foregut spheroids grown on a scaffold and transplanted into the mouse fatpad expressed lung markers when harvested at 4 weeks. (A) PLG scaffolds were coated with a mix of Matrigel and DMEM/F12. Foregut spheroids were then seeded onto the scaffold in 100% Matrigel. The scaffolds were cultured for 5 to 7 days *in vitro* in media supplemented with FGF10. The scaffolds were retrieved after 4 weeks. (B) Whole mount image of foregut spheroids seeded on the scaffold and cultured for 5 days *in vitro*. (C) Tissue retrieved after 4 weeks expressed lung marker NKX2.1 (green) and human maker, huMITO (white) within the airway-like structures 4week: n=4. Scale bars in B represent 500µm and in C represent 50µm.

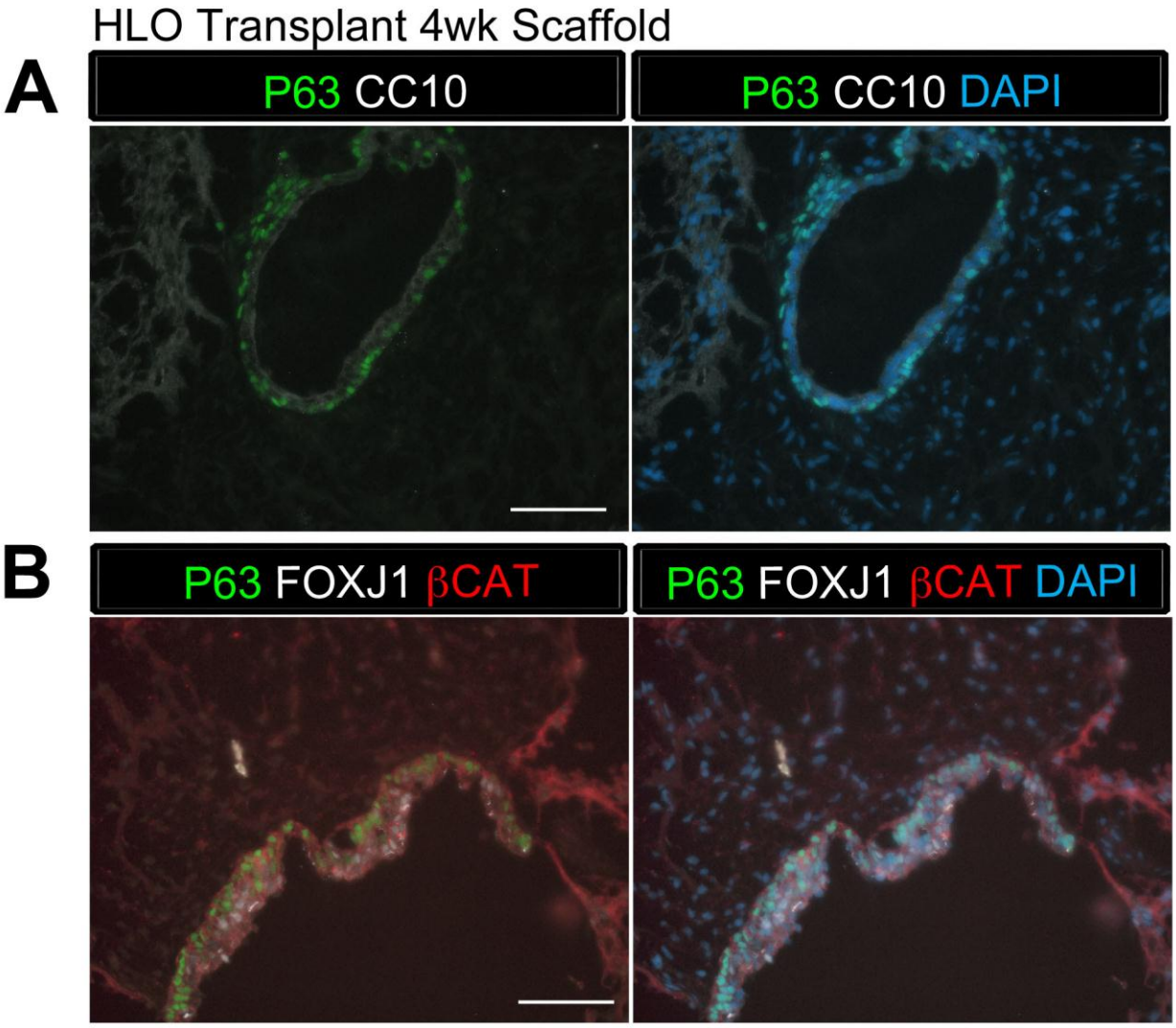

Figure 4.4 Transplanted scaffolds retrieved after 4 weeks possessed airway-like structures similar to HLOs grown *in vitro.* (A) Foregut spheroids transplanted on a scaffold into the mouse fat pad and retrieved after 4 weeks had airway-like structures that expressed basal cell marker P63 (green), but did not express club cell marker CC10 (white). (B) Airway-like structures also expressed ciliated cell marker FOXJ1 (white) along with P63 (green). β-Catenin (βCAT, red) outlines the epithelium n=4. Scale bars represent in A-B 50μm.

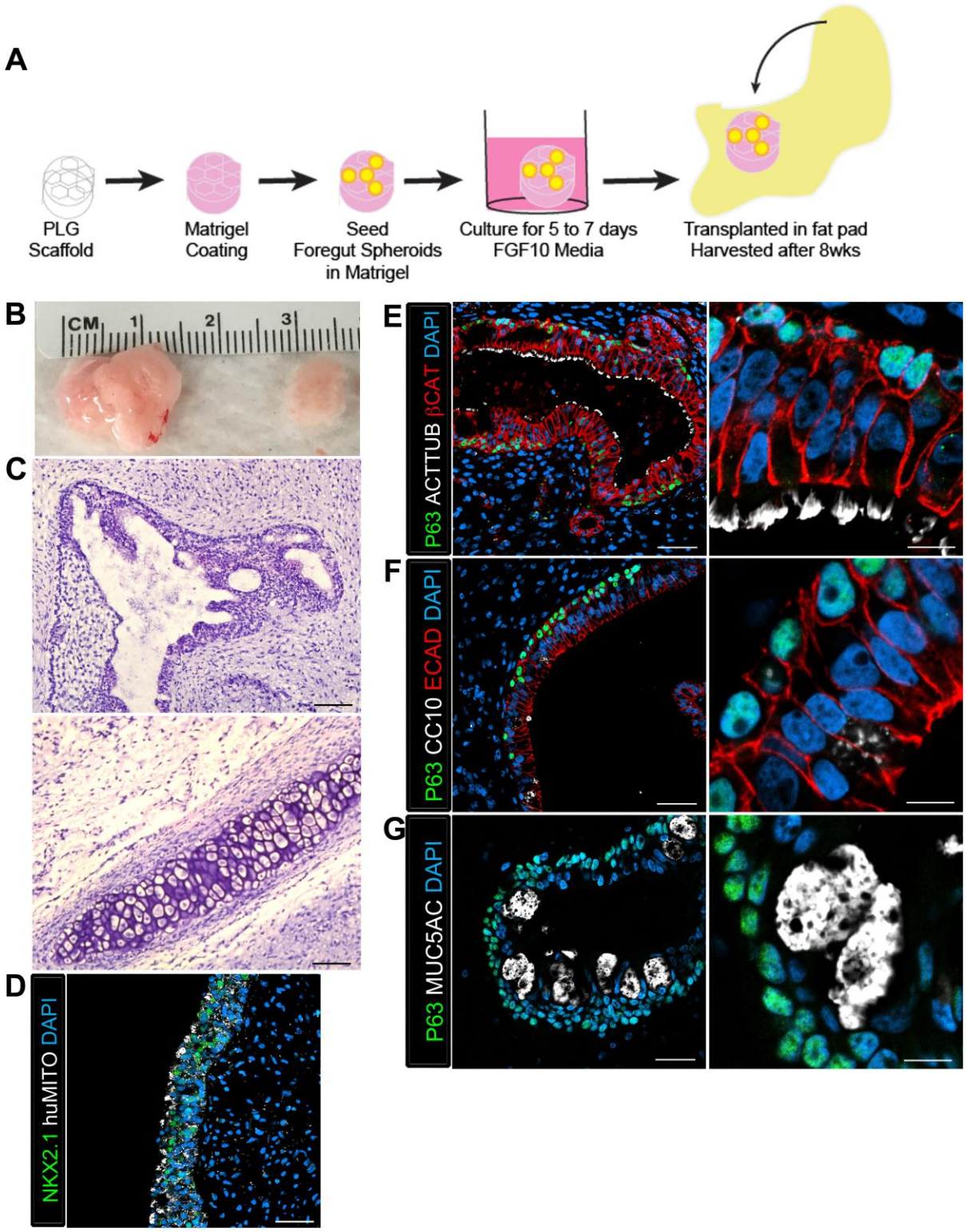

Figure 4.5 Transplanted foregut spheroids harvested at 8 weeks outgrew the scaffold and possessed mature airway-like structures. (A) PLG scaffold was coated with Matrigel diluted in DMEM/F12 then foregut spheroids were seeded onto the

scaffold in 100% Matrigel. The scaffolds were cultured for 5 to 7 days *in vitro* in media supplemented with FGF10. The scaffold were then placed in the mouse fat pad and retrieved after 8 weeks. (B) Whole mount image of transplanted human lung organoids (tHLOs). The tHLOs ranged from 0.5cm to 1.5cm length. (C) H&E of tHLOs showed airway like structures (top panel) and clusters of cartilage (bottom panel). (D) Tissue retrieved after 8 weeks expressed lung marker NKX2.1 (green) and human maker, huMITO (white) within the airway-like structures (E-F) 8 week transplants possessed airway structures organized into a pseudostratified epithelium outlined by βCAT (red). (E) The airway-like structures expressed basal cell marker P63 (green) that lined the basal lamina of the epithelium outlined by β-Cat (red). The majority of the cells adjacent to the cells lining the basal lamina were multiciliated cells positive for acetylated tubulin with the cilia facing in toward the lumen area (ACTTUB, white). (F) The airway-like structures lined with basal cell marker P63 (green) also expressed club cell marker CC10 (white), in which the high mag image on the right shows the punctate staining of the secreted protein stain. (G) Transplanted organoids expressed goblet cell marker MUC5AC (white) that was secreted in toward the lumen area and lined with P63+cells (green) n=12. 7 out of 8 tHLOs possessed airway structures. Scale bars in C represent 50µm, in D-G low mag scale bars represent 50µm and E-G high mag represent 10µm.

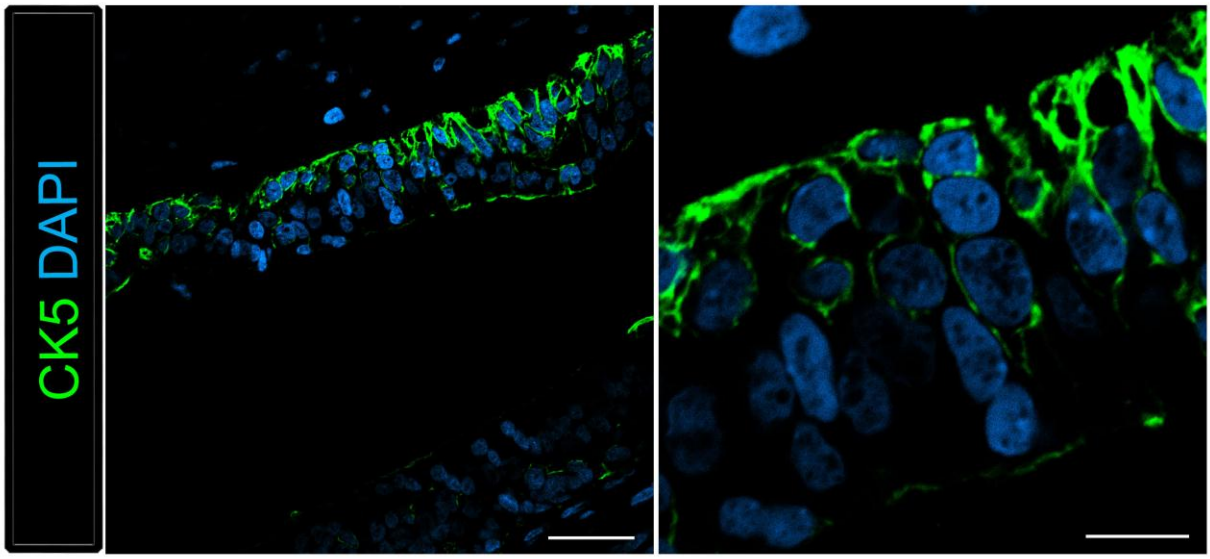

Figure 4.6 Transplanted organoids expressed basal cell marker Cytokeratin5. Airway-like structures possessed cells lining the basal lamina that expressed basal cell marker Cytokeratin5 (CK5, green). Scale bars represent 50μm in the low mag image and 10μm in the high mag image.

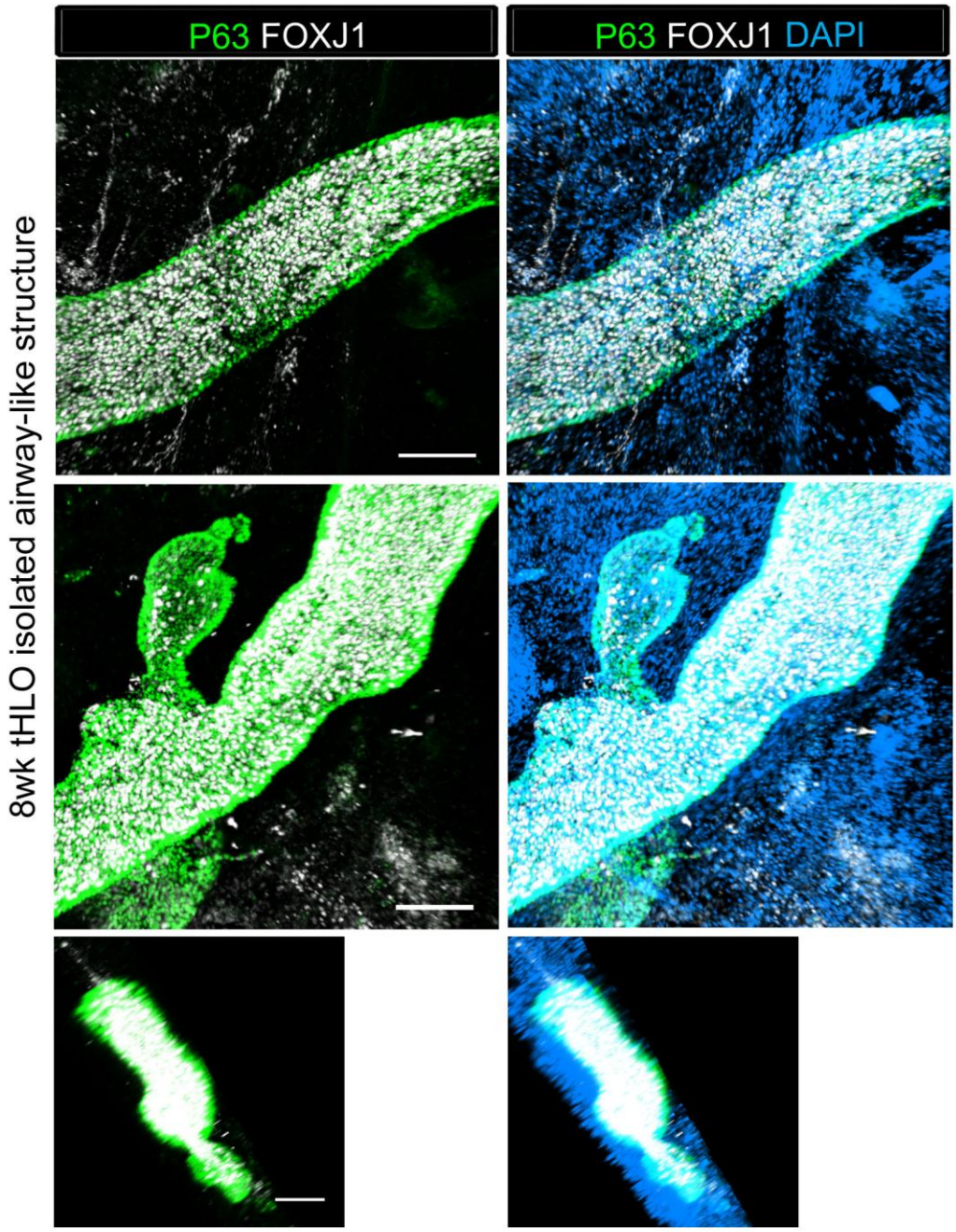

Figure 4.7 tHLOs possessed airway-like structures that expressed airway markers within a tube structure. 3D rendering of z-stack images revealed tube structures that were outlined by basal cell marker P63 (green) and within the tube cells expressed ciliated cell marker FOXJ1 (white). Bottom panel is the z-stack images stacked looking through the tube where the P63 (green) outlines the tube and the FOXJ1 (white) is within the tube. The lumen (L) is not visible because the cells are stacked one on top of each other. Scale bars represent 100μm.

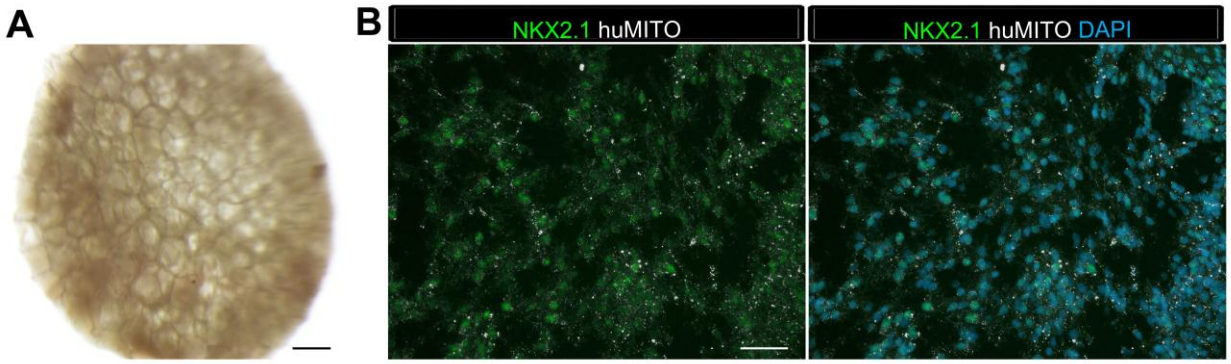

Figure 4.8 Foregut spheroids grown on PLG scaffolds *in vitro* maintained the lung identity but did generate airway-like structures. (A) Whole mount image of scaffold grown for 8 weeks *in vitro*. Organoid tissue stayed within the scaffold. (B) The tissue within the scaffold expressed lung marker NKX2.1 (green) and huMITO (white), but did not form airway-like structures. Scale bars represent 500µm in A and 50µm in B.

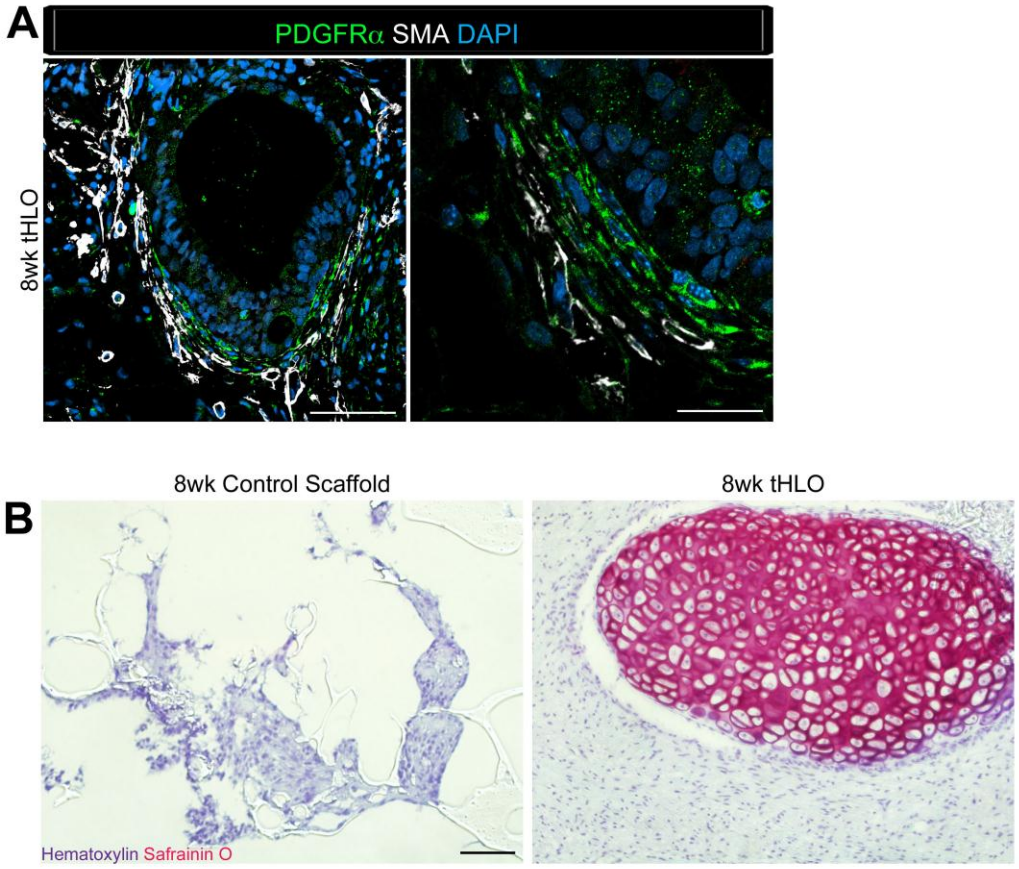

Figure 4.9 Transplanted organoids consisted of different mesenchymal cells. (A) Cells surrounding the airway-like structures expressed myofibroblast markers PDGFRα (green) SMA (white) and expressed smooth muscle markers PDGFRα-/SMA+ (white only). (B) Cartilage stain SafraninO showed clusters of cartilage in the 8wk tHLO (right panel) while there was no cartilage in the scaffold grown *in vitro* for 8 weeks (left panel). Scale bars in A represent 50μm lower mag image (left panel) 25μm in bottom panel in lower mag image (right panel). Scale bar in B represent 100μm.

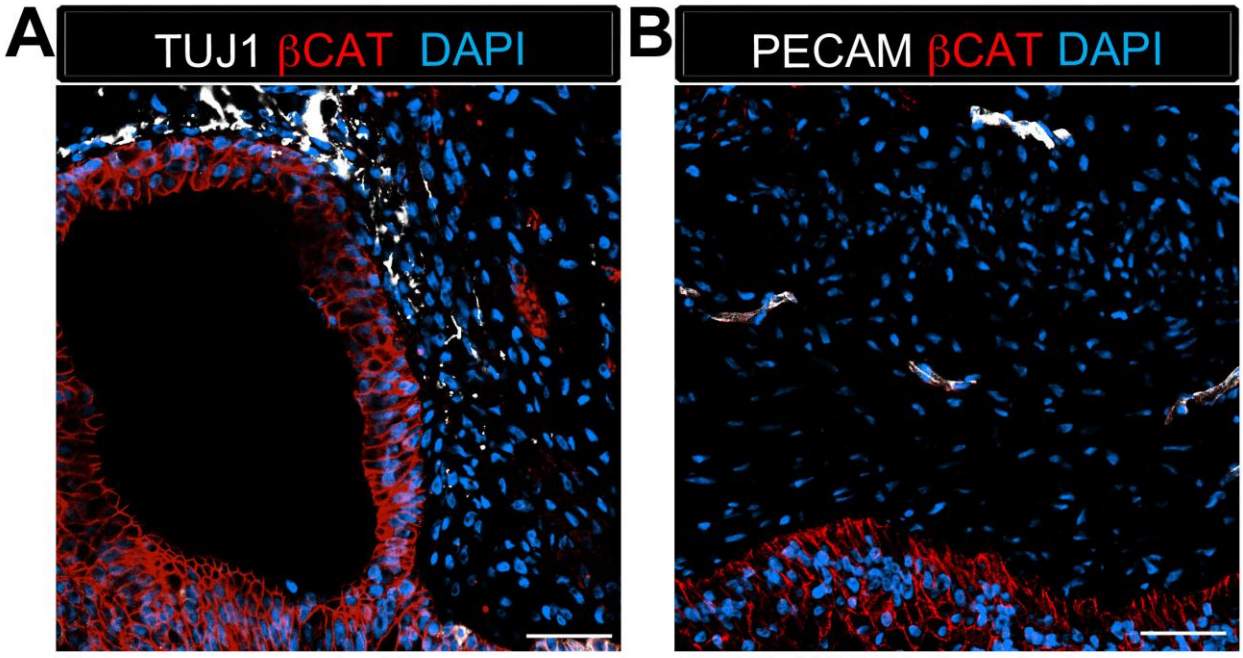

Figure 4.10 tHLO airway-like structures were surrounded by cells expressing neuron markers and vasculature markers. (A-B) Some of the cells surrounding the airway-like structures outlined by βCAT (red) expressed (A) neuron marker TUJ1 (white) and (B) vasculature marker PECAM (white). Scale bars represent 50μm.

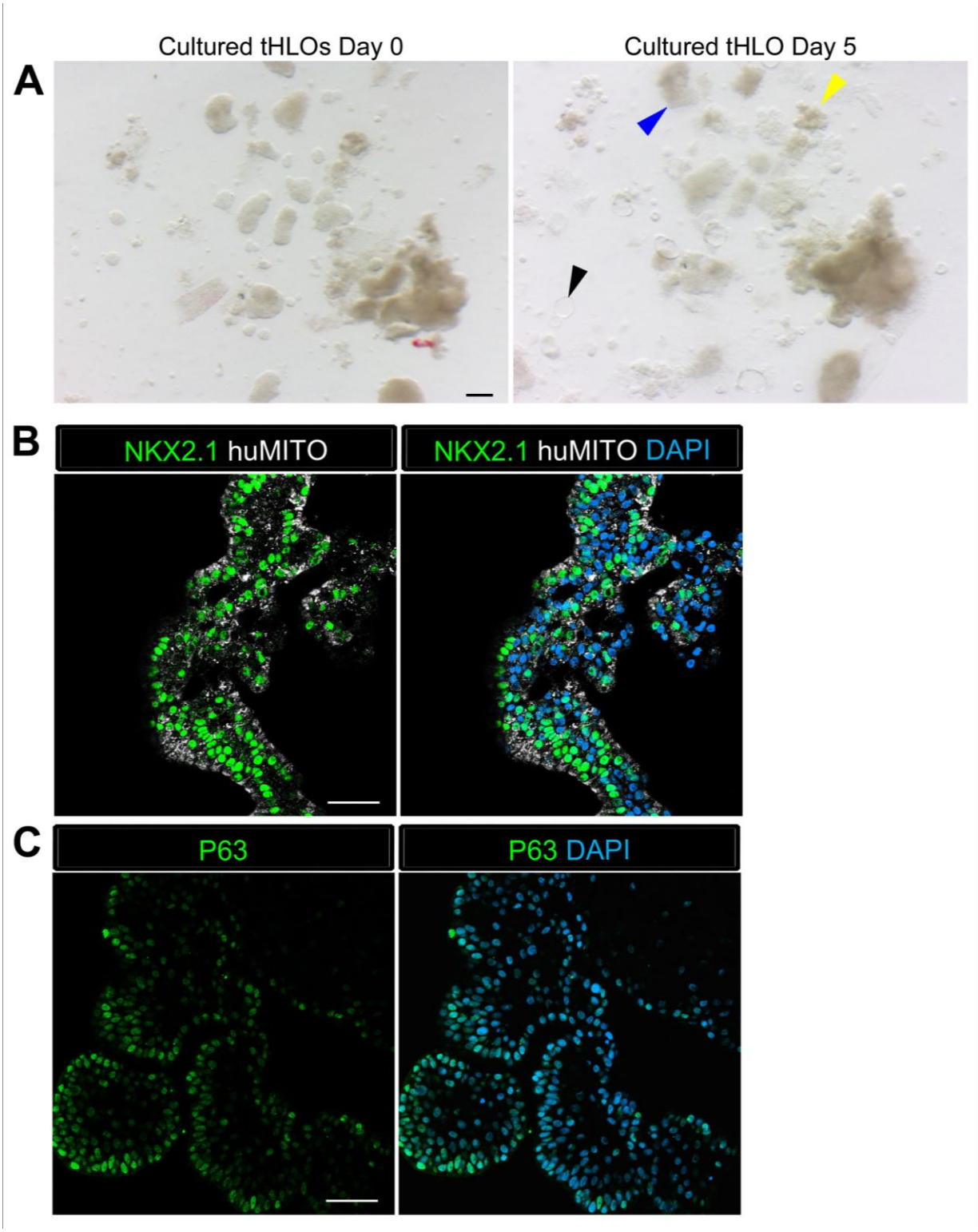

Figure 4.11 Transplanted tissue can be cultured *in vitro*. (A) Whole mount image of transplanted airway cultures from day 0 (left panel) and after 5 days in culture (right panel). After 5 days the cultures formed cyst structures (black arrowhead), dense

cultures (blue arrowhead), and budded structures (yellow arrowhead). (B) 5 day tHLO cultures expressed lung marker NKX2.1 (green) and huMITO (white). (C)The majority of the cells expressed basal cell marker P63 (green) in 5 day tHLO cultures. Scale bars in A represent 250µm and in B-C represent 50µm.

Table 4.1 List of primary and secondary antibodies

Primary Antibody	Source	Catalog #	Dilution	Clone
Goat anti-β-Catenin (βCAT)	Santa Cruz Biotechnology	sc-1496	1:200	C-18
Goat anti-CC10	Santa Cruz Biotechnology	sc-9770	1:200	C-20
Goat anti-SOX9	R&D Systems	AF3075	1:500	polyclonal
Goat anti-VIMENTIN (VIM)	Santa Cruz Biotechnology	sc-7558	1:100	S-20
Mouse anti-Acetylated Tubulin (ACTTUB)	Sigma-Aldrich	T7451	1:1000	6-11B-1
Mouse anti-E-Cadherin (ECAD)	BD Transduction Laboratories	610181	1:500	36/E-Cadherin
Mouse anti-FOXJ1	eBioscience	14-9965-82	1:500	2A5
Mouse anti- Human Mitochondria (huMITO)	Millipore	MAB1273	1:500	113-1
Rabbit anti-Cytokeratin5 (CK5)	Abcam	ab53121	1:500	polyclonal
Rabbit anti-NKX2.1	Abcam	ab76013	1:200	EP1584Y
Rabbit anti-P63	Santa Cruz Biotechnology	sc-8344	1:200	H-129
Rabbit anti-PDGFRα	Santa Cruz Biotechnology	sc-338	1:100	C-20
Rabbit anti-SOX2	Seven Hills Bioreagents	WRAB-SOX2	1:500	polyclonal
Biotin-Mouse anti MUC5AC*	Abcam	ab79082	1:100	MonoClonal
Cy3- Mouse anti Actin-alpha smooth muscle (SMA)*	Sigma	C6198	1:400	MonoClonal
Secondary Antibody	**Source**	**Catalog #**	**Dilution**	
Donkey anti-goat 488	Jackson Immuno	705-545-147	1:500	
Donkey anti-goat 647	Jackson Immuno	705-605-147	1:500	
Donkey anti-goat Cy3	Jackson Immuno	705-165-147	1:500	
Donkey anti-mouse 488	Jackson Immuno	715-545-150	1:500	
Donkey anti-mouse 647	Jackson Immuno	415-605-350	1:500	
Donkey anti-mouse Cy3	Jackson Immuno	715-165-150	1:500	
Donkey anti-rabbit 488	Jackson Immuno	711-545-152	1:500	
Donkey anti-rabbit 647	Jackson Immuno	711-605-152	1:500	
Donkey anti-rabbit Cy3	Jackson Immuno	711-165-102	1:500	
Donkey anti-goat 488	Jackson Immuno	705-545-147	1:500	
Donkey anti-goat 647	Jackson Immuno	705-605-147	1:500	
Donkey anti-goat Cy3	Jackson Immuno	705-165-147	1:500	
Donkey anti-mouse 488	Jackson Immuno	715-545-150	1:500	

Donkey anti-mouse 647	Jackson Immuno	415-605-350	1:500	
Donkey anti-mouse Cy3	Jackson Immuno	715-165-150	1:500	
Donkey anti-rabbit 488	Jackson Immuno	711-545-152	1:500	
Donkey anti-rabbit 647	Jackson Immuno	711-605-152	1:500	
Donkey anti-rabbit Cy3	Jackson Immuno	711-165-102	1:500	

***Secondary antibody conjugated to the primary antibody**

CHAPTER 5

DISCUSSION

Contribution of work

The work presented in Chapter 2 of this dissertation assigns a novel functional role to the transcription factor Sox9 during lung development, and indicates that it is an important factor for proper branching morphogenesis. Previously, Sox9 had been shown to be expressed in the actively branching epithelium during development, but was concluded to have no role in branching morphogenesis (1). By using a ShhCre driver to delete Sox9 in the lung epithelium during lung induction, we have demonstrated that Sox9 is necessary for proper branching morphogenesis. With further characterization, we illustrated that Sox9 regulates extracellular matrix (ECM) protein deposition of Col2a1 and laminin. This relationship between distal progenitor marker Sox9 and epithelial ECM deposition is a novel connection and will further our understanding of the interactions of the branching epithelium and the ECM. These results shed new light on the importance of the physical environment surrounding the bud tip, and highlight an important transcriptional role for Sox9 in regulating this physical environment.

Chapter 3 and 4 of this dissertation described methods to generate immature human lung organoids from pluripotent stem cells, and further showed that transplantation of these organoids into mice resulted in structural and cellular

maturation. These studies made several major contributions to the field. Our studies were the first to show that hPSCs could be used to generate three-dimensional lung tissue with appropriate architecture and cellular composition. Previous studies have demonstrated differentiation of lung tissue from hPSC in 2D culture conditions (2-8). The three-dimensional cultures allowed for relevant structures to form including lung airway-like structures. Having such relevant structures is necessary in order to study complex cell-cell interactions and tissue remodeling during a disease or injured context. For instance, the HLO model has airway-like structures that are lined with cells expressing basal cell markers that are adjacent to multi-ciliated cells. The basal cell is the adult stem cell of the airway and can give rise to ciliated cells upon injury (9-14). This cellular organization allows for complex signaling between basal and ciliated cells thus recapitulating human airway homeostasis.

In addition, the HLOs possess both lung epithelium and mesenchyme, whereas all other hPSC-derived models only possess lung epithelial cells (2-8, 15-17). Having both cellular compartments allows for cross talk between the epithelium and mesenchyme as it does in the native lung during development and adult homeostasis. In addition, lung diseases can originate in the lung epithelium, mesenchyme, or both. Thus, having both epithelium and mesenchyme will allow us to better simulate complex tissue crosstalk that may be necessary for understanding multi-faceted diseases such as pulmonary fibrosis. For example, pulmonary fibrosis is thought to originate from epithelial defects, which subsequently lead to activation and remodeling of mesenchymal cells that produces dense tissue in the distal airway spaces (18-21). Currently, HLOs are the only human lung model that contains both epithelial and

mesenchymal tissue, which are both important contributors to human pulmonary disease and will allow for more accurate recapitulation of complex diseases *in vitro*. Taken together the HLOs possess multiple lung tissues (epithelium and mesenchyme), diverse cell types, and structures similar to the native lung that result in an ideal model study development, homeostasis and diseases.

Future Directions

In chapter 2, our studies in the developing mouse lung suggest that Sox9 is a crucial regulator of epithelial movement in the lung epithelium by directly and indirectly affecting the ECM and cytoskeleton. Consistent with this idea, Sox9 regulates cell movement during other developmental and disease contexts. For example, high levels of Sox9 are associated with invasiveness and lower survival in several cancers, including non-small cell lung cancer (22-28). During development Sox9 is necessary for neural crest cell migration (29). Lastly, Sox9 directly regulates various ECM genes in chondrocytes including Col2a1 (30). Therefore, future studies could explore the mechanisms by which Sox9 regulates the ECM and cytoskeleton in the developing lung in order to coordinate cellular movement at the branch tips.

During branching morphogenesis the physical environment plays an important role regulating the branching pattern (31-33). We have shown at the different stages of a branch bifurcation, there is a thicker deposition of ECM protein laminin where the cleft of the bifurcation will form and a thinner layer of laminin where the buds will grow out from and become two new branches (33). This pattern is consistent with ECM protein fibronectin, which is distributed in a similar manner (34). More recently, the degradation

of the ECM during branching morphogenesis was observed in real time through live imaging of ECM proteins collagenIV, laminin, and perlecan. This revealed that the ECM forms a mesh-like network around the epithelial bud tip to allow parts of the basal surface of the epithelial cells to poke through the ECM as the entire epithelial bud branches (32). Lastly, isolated mouse epithelial lung buds cultured in different matrix stiffness's caused different number of branch tips to form (35). Therefore, the ECM composition affects branching, but how the ECM is regulated is unknown. Our results showed that Sox9 regulates the ECM, either directly or indirectly, therefore; using genetic mouse models (gain- and loss-of-function) will allow us to define a mechanism for how Sox9 regulates the ECM, which will then further our understanding of how the ECM regulates branching morphogenesis.

In order to define the mechanism of Sox9 during branching morphogenesis, a careful study of migration and ECM at the branching tips needs to be conducted. By using explant cultures as demonstrated in Chapter 2, epithelial migration during branching morphogenesis can be recorded and compared in both $Sox9^{LOF}$ and $Sox9^{GOF}$ E12.5 mouse lung. Similar to Harunaga et al. 2014, the mesh network of ECM proteins laminin and Col2a1 can be compared between $Sox9^{LOF}$ and $Sox9^{GOF}$ lungs in order to test if the level of Sox9 expression affects the ECM network. Lastly, a scratch assay on epithelial bud cultures in control and $Sox9^{LOF}$ distal lung epithelium demonstrated in Chapter 2, can be used to measure changes in epithelial cell migration when the cells are grown on different ECM protein combinations. This assay will first test if the ECM composition affects overall *in vitro* lung epithelial cell migration and then more specifically if the delayed $Sox9^{LOF}$ epithelial cell migration can be rescued with different

ECM combinations. There are still many unanswered questions regarding the role and regulation of ECM and cytoskeleton during branching morphogenesis. For example, does epithelial cell cytoskeleton disruption lead to aberrant ECM protein deposition, or do these defects occur independently of one another? Does Sox9 directly or indirectly regulate cytoskeletal proteins and ECM proteins? Is the cytoskeletal defect in $Sox9^{LOF}$ epithelium secondary to improper ECM protein deposition?

There are also several unanswered questions and outstanding problems in the field of pluripotent stem cell differentiation that remain. For example, in Chapters 3 and 4, I demonstrated that 3-dimensional lung organoid tissue can be derived from hPSCs, however; there are currently no *in vitro* human lung models to study branching morphogenesis. More specifically, the HLO model begins as a lung progenitor population expressing the lung marker NKX2.1 and then directly differentiates into pockets of distal epithelium and proximal airway-like structures, seemingly without going through a stage of branching morphogenesis. Thus, HLOs and tHLOs lack the complex, arborized tree-like network of the adult lung, and tHLOs appear only to possess airway-like structures. Therefore, a major direction of future research will be to determine the appropriate chemical and physical environment that will allow *in vitro* development of HLOs to undergo branching morphogenesis and establish proximal-distal axis, ultimately giving rise to the adult lung structures.

Branching morphogenesis is a dynamic process involving both directional chemical and physical cues. The chemical environment consist of signaling factors that are important for both branch growth and for establishing the proximal-distal axis including. Several pathways are known to play very important roles during this process,

including Wnts, BMP4, FGFs, and SHH (36-38). Currently we grow the HLOs in media supplemented with high FGF10. FGF10 is known to promote epithelial growth, and during late development FGF10 is necessary to maintain the basal cell population in the mouse trachea (39-41). Therefore, high FGF10 in the HLO cultures maintains epithelial growth and may be inducing and maintaining cells that express basal cell markers, but this growth factor does not appear to induce branching morphogenesis *in vitro*. Recently it has been shown for *in vitro* mouse bud cultures with no mesenchyme present that FGF1 and FGF9 cause extensive epithelial budding (42). Therefore, it is possible that other FGFs besides FGF10 may be important for branching. A simple experiment to perform would be to supplement the media with FGF9 and FGF1 in order to induce budding as seen in the mouse bud cultures. Such a finding would also be very interesting, as it would provide a system to understand how a tissue responds differently to signaling ligands from a single family in order to give diverse biological outcomes. As mentioned earlier, the ECM also plays a significant role in epithelial movement during branching (31-33). Therefore, the matrix surrounding the HLOs could affect epithelial movement, and their ability or inability to branch *in vitro*. To date, we have grown HLOs in Matrigel, which is enriched in laminin (43). The native lung ECM consists of many proteins including laminin, collagen, perlecan, fibronectin, and elastin (35, 44). Therefore, by changing the matrix composition to represent the native lung ECM, we may predict that the change in environment would induce HLOs to form branching structures. Lastly, the surrounding vasculature and the invading neural crest cells, which give rise to neurons, are both important for branching morphogenesis (45-52). It is possible that HLOs do not branch because they are missing these cellular components.

By deriving endothelial cells and neural crest cells from hPSCs and combining these cells with the foregut spheroids, which consist of lung progenitors and mesenchyme, it is possible that HLOs will form budding structures (53-58). This would be an interesting result, and would lead to further exploration on understanding the mechanistic basis by which tissue-tissue interactions or signaling between different tissues could promote branching morphogenesis.

As branching occurs, a proximal-distal axis is established in which the proximal epithelium will give rise to the conducting airways and the distal epithelium will give rise to the alveoli where gas exchange occurs. Although the HLO model does not undergo branching morphogenesis, the HLOs have clusters of proximal and distal cell types. However, we do not know the exact factors or the overall environment that induces a proximal cell instead of a distal cell. In order to generate specific structures of the lung, proximal and distal identities need to be established. During branching morphogenesis, the proximal epithelium expresses Sox2 while the distal epithelium expresses Sox9/Id2/Nmyc (1, 33, 59, 60). Wnt2/2b, BMP4, and FGF10 are expressed at high levels in the distal mesenchyme and Wnt7a from the distal epithelium signal to the distal epithelium establish distal identity in mouse lungs (39-41, 61-65). In addition, loss of Wnt signaling in mice causes an expansion of the proximal domain during lung development (65, 66). In order to screen the different signaling factors, mouse embryonic epithelial bud tips can be cultured in different combinations of Wnt, BMP, and FGFs to see if the buds maintain Sox9 expression or turn off Sox9 and express Sox2. This screen will then show the essential growth factors to maintain distal or proximal identity. The top candidates of growth factor combinations from the mouse bud screen

could then be applied to the HLO cultures, which may create an environment to develop either proximal conducting airways or distal alveoli accordingly. However, many questions remain with regards to deriving airways and/or alveoli including: How do you generate alveolar structures without the support of a scaffold? How can we set up a chemical gradient to establish a proximal-distal axis *in vitro*? If we can form budding structures that resemble branches, will the budding structures eventually become airway or alveoli and can we induce one over the other by changing the physical and chemical environment?

Currently, both HLOs and tHLOs can be applied to model diseases affecting the airway. HLOs and tHLOs possess lumens similar to the intestinal organoids. The intestinal organoids are able to be injected with various substrates including pathogens and chemicals (67). We can apply this approach to HLOs and tHLOs and microinject pathogens that are known to infect the airway epithelium such as human respiratory syncytial virus infection (68), or microinject chemicals that induce injury including SO2, naphthalene, and allergens (69-72). We can then model human airway epithelial reaction and regeneration. More specifically, HLOs and tHLOs possess cells expressing basal cell markers, which are the adult stem cell of the airways (9-14); thus we can study basal cell maintenance and the balance of the secretory and ciliated cell populations. Both organoid systems, HLO and tHLO provide a developmental and adult lung context respectively to study airway disease and regeneration.

Taken together, the work presented in this dissertation has utilized both animal models and human pluripotent stem cells to generate three-dimensional human lung tissue models in order to better understand how the lung develops. In the future, it will

be interesting to see how these models can be leveraged to further our understanding of human development and adult lung diseases.

References

1. Perl A-KT, Kist R, Shan Z, Scherer G, Whitsett JA (2005) Normal lung development and function afterSox9 inactivation in the respiratory epithelium. *genesis* 41(1):23–32.

2. Huang SXL, et al. (2013) Efficient generation of lung and airway epithelial cells from human pluripotent stem cells. *Nature Biotechnology*. doi:10.1038/nbt.2754.

3. Longmire TA, et al. (2012) Efficient Derivation of Purified Lung and Thyroid Progenitors from Embryonic Stem Cells. *Stem Cell* 10(4):398–411.

4. Wong AP, et al. (2012) Directed differentiation of human pluripotent stem cells into mature airway epithelia expressing functional CFTR protein. *Nature Biotechnology* 30(9):875–881.

5. Hannan NRF, Sampaziotis F, Segeritz C-P, Hanley NA, Vallier L (2015) Generation of Distal Airway Epithelium from Multipotent Human Foregut Stem Cells. *Stem Cells Dev* 24(14):1680–1690.

6. Firth AL, et al. (2014) Generation of multiciliated cells in functional airway epithelia from human induced pluripotent stem cells. *Proceedings of the National Academy of Sciences* 111(17):E1723–30.

7. Ghaedi M, et al. (2014) Alveolar epithelial differentiation of human induced pluripotent stem cells in a rotating bioreactor. *Biomaterials* 35(2):699–710.

8. Mou H, et al. (2012) Generation of Multipotent Lung and Airway Progenitors from Mouse ESCs and Patient-Specific Cystic Fibrosis iPSCs. *Stem Cell* 10(4):385–397.

9. Rock JR, et al. (2009) Basal cells as stem cells of the mouse trachea and human airway epithelium. *Proceedings of the National Academy of Sciences* 106(31):12771–12775.

10. Hackett T-L, et al. (2008) Characterization of side population cells from human airway epithelium. *STEM CELLS* 26(10):2576–2585.

11. Hong KU, Reynolds SD, Watkins S, Fuchs E, Stripp BR (2004) Basal cells are a multipotent progenitor capable of renewing the bronchial epithelium. *AJPA* 164(2):577–588.

12. Boers JE, Ambergen AW, Thunnissen FB (1998) Number and proliferation of basal and parabasal cells in normal human airway epithelium. *Am J Respir Crit Care Med* 157(6 Pt 1):2000–2006.

13. Pardo-Saganta A, et al. (2015) Injury induces direct lineage segregation of functionally distinct airway basal stem/progenitor cell subpopulations. *Cell Stem Cell* 16(2):184–197.

14. Nakajima M, et al. (1998) Immunohistochemical and ultrastructural studies of basal cells,

Clara cells and bronchiolar cuboidal cells in normal human airways. *Pathol Int* 48(12):944–953.

15. Konishi S, et al. (2016) Directed Induction of Functional Multi-ciliated Cells in Proximal Airway Epithelial Spheroids from Human Pluripotent Stem Cells. *Stem Cell Reports* 6(1):18–25.

16. Gotoh S, et al. (2014) Generation of alveolar epithelial spheroids via isolated progenitor cells from human pluripotent stem cells. *Stem Cell Reports* 3(3):394–403.

17. Ghaedi M, et al. (2013) Human iPS cell-derived alveolar epithelium repopulates lung extracellular matrix. *J Clin Invest* 123(11):4950–4962.

18. Leng D, et al. (2013) Meta-analysis of genetic programs between idiopathic pulmonary fibrosis and sarcoidosis. *PLoS ONE* 8(8):e71059.

19. Rojas M, et al. (2015) Aging and Lung Disease. Clinical Impact and Cellular and Molecular Pathways. *Ann Am Thorac Soc* 12(12):S222–7.

20. King TE, Pardo A, Selman M (2011) Idiopathic pulmonary fibrosis. *Lancet* 378(9807):1949–1961.

21. Selman M, Pardo A (2002) Idiopathic pulmonary fibrosis: an epithelial/fibroblastic cross-talk disorder. *Respir Res* 3:3.

22. Zhou C-H, et al. (2012) Clinical significance of SOX9 in human non-small cell lung cancer progression and overall patient survival. *J Exp Clin Cancer Res* 31:18.

23. Matheu A, et al. (2012) Oncogenicity of the developmental transcription factor Sox9. *Cancer Research* 72(5):1301–1315.

24. Chakravarty G, et al. (2011) Prognostic significance of cytoplasmic SOX9 in invasive ductal carcinoma and metastatic breast cancer. *Exp Biol Med (Maywood)* 236(2):145–155.

25. Thomsen MK, et al. (2010) SOX9 elevation in the prostate promotes proliferation and cooperates with PTEN loss to drive tumor formation. *Cancer Research* 70(3):979–987.

26. Jiang SS, et al. (2010) Upregulation of SOX9 in lung adenocarcinoma and its involvement in the regulation of cell growth and tumorigenicity. *Clin Cancer Res* 16(17):4363–4373.

27. Rao P, Fuller GN, Prieto VG (2010) Expression of Sox-9 in metastatic melanoma--a potential diagnostic pitfall. *Am J Dermatopathol* 32(3):262–266.

28. Pritchett J, Athwal V, Roberts N, Hanley NA, Hanley KP (2011) Understanding the role of SOX9 in acquired diseases: lessons from development. *Trends Mol Med* 17(3):166–174.

29. Betters E, Liu Y, Kjaeldgaard A, Sundström E, García-Castro MI (2010) Analysis of early human neural crest development. *Developmental Biology* 344(2):578–592.

30. Oh C-D, et al. (2010) Identification of SOX9 Interaction Sites in the Genome of Chondrocytes. *PLoS ONE* 5(4):e10113.

31. Kim HY, Varner VD, Nelson CM (2013) Apical constriction initiates new bud formation during monopodial branching of the embryonic chicken lung. *Development*. doi:10.1242/dev.093682.

32. Harunaga JS, Doyle AD, Yamada KM (2014) Local and global dynamics of the basement membrane during branching morphogenesis require protease activity and actomyosin contractility. *Developmental Biology* 394(2):197–205.

33. Rockich BE, et al. (2013) Sox9 plays multiple roles in the lung epithelium during branching morphogenesis. *Proceedings of the National Academy of Sciences* 110(47):E4456–64.

34. Sakai T, Larsen M, Yamada KM (2003) Fibronectin requirement in branching morphogenesis. *Nature* 423(6942):876–881.

35. Kim HY, Nelson CM (2012) Extracellular matrix and cytoskeletal dynamics during branching morphogenesis. *organogenesis* 8(2):56–64.

36. Morrisey EE, Hogan BLM (2010) Preparing for the First Breath: Genetic and Cellular Mechanisms in Lung Development. *Dev Cell* 18(1):8–23.

37. Rawlins EL, Ostrowski LE, Randell SH, Hogan BLM (2007) Lung development and repair: contribution of the ciliated lineage. *Proc Natl Acad Sci USA* 104(2):410–417.

38. Herriges M, Morrisey EE (2014) Lung development: orchestrating the generation and regeneration of a complex organ. *Development* 141(3):502–513.

39. Bellusci S, Grindley J, Emoto H, Itoh N, Hogan BL (1997) Fibroblast growth factor 10 (FGF10) and branching morphogenesis in the embryonic mouse lung. *Development* 124(23):4867–4878.

40. Nyeng P, Norgaard GA, Kobberup S, Jensen J (2008) FGF10 maintains distal lung bud epithelium and excessive signaling leads to progenitor state arrest, distalization, and goblet cell metaplasia. *BMC Dev Biol* 8:2.

41. Volckaert T, et al. (2013) Localized Fgf10 expression is not required for lung branching morphogenesis but prevents differentiation of epithelial progenitors. *Development* 140(18):3731–3742.

42. Goto A, Yamazaki N, Nogawa H (2014) Characterization of FGF family growth factors concerning branching morphogenesis of mouse lung epithelium. *Zool Sci* 31(5):267–273.

43. Hughes CS, Postovit LM, Lajoie GA (2010) Matrigel: a complex protein mixture required for optimal growth of cell culture. *Proteomics* 10(9):1886–1890.

44. Bonnans C, Chou J, Werb Z (2014) Remodelling the extracellular matrix in development and disease. *Nat Rev Mol Cell Biol* 15(12):786–801.

45. Barkauskas CE, et al. (2013) Type 2 alveolar cells are stem cells in adult lung. *J Clin Invest* 123(7):3025–3036.

46. van Tuyl M, et al. (2007) Angiogenic factors stimulate tubular branching morphogenesis of sonic hedgehog-deficient lungs. *Developmental Biology* 303(2):514–526.

47. Del Moral P-M, et al. (2006) VEGF-A signaling through Flk-1 is a critical facilitator of early embryonic lung epithelial to endothelial crosstalk and branching morphogenesis. *Developmental Biology* 290(1):177–188.

48. Franzdóttir SR, et al. (2010) Airway branching morphogenesis in three dimensional culture. *Respir Res* 11:162.

49. Lee J-H, et al. (2014) Lung stem cell differentiation in mice directed by endothelial cells via a BMP4-NFATc1-thrombospondin-1 axis. *Cell* 156(3):440–455.

50. Bower DV, et al. (2014) Airway branching has conserved needs for local parasympathetic innervation but not neurotransmission. *BMC Biol* 12:92.

51. Freem LJ, et al. (2010) The intrinsic innervation of the lung is derived from neural crest cells as shown by optical projection tomography in Wnt1-Cre;YFP reporter mice. *J Anat* 217(6):651–664.

52. Aven L, Ai X (2013) Mechanisms of respiratory innervation during embryonic development. *organogenesis* 9(3):194–198.

53. Levenberg S, Golub JS, Amit M, Itskovitz-Eldor J, Langer R (2002) Endothelial cells derived from human embryonic stem cells. *Proc Natl Acad Sci USA* 99(7):4391–4396.

54. Kane NM, et al. (2010) Derivation of endothelial cells from human embryonic stem cells by directed differentiation: analysis of microRNA and angiogenesis in vitro and in vivo. *Arterioscler Thromb Vasc Biol* 30(7):1389–1397.

55. Costa M, et al. (2013) Derivation of endothelial cells from human embryonic stem cells in fully defined medium enables identification of lysophosphatidic acid and platelet activating factor as regulators of eNOS localization. *Stem Cell Res* 10(1):103–117.

56. Lian X, et al. (2014) Efficient differentiation of human pluripotent stem cells to endothelial progenitors via small-molecule activation of WNT signaling. *Stem Cell Reports* 3(5):804–816.

57. Avery J, Dalton S (2016) Methods for Derivation of Multipotent Neural Crest Cells Derived from Human Pluripotent Stem Cells. *Methods Mol Biol* 1341:197–208.

58. Lee G, et al. (2007) Isolation and directed differentiation of neural crest stem cells derived from human embryonic stem cells. *Nature Biotechnology* 25(12):1468–1475.

59. Okubo T (2005) Nmyc plays an essential role during lung development as a dosage-sensitive regulator of progenitor cell proliferation and differentiation. *Development* 132(6):1363–1374.

60. Rawlins EL, Clark CP, Xue Y, Hogan BLM (2009) The Id2+ distal tip lung epithelium contains individual multipotent embryonic progenitor cells. *Development* 136(22):3741–3745.

61. Weaver M, Yingling JM, Dunn NR, Bellusci S, Hogan BL (1999) Bmp signaling regulates proximal-distal differentiation of endoderm in mouse lung development. *Development* 126(18):4005–4015.

62. De Langhe SP, Reynolds SD (2008) Wnt signaling in lung organogenesis. *organogenesis* 4(2):100–108.

63. Kadzik RS, et al. (2014) Wnt ligand/Frizzled 2 receptor signaling regulates tube shape and branch-point formation in the lung through control of epithelial cell shape. *Proceedings of the National Academy of Sciences* 111(34):12444–12449.

64. Rajagopal J, et al. (2008) Wnt7b stimulates embryonic lung growth by coordinately increasing the replication of epithelium and mesenchyme. *Development* 135(9):1625–1634.

65. Shu W, et al. (2005) Wnt/β-catenin signaling acts upstream of N-myc, BMP4, and FGF signaling to regulate proximal–distal patterning in the lung. *Developmental Biology* 283(1):226–239.

66. Mucenski ML, et al. (2003) beta-Catenin is required for specification of proximal/distal cell fate during lung morphogenesis. *J Biol Chem* 278(41):40231–40238.

67. Leslie JL, et al. (2015) Persistence and toxin production by Clostridium difficile within human intestinal organoids result in disruption of epithelial paracellular barrier function. *Infect Immun* 83(1):138–145.

68. Collins PL, Graham BS (2008) Viral and host factors in human respiratory syncytial virus pathogenesis. *J Virol* 82(5):2040–2055.

69. Borthwick DW, Shahbazian M, Krantz QT, Dorin JR, Randell SH (2001) Evidence for stem-cell niches in the tracheal epithelium. *American Journal of Respiratory Cell and Molecular Biology* 24(6):662–670.

70. Rawlins EL, Hogan BLM (2008) Ciliated epithelial cell lifespan in the mouse trachea and lung. *Am J Physiol Lung Cell Mol Physiol* 295(1):L231–4.

71. Stripp BR, Maxson K, Mera R, Singh G (1995) Plasticity of airway cell proliferation and gene expression after acute naphthalene injury. *Am J Physiol* 269(6 Pt 1):L791–9.

72. Rock JR, Randell SH, Hogan BLM (2010) Airway basal stem cells: a perspective on their roles in epithelial homeostasis and remodeling. *Dis Model Mech* 3(9-10):545–556.

APPENDIX: PUBLICATIONS

1. Liu Q, Chen Y, Copeland D, Ball H, Duff RJ, **Rockich (Dye) B**, Londraville RL. Expression of leptin receptor gene in developing and adult zebrafish. General and Comparative Endocrinology 2010 Apr 1. PMCID: PMC3408649

2. **Rockich (Dye) BE**, Hrycaj SM, Shih H-P, Nagy MS, Ferguson MAH, Kopp JL, Sander M, Wellik DM, Spence JR. Sox9 plays multiple roles in the lung epithelium during branching morphogenesis. Proceedings of the National Academy of Sciences. 2013 Nov 4. PMCID: PMC3839746 (Chapter 2)

3. McCracken KW, Catá EM, Crawford CM, Schumacher M, **Rockich (Dye) BE**, Tsai YH, Mayhew CN, Spence JR, Zavros Y, Wells JM. Modelling human development and disease in pluripotent stem cell-derived gastric organoids. Nature 2014 Dec 18. PMCID: PMC4270898

4. **Dye BR**, Hill DR, Ferguson MAH, Tsai YH, Dyal R, Wells JM, Mayhew CN, Nattiv R, Klein OD, White ES, Deutsch GH, Spence JR. In vitro generation of three dimensional lung organoids from human pluripotent stem cells. Elife 2015 Mar 24 PMCID: PMC4370217 (Chapter 3)

5. Hrycaj SM, **Dye BR**, Baker NC, Larsen BM, Burke AC, Spence JR, Wellik DM. Hox5 Genes Regulate the Wnt2/2b-Bmp4-Signaling Axis during Lung Development. Cell Reports 2015 Aug 11 PMCID: PMC4536095

6. Tsai YH, Hill DR, Kumar N, Huang S, Chin AM, **Dye BR**, Verzi MP, Spence JR. LGR4 and LGR5 function redundantly during human endoderm differentiation. Submitted.

7. **Dye BR**, Miller AJ, Spence JR. How to grow a lung: Applying principles of developmental biology to generate lung lineages from human pluripotent stem cells. Under review at Current Pathobiology Reports (Chapter 1)